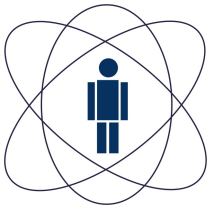

CBPF

Centro Brasileiro de Pesquisas Físicas

Tese de Doutorado

Potenciais dependentes de spin, *axion-like particles* e violação da simetria de Lorentz: fenomenologia de cenários além do Modelo Padrão na fronteira de baixas energias da física

Pedro Cavalcanti Malta

Rio de Janeiro, Junho de 2017

ABSTRACT

Spin-dependent potentials, axion-like particles and Lorentz-symmetry violation: beyond the Standard Model phenomenology at the low-energy frontier of physics

Pedro Cavalcanti Malta

Co-supervisor: Prof. Dr. José Abdalla Helayël-Neto (CBPF)

Co-supervisor: Prof. Dr. Jörg Jäckel (ITP, University of Heidelberg)

Abstract of the doctoral thesis submitted to the Graduate Program in Physics of the Brazilian Centre for Research in Physics (CBPF, Rio de Janeiro, Brazil) and to the Combined Faculties of the Natural Sciences and Mathematics of the Ruperto-Carola University of Heidelberg (Heidelberg, Germany) as part of the requirements necessary to the obtainment of the title of Doctor in natural sciences.

It is well known that the Standard Model is not complete and many of the theories that seek to extend it predict new phenomena that may be accessible in low-energy settings. This thesis deals with some of these, namely, novel spin-dependent interparticle potentials, axion-like particles and Lorentz-symmetry violation. In Part I we discuss the spin-dependent potentials that arise due to the exchange of a topologically massive mediator, and also pursue a comparative study between spin-1/2 and spin-1 sources. In Part II we treat massive axion-like particles that may be copiously produced in core-collapse supernovae, thus leading to a non-standard flux of gamma rays. Using SN 1987A and the fact that after its observation no extra gamma-ray signal was detected, we are able to set robust limits on the parameter space of axion-like particles with masses in the $10\,\mathrm{keV} - 100\,\mathrm{MeV}$ range. Finally, in Part III we investigate the effects of Lorentz-breaking backgrounds in QED. We discuss two scenarios: a modification in the Maxwell sector via the Carroll-Field-Jackiw term and a new non-minimal coupling between electrons and photons. We are able to set upper limits on the coefficients of the backgrounds by using laboratory-based measurements.

Keywords: physics beyond the Standard Model; low-energy phenomenology; spin-dependent potentials; axion-like particles; Lorentz-symmetry violation.

Rio de Janeiro,
June 2017.

ZUSAMMENFASSUNG

Spin-abhängige Potenziale, axion-artige Teilchen und
Lorentz-Symmetrie-Brechung:Phenomenologie von Szenarien
jenseits-des-Standardmodells an der niederenergetischen Grenze der Physik

Pedro Cavalcanti Malta
Erster Betreuer: Prof. Dr. José Abdalla Helayël-Neto (CBPF)
Zweiter Betreuer: Prof. Dr. Jörg Jäckel (ITP, Universität Heidelberg)

Zusammensfassung zur beim *Graduate Program in Physics* vom brasilianischen Zentrum für physikalische Forschung (CBPF, Rio de Janeiro, Brasilien) und bei der Naturwissenschaftlich-Mathematische Gesamtfakultät der Ruprecht-Karls Universität Heidelberg (Heidelberg, Deutschland) eingereichten Doktorarbeit als teilweise Voraussetzung für die Verleihung des Doktortitels (Dr. rer. nat.).

Es ist bekannt, dass das Standardmodell nicht vollständig ist. Viele Theorien, die versuchen es zu erweitern, sagen neue Phänomene voraus, die bei niedrigen Energien detektiert werden können. Diese Doktorarbeit befasst sich mit einigen davon: neue spin-abhängige Potenziale, axion-artige Teilchen und Brechung der Lorentz-Symmetrie. Im I. Teil diskutieren wir spin-abhängige Potenziale, die durch topologisch massive Austauschbosonen verursacht werden können. Wir unternehmen auch einen Vergleich zwischen den Wechselwirkungen von spin-1/2 und spin-1 Quellen. Im II. Teil beschäftigen wir uns mit massiven axion-artigen Teilchen, die durch Kernkollaps-Supernovae reichlich produziert werden können und damit einen nichtstandardmäßigen Fluß von Gamma-Strahlung erzeugen können. Mithilfe von SN 1987A und der Tatsache, dass nach deren Betrachtung kein unerwartetes Signal gemessen wurde, haben wir robuste Grenzen auf den Parameterraum von axionartigen Teilchen mit Massen im Bereich $10\,\mathrm{keV} - 100\,\mathrm{MeV}$ gesetzt. Schließich, im III. Teil untersuchen wir die Effekte von Lorentz-Symmetrie-brechenden Hintergründen beim QED. Wir befassen uns mit zwei Szenarien: einem durch den Carroll-Field-Jackiw-Term veränderten Maxwell-Sektor und einem zweiten mit einer neuen nichtminimalen Kopplung zwischen Elektronen und Photonen. Wir haben durch auf der Erde basierte Laborexperimente obere Grenzen auf die Koeffizienten der Lorentzbrechenden Hintergründe gesetzt.

Schlüsselwörter: Physik jenseits des Stadardmodells; niederenergetische Phänomenologie; spin-abhängige Potenziale; axion-artige Teilchen; Brechung der Lorentz-Symmetrie.

Rio de Janeiro,
Juni 2017.

RESUMO

Potenciais dependentes de spin, *axion-like particles* e violação da simetria de Lorentz: fenomenologia além do Modelo Padrão na fronteira de baixas energias da física

Pedro Cavalcanti Malta
Co-orientador: Prof. Dr. José Abdalla Helayël-Neto (CBPF)
Co-orientador: Prof. Dr. Jörg Jäckel (ITP, Universidade de Heidelberg)

Resumo da Tese de Doutorado submetida ao Programa de Pós-graduação em Física do Centro Brasileiro de Pesquisa em Física (CBPF, Rio de Janeiro, Brasil) e às Faculdades Combinadas de Ciências Naturais e Matemática da Universidade Ruperto-Carola de Heidelberg (Heidelberg, Alemanha) como parte dos requisitos necessários à obtenção do título de Doutor em Ciências (Física).

É bem conhecido o fato de que o Modelo Padrão não é completo e que diversas teorias que tentam estendê-lo predizem novos fenômenos que podem ser accessíveis em baixas energias. Esta tese trata de alguns destes aspectos, a saber: novos potenciais dependentes de spin, *axion-like particles* e violação da simetria de Lorentz. Na Parte I nós discutimos potenciais interpartícula que ocorrem devido à troca de mediadores topologicamente massivos, assim como traçamos um estudo comparado das interações entre fontes de spin-1/2 e spin-1. Na Parte II nós tratamos *axion-like particles* massivos que podem ser copiosamente produzidos em supernovas com colapso de caroço (*core collapse*), gerando assim um fluxo não-padrão de raios gama. Usando SN 1987A e o fato de que após sua observação nenhum excesso de raios gama for detectado, nós podemos obter limites robustos no espaço de parâmetros de *axion-like particles* com massas em torno de $10\,\mathrm{keV} - 100\,\mathrm{MeV}$. Finalmente, na Parte III nós investigamos os efeitos de vetores de fundo que quebram a simetria de Lorentz na EDQ. Nós discutimos dois cenários: a modificação do setor de Maxwell através do termo de Carroll-Field-Jackiw e de um acoplamento não-mínimo entre elétrons e fótons. Utilizando medidas em laboratórios terrestres nós obtemos limites superiores para os diferentes coeficientes dos vetores de fundo.

Palavras-chave: física além do Modelo Padrão; fenomenologia em baixas energias; potenciais dependentes de spin; *axion-like particles*; violação da simetria de Lorentz.

Rio de Janeiro,
Junho de 2017.

Acknowledgements[1]

This PhD work, though being a great personal achievement, owes its results not only to my individual efforts, but also to the help from many others who were by my side during the years necessary to its completion. The time as a PhD student was certainly full of ups and downs (hopefully on average more ups) and I wish to dedicate this thesis to all those who believed in and supported me. Accepting the risk of forgetting someone (sorry), below I mention a few of the most important people that made this PhD possible.

My Brazilian advisor, José Abdalla Helayël-Neto (CBPF), who, with infinite patience and wisdom, guided me throughout many complicated topics and decisions, and showed that science without humanity is not worth pursuing. I am specially thankful for his great partnership and trust during the first two and a half years of my PhD, when I needed to travel and be absent for long periods to be with my (at the time not yet) wife. Without his attention and above all understanding, both my doctorate and my marriage would not be possible.

My German advisor, Jörg Jäckel (ITP, Heidelberg), who enthusiastically accepted to advise me and promptly worked alongside the University of Heidelberg to tackle the initial bureaucracy and make it possible for me to have a smooth transition between CBPF and the ITP – Heidelberg. I thank him specially for his patience and great attention to detail, as well as his willingness to discuss and support new ideas. It has been a great pleasure to work on phenomenology with him and try to grasp a bit of the *higher art of estimation*.

My wife, Karoline Selbach, whom I have met in a Physics conference in 2013 (CLASHEP, at Arequipa, Peru) and, after that, has turned my life upside down, for the better. Her intelligence, sensibility and clear-mindedness inspire and motivate me every day to be a better person. For her I litearlly went to the end of the world (a.k.a. Japan) and, to be together, we have flown more than 145.000 km – half way to the Moon – and I would do it again. I thank her for her immense support and dedication during this – at times troubled – but mostly very happy period, always by my side, always there when I needed. I love you!

My family (Ana, Paulo and João), who always supported me by making life a bit easier in the hardest times. You have allowed me to follow my dream with Karoline even if this meant me not being around anymore. Thank you for the whole-hearted love and warmth and care, and please know that there has not been one day in the last three years that passed without me missing you. Thank you for everything, I love you! I also dedicate this thesis *in memorium* to Catarina and Manuela, whose short time on this Earth made my life a lot brighter by showing how inconditional love can be. I miss you!

My newer family (Dagmar, Sylvia and Jürgen + Willi and Petra), who took me with great enthusiasm and made me feel one of your own. It has not been always easy: I needed one year to be reasonably proficient in German (still not in bergisch Blatt, sorry Oma). There are so many differences in cultural backgrounds

[1] "The universe is made of stories not of atoms", Muriel Rukeyser (1913 - 1980), american poet.

and every detail is a new discovery. You have been great, thank you so much for all the patience, support and, above all, for the continued understanding and care.

My friends from both UFRJ and CBPF, for their presence and everlasting friendship and partnership. Without you this PhD would be very hard to accomplish. In the wise words of Cicero (106 - 43 BC), "the shifts of Fortune test the reliability of friends", and I am very happy to have this amazing group of friends and colleagues to whom I owe so much: Michael Moraes, Daniel Kroff, Anderson Kendi, Marcelo Vargas, Carlos Zarro, Daniel Niemeyer, Mauricio Hippert, Celio Marlier, Gustavo Pazzini, Pedro Costa, Yuri Müller, Lais Lavra, Leonardo Ospedal, André Persechino, Judismar Guaitolini, Kim Veiga, Fabio Lucio Alves, Luís Santos and Felipe Gomes.

I am also very thankful for the friendship with Jonas and Clara, with whom I have had so many interesting and funny conversations in Heidelberg and Stuttgart (more to come in München, I hope). Furthermore, I would like to thank my friends from Leme (Fernando, Pablo, Alexandre and Marcio) for nice times surfing, as well as my dear friends acquired during my German course in Dresden (Bruno, Fabi, Ramon, Thiago, Luiza, Hermógenes and Márcia), which have been great during the second half of my PhD time; hopefully we will keep in touch for the years to come.

I dedicate this thesis *in memorium* to my father, Paulo Jorge de Barros Malta, who passed away on the 12 of March 2017 after fighting against an aneurism in the aorta. A loving and caring father, a great supporter of my development, a very cultivated and bright man. A wonderful guy. Esta tese de doutorado é para você, papai! Te amo!

The known is finite, the unknown infinite; intellectually we stand on an islet in the midst of an illimitable ocean of inexplicability. Our business in every generation is to reclaim a little more land.

Thomas Henry Huxley

Contents

Presentation

The Standard Model and beyond

The Standard Model (SM) is the theoretical framework which currently most accurately describes the phenomena in the atomic and sub-atomic scales. It is the result of cumulative theoretical and experimental work done basically since the discovery of the electron by J.J. Thomson in 1897 [1]. Since then the list of known particles has considerably grown with the latest big discovery being made in 2012, when the Higgs boson was first detected[2].

Some of the particles discovered are not actually elementary, but rather composite objects that can be described by more fundamental entities[3]. As we currently understand it, the truly fundamental ingredients of the SM belong to two categories: fermions and bosons. The elementary fermions are the charged leptons (e, μ, τ) and associated neutrinos (ν_e, ν_μ, ν_τ), and the fractionally charged quarks (u, d, c, s, b, t), all with spin-1/2. In the boson sector we have the massless photon, the heavy $W^\pm$ and Z^0, and the eight massless gluons, all with spin-1, the graviton with spin-2 and the Higgs with spin-0. A comprehensive list of particles – elementary or not – and their known properties can be found in Ref. [2].

The particles cited above interact with each other in such a way that the fermions are the usual (matter) sources, typically represented by electrons, protons, neutrons and agglomerations thereof (i.e., atoms, molecules, etc), whereas the bosons – except the Higgs! – are responsible for mediating the interactions. In this sense, presently we have been able to identify four fundamental forces, namely: weak and strong nuclear forces, electromagnetic and gravitation. The first two are limited to nuclear ranges ($\lesssim 10^{-10}$ m) and do not have significant effects outside the atomic nucleus. The second two are unlimited in range and shape our everyday world from the micrometer scales up to astronomical ones.

[2]For a nice timeline, see Ref. [1].

[3]Incidentally, the rate of discoveries is usually correlated with our ability to increase the energy available in experiments. With more energy one can probe deeper into the structure of matter and resolve finer details. This is essentially the way that the nucleus was discovered by Rutherford.

Nowadays fundamental interactions are seen as a consequence of symmetry. This started with the classical electromagnetic theory and evolved until the SM, which is built upon the principle of gauge symmetry[4]. The golden standard to this is quantum electrodynamics (QED), where the interaction of charged particles with the electromagnetic field naturally emerges when we assume that charged matter transforms differently depending on the point in spacetime. The more complicated weak and strong interactions (non-Abelian, Yang-Mills theories) are described similarly, *mutatis mutandis* [4].

Important clues regarding which symmetries are important in the SM have been found in the 1950's, when it became clear that weak interactions differentiate between left- and right-handed fermions [5–7]. In the 1960's Salam, Weinberg and Glashow [8–11] formulated the SM based upon gauged $SU(2)_L \otimes U(1)_Y$, which is as we know it today. One of the most important ingredients, however, is spontaneous symmetry breaking via a scalar field (the Higgs), which leads to the low-energy $U(1)_{\rm em}$. The Higgs boson is a cornerstone of the Salam-Weinberg-Glashow model: as it acquires its expectation value and breaks the symmetry, it also generates mass for gauge bosons, itself and fermions (except neutrinos) [4].

The Salam-Weinberg-Glashow model with Higgs mechanism is ultimately based upon the unification of electromagnetism and weak interactions[5] and successfully predicts neutral currents [12], as well as the masses of the $W^{\pm}$ and Z^0 bosons (first observed in 1983 [13, 14]) and the newly discovered Higgs [15, 16]. For reviews, see e.g. Refs. [1, 4, 17, 18].

However, the story of the SM is not only made of successes [19]. Theoretically, some issues are not satisfactorily explained, e.g., the quantization of electric charge, the number of families or the mass hierarchy of leptons and quarks (which span several orders of magnitude). Other issues are more pressing, such as the observed matter-antimatter asymmetry, neutrino masses[6], the identification of what are dark matter and dark energy, and a theory of quantum gravity, just to quote a few.

[4] In the words of Salam and Ward: "Our basic postulate is that it should be possible to generate strong, weak and electromagnetic interaction terms (with all their correct symmetry properties and also with clues regarding their relative strengths) by making local gauge transformations on the kinetic–energy terms in the free Lagrangian for all particles" [3].

[5] The most visible signal of this unification is displayed in the relation between the electric charge e, weak angle θ_W and weak isospin coupling constant g, $e = g \sin\theta_W$ [4].

[6] All started with the so-called neutrino anomalies, an unexpected difference in the number of neutrinos observed relative to the theoretical predictions. The currently accepted solution was first suggested by Pontecorvo [20] and is based upon flavor oscillation. This means that the interaction eigenstates (e, μ, τ) are not propagation – i.e., mass – eigenstates, therefore it is not really meaningful to talk about the mass of the electron neutrino, muon neutrino, etc. In any case, the oscillation phenomenon depends only upon the difference of the squared masses, so the determination of the individual masses is still an open challenge [21].

All these points indicate that the SM is somehow not complete and must be augmented by some kind of new physics. The current understanding is that the SM is a low-energy limit ($E \sim m_W \sim 100$ GeV) of a more complete theory, which should be valid up to very high energy scales, maybe the Planck scale $M_{\rm Pl} \sim 10^{19}$ GeV. Given the historical development of physical models through consecutive unification of previously separate concepts[7], it is also believed that the SM should be a sub-set of some larger theory.

With the aforementioned arguments in mind, many beyond the SM (BSM) scenarios have been developed over the last decades, such as extra dimensions [22], supergravity [23], supersymmetry[8] and grand unified theories [24–27]. Another possible – and interesting – BSM scenario is string theory[9] (for an overview, see Ref. [28] and references therein). As the name indicates, there the fundamental objects are not point-like particles, but rather extended 1-D strings. It provides a quantum-mechanical theory for gravitation (and gauge interactions) which reduces to Einstein's general relativity (and SM) below a characteristic string scale $v_{\rm Fermi} \ll M_s \lesssim M_{\rm Pl}$ [29]. In particular, this means that the stringy behavior is only visible at a very high energy (mass) scale – or very small distance – and, below it, the usual point-like behavior should be recovered.

An important feature of string theories is that higher-dimensional spacetimes are needed for consistency: $D = 10$ in the case of (super)strings [29]. While this is quite interesting[10], it also poses a problem: where are the extra six dimensions? The way out is to compactify the extra dimensions into small internal manifolds, thus avoiding problems with established phenomenology (i.e., no evidence of *large* extra dimensions has ever been found). Due to its topological nature, low-energy phenomenology is influenced by the way compactifications are performed and the physics in the remaining large $(1 + 3)$ dimensions is therefore affected by the way the other compact dimensions are arranged.

---

[7] This trend started with Newton showing that gravity acted similarly on Earth and in the cosmos, followed by Faraday and Maxwell who recognized the unity behind electricity and magnetism, and passed by Einstein, Lorentz and Hertz that constructed the unified concept of spacetime. The latest and – to me – most impressive feat was the demonstration of electroweak unification at the Fermi scale.

[8] The prefix *super* is related to the fact that a new spacetime symmetry can be added to Poincaré symmetry producing a transformation relating fermions and bosons. In particular, this means that at some energy scale, each SM particle has a superpartner with the same mass. Since we have not observed any such particle until today, we assume that some kind of symmetry breaking takes place at high energies ($v_{\rm susy} \gtrsim 1$ TeV).

[9] As a matter of fact, string theories include some aspects of other candidate models, such as supersymmetry and unification of the coupling constants at some high-energy scale. Some string models only have bosonic degrees of freedom and need supersymmetry to produce a fermionic spectrum.

[10] The theory *provides* the dimensionality of spacetime instead of taking it as an input variable.

In string-based models gravitons are represented by closed strings, spin-1 fields are represented by open strings, while fermions are obtained as intersections of higher-dimensional objects (branes) [30, 31]. In this sense, depending on the details of the topology (e.g. compactification), the theory may contain a plethora of particles in its low-energy limit, including the well-known spectrum of the SM.

This fact is especially interesting from the phenomenological point of view, as basically all BSM scenarios include new degrees of freedom in the form of scalars, vectors and tensors (and respective pseudo versions). In fact, in string-based models there is an infinite number of them with masses $M^2 \sim M_s^2\,(N-1)$, $N = 0, 1, 2, \cdots$ [29]. The lightest modes could indeed have tangible effects in our low-energy world. Common examples are axions and axion-like particles [32–40], and hidden (dark) photons kinetically mixed with the usual photon [41–43]. Yet another interesting effect is the possibility that Lorentz symmetry itself is spontaneously broken, thus producing non-dynamical tensor-like (fixed) backgrounds that would break spacetime isotropy [44, 45]. Topologically massive 2-rank tensors may also be featured in supergravity and string models coupled to 4-vector potentials. The latter are studied in Part I, axion-like particles will be the topic of Part II, whereas Lorentz-symmetry violation will be the focus of Part III.

These new BSM-inspired particles may be a blessing as they can potentially help solve some of the problems of the SM[11]. A typical example, outside the scope of this thesis, is that of supersymmetric particles which could help stabilize the electroweak vacuum [46]. In general, new phenomenology may have one of two possible origins: either it is custom tailored to solve some specific problem in a bottom-up approach (e.g. the QCD axion is designed to solve the strong CP problem, cf. Chapter 4), or it stems from some extension of the SM in a top-down approach (e.g. Kalb-Ramond 2-rank tensors, axion-like particles and Lorentz-violating backgrounds). This thesis will be focused on the latter case, i.e., on the signals coming from the low-energy limit of high-energy BSM extensions.

From the 2008 start of the LHC, we have reached TeV energies for the first time, what led to the discovery of the 125 GeV Higgs in 2012. Although being able to look for new, even heavier particles, we must also entertain the possibility that new physics may manifest itself in sub-TeV scales. The main objective of this thesis is to report on the progress in constraining some sectors of BSM scenarios on the other side of the energy scale, i.e., in the low-energy frontier of physics.

[11] Even though, in fairness, the elevated number of possible new particles and, most importantly, their masses – which are increasingly larger – deems most of them to ostracism, as larger masses can usually only be produced with higher energies (see the example of the three heavy electroweak bosons). Anything larger than a few TeV is currently hard to directly study in the laboratory.

The low-energy frontier

An important issue is that of the energy scales involved. Based on dimensional analysis, the natural mass scale where gravitation ($G_{\rm N}$) and quantum ($\hbar$) effects meet is the Planck scale[12] $M_{\rm Pl} = \sqrt{\hbar c^5/G_{\rm N}} \simeq 10^{19}$ GeV. Needless to say that this is out of current or future experimental reach. Another important – and more accessible – scale is the Fermi scale $v_{\rm Fermi} \approx 250$ GeV, whereupon electromagnetic and weak interactions merge into the unified electroweak interaction [4]. The gap between these scales is so vast and potentially empty that it has been referred to as a desert, a kind of *terra nullius*.

Beyond the SM scenarios usually contain a natural scale of their own, e.g. QCD axions have a Peccei-Quinn scale f_a with which mass and coupling (to photons, gluons, etc) are related via m_a, $g_{a\gamma,\,e} \sim f_a^{-1}$ (cf. Chapter 4) [47], whereas Lorentz-symmetry breaking effects usually appear in combination with $\sim M_{\rm Pl}^{-k}$, cf. eq.(6.3). Again, following the trend, these scales are usually related to the breakdown of some more fundamental symmetry and are typically somewhere between the electroweak and Planck scales, thus helping populate the aforementioned desert.

In fact, the appearance of inverse powers of such scales leads to a suppression of the effects related to them. This is nothing new: take muon decay for example. The decay is mediated by a heavy W boson, but, at energies below $m_W \sim 100$ GeV, the propagator behaves as $(q^2 - m_W^2)^{-1} \to m_W^{-2}$, so that the *effective* (Fermi) coupling constant is $G_{\rm F} \sim m_W^{-2}$. In a way, the "dimensionfullness" of $G_{\rm F}$ indicates that some underlying physics is at play, albeit somewhat implicitly[13]. In analogy with the originally W-mediated Fermi interaction (which in low energies looks like a point interaction), we see that BSM scenarios, which may not even be based on localized interactions, appear as low-energy effective theories with localized vertices connecting SM and novel BSM sectors suppressed by large mass scales.

This suppression is directly responsible for the smallness of the physical effects remnant of the original BSM theory. That this should be the case is obvious from the fact that, if it was not so, we would have noticed before (maybe then the SM would be *par default* larger). This brings us to an important question: where do we have to look to find the signals of the underlying BSM theories? Which route is the best, high- or low-energy experiments?

[12]Note that this is similar to the unified relationship between electric charge, weak isospin coupling and weak (Weinberg) angle discussed above. In this sense, the Planck mass should be pointing at the approximate energy scale of unification between gravity and quantum mechanics.

[13]This has to do with the renormalizability of the low-energy theory. In the previous example, the four-fermion Fermi contact interaction is not renormalizable. Its high-energy completion, the SM, on the other hand, is.

Traditionally, a particle physicist would say that smashing things (usually electrons and positrons, or hadrons) at high energies is the way to go: historically this path has indeed proved to be fruitful, specially in unveiling the compositeness of objects such as protons and neutrons. While this strategy has the potential to lead to discoveries, it has the disadvantage that it is not the most precise measurement technique available and the effects we are looking for are assumedly tiny.

Already since the 1970's many extensions to the then new SM were proposed[14]. These proposals usually predict the existence of new particles, which, in order to be detectable, must be coupled to some sector of the SM. These may be quite heavy and their production typically requires energies of the order of their mass. High-energy colliders are fit for the task of producing such heavy particles[15], especially given the relatively fast pace in reaching higher energies (the LHC aims at 14 TeV).

An example in this direction is the search for heavy ($m_a >$ GeV) axion-like particles (ALPs) at colliders. Due to their coupling to photons, they have been searched for in connection to processes with final-state photons, such as $p + p \to \gamma + a$ or $3\,\gamma$. Depending on mass and coupling, ALPs may decay either inside the detector, leading to three photons, or outside, where only one photon is detected and the ALPs are "seen" as missing energy[16]. Simulations found no significant deviations from the expected background, thus setting upper bounds around $g_{a\gamma\gamma} \lesssim 10^{-3}\,\mathrm{GeV}^{-1}$ [54, 55]. Incidentally, from Fig. 5.11 we see that, in terms of range in coupling, colliders are limited as probes of massive ALPs in comparison to astrophysical scenarios, e.g., supernovae, where ALPs may be copiously produced.

In this respect, Payez *et al.* [56] used data on gamma rays from the famous supernova of 1987 (SN 1987A) to obtain limits on very light ($m_a \lesssim 10^{-10}$ eV) and weakly coupled ALPs. Assuming $g_{a\gamma\gamma} = 10^{-10}\,\mathrm{GeV}^{-1}$ initially, they calculated the ALP production spectrum and estimated that the ALPs, each with $\langle E_a \rangle \sim$ 100 MeV, carry away a total amount of energy of $E_{\mathrm{tot}} \sim 8 \times 10^{49}\,\mathrm{erg} \sim 5 \times 10^{55}\,\mathrm{MeV}$. Given that the ALPs are too weakly coupled to be re-absorbed, the total number of ALPs emitted would be $N_{\mathrm{tot}} \approx E_{\mathrm{tot}}/\langle E_a \rangle$, so that the core collapse would have generated $N_{\mathrm{tot}} \sim 5 \times 10^{53}$ ALPs. With this, in principle, on Earth[17] we should have an overall fluence (particles per unit area) of $N_{\mathrm{tot}}/4\pi d_{\mathrm{SN}}^2 \sim 10^6$ ALPs·cm^{-2}.

[14] Notably popular – and searched for – are supersymmetry [48–50] and extra dimensions [51–53].

[15] Z-mediated processes were only observed when the energies reached $m_{\mathrm{Z}} \simeq 90$ GeV.

[16] Missing energy is a generic denomination for final states that escape detection because they are too weakly coupled (an usual example are neutrinos). Typically, the initial transverse momentum (or energy) is known to be zero and momentum (and energy) conservation holds. If the transverse momentum of the total "visible" particles in the final state is not zero, then we say that something escaped detection, therefore the denomination of "missing energy".

[17] The SN-Earth distance is $d_{\mathrm{SN}} = 51.4\,\mathrm{kpc} = 1.52 \times 10^{23}$ cm.

Very light ALPs may oscillate into photons in the presence of an external electromagnetic field. Hence, there is a finite probability (estimated to be ~ 0.1) of photo-regeneration in the magnetic field of the galaxy. With this, the effective number of ALP-originated photons on Earth would be $\sim 10^5\,\gamma\cdot\mathrm{cm}^{-2}$ – a very close estimate to the state-of-the-art value reported in Ref. [56]. The experimental upper limit on the gamma-ray fluence from SN 1987A (after 10 s) is $0.6\,\gamma\cdot\mathrm{cm}^{-2}$ [57], and, noting that N_{tot} scales with the coupling as $N_{\mathrm{tot}}\sim g_{a\gamma\gamma}^4$, one finds $g_{a\gamma\gamma}\lesssim 10^{-11}\,\mathrm{GeV}^{-1}$, which is much more strict than the bound from colliders [54].

The improvement here is not due to a much better experimental resolution or TeV-like energies, but simply due to the huge number of ALPs produced in the process under examination. It is therefore the overwhelming production of ALPs in the collapsing star that overcomes the smallness of the production cross section itself, which is a limiting factor in collider experiments.

Despite of the impressive *total* energy involved in the (hypothetical) ALP burst during a supernova event, ALP production itself is not a high-energy process. In fact, the energies involved are of the order of the core temperature, $T\sim 10^{11}\,\mathrm{K}\approx$ ten MeV, in the case of SN 1987A. This is way below the TeV-scale energies attained in high-energy experiments. As discussed in Chapter 5, even if we consider relatively heavy ALPs ($10\,\mathrm{keV}\lesssim m_a\lesssim 100$ MeV), SN 1987A still allows us to probe very small couplings $\sim 10^{-12}\,\mathrm{GeV}^{-1}$, cf. Figs. 5.8 and 5.11.

We have seen that low-energy observations (up to MeV) are effective means to constrain ALPs in an ample mass range. Low-energy configurations may be useful also when dealing with new physics *without* new particles. Lorentz-symmetry violation (LSV), for example, has received considerable attention in the last decades and a number of experimental tests has been applied to search for its effects [58] – this is the central topic in Part III. In Chapter 7 we investigate a LSV modification in the photon sector in the light of laboratory experiments.

This sector in LSV QED produces a number of potentially observable effects as it modifies the behavior of light. The LSV coefficients are strongly constrained via astrophysical observations, so, in order to extract competitive limits, in the context of this thesis we have looked for precise laboratory-based tests. Particularly interesting are: hydrogen spectroscopy [59], measurements of the electric dipole moment of the electron [60] and of vacuum birefringence [61]. Once more, these are low-energy experiments[18] that can sensitively test features of BSM scenarios. With them, in the context of Lorentz violation, we have been able to extract laboratory-based upper limits that complement astrophysical ones.

[18]For example, the PVLAS experiment uses a laser with 1064 nm (≈ 1 eV) and 1 W of power.

Also in the context of LSV, but a bit off the (very) low-energy domain we have explored so far, collider tests have not been broadly used, as these are usually not the most precise. Nevertheless, they might bring interesting information. In Chapter 8 we discuss the case of a non-minimal coupling involving a LSV 4-vector and, besides obtaining upper limits on some of its components, we show that anisotropies may be introduced, specially through a dependence of the modified (differential) cross sections on the azimuthal scattering angle [71]. This distinctive feature – absent in many QED processes – may be searched for in high-energy experiments, but, in general Lorentz violation has proved to be an instance where, indeed, low-energy tests are more efficient in constraining new physics.

Finally, in Chapters 2 and 3 we discuss spin-dependent interactions. Interparticle potentials are non-relativistic constructions applicable to both classical and quantum systems that transmit important information on the structure of the sources and mediator. The discussion is conducted in two fronts: in Chapter 2 we discuss how a topologically massive spin-1 boson may intermediate new spin-dependent interactions between spin-1/2 sources and next, in Chapter 3, we compare spin-1/2 and spin-1 sources and how their interaction via standard mediators differ (or not) in terms of spin dependence.

The main objective is not (yet) to set upper limits on couplings and masses of new mediators. Rather, the goal is to comparatively study the various spin-dependent potentials. Such interactions, which may be due to BSM physics, may have macroscopic consequences and can be tested using table-top settings, such as torsion balances, a traditional – but effective – low-energy method that played an important role in early studies of gravitation [62, 63]. Despite being originally designed to test gravity, this and other methods are actually sensitive probes to BSM scenarios, where long-range interactions may be dictated by "charges" other than the mass. Besides, Newtonian gravity is classical and does not "feel" (intrinsic) spin, so that novel spin-dependent interactions may compete with gravitational forces[19].

In summary, the works presented in this thesis discuss phenomena that can be explored in sub-TeV scenarios. This shows that the footprints of theories whose typical energy scales lie around $M_{\rm Pl}$ need not be searched exclusively in the high-energy domains of the LHC and the like, but also in the (relatively) low-energy environments in spectroscopy or even in nuclear reactions in stars. The examples discussed in this thesis – and others more [65] – indicate that there is a strong case for looking for new phenomena at the low-energy frontier of physics.

[19]These methods have also been used to study modifications of the inverse-square law induced by e.g. extra dimensions, where it was shown that the latter should be $\lesssim 40\,\mu$m [64].

Organization of this thesis

Despite appearing disconnected, we have seen that BSM theories are behind all the topics discussed in this thesis, so we may consider their investigation a study of the phenomenology of BSM scenarios. Furthermore, low-energy tests may provide good sensitivity to these non-standard effects, thus allowing to constrain the associated physical parameters[20]. With this in mind, I decided to divide the thesis in three parts (I, II and III), one for each main topic, and include an independent introduction to each of them as a first chapter, even though each individual chapter also has a more specific introduction of its own.

The contents of the chapters stem primarily from published papers [66–71] and, as such, will be hopefully self-consistent. Furthermore, for the sake of a clearer exhibition, I have taken liberty to expand them. The respective introduction to each chapter is followed by the main results and in the end there is a section with (partial) conclusions to help summarize and highlight the original contributions presented. This thesis is organised as follows:

- **Chapter 1**: I discuss the topologically massive Cremmer-Scherk-Kalb-Ramond (CSKR) system, introducing the necessary tools used in Chapter 2.

- **Chapter 2**: using the results from the preceding chapter I obtain the different spin-dependent interparticle potentials between spin-1/2 sources mediated via the CSKR system [66].

- **Chapter 3**: applying the general methodology employed in the previous chapters, here I develop a systematic comparison between the interaction potentials between spin-1/2 and spin-1 sources [67, 68].

- **Chapter 4**: in this chapter I briefly introduce the axion (and axion-like particles) in preparation for the discussion presented in Chapter 5.

- **Chapter 5**: I discuss heavy axion-like particles (ALPs) in the context of SN 1987A. Taking into account production, propagation and subsequent decay into photons, we obtain competitive limits on the ALP parameter space [69].

- **Chapter 6**: an introduction to the topic of Lorentz-symmetry violation (LSV) is presented as a preparation for the discussions in the next two chapters.

[20] The experimental inputs used throughout this thesis do not show signs of new physics. These null results, together with small experimental uncertainties, allow us only to place upper limits on the parameter space of BSM physics.

- **Chapter 7**: here I discuss LSV in the photon sector via the Carroll-Field-Jackiw term, which introduces a fixed background, giving rise to modified electrodynamics. We obtain competitive laboratory-based limits [70].

- **Chapter 8**: finally, here I investigate the role of another LSV background 4-vector, but in the electron-photon sector. This non-minimal coupling modifies the usual QED vertex and its effects in some tree-level processes in QED are discussed [71].

The last chapter (Concluding remarks) is devoted to a brief overview of the works presented, as well as a discussion of possible future projects.

Contributions of the author

Some of the problems investigated during my doctorate have evolved into projects and have been completed, thus resulting in the following papers:

- F.A. Gomes Ferreira, P.C. Malta, L.P.R. Ospedal, J.A. Helayël-Neto, *Topologically massive spin-1 particles and spin-dependent potentials*, Eur. Phys. J. C **75**, 232 (2015). ArXiv:hep-th/1411.3991v2.

- P.C. Malta, L.P.R. Ospedal, K. Veiga, J.A. Helayël-Neto, *Comparative aspects of spin-dependent interaction potentials for spin-1/2 and spin-1 matter fields*, Adv. High Energy Phys. **2016**, 2531436 (2016)[21]. ArXiv:hep-th/1510.03291v6.

- J. Jaeckel, P.C. Malta, J. Redondo, *Decay photons from the ALP burst of type-II supernovae.* ArXiv:hep-ph/1702.02964.

- Y.M.P. Gomes, P.C. Malta, *Laboratory-based limits on the Carroll-Field-Jackiw Lorentz-violating electrodynamics*, Phys. Rev. D **94**, 025031 (2016). ArXiv:hep-ph/1604.01102v4.

- G.P. de Brito, J.T. Guaitolini Junior, D. Kroff, P.C. Malta, C. Marques, *Lorentz violation in simple QED processes*, Phys. Rev. D **94**, 056005 (2016). ArXiv:hep-ph/1605.08059v3.

[21] A corrigendum to this paper was included, cf. Chapter 2. It has two versions, a long and a short one. The longer version can be found – along with the published version of the main manuscript – at arXiv:hep-th/1510.03291v5. The shorter version of the corrigendum is at arXiv:hep-th/1510.03291v6 and published under Adv. High Energy Phys. **2017**, 9152437 (2017).

In the papers above I have closely collaborated with different people, including: Gustavo P. de Brito, Celio Marques, Judismar T. Guaitolini Jr, Yuri M. P. Gomes, Leonardo P. R. Ospedal, Kim Veiga, and Felipe A. G. Ferreira (PhD students from our group at CBPF), and Daniel Kroff (IFT - Institute for Theoretical Physics, São Paulo, Brazil). Furthermore, I have collaborated with J. Redondo (Uni. Zaragoza, Spain), and my advisors, J. Jaeckel (ITP, Heidelberg, Germany) and J. A. Helayël-Neto (CBPF, Rio de Janeiro, Brazil).

The ideas for the first two papers (as listed above) originated during lectures from my Brazilian advisor and evolved eventually into publishable work. The third paper was developed during my stay at the ITP, Heidelberg, and was conducted in collaboration with my German advisor. The fourth and fifth papers were developed independently in collaboration with fellow PhD students from CBPF, Rio de Janeiro, and IFT, São Paulo.

A sixth and last paper [72] – fruit of an independent investigation with fellow students – has also been published[22]

- G.P. de Brito, P.C. Malta, L.P.R. Ospedal, *Spin- and velocity-dependent non-relativistic potentials in generalized electrodynamics*, Phys. Rev. D **95**, 016006 (2017). ArXiv:hep-th/1612.01181v2.

I have actively participated in the preparation of all papers listed above, both in the conceptual and calculational works, as well as in the writing process. In the first two papers I have shared the writing efforts with the co-authors and we have performed all calculations together. In the third paper I have done most of the writing and have performed most of the calculations; I have also written and run the simulations, and produced the images and plots used. For the fourth paper I have done practically all the writing, while the calculations were done in parallel with the co-author. In the fifth paper I have written two main sections and most of the introduction and conclusion. Similar distribution of tasks took place in the production of the sixth and last paper. All the co-authors are aware and approve of the inclusion of their partial contributions (all duly acknowledged) in this thesis.

[22] Its contents are aligned with the first two papers, but this last paper is **not** included here, as it was part of Leonardo Ospedal's PhD thesis.

Part I

Chapter 1

The topologically massive CSKR system

1.1 Introduction

As mentioned in the Presentation, in this first part of the thesis we will focus on the non-relativistic interaction between sources in an effort to better understand the ensuing interactions depending on the kind of sources and mediators. In this chapter and the next we take two spin-1/2 fermions whose interactions are mediated by massive vector neutral bosons.

The spin-1 messenger may be represented by the typical Proca field, but this is not the only option: here we also consider the less trivial combination of a 4-vector and a rank-2 tensor gauge potentials connected via a Chern-Simons-like topological mixing term. Our task in this chapter is to present this scenario and discuss a few of its properties and physical interpretations.

The archetypical way of representing a spin-1 neutral particle is through a 4-vector A^μ, whose Maxwell-like Lagrangian (density) reads

$$\mathcal{L}_{\text{Proca}} = -\frac{1}{4} F_{\mu\nu}^2 + \frac{1}{2} m_0^2 A_\mu^2, \tag{1.1}$$

where m_0 is the mass and $F_{\mu\nu} = \partial_\mu A_\nu - \partial_\nu A_\mu$ is the usual Abelian anti-symmetric field-strength tensor. The equations of motion follow from the variational principle and read $\partial_\mu F^{\mu\nu} + m_0^2 A^\nu = 0$, while the Bianchi identities still hold unchanged, i.e., $\partial_\mu \tilde{F}^{\mu\nu} = 0$, where the dual of the field-strength tensor is defined as $\tilde{F}^{\mu\nu} = \frac{1}{2}\epsilon^{\mu\nu\alpha\beta} F_{\alpha\beta}$. These equations reproduce the standard Maxwell equations in the $m_0 \to 0$ limit, while, in the massive case, they give the Proca equations [73]. Notice that the mass term destroys gauge invariance.

The last statement regarding the transition from massive to massless is true at the Lagrangian level, but it does not work so nicely when one considers the propagator, as the mass shows up in the denominator of the longitudinal piece, cf. eq.(1.15). Another instance where trouble may arise is when one considers the emission of massive bosons and one takes the massless limit, whereby infinitely energetic radiation may be sent out[1] [74]. The transition from massive to massless is therefore a bit tricky and the difficulty lies actually on gauge invariance. The massless (Maxwell) case is perfectly gauge invariant, but this is clearly not the case in Lagrangian (1.1), and the mass term is to blame. The loss of gauge invariance complicates the passage $m_0 \to 0$, but, as we shall see in what follows, the topological formulation solves this issue (cf. Section 1.3).

To see that eq.(1.1) indeed describes a particle of vector nature, it suffices to check that the original four degrees of freedom (d.o.f.) related to the components of A^μ are reduced to three due to the subsidiary condition $\partial_\mu A^\mu = 0$, which follows from the anti-symmetry of the field-strength tensor. This eliminates the necessity of introducing an extra gauge-fixing term by hand, as in usual electromagnetism. In the massless case, the lack of an automatic subsidiary condition gives rise to a gauge freedom, which translates into the possibility of implementing transformations such as $A^\mu(x) \to A^\mu(x) + \partial_\mu \alpha(x)$, with $\alpha(x)$ a scalar (gauge) function of spacetime, without affecting the equations of motion, or the action, for that matter.

Historically, this issue was very important, since weak interactions were expected[2] to be mediated by heavy particles and a gauge-invariant formulation à la QED was the trend to be followed. It soon became clear that gauge invariance and massive bosons were not easily reconciled and mass-generation mechanisms were devised to circumvent the difficulties, the best candidate being the by-now renowned Higgs mechanism[3].

For simplicity, let us consider the local $U(1)$ case, where a complex scalar field ϕ couples minimally to an Abelian 4-potential A^μ. In this case, if the scalar boson happens to be self-interacting according to the usual Mexican-hat potential, it may develop a non-vanishing vacuum expectation value (VEV) $\langle \phi \rangle = v \neq 0$, around which the physical fields oscillate as excitations. After expanding the potential

[1] This can be seen by considering an arbitrary 4-current J coupled to the vector boson and the associated emission rate. The latter is proportional to $\sim J_\mu J_\nu \left(\eta^{\mu\nu} - k^\mu k^\nu / m_0^2\right)$ and, in the limit where $m_0 \to 0$, it is clear that such a rate would blow up. This is nonetheless generally avoided if one demands that the current J be conserved.

[2] The suggestion that intermediate vector bosons played a role in weak interactions was made as early as 1930's, by Klein [4, 75].

[3] To avoid historical injustice I would like to mention that this mechanism was proposed almost simultaneously by Brout and Englert [76], Guralnik, Hagen and Kibble [77], and Higgs [78].

around this minimum configuration, the gauge boson, which was initially massless, appears to acquire a mass, while one of the components of the complex scalar field remains massive – it is the Higgs scalar – and the other vanishes[4].

This clever procedure relies on the prescription of a new complex field, which, due to its minimal coupling to the Abelian gauge potential, makes the latter transition from massless to massive at the expense of one of its degrees of freedom – this is the Goldstone theorem in a nutshell. Nevertheless, this simple Abelian picture was not enough to describe e.g. the appearance of only left-handed neutrinos (and right-handed anti-neutrinos) in the weak interactions, thus suggesting that the symmetry behind the soon-to-be Standard Model should be more elaborated, i.e., non-Abelian.

The corresponding non-Abelian generalization of the Higgs mechanism was put forward mainly by Salam, Glashow and Weinberg in the 1960-70's [8–11] and its predictions were successfully confirmed in the 1980's by the measurements of the masses of the $W^{\pm}$ and Z^0 bosons and, most recently in 2012, by the observation of a neutral scalar of mass 126 GeV at CERN [15, 16], which is (so far) compatible with the properties expected from the Higgs boson.

Nevertheless, during the almost 50 years between Higgs' original proposal (1964) and its confirmation (2012), it was not clear whether the Higgs mechanism was not only theoretically pleasing, but also actually realized in nature. In the mean time other alternative ideas were presented [79–84], all trying to avoid a new scalar (Higgs) particle that could turn out not being found. These models do not rely on spontaneous symmetry breaking, but rather represent dynamical mass generation mechanisms. In Section 1.3 we describe this topic, in the context of this thesis, in further detail.

One such mechanism was proposed by Cremmer and Scherk in the context of dual models applied to strong interactions and is based on a pair of fields, namely, a 2-rank anti-symmetric tensor and a 1-form (i.e., a 4-vector), the two being connected via a topological mixing term [85]. This term turns out to be able to generate mass to the 4-vector without the introduction of an extra scalar field. Almost simultaneously, Kalb and Ramond introduced a similar system of fields in the study of the classical interaction between strings [86]. We shall not go into the details of the original works, but we note that 2-form gauge fields are present in some beyond the Standard Model scenarios, being typical of e.g. off-shell supergravity in four or higher dimensions [87–91].

[4]This component is actually eliminated by a suitable $U(1)$ transformation, which amounts to a choice of the gauge function so as to eliminate it at every point in spacetime. The respective d.o.f. do not disappear, however, but are transferred via the same transformation to the gauge fields, therefore generating the respective masses.

The objective in the next sections is to review the properties of this topologically mixed system, as well as explicitly show that it indeed serves to dynamically generate mass for a neutral vector boson.

1.2 The Cremmer-Scherk-Kalb-Ramond field

In the previous section we briefly discussed the historial need of Higgsless models from the point of view of gauge mass generation and the (then real) possibility that no Higgs would be found. We now depart from this route and focus on the general properties of the topologically massive fields discussed above.

As also stated above and in the Presentation, most scenarios of physics beyond the Standard Model need to extend the known particle spectrum by postulating new (pseudo-)scalar, vector and/or tensor fields. While the first possibility will be the object of our investigations in the second part of this thesis, here we shall discuss some general aspects of the fields proposed by Cremmer, Scherk, Kalb and Ramond – from here on dubbed the CSKR system[5].

The Proca vector field transforms under the $\left(\frac{1}{2},\frac{1}{2}\right)$-representation of the Lorentz group and its Lagrangian, eq.(1.1), is the simplest extension of standard electromagnetism leading to a massive intermediate vector boson, but it is not the only one. A massive spin-1 particle can also be described through a vector and a tensor field connected by a mixing topological mass term, what would also do the trick. Both the vector X_μ and the tensor $B_{\mu\nu}$ are gauge fields described by the following Lagrangian[6]

$$\mathcal{L}_0 = -\frac{1}{4}\,F_{\mu\nu}^2 + \frac{1}{6}\,G_{\mu\nu\kappa}^2 + \frac{m_0}{\sqrt{2}}\,\epsilon^{\mu\nu\alpha\beta}\,X_\mu\partial_\nu B_{\alpha\beta}, \tag{1.2}$$

where the field-strength tensors are defined as: $F_{\mu\nu} = \partial_\mu X_\nu - \partial_\nu X_\mu$ and $G_{\mu\nu\kappa} = \partial_\mu B_{\nu\kappa} + \partial_\nu B_{\kappa\mu} + \partial_\kappa B_{\mu\nu}$.

The origin of the denomination "topological" lies in the fact that this term does not involve the Minkowski metric, so that its contribution to the energy-momentum tensor is zero. It is important to note that, contrary to the typical Proca case, the topological mass term does not break gauge invariance and no spontaneous symmetry breaking is invoked. The action is invariant under the independent, but

[5]This is not the name usually found in the literature (there is no consensus, actually), but we use it here for simplicity to indicate the pair $\{X_\mu, B_{\nu\kappa}\}$.

[6]Here we deviate from the notation in our published work [66] by using the letter X for the 4-vector in the topological system, as opposed to A used in the paper (here A is reserved for the Proca field). We keep nevertheless the letter F for both field-strength tensors.

simultaneous, local Abelian gauge transformations given by

$$X'_\mu = X_\mu - \partial_\mu \alpha \tag{1.3}$$

$$B'_{\mu\nu} = B_{\mu\nu} + \partial_\mu \beta_\nu - \partial_\nu \beta_\mu. \tag{1.4}$$

Besides these, due to the anti-symmetry of the last two terms in eq.(1.4), the vector function β_μ may also undergo a gauge transformation of its own, namely, $\beta_\mu(x) \to \beta_\mu(x) + \partial_\mu f(x)$, without changing the "primary" gauge transformations themselves or the physical field, $B^{\mu\nu}$. This means that, from the original 4 d.o.f. from X^μ, one is eliminated by a gauge choice due to eq.(1.3). Similarly, from the 6 independent components of the 2-rank anti-symmetric potential $B^{\mu\nu}$, eq.(1.4) combined with the gauge transformation for β_μ itself leave only 3 d.o.f. untouched[7]. It is clear that having extra gauge symmetries constrains the system and reduces its physical (active) components.

A transparent way to see this is by writing the fields in momentum space as combinations of linearly independent (momentum) 4-vectors and attribute one d.o.f. for each of the coefficients of the combination. The aforementioned gauge transformations amount then to connecting the set of primed and unprimed coefficients (cf. eqs.(1.3) and (1.4)) and this shows that, in the case of eq.(1.3), one of them is actually a function of the gauge parameter α, being therefore non-physical[8]. Analogous considerations apply for $B^{\mu\nu}$.

All these statements are made based on the analysis of the symmetries alone, no mention of the equations of motion has yet been made, from which we expect further constraints. Let us then apply the variational principle to $\mathcal{L}_0$, from which we obtain

$$\partial_\mu F^{\mu\nu} + \sqrt{2} m_0 \tilde{G}^\nu = 0 \tag{1.5}$$

$$\partial_\mu G^{\mu\nu\kappa} - \frac{m_0}{\sqrt{2}} \tilde{F}^{\nu\kappa} = 0 \tag{1.6}$$

where the dual field-strength for $B^{\mu\nu}$ is given by $\tilde{G}^\nu = \frac{1}{6}\epsilon^{\nu\alpha\beta\lambda} G_{\alpha\beta\lambda}$. The duals fulfil the usual Bianchi identities $\partial_\mu \tilde{F}^{\mu\nu} = 0$ and $\partial_\mu \tilde{G}^\mu = 0$. We notice that the dual field strengths play the role of sources and that m_0 parametrizes the coupling to these sources, i.e., the mass parameter is responsible for the mixing between the vector and tensor fields.

[7] Even though β_μ has 4 d.o.f., its own gauge transformation reduces this to 3, so its capacity of gauging away d.o.f. from $B^{\mu\nu}$ is correspondingly reduced.

[8] In the sense that, upon an adequate choice of the function α, this coefficient may be completely eliminated. In other words, if the physics cannot depend on gauge choices, then all gauge-dependent parameters must be dispensable.

Before proceeding with the analysis, we would like to briefly comment on the spectrum of the model without a mass term, that is, with $m_0 = 0$. In this case the two fields, X^μ and $B^{\mu\nu}$, are completely decoupled and one has $\partial_\mu\{\cdots\} = 0$, with $\{\cdots\} = F^{\mu\nu}$, or $G^{\mu\nu\kappa}$. Together with the Bianchi identities and gauge transformations, this set of equations of motion tells us that both fields are massless, but also that X^μ is essentially equivalent to the electromagnetic photon, thus possessing two d.o.f.. Similarly, we may solve the equations for G by using $G_{\mu\beta\lambda} = \epsilon_{\mu\beta\lambda\sigma}\partial^\sigma\xi$, ξ being a scalar function. This shows that, effectively, the free $B^{\mu\nu}$ is characterized by just one massless scalar d.o.f. carried by ξ. Incidentally, when we consider the full theory with $m_0 \neq 0$, this scalar will be transferred to the longitudinal sector of X^μ and will be responsible for its massive propagation – a phenomenon similar to the one behind the unitary gauge transformations in the $SU(2) \otimes U(1)$ electroweak theory.

Finally, let us focus on the topologically mixed theory, where we keep a non-zero mass parameter in $\mathcal{L}_0$. By acting on eqs.(1.5) and (1.6) above with $\epsilon\partial$ (Lorentz indices omitted for simplicity) and using the respective Bianchi identities, we extract two wave equations for the dual field strengths, namely

$$\left(\Box + m_0^2\right)\tilde{G}^\mu = 0 \quad \text{and} \quad \left(\Box + m_0^2\right)\tilde{F}^{\mu\nu} = 0, \tag{1.7}$$

from where we see that the excitations described by the fields are indeed massive, as anticipated[9]. One smart way [94] to see what is happening is by writing $\tilde{G}^\nu = \partial^\nu\phi + \frac{m_0}{\sqrt{2}}X^\nu$, which solves eq.(1.6) and allows us to write eq.(1.5) as

$$\left(\Box + m_0^2\right)X^\mu - \partial^\mu\left[\partial_\nu X^\nu - \sqrt{2}m_0\phi\right] = 0. \tag{1.8}$$

If we make the (gauge) choice $\partial_\nu X^\nu = \sqrt{2}m_0\phi$, the equation above describes a free massive vector boson. Additionally, this choice indicates that the longitudinal part of X^μ is determined by the scalar d.o.f. originally belonging to $B^{\mu\nu}$, i.e., a dynamical transfer of d.o.f. between the fields X^μ and $B^{\mu\nu}$ took place, what was only possible due to the topological mixing. This construction carries the same spirit as the Higgs mechanism in the unitary gauge, but with the advantage of preserving gauge invariance throughout. Now we can also justify the weird $1/\sqrt{2}$ in the mass term in eq.(1.2): it makes the wave equation for massive X^μ look simpler.

[9] An alternative and interesting way to show this is by writing the field strengths in terms of electric and magnetic fields as $F^{\mu\nu} = \{\mathbf{E}, \mathbf{B}\}$ and $G^{\mu\nu\kappa} = \{b, \mathbf{e}\}$. Working out the equations of motion one finds that $\mathbf{B}, b$ and $\mathbf{e}$ may all be expressed in terms of the electric field, $\mathbf{E}$, and its wave vector, $\mathbf{k}$. It is also clear that the vector potential also possesses a longitudinal component inherited from the rank-2 tensor – a clear indication of its massive character (see Refs. [92, 93]).

At this point we can distinguish between the number of d.o.f. comported by the topological model in its off- and on-shell levels. The former is understood as the situation where the fields are still not constrained by Noether's variational procedure, so that the only *a priori* constraints come from the gauge symmetries allowed by the Lagrangian. In this sense, in the off-shell regime, the topological $\{X_\mu, B_{\nu\kappa}\}$ system displays $3 + 3 = 6$ d.o.f. altogether.

On the other hand, in the on-shell regime, when the equations of motion are taken into account, the number of constraints increases and, as seen above, we end up with 3 d.o.f., which are sufficient to describe a massive vector neutral particle. It is important to highlight that, at this point, the 3 d.o.f. available may be accredited to either X^μ or $B^{\mu\nu}$, as long as they are considered *together*.

1.3 Mass generation à la Cremmer-Scherk

The discussion above around the wave equation for the massive X^μ opens the following question: would it then be possible to completely eliminate the more complicated 2-rank tensor from the theory already at the Lagrangian level? That is, could we redefine the fields in such a way that $\mathcal{L}_0 \to \mathcal{L}_{\text{Proca}}$, thus avoiding the trouble of working with the cumbersome topological mixing term? In this section we briefly review the main arguments presented in Ref. [85] to show that the answer is "yes", though at the cost of introducing non-local field redefinitions.

Let us consider the CSKR Lagrangian, eq.(1.2), and, more specifically, the topological mixing term, and try to write it fully in terms of $\tilde{G}^\mu$. This can be done by using the relations $G_{\mu\nu\kappa} = \epsilon_{\mu\nu\kappa\lambda}\tilde{G}^\lambda$ and $\epsilon_{\mu\nu\alpha\beta}\partial^\nu B^{\alpha\beta} = -2\tilde{G}_\mu$, so that $\mathcal{L}_0$ becomes[10]

$$\mathcal{L}_0 = -\frac{1}{4}F_{\mu\nu}^2 - \tilde{G}_\mu\tilde{G}^\mu - \sqrt{2}m_0 X_\mu\tilde{G}^\mu. \tag{1.9}$$

Even though all the steps we followed were valid, we see that, through the aforementioned substitution, there are no derivatives acting on $\tilde{G}$. There is therefore no kinetic term for $\tilde{G}$, so we have left something out: the Bianchi identity, $\partial_\mu\tilde{G}^\mu = 0$. To re-establish it, we may introduce a Lagrange multiplier Λ, so that the Lagrangian becomes

$$\mathcal{L}_0 = -\frac{1}{4}F_{\mu\nu}^2 - \tilde{G}_\mu\tilde{G}^\mu - \sqrt{2}m_0 X_\mu\tilde{G}^\mu - \tilde{G}_\mu\partial^\mu\Lambda, \tag{1.10}$$

and now the Bianchi identity is included and we should have a model equivalent to

[10] Here we use that $\epsilon_{\mu\alpha\beta\gamma}\epsilon^{\nu\alpha\beta\gamma} = -6\delta_\mu^\nu$ in Minkowski (3+1) spacetime.

the original CSKR one. However, we see that the last two terms may be written as

$$-\sqrt{2}m_0 X_\mu \tilde{G}^\mu - \tilde{G}_\mu \partial^\mu \Lambda = -\left[\sqrt{2}m_0 X^\mu + \partial^\mu \Lambda\right] \tilde{G}_\mu,$$

which suggests the following field redefinition:

$$X'^\mu = X^\mu + \frac{1}{\sqrt{2}m_0}\partial^\mu \Lambda, \tag{1.11}$$

whereby the field-strength tensor is left unchanged, i.e., $F'_{\mu\nu} = F_{\mu\nu}$.

In terms of the new primed field, we have then

$$\mathcal{L}_0 = -\frac{1}{4}F'^2_{\mu\nu} + \frac{1}{2}m_0^2 X'_\mu X'^\mu - a_\mu a^\mu \tag{1.12}$$

with $a^\mu = \tilde{G}^\mu + \frac{m_0}{\sqrt{2}}X'^\mu$, which is a non-dynamical new field, which is left uncoupled to the other field in the model, X'^μ. Equation (1.12) is formally identical to $\mathcal{L}_{\text{Proca}}$, eq.(1.1), so what we actually achieved was to bring the topological construction to the form of a simple Proca Lagrangian, but with a twist: interestingly enough, it is gauge preserving[11] [85]. We must point out, however, that this rather simple-looking transition from a topological Lagrangian to a Proca-like one is actually based on the exchange of the rank-2 tensor $B^{\mu\nu}$ by its dual field strength $\tilde{G}^\mu$, which is then eliminated by the mechanism described above.

The reason why this matters to our current discussion is that, in Chapter 2, we are going to study the interactions between spin-1/2 sources mediated by spin-1 neutral bosons. We will not restrict ourselves to the well-known vector current, $j^\mu \sim \bar{\psi}\gamma^\mu\psi$, which is conserved in view of the Dirac equation, but we extend our study to a broader variety of currents (sources), including pseudo-vector and tensorial ones. In this case we end up with a direct interaction involving the $B^{\mu\nu}$ field and the tensor current $j^{\mu\nu} \sim \bar{\psi}\Sigma^{\mu\nu}\psi$, where $\Sigma^{\mu\nu}$ is the spin matrix in its spinor representation.

Such an interaction, $\mathcal{L}_{\text{int}} \sim j_{\mu\nu}B^{\mu\nu}$, would then frustrate our attempt to eliminate the tensor field in favor of the dual field strength, as it would demand that, in the process, we make the effective substitution $B \to \frac{1}{\partial}\tilde{G}$, due to $\epsilon_{\mu\nu\alpha\beta}\partial^\nu B^{\alpha\beta} = -2\tilde{G}^\mu$, which introduces a non-local interaction. Therefore, in order to avoid problematic interactions arising with the "inverse" derivative, we refrain from using the techniques developed above (following Ref. [85]) and take $\mathcal{L}_0$, eq.(1.2), as an independent formulation for a spin-1 massive neutral boson, specially in the presence of an interaction such as $\mathcal{L}_{\text{int}} \sim j_{\mu\nu}B^{\mu\nu}$.

[11] This can be done by allowing the simultaneous gauge transformation: $\Lambda' = \Lambda + \sqrt{2}m_0\alpha$ (cf. eq.(1.3)).

Finally, we point out the paper by Kamefuchi *et al.* [95] that discusses the conditions on field reshufflings which do not change the physical results, namely, the S-matrix elements. A crucial requirement is that the change of basis in field space does not yield non-local interactions. Therefore, as we shall introduce tensorial currents, in the next sections we will try to characterize the spin-1 mediation in terms of the Proca and CSKR system as independent physical models in their own right. In Chapter 2 we study the interparticle potentials arising from their exchange and, as can be already expected, the interactions which do not involve tensor currents will be essentially identical for vector-boson exchange, but when we consider mixed propagators, more interesting potentials will appear.

1.4 Propagators

As will be discussed further in Chapter 2, our objective is to study the interaction between fermionic sources via the exchange of massive spin-1 bosons, these being described by either a Proca field or the CSKR system. To accomplish this, it is important to obtain the propagator of this intermediate particle. In this section we extract the respective propagators, which will find their final use in Chapter 2 as we calculate the interparticle potentials for the two models.

Let us start by the simplest Proca field. The propagator $\langle A_\mu A_\nu \rangle$ is obtained from the kinetic, i.e., quadratic, part of the Lagrangian, eq.(1.1), which can be suitably rewritten as $\frac{1}{2}A^\mu \mathcal{O}_{\mu\nu} A^\nu$, in which the wave operator $\mathcal{O}_{\mu\nu}$ – essentially the inverse of the propagator – is $\mathcal{O}_{\mu\nu} = (\Box + m_0^2)\,\theta_{\mu\nu} + m_0^2 \omega_{\mu\nu}$. Here we have introduced the transverse and longitudinal projection operators defined as

$$\theta_{\mu\nu} \equiv \eta_{\mu\nu} - \frac{\partial_\mu \partial_\nu}{\Box}, \tag{1.13}$$

$$\omega_{\mu\nu} \equiv \frac{\partial_\mu \partial_\nu}{\Box}, \tag{1.14}$$

which satisfy $\theta^2 = \theta$, $\omega^2 = \omega$, $\theta\omega = 0$ and $\theta + \omega = 1$. Due to these simple algebraic properties it is easy to invert $\mathcal{O}_{\mu\nu}$ and, transforming to momentum space ($\partial_\mu \to i p_\mu$), we finally have

$$\langle A_\mu A_\nu \rangle = -\frac{i}{k^2 - m_0^2}\left(\eta_{\mu\nu} - \frac{k_\mu k_\nu}{m_0^2}\right). \tag{1.15}$$

So far, so good, but as can be guessed from the unusual form of the topological term, the propagator for the CSKR system will not be so simple. Most importantly, it is fundamental to find suitable projection operators in order to obtain the propagators of the model, in close analogy to what we did above.

These operators appear as we try to write the pure G-dependent piece of $\mathcal{L}_0$ as a quadratic combination of the more basic B-fields:

$$\frac{1}{6}G^2_{\mu\nu\kappa} = \frac{1}{2}B^{\mu\nu}\left[(P_e) - 1^{\text{a.s.}}\right]_{\mu\nu,\,\kappa\lambda} B^{\kappa\lambda}, \tag{1.16}$$

and we define the spin operators that act on an anti-symmetric 2-form as

$$\begin{aligned}
(P_b)_{\mu\nu,\,\rho\sigma} &\equiv \frac{1}{2}\left(\theta_{\mu\rho}\,\theta_{\nu\sigma} - \theta_{\mu\sigma}\,\theta_{\nu\rho}\right) && (1.17)\\
(P_e)_{\mu\nu,\,\rho\sigma} &\equiv \frac{1}{2}\left(\theta_{\mu\rho}\,\omega_{\nu\sigma} + \theta_{\nu\sigma}\,\omega_{\mu\rho} - \theta_{\mu\sigma}\,\omega_{\nu\rho} - \theta_{\nu\rho}\,\omega_{\mu\sigma}\right) && (1.18)\\
(P_b + P_e)_{\mu\nu,\,\rho\sigma} &= \frac{1}{2}\left(\eta_{\mu\rho}\eta_{\nu\sigma} - \eta_{\mu\sigma}\eta_{\nu\rho}\right) \equiv 1^{a.s.}_{\mu\nu,\,\rho\sigma} && (1.19)
\end{aligned}$$

which are anti-symmetric generalizations of the projectors $\theta_{\mu\nu}$ and $\omega_{\mu\nu}$ [96–98]. The comma indicates that we have anti-symmetry in changes $\mu \leftrightarrow \nu$ or $\rho \leftrightarrow \sigma$. These operators satisfy the following algebra:

$$(P_b)_{\mu\nu,\,\alpha\beta}\,(P_b)^{\alpha\beta}{}_{,\,\rho\sigma} = (P_b)_{\mu\nu,\,\rho\sigma} \tag{1.20}$$

$$(P_e)_{\mu\nu,\,\alpha\beta}\,(P_e)^{\alpha\beta}{}_{,\,\rho\sigma} = (P_e)_{\mu\nu,\,\rho\sigma} \tag{1.21}$$

$$(P_b)_{\mu\nu,\,\alpha\beta}\,(P_e)^{\alpha\beta}{}_{,\,\rho\sigma} = 0 \tag{1.22}$$

$$(P_e)_{\mu\nu,\,\alpha\beta}\,(P_b)^{\alpha\beta}{}_{,\,\rho\sigma} = 0. \tag{1.23}$$

We notice that the mixing term between X_μ and $B_{\mu\nu}$ introduces a new operator, $S_{\mu\nu\kappa} \equiv \epsilon_{\mu\nu\kappa\lambda}\,\partial^\lambda$, which is *not* a projector and satisfies

$$\epsilon^{\mu\nu\alpha\beta}\,X_\mu \partial_\nu B_{\alpha\beta} = \frac{1}{2}\left[X^\mu\,S_{\mu\kappa\lambda}B^{\kappa\lambda} - B^{\kappa\lambda}\,S_{\kappa\lambda\mu}\,X^\mu\right],$$

so that we need to study the algebra of $S_{\mu\nu\kappa}$ with the projectors (1.17) and (1.18) in order to proceed with the inversion.

The following relations are found to hold:

$$S_{\mu\nu\alpha}S^{\alpha\kappa\lambda} = -2\Box\left(P^1_b\right)_{\mu\nu,}{}^{\kappa\lambda} \tag{1.24}$$

$$\left(P^1_b\right)_{\mu\nu,\,\alpha\beta} S^{\alpha\beta\kappa} = S_{\mu\nu}{}^{\kappa} \tag{1.25}$$

$$S^{\kappa\alpha\beta}\left(P_b^1\right)_{\alpha\beta,}{}^{\mu\nu} = S^{\kappa\mu\nu} \tag{1.26}$$

$$\left(P_e^1\right)_{\mu\nu,\,\alpha\beta} S^{\alpha\beta\kappa} = 0 \tag{1.27}$$

$$S^{\kappa}{}_{\alpha\beta}\left(P_e^1\right)^{\alpha\beta,\,\mu\nu} = 0 \tag{1.28}$$

$$S_{\mu\alpha\beta}S^{\alpha\beta}_{\ \ \nu} = -2\Box\theta_{\mu\nu}. \tag{1.29}$$

Besides $\mathcal{L}_0$, which is gauge invariant, it is necessary to add appropriate gauge-fixing terms

$$\mathcal{L}_{\text{g.f.}} = \frac{1}{2\xi_X}\,(\partial_\mu X^\mu)^2 + \frac{1}{2\xi_B}\,(\partial_\mu B^{\mu\nu})^2 \tag{1.30}$$

which may also be written as

$$\mathcal{L}_{\text{g.f.}} = -\frac{1}{2\xi_X}X^\mu\Box\omega_{\mu\nu}X^\nu - \frac{1}{2\xi_B}B^{\mu\nu}\frac{\Box}{2}\,(P_e)_{\mu\nu,\,\kappa\lambda}\,B^{\kappa\lambda}, \tag{1.31}$$

so the full Lagrangian $\mathcal{L} = \mathcal{L}_0 + \mathcal{L}_{\text{g.f.}}$ may now be cast in a simpler quadratic form in terms of the projection operators:

$$\mathcal{L} = \frac{1}{2}\begin{pmatrix} X^\mu & B^{\kappa\lambda}\end{pmatrix}\begin{pmatrix} P_{\mu\nu} & Q_{\mu\rho\sigma} \\ R_{\kappa\lambda\nu} & \mathbf{S}_{\kappa\lambda,\,\rho\sigma}\end{pmatrix}\begin{pmatrix} X^\nu \\ B^{\rho\sigma}\end{pmatrix}, \tag{1.32}$$

where we identify

$$P_{\mu\nu} \equiv \Box\theta_{\mu\nu} - \frac{\Box}{\xi_X}\omega_{\mu\nu} \tag{1.33}$$

$$Q_{\mu\rho\sigma} \equiv m_0\,S_{\mu\rho\sigma}/\sqrt{2} \tag{1.34}$$

$$R_{\kappa\lambda\nu} \equiv -m_0\,S_{\kappa\lambda\nu}/\sqrt{2} \tag{1.35}$$

$$\mathbf{S}_{\kappa\lambda,\,\rho\sigma} \equiv -\Box\,(P_b)_{\kappa\lambda,\,\rho\sigma} - \frac{\Box}{2\xi_B}\,(P_e)_{\kappa\lambda,\,\rho\sigma}\,. \tag{1.36}$$

We are now in position to fully appreciate the effort of building a closed algebra for the projection operators, as it will allow us to complete the inversion[12] of the matrix in eq.(1.32). We may then invert the matrix wave operator in (1.32) and read off the $\langle X_\mu X_\nu\rangle$, $\langle X_\mu B_{\kappa\lambda}\rangle$ and $\langle B_{\mu\nu}B_{\kappa\lambda}\rangle$ momentum-space propagators, which

[12]The technique to invert eq.(1.32) is quite simple: we write its inverse as a general matrix in the 2×2 space of the operators given in eq.(1.36) and apply the (now) closed algebra of the spin operators to solve the coupled equations. Without the algebra developed above, this task would be much more difficult to be undertaken.

turn out to be given by

$$\langle X_\mu X_\nu \rangle = -\frac{i}{k^2 - m_0^2}\,\eta_{\mu\nu} + i\left(\frac{1}{k^2 - m_0^2} + \frac{\xi_X}{k^2}\right)\frac{k_\mu k_\nu}{k^2} \tag{1.37}$$

$$\langle B_{\mu\nu} B_{\kappa\lambda} \rangle = \frac{i}{k^2 - m_0^2}\,\left(P_b\right)_{\mu\nu,\,\kappa\lambda} + \frac{2i\xi_B}{k^2}\,\left(P_e\right)_{\mu\nu,\,\kappa\lambda} \tag{1.38}$$

$$\langle X_\mu B_{\nu\kappa} \rangle = \frac{m_0/\sqrt{2}}{k^2\,(k^2 - m_0^2)}\,\epsilon_{\mu\nu\kappa\lambda}\,k^\lambda. \tag{1.39}$$

From the propagators above, we see that the massive pole $k^2 = m_0^2$, present in (1.37)-(1.39), actually describes the spin-1 massive excitation carried by the set $\{X_\mu, B_{\nu\kappa}\}$. In contrast to the off-shell regime of the so-called BF-model [99], the non-diagonal $\langle X_\mu B_{\nu\kappa} \rangle$ propagator exhibits a massive pole and it cannot be considered separately from the $\langle X_\mu X_\nu \rangle$ and $\langle X_\mu B_{\kappa\lambda} \rangle$ propagators: only the full set of fields together correspond to the 3 d.o.f. of the on-shell massive spin-1 boson we consider in our study.

An interesting aspect we would like to highlight at this point is the connection with the $m_0 \to 0$ limit. As mentioned in Section 1.1, this limit is rather ill-defined for the usual Proca formulation, specially when one observes its propagator, eq.(1.15). Here, however, by looking at eq.(1.37) ones sees that no problems arise in the transition to the massless limit: this is due to the preservation of gauge invariance, which is left untouched by the topological mass term.

Another important point to be noticed is that in the CSKR system the gauge-fixing parameters, ξ_X and ξ_B, are present in the $\langle X_\mu X_\nu \rangle$ and $\langle B_{\mu\nu} B_{\kappa\lambda} \rangle$ propagators; a similar situation happens in (massless) electrodynamics, also in the longitudinal sector. This is naturally expected and, by the definition of $\left(P_e\right)_{\mu\nu,\,\kappa\lambda}$, eq.(1.18), we see that the gauge-dependent pieces of the propagators do not contribute when conserved currents are attached to them. This is due to the presence of the longitudinal projector, $\omega_{\mu\nu}$ (cf. eq.(1.14)), for which $\omega_{\mu\nu} j^\nu \sim \partial_\nu j^\nu = 0$, for conserved j^μ.

Different from the point of view adopted in Ref. [94], where the authors treat the topological mass term as a vertex insertion (they keep the $\langle X_\mu X_\nu \rangle$ and $\langle B_{\mu\nu} B_{\kappa\lambda} \rangle$ propagators separately and with a trivial pole $k^2 = 0$), we consider it as a genuine bilinear term and include it in the sector of 2-point functions. For that, we introduce the mixed spin operator $S_{\mu\nu\kappa}$ in the operator algebra and its final effect is to yield the mixed $\langle X_\mu B_{\nu\kappa} \rangle$ propagator. The common pole at $k^2 = m_0^2$ does not describe different particles, but a single massive spin-1 excitation described by the combined $\{X_\mu,\, B_{\nu\kappa}\}$ fields. Reference [94] sums up the (massive) vertex insertions into the $\langle X_\mu X_\nu \rangle$ propagator which develops a pole at $k^2 = m_0^2$. They leave the $\langle B_{\mu\nu} B_{\kappa\lambda} \rangle$

propagator because the $B_{\mu\nu}$ field does not interact with the fermions; the latter are only minimally coupled to X_μ.

On the other hand, in Ref. [100], the topological mass term that mixes X_μ and $B_{\nu\kappa}$ is generated by radiative corrections induced by 4-fermion interactions. So, for the sake of their calculations, the authors work with a massless vector propagator whose mass is dynamically generated. This is not what we do here. In a more recent paper [101], again an induced topological mass term mixes X_μ and $B_{\nu\kappa}$ but, in this case, it is a topological current that radiatively generates the mass.

Here we point out once again the seminal paper by Cremmer and Scherk [85] (cf. Section 1.3), where they show that, for the analysis of the spectrum, it is possible to take the field strength $G^{\mu\nu\kappa}$ and its dual $\tilde{G}^\mu$, as fundamental fields, thus enabling them to go into a new field basis where a Proca-like field emerges upon a field redefinition. We cannot follow this road here, for our $B_{\mu\nu}$ is coupled to tensor and pseudo-tensor currents in the process of evaluating some of our potentials. This prevents us from adopting $\tilde{G}^\mu$ as a fundamental field, as it is done in Ref. [85]; this would be conflicting with the locality of the action. But, for the sake of analysing the spectrum, Cremmer and Scherk's procedure works perfectly well.

To conclude the present discussion about the propagators, we reinforce that once the X_μ and $B_{\mu\nu}$ fields interact with external currents, the diagonalization of the (free) bilinear piece of the Lagrangian is not a good procedure, the reason being that the topological mass term has a derivative operator, which would imply non-local interactions between the new (diagonalized) fields and the external currents, so that the physical equivalence stated by Kamefuchi, O'Raifeartaigh and Salam [95] can no longer be undertaken.

1.5 Partial conclusions

In this chapter we reviewed some aspects of the Proca field and the CSKR system and discussed the degrees of freedom described by each of them. We also followed the discussion from Cremmer and Scherk [85] to show that the topological connection between a rank-2 tensor and a 4-vector plays the role of a mass generating mechanism, albeit introducing a potentially non-local field redefinition.

We have also obtained the propagators for both models, as well as developed the algebraic spin operators related to the topological system. These operators are fundamental tools in order to obtain the propagators, as they possibilitate the inversion of the quadratic part of the Lagrangian.

We would like to remark that, although we followed a line of thought which passed by non-Abelian gauge bosons, the CSKR model discussed above is Abelian and its generalization to non-Abelian symmetry groups is by no means trivial and constitutes a so far unsolved problem – see e.g. Refs. [102, 103]. For this reason, in our work [66] and in this thesis, we focus only on Abelian symmetries and gauge potentials, thus leaving its non-Abelian generalization and its associated issues untouched.

The study of the propagators is an important step in the direction we are following: the calculation of the interparticle potentials between spin-1/2 sources mediated by either the Proca field or the CSKR system. Naturally, the other indispensable ingredient for interaction is the matter sector, which is codified in fermionic bilinears (currents). We wish to determine how the different currents are expressed in the non-relativistic limit we are interested in and this is done in the next chapter, where we also perform the calculation of the potentials for a variety of fermionic sources with different symmetry properties, namely, pseudo-vector, vector, pseudo-tensor and tensor.

The content of this introductory chapter stems from the cited references and original independent modifications thereof. This introduction will also serve as (partial) basis for Chapter 3, which is based (with original expansion made by myself) upon my second publication [67]. Some of the topics presented here also (partially) stem from the material covered in lectures given by my Brazilian advisor, prof. J.A. Helayël-Neto, at CBPF[13].

[13]Since 2008, most of the lectures given by members of our research group is recorded in video and is publicly available at the website: `www.professorglobal.com.br/fisica`.

Chapter 2

Topologically massive spin-1 particles: spin-dependent potentials

This chapter is based upon the published work "Topologically massive spin-1 particles and spin-dependent potentials" [66] whose content has been significantly expanded to help clarify the discussion. This work was done in collaboration with L.P.R. Ospedal, F.A.G. Ferreira and J.A. Helayël-Neto (advisor), and we have shared both writing and calculational work.

2.1 Introduction

Most macroscopic phenomena originate either from gravitational or electromagnetic interactions since weak and strong nuclear forces are too short ranged to act outside the nucleus. There has been some experimental effort over the past decades towards the improvement of low-energy measurements of the inverse-square law with fairly good agreement between theory and experiment [104, 105]. The equivalence principle has also been recently tested to search for a possible spin-gravity coupling [106], something that is not classically allowed.

On the other hand, a number of scenarios beyond the Standard Model (BSM) motivated by high-energy phenomena predict very light, weakly interacting sub-eV particles (WISPs) that could generate new long-range forces, such as hidden photons [41–43], axions [107] – see Chapter 4 – or SUSY-motivated particles [108]. The aforementioned experimental tests have set strong upper limits on deviations from well-established physics.

Besides the Coulomb-like "monopole-monopole" force, it is also possible that new spin-dependent forces arise from monopole-dipole and dipole-dipole (spin-spin) interactions. Those types of behavior are closely related to two important aspects of any interacting theory: matter-mediator interaction vertices and the propagator of intermediate particles. This chapter is mainly concerned with this issue and its consequences on the interaction potential between fermionic sources[1].

Propagators are read off from the quadratic part of a given Lagrangian density and depend on intrinsic attributes of the fields, such as their spin. Most of the literature is concerned with spin-1 bosons in the $\left(\frac{1}{2},\frac{1}{2}\right)$-representation of the Lorentz group (e.g., photon). Here, we would like to address the following questions: for two different fields representing the same sort of (on-shell) spin-1 particle, which role does a particular representation play in the final form of the interaction? Is the form of the mass term (corresponding to some specific mass-generation mechanism) determinant for the macroscopic characterization of the interparticle potential?

The amplitude for the elastic scattering of two fermions is sensitive to the fundamental, microscopic properties of the intermediate boson. We set out to study the potential generated by the exchange of two different classes of neutral particles: a Proca (vector) boson and a 2-rank anti-symmetric tensor, the Kalb-Ramond field [85, 86], combined with a vector boson, i.e., the $\{X_\mu, B_{\nu\kappa}\}$ (CSKR) system with a topological mixing term, cf. Chapter 1. Our main motivation to take the CSKR system into consideration is two-fold:

- **i)** They may be the messenger, or the remnant, of some BSM physics. This is why we are interested in understanding whether we may find out the track of a 2-rank gauge sector in the profile of spin-dependent potentials.

- **ii)** In four spacetime dimensions, a pure on-shell 2-rank gauge potential actually describes a scalar particle. However, off-shell it is not so (cf. Section 1.2). This means that the quantum fluctuations of a 2-rank gauge field may induce a new pattern of spin dependence. Moreover, its mixing with an Abelian gauge potential sets up a different scenario to analyse interparticle potentials induced by massive vector particles.

Our object of interest is a neutral massive spin-1 mediating particle, which we might identify as a sort of massive photon. Such a particle is extensively discussed in the literature, often dubbed $Z^{0'}$. In Refs. [110–112] the authors present an exhaustive list of different candidate $Z^{0'}$ particles and phenomenological constraints

[1]Other sources (systems) involving neutral as well as charged particles, with or without spin, have also been considered by Holstein [109].

on their masses and couplings. In this thesis we study interaction potentials between fermionic currents as induced by $Z^{0'}$-like virtual particles. Their effects are then included in the interpaticle potentials we are going to work out. Therefore, the velocity- and spin- dependence of our potentials appear as an effect of the interchange of a virtual $Z^{0'}$-like particle with possible topological origins.

We exploit a variety of couplings to ordinary matter in order to extract possible experimental signatures that allow to distinguish between the two types of mediation in the regime of low-energy interactions. From the physical side, we expect those potentials to exhibit a polynomial correction (in powers of $1/r$) to the well-known $e^{-m_0 r}/r$ Yukawa potential [113]. This means that a laboratory apparatus with typical dimensions of $\sim$ mm could be used to examine the interaction mediated by massive bosons with $m_0 \sim 10^{-3}\,\mathrm{eV}$.

Developments in the measurement of macroscopic interactions between unpolarized and polarized objects [104, 105, 114–117] are able to constrain many of the couplings between electrons and nucleons (protons and neutrons), so we can concentrate on more fundamental matters, such as the impact of the particular field representation of the intermediate boson in the fermionic interparticle potential. To this end, we discuss the case of monopole-dipole interactions in order to directly compare the Proca and $\{X_\mu, B_{\nu\kappa}\}$ mechanisms. This is an interesting instance where the direct coupling of the tensor gauge potential to a tensor current may modify the usual Proca interaction profile (cf. Chapter 1).

It is worthwhile pointing out that the main contribution here is actually to associate different field representations, which differ from each other by their respective off-shell d.o.f., to the explicit spin dependence in the particle potentials we derive. Rather than focusing on setting constraints on the BSM parameters associated to the new interactions, we aim at a better understanding of the interplay between different field representations for a given spin and the spin dependence of the potentials that appear from the associate models. This shall be explicitly highlighted in the end of Section 2.5.

We anticipate here, however, that four particular types of spin dependence show up only in the topologically massive case, thus being a distinguishing feature of CSKR-mediated interactions. The Proca-type massive exchange does exclude these four distinctive interaction types, as it will become clear also in Section 2.5. As a preliminary step, in the next section we briefly review some aspects necessary to develop the non-relativistic (NR) expansions of the spin-1/2 currents.

2.2 Basic conventions

The basic spinors used to compose the scattering amplitude are the positive energy solutions to the Dirac equation in momentum space [73], namely[2]

$$u(P) = N_f \begin{pmatrix} \xi \\ \frac{\boldsymbol{\sigma}\cdot\mathbf{P}}{E+m}\,\xi \end{pmatrix} \tag{2.1}$$

where $|N_f|^2 = E + m$. Here $E = \sqrt{|\mathbf{P}|^2 + m^2}$ with m being the electron's (or, more generally, the fermion's) mass and $\xi = \begin{pmatrix} 1 \\ 0 \end{pmatrix}$ or $\xi = \begin{pmatrix} 0 \\ 1 \end{pmatrix}$ are the basic bi-spinors for spin-up and -down states, respectively. The orthonormality relation $\xi_r'^{\dagger}\xi_s = \delta_{rs}$ is supposed to hold and we will usually suppress spinor indices (rs).

The gamma matrices are expressed in the standard Dirac basis, i.e.,

$$\gamma^0 = \begin{pmatrix} 1 & 0 \\ 0 & -1 \end{pmatrix}, \gamma^i = \begin{pmatrix} 0 & \sigma_i \\ -\sigma_i & 0 \end{pmatrix} \text{ and } \gamma_5 = \begin{pmatrix} 0 & 1 \\ 1 & 0 \end{pmatrix}, \tag{2.2}$$

and we denote the generators of the boosts and rotations by

$$\Sigma^{\mu\nu} \equiv \frac{i}{4}\left[\gamma^\mu, \gamma^\nu\right]. \tag{2.3}$$

From here on we define $\langle\sigma_i\rangle \equiv \xi'^{\dagger}\,\sigma_i\,\xi$. The metric and Levi-Civita symbol are defined so that $\eta^{\mu\nu} = \mathrm{diag}(+,-,-,-)$ and $\epsilon^{0123} = +1$, respectively. We adopt natural units $\hbar = c = 1$ throughout.

2.2.1 Current decompositions in the non-relativistic limit

In order to calculate the spin-dependent potentials, it is useful to have the non-relativistic limit of the source currents, where we assume the following approximations:

1) $|\mathbf{p}|^2/m^2 \sim \mathcal{O}(v^2) \to 0$

2) Small momentum transfer: $|\mathbf{q}|^2/m^2 \to 0$

3) The cross product of $\mathbf{p}$ and $\mathbf{q}$ tends to zero since $|\mathbf{p}|/m$ and $|\mathbf{q}|/m$ are small and energy-momentum conservation implies $\mathbf{p}\cdot\mathbf{q} = 0$

[2]Contrary to the individual components of the 3-vectors, which are in boldface (occasionally also with indices), the Pauli and Dirac gamma matrices will not be boldfaced, unless they are contracted with another 3-vector.

In such an approximation scheme we may re-express the positive-energy solution spinor, eq.(2.1), as

$$u(P) = \sqrt{2m} \begin{pmatrix} \xi \\ \frac{\boldsymbol{\sigma}\cdot\mathbf{P}}{2m}\,\xi \end{pmatrix}, \tag{2.4}$$

where we have taken $|N_f|^2 \simeq m + \frac{|\mathbf{P}|^2}{2m} + m = 2m + \mathcal{O}(|\mathbf{P}|^2/m^2)$, as well as $E + m \simeq 2m$ in the denominator of the "small component". This is justified – up to the desired order in $|\mathbf{p}|/m$ – given that we already have a factor of $|\mathbf{p}|/m$ in this component.

Here we show the result of the application of eq.(2.4) in the non-relativistic limit as a building block for the different fermionic currents. The fully relativistic form of the currents is shown in Appendix A. We adopt the parametrization for the first current (i.e., first vertex) following Fig. 2.1. Making use of the Dirac spinor conjugate, $\bar{u} \equiv u^\dagger \gamma^0$, we may use the explicit form of the basic low-energy spinor, eq.(2.4), to obtain the following set of identities (omitting the coupling constants for the sake of simplicity):

1) Scalar current (S):

$$\bar{u}(p + q/2)\, u(p - q/2) \approx \delta\,. \tag{2.5}$$

2) Pseudo-scalar current (PS):

$$\bar{u}(p + q/2)\, i\gamma_5\, u(p - q/2) = -\frac{i}{2m}\, \mathbf{q} \cdot \langle \boldsymbol{\sigma} \rangle \tag{2.6}$$

3) Vector current (V):

$$\bar{u}(p + q/2)\, \gamma^\mu\, u(p - q/2), \tag{2.7}$$

3i) For $\mu = 0$,

$$\bar{u}(p + q/2)\, \gamma^0\, u(p - q/2) \approx \delta \tag{2.8}$$

3ii) For $\mu = i$,

$$\bar{u}(p + q/2)\, \gamma^i\, u(p - q/2) = \frac{\mathbf{p}_i}{m}\, \delta - \frac{i}{2m}\, \epsilon_{ijk}\, \mathbf{q}_j\, \langle \sigma_k \rangle \tag{2.9}$$

4) Pseudo-vector current (PV):

$$\bar{u}(p + q/2)\gamma^\mu\gamma_5 u(p - q/2) \tag{2.10}$$

4i) For $\mu = 0$,

$$\bar{u}(p+q/2)\,\gamma^0\,\gamma_5\,u(p-q/2) = \frac{1}{m}\,\langle\boldsymbol{\sigma}\rangle\cdot\mathbf{p} \tag{2.11}$$

4ii) For $\mu = i$,

$$\bar{u}(p+q/2)\,\gamma^i\,\gamma_5\,u(p-q/2) \;\approx\; \langle\sigma_i\rangle \tag{2.12}$$

5) Tensor current (T):

$$\bar{u}(p+q/2)\,\Sigma^{\mu\nu}\,u(p-q/2) \tag{2.13}$$

5i) For $\mu = 0$ and $\nu = i$,

$$\bar{u}(p+q/2)\,\Sigma^{0i}\,u(p-q/2) = -\frac{1}{2m}\,\epsilon_{ijk}\,\mathbf{p}_j\,\langle\sigma_k\rangle - \frac{i}{4m}\,\delta\,\mathbf{q}_i \tag{2.14}$$

5ii) For $\mu = i$ and $\nu = j$,

$$\bar{u}(p+q/2)\,\Sigma^{ij}\,u(p-q/2) \approx \frac{1}{2}\,\epsilon_{ijk}\langle\sigma_k\rangle \tag{2.15}$$

6) Pseudo-tensor current (PT):

$$\bar{u}(p+q/2)\,i\,\Sigma^{\mu\nu}\,\gamma_5\,u(p-q/2) \tag{2.16}$$

6i) For $\mu = 0$ and $\nu = i$,

$$\bar{u}(p+q/2)\,i\,\Sigma^{0i}\,\gamma_5\,u(p-q/2) \approx -\frac{1}{2}\langle\sigma_i\rangle \tag{2.17}$$

6ii) For $\mu = i$ and $\nu = j$

$$\bar{u}(p+q/2)\,i\,\Sigma^{ij}\,\gamma_5\,u(p-q/2) = -\frac{1}{2m}\,\left(\mathbf{p}_i\langle\sigma_j\rangle - \mathbf{p}_j\langle\sigma_i\rangle\right) - \frac{i}{4m}\,\delta\,\epsilon_{ijk}\,\mathbf{q}_k \tag{2.18}$$

In the manipulations above we have kept the rs indices implicit in the δ_{rs}, as mentioned above, pointing out only the particle label. Besides omitting the respective coupling constants, we have not included the common $2m$ pre-factor – this makes the non-relativstic approximation more explicit at the current level (see Section 2.3). Due to momentum conservation and our choice of reference frame (cf. Fig. 2.1), the second current (or second vertex) can be obtained by performing the changes $\mathbf{q} \to -\mathbf{q}$ and $\mathbf{p} \to -\mathbf{p}$ in the first one, which is the set displayed above.

2.3 Methodology

Let us first establish the kinematics of our problem. We are dealing with two fermions, 1 and 2, which scatter elastically. If we work in the center of mass (CM) reference frame, we can assign them momenta as indicated in Fig. 2.1 below, where $\mathbf{q}$ is the momentum transfer and $\mathbf{p}$ is the average momemtum of fermion 1 before and after the scattering.

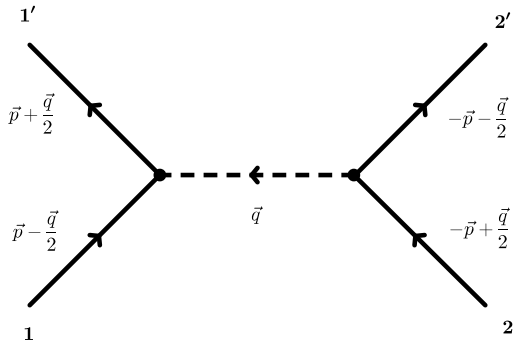

Figure 2.1: Basic vertex structure and momentum assignments. The arrows above the momenta are simply to highlight the 3-vector nature.

Given energy conservation and our choice of reference frame, one can show that $\mathbf{p}\cdot\mathbf{q}=0$ and that q^μ is space-like: $q^2=-\mathbf{q}^2$ (i.e., $q^0=0$). The amplitude will be expressed in terms of $\mathbf{p}$ and $\mathbf{q}$ and we shall keep only terms linear in $|\mathbf{p}|/m_{1,2}$. It will also include the spin of the particles involved, as the current decompositions discussed in Section 2.2.1 already indicate.

Our objective is to extract the interparticle potential (energy) generated by two sources via the exchange of a mediator. This may be done by using the first Born approximation [118], which gives the two-fermion potential generated by a one-boson exchange. It is essentially the Fourier transform of the tree-level momentum-space (non-relativistic) amplitude[3] with respect to the momentum transfer $\mathbf{q}$, that is

$$V(r,v)=-\int\frac{d^3\mathbf{q}}{(2\pi)^3}\,e^{i\mathbf{q}\cdot\mathbf{r}}\,\mathcal{A}(\mathbf{q},m\mathbf{v}), \tag{2.19}$$

where $\mathbf{r}$, r and $v=|\mathbf{p}|/m_{1,2}$ are the relative position vector, its modulus and average velocity of the fermions, respectively.

[3]The minus sign in eq.(2.19) is tied to the non-trivial elements of the S matrix, $S_{fi}=\delta_{fi}+i\,(2\pi)^4\,\delta^4\,(\Sigma p_f-\Sigma p_i)\,T_{fi}$, where $T_{fi}\sim\mathcal{M}_{fi}$, modulo normalization factors. We highlight that this is simply a convention, which must be kept throughout, but not all authors use the same. For instance, the minus sign for the potential along with $i\mathcal{M}$ are used by Moody & Wilczek [107] and Dobrescu & Mocioiu [113], whereas the opposite signs are used by Sucher *et al.* [122].

An important issue is the connection between the fully relativistic Feynman amplitude – let us denote it by $\mathcal{M}$ – and the non-relativistic one, $\mathcal{A}$ [118]. The two amplitudes are related[4] via

$$\mathcal{A} = \prod_{j=1,2} (2E_j)^{-1/2} \prod_{k=1',2'} (2E_k)^{-1/2} \mathcal{M} \tag{2.20}$$

which shows that the bridge between $\mathcal{A}$ and $\mathcal{M}$ is built on energy-dependent factors. These come from the different conventions used to normalize the one-particle states in relativistic and non-relativistic quantum mechanics[5].

Incidentally, one notices that the multiplicative factors from eq.(2.20) are exactly cancelled[6] by the normalization factors of the spinors, cf. eq.(2.4). We are therefore free to directly use the current decompositions listed in Section 2.2.1, for their $2m$ pre-factors are already factored out and are washed away by the respective $2E \approx 2m$ factors from the relation above.

We restrict ourselves to tree-level amplitudes, i.e., one-boson exchange, since we are considering weakly interacting particles carrying tiny coupling constants suppressing higher-order diagrams (higher-order and quantum corrections may also be calculated, see e.g. Refs. [119–121]). The typical outcomes are Yukawa-like inter-particle potentials with extra $1/r$ contributions[7] which also depend on the spin of the sources, as well as on their velocity. Contrary to the usual Coulomb case, spin- and velocity-dependent terms are the rule, not the exception.

2.4 The potentials: Proca

In the previous section and in Chapter 1 we have introduced the two key elements necessary to our analysis, namely, the propagators and the currents expressed in the low-energy regime. Before we explore the more involved case of the topological system, it is worthwhile checking our method in the more conventional context of the exchange of a single neutral Proca particle.

[4] Volume factors have been omitted since we are not explicitly working with decay rates or cross sections, where possible boundary conditions may play a role.

[5] In non-relativistic quantum mechanics one does not need to care about the Lorentz properties of the normalization – possibly only the ones related to rotations, etc. However, in the relativistic case one needs to include Lorentz-invariant norms and this leads to extra energy factors; these end up impacting on the amplitudes and are made explicit in eq.(2.20).

[6] This is due to the approximation level in which we are working. If one goes up to $\mathcal{O}(|\mathbf{p}|^2/m^2)$ this will impact on the explicit form of the spinor (2.1), whose (upper) "large" component will generally differ from the expression shown in eq.(2.4). This observation will become relevant in Chapter 3, where we go one order higher in the non-relativistic limit.

[7] These factors arise due to the extra $\mathbf{q}$ terms in the amplitudes, as well as the modified propagators, specially the mixed ones.

Using the parametrization of Fig. 2.1 and applying the Feynman rules, we get

$$\begin{aligned} i\mathcal{A}^{\text{Proca}}_{\text{V}-\text{V}} &= \bar{u}(p+q/2)\left\{ig_1^V\gamma^\mu\right\}u(p-q/2)\langle A_\mu A_\nu\rangle \\ &\times \bar{u}(-p-q/2)\left\{ig_2^V\gamma^\nu\right\}u(-p+q/2) \end{aligned}$$

with g_1^V and g_2^V referring to the coupling constants. In the vector case we may identify the coupling constant with the electric charge, since an analogous current is obtained via the Noether procedure for the usual Dirac field coupled to the electromagnetic potentials, ϕ and $\mathbf{A}$ – this is specially true in the massless limit of eq.(1.1). In Chapter 3 we shall make this difference explicit by denoting $g_V \equiv e$, with the latter being the usual electric charge.

Following the discussion above, we ignore normalization and energy pre-factors, which have been already implicitly cancelled. The equation above can be put in the simpler form:

$$\mathcal{A}^{\text{Proca}}_{\text{V}-\text{V}} = i\, J_1^\mu\, \langle A_\mu A_\nu\rangle\, J_2^\nu. \tag{2.21}$$

If we use current conservation and that $q^0 = 0$ we find that the amplitude is $\mathcal{A}^{\text{Proca}}_{V-V} = -\frac{1}{\mathbf{q}^2+m_0^2} J_1^\mu\, J_{2\mu}$ and, according to eq.(2.9), we have $J_1^i\, J_{2i} \sim \mathcal{O}(v^2)$. Therefore, only the term $J_1^0\, J_{20} \approx g_1^V g_2^V \delta_1\delta_2$ contributes. The NR amplitude reads, then

$$\mathcal{A}^{\text{Proca}}_{V-V} = -g_1^V g_2^V\, \frac{\delta_1\delta_2}{\mathbf{q}^{\,2}+m_0^2}, \tag{2.22}$$

where δ_i is such that $\delta_i = +1$ if the i-th particle experiences no spin flip in the interaction and $\delta_i = 0$ otherwise. The global term $\delta_1\delta_2$ indicates that the amplitude is non-trivial only if both particles do not flip their respective spins. If one of them does, the potential vanishes identically, meaning that this interaction only occurs with no spin flip – this is similar to the usual Coulomb case in lowest order. In what follows, we shall come across situations where only a single δ_i appears, thus justifying the effort to keep the δ_i explicit.

Finally, taking the Fourier transform we obtain the potential between two static vector currents, namely,

$$V^{\text{Proca}}_{\text{V}-\text{V}} = \frac{g_1^V g_2^V \delta_1\delta_2}{4\pi}\, \frac{e^{-m_0 r}}{r}, \tag{2.23}$$

which displays the well-known exponentially suppressed repulsive Yukawa behaviour typical of a massive vector boson exchange. In our notation the potential is indicated as $V_{v_1-v_2}$, where $v_{1,2}$ refer to the vertices related to the particles 1 and 2. In the case above, the subscripts V stand for vector currents. As already indicated, the typical interaction length of such an interaction is $\sim m_0^{-1}$.

Following the same procedure we can exploit other situations, namely: vector with pseudo-vector currents and two pseudo-vector currents. The results are the following:

$$V_{\rm V-PV}^{\rm Proca} = -\frac{g_1^V g_2^{PV}}{4\pi}\Bigg\{\delta_1\left(\frac{1}{m_1}+\frac{1}{m_2}\right)\,\mathbf{p}\cdot\langle\boldsymbol{\sigma}\rangle_2 + + \frac{(1+m_0 r)}{2m_1 r}\,\left[\langle\boldsymbol{\sigma}\rangle_1\times\langle\boldsymbol{\sigma}\rangle_2\right]\cdot\hat{\mathbf{r}}\Bigg\}\,\frac{e^{-m_0 r}}{r} \tag{2.24}$$

$$V_{\rm PV-PV}^{\rm Proca} = -\frac{g_1^{PV} g_2^{PV}}{4\pi}\,\langle\boldsymbol{\sigma}\rangle_1\cdot\langle\boldsymbol{\sigma}\rangle_2\,\frac{e^{-m_0 r}}{r}, \tag{2.25}$$

where we indicate that the longitudinal sector of the propagator is eliminated by the conserved V current in $V_{\rm V-V}^{\rm Proca}$. The same is not true for $V_{\rm PV-PV}^{\rm Proca}$ since the PV current for spin-1/2 sources is not conserved. However, due to the compromise of discarding terms of $\mathcal{O}(|\mathbf{p}|^2/m^2)$ – and here we assume also $\mathcal{O}(|\mathbf{q}|^2/m_0^2)$ to be negligeable – one finds no longitudinal correction to the $PV-PV$ potential. In the potentials above we find all kinds of spin-dependent interactions, while the r factors are limited to r^{-2}.

If one lifts the restriction of $|\mathbf{q}|^2/m_0^2 \ll 1$ and allows terms of $\mathcal{O}(|\mathbf{q}|^2/m_0^2)$, then eq.(2.25) receives a correction, namely,

$$V_{\rm PV-PV}^{\rm Proca} \;\to\; V_{\rm PV-PV}^{\rm Proca} + \frac{g_1^{PV} g_2^{PV}}{4\pi}\,\frac{e^{-m_0 r}}{m_0^2 r^3}\Bigg\{\left[3+3m_0 r+m_0^2 r^2\right]\left(\langle\boldsymbol{\sigma}\rangle_1\cdot\hat{\mathbf{r}}\right)\left(\langle\boldsymbol{\sigma}\rangle_2\cdot\hat{\mathbf{r}}\right) + -(1+m_0 r)\langle\boldsymbol{\sigma}\rangle_1\cdot\langle\boldsymbol{\sigma}\rangle_2\Bigg\}, \tag{2.26}$$

which is equal to $V_{\rm PV-PV-LONG}^{s=1/2}$, eq.(3.48). This pure spin-spin (dipole-dipole) term has been neglected in our work [66], but, since we did not limit the analysis to any specific application, the value of the mass m_0 was kept open, so we recover our previous results if we take, as mentioned above, the limit where $\mathcal{O}(|\mathbf{q}|^2/m_0^2)$ is negligeable (in the amplitude[8]).

In fact, in our original published work [66], we assumed that all currents are actually conserved, as the non-vector interactions may stem from some BSM scenario where the associated symmetries hold and currents are conserved. In the next sections we shall therefore neglect such longitudinal contributions on the grounds discussed above.

[8]Besides this, the r-dependence of this correction shows that such term is important only for short distances, so that, for macroscopic, i.e., long-range, interactions this term may be dropped.

In what follows we will see that a richer class of potentials is generated if the massive spin-1 Abelian boson exhibits a gauge-invariant mass term that comes from a topological mixing. This will be mainly due to the presence of the tensor field in the mixed propagator, as well as in the pure tensor-tensor one.

2.5 The potentials: CSKR

We have already discussed the procedure to obtain the potentials, so now we are ready to focus on the more interesting topological sector. As a concrete and explicit example, let us work out the particular case in which we have the propagator $\langle B_{\mu\nu}B_{\kappa\lambda}\rangle$ and two tensor currents. In the following, we adopt the parametrization of Fig. 2.1.

After applying the Feynman rules, we can rewrite the scattering amplitude for this process as

$$\mathcal{A}^{\langle BB\rangle}_{\mathrm{T-T}} = iJ_1^{\mu\nu}\langle B_{\mu\nu}B_{\kappa\lambda}\rangle J_2^{\kappa\lambda} \tag{2.27}$$

with the tensor currents given by eq.(2.13). Substituting the propagator (1.38) in eq.(2.27) and eliminating its longitudinal sector (see discussion below eq.(2.26)), we end up with $\mathcal{A}^{\langle BB\rangle}_{\mathrm{T-T}} = -\frac{1}{q^2-m_0^2}J_1^{\mu\rho}J_{2\,\mu\rho}$.

The product of currents leads to $J_1^{\mu\rho}J_{2\,\mu\rho} = 2J_1^{0i}J_{2\,0i} + J_1^{ij}J_{2\,ij}$ but, according to eq.(2.14), we conclude that $J_1^{0i}J_{2\,0i} \sim \mathcal{O}(v^2)$ does not contribute. The term $J_1^{ij}J_{2\,ij}$ can be simplified by using eq.(2.15) (with the appropriate changes to the second current), so that we get

$$\mathcal{A}^{\langle BB\rangle}_{\mathrm{T-T}} = \frac{1}{2}\,\frac{g_1^T g_2^T}{\mathbf{q}^2+m_0^2}\,\langle\boldsymbol{\sigma}\rangle_1\cdot\langle\boldsymbol{\sigma}\rangle_2 \tag{2.28}$$

and, performing the Fourier integral, we obtain the NR spin-spin potential, namely

$$V^{\langle BB\rangle}_{\mathrm{T-T}} = -\frac{g_1^T g_2^T}{8\pi}\,\langle\boldsymbol{\sigma}\rangle_1\cdot\langle\boldsymbol{\sigma}\rangle_2\frac{e^{-m_0 r}}{r}. \tag{2.29}$$

Similarly, we find the interaction potentials between tensor and pseudo-tensor currents to be

$$\begin{aligned} V^{\langle BB\rangle}_{\mathrm{T-PT}} &= \frac{g_1^T g_2^{PT}}{8\pi r}\left\{\left(\frac{1}{m_1}+\frac{1}{m_2}\right)\mathbf{p}\cdot(\langle\boldsymbol{\sigma}\rangle_1\times\langle\boldsymbol{\sigma}\rangle_2) + \right. \\ &+ \left.\frac{(1+m_0 r)}{2r}\left(\frac{\delta_2}{m_2}\langle\boldsymbol{\sigma}\rangle_1 - \frac{\delta_1}{m_1}\langle\boldsymbol{\sigma}\rangle_2\right)\cdot\hat{\mathbf{r}}\right\}e^{-m_0 r} \end{aligned} \tag{2.30}$$

as well as between two pseudo-tensors

$$V^{\langle BB\rangle}_{\rm PT-PT} = \frac{g_1^{PT} g_2^{PT}}{8\pi}\,\langle\boldsymbol{\sigma}\rangle_1\cdot\langle\boldsymbol{\sigma}\rangle_2\frac{e^{-m_0 r}}{r}. \tag{2.31}$$

It is worthwhile comparing the potentials (2.29) and (2.31). We observe that they only differ by a relative minus sign. This means that they exhibit opposite behaviors for a given spin configuration: one is attractive while the other is repulsive. The physical reason is that the $PT-PT$ and $T-T$ potentials stem from different sectors of the respective currents. The $PT-PT$ amplitude is composed by the $(0i)-(0j)$ terms of the currents, whereas the $T-T$ amplitude arises from the $(ij)-(kl)$ components, as it can be seen from eq. (2.27).

To gain a better insight, let us check the structure of the $\langle B_{\mu\nu}B_{\kappa\lambda}\rangle$ propagator, specially the pieces which participate in each of the potentials. It becomes clear that, in the case of the $PT-PT$ interactions, the relevant part of the full propagator is $\langle B_{0i}B_{0j}\rangle \sim \frac{i}{\mathbf{q}^2+m_0^2}\delta_{ij}$. This is typical of the propagator of a scalar mediator, thus leading us to conclude that an $s=0$ mode was exchanged. In contrast, in the $\langle B_{ij}B_{kl}\rangle$ sector, the only exchange is of a pure spin-1 mode. It is well-known, however, that the exchange of a scalar and a vector boson between sources of equal charges yields respectively attractive and repulsive interactions, therefore justifying the aforementioned sign difference between eqs.(2.29) and (2.31).

For the mixed propagator $\langle X_\mu B_{\kappa\lambda}\rangle$, eq.(1.39), we have four possibilities involving the following currents: vector with tensor, vector with pseudo-tensor, pseudo-vector with tensor and pseudo-vector with pseudo-tensor. The results are given below:

$$V^{\langle XB\rangle}_{\rm V-T} = \frac{g_1^V g_2^T \delta_1}{4\pi\sqrt{2}m_0 r^2}\left[1-(1+m_0 r)\,e^{-m_0 r}\right]\langle\boldsymbol{\sigma}\rangle_2\cdot\hat{\mathbf{r}} \tag{2.32}$$

$$V^{\langle XB\rangle}_{\rm PV-T} = \frac{g_1^{PV} g_2^T}{4\pi\sqrt{2}m_0\mu r^2}\left[1-(1+m_0 r)\,e^{-m_0 r}\right](\langle\boldsymbol{\sigma}\rangle_1\cdot\mathbf{p})\,(\langle\boldsymbol{\sigma}\rangle_2\cdot\hat{\mathbf{r}}) \tag{2.33}$$

$$\begin{aligned} V^{\langle XB\rangle}_{\rm PV-PT} &= \frac{g_1^{PV} g_2^{PT}}{\sqrt{2}4\pi r m_0}\Bigg\{\frac{\delta_2 m_0^2 e^{-m_0 r}}{2m_1 m_2}\langle\boldsymbol{\sigma}\rangle_1\cdot\mathbf{p}+ \\ &+ \frac{1}{r}\left[1-(1+m_0 r)\,e^{-m_0 r}\right](\langle\boldsymbol{\sigma}\rangle_2\times\langle\boldsymbol{\sigma}\rangle_1)\cdot\hat{\mathbf{r}}\Bigg\}. \end{aligned} \tag{2.34}$$

The richest potential is the one between vector and pseudo-tensor sources, given by

$$\begin{aligned} V_{\mathrm{V-PT}}^{\langle XB\rangle} &= \frac{\sqrt{2}g_1^V g_2^{PT}}{4\pi m_0 r}\Bigg\{\frac{\delta_1\delta_2 m_0^2 e^{-m_0 r}}{4m_2} + \\ &+ \frac{\delta_1}{2\mu r^2}\left[1-(1+m_0 r)\,e^{-m_0 r}\right]\mathbf{L}\cdot\langle\boldsymbol{\sigma}_2\rangle + \\ &- \frac{1}{4m_1 r^2}\left[1+\left(1+m_0 r-m_0^2 r^2\right)e^{-m_0 r}\right]\langle\boldsymbol{\sigma}_1\rangle\cdot\langle\boldsymbol{\sigma}_2\rangle + \\ &+ \frac{1}{4m_1 r^2}\left[3+\left(3+3m_0 r+m_0^2 r^2\right)e^{-m_0 r}\right](\langle\boldsymbol{\sigma}_1\rangle\cdot\hat{\mathbf{r}})\,(\langle\boldsymbol{\sigma}_2\rangle\cdot\hat{\mathbf{r}})\Bigg\} \quad (2.35) \end{aligned}$$

where we have introduced the reduced mass of the fermion system $\mu^{-1}=m_1^{-1}+m_2^{-1}$ and defined $\mathbf{L}=\mathbf{r}\times\mathbf{p}$.

One interesting observation is the *absence* of contact terms (Dirac deltas) in the potentials above. Our precaution of keeping terms $\sim\mathbf{q}^2$ in the amplitude – even though this is beyond our approximation level (NR) – turns out to be excessive. This is a peculiarity of the mixed $\langle X_\mu B_{\kappa\lambda}\rangle$ propagator, which factorizes into $\sim\frac{1}{\mathbf{q}^2}-\frac{1}{\mathbf{q}^2+m_0^2}$, thus allowing for the accidental cancellation of the contact terms.

The minus sign is very important, as it eliminates the mass-independent contact terms which appear in the integrals (A.36) and (A.37). Incidentally, this also happens in the $V_{\mathrm{PV-PT}}^{\langle XB\rangle}$ potential. We would like to highlight here that this type of cancellation also takes place in other scenarios, such as in the Podolsky-Lee-Wick electrodynamics [72], where the propagators exhibit a similar structure.

For the propagator $\langle X_\mu X_\nu\rangle$, eq,(1.37), whenever it is coupled to a conserved current – here this is explicitly true for the V current – we find the same results as the ones with $\langle A_\mu A_\nu\rangle$ (cf. Section 2.4). This is due to current conservation, which eliminates the gauge-fixing dependent piece of $\langle X_\mu X_\nu\rangle$ and the longitudinal sector in $\langle A_\mu A_\nu\rangle$ (see discussion at the end of Section 2.4). This means that, even though the vector field appears now mixed with the $B_{\mu\nu}$ field with a gauge-preserving mass term, for the sake of the interaction potentials, the results are the same as in the Proca case as far as (only) X_μ-field exchange is concerned.

Furthermore, we point out that experiments with rare earth iron garnet test masses [124] could be a possible scenario to distinguish the two different mass terms. In the Proca case we obtained the following spin- and velocity-dependences: $\mathbf{p}\cdot\boldsymbol{\sigma}$, $(\boldsymbol{\sigma}_1\times\boldsymbol{\sigma}_2)\cdot\hat{\mathbf{r}}$ and $\boldsymbol{\sigma}_1\cdot\boldsymbol{\sigma}_2$. These also appear in the topologic gauge-preserving mass, but there we have additional profiles, given by $(\boldsymbol{\sigma}_1\times\boldsymbol{\sigma}_2)\cdot\mathbf{p}$, $\boldsymbol{\sigma}\cdot\hat{\mathbf{r}}$, $(\boldsymbol{\sigma}_1\cdot\mathbf{p})(\boldsymbol{\sigma}_2\cdot\hat{\mathbf{r}})$ and $(\hat{\mathbf{r}}\times\mathbf{p})\cdot\boldsymbol{\sigma}$.

The aforementioned experiment provides six configurations $(C1, ..., C6)$ by changing the relative orientation of the detector and the test mass with respective spin polarizations and relative velocities. One of these configurations is interesting to our work, namely, $C5$ is sensitive only to $(\hat{\mathbf{r}} \times \mathbf{p}) \cdot \boldsymbol{\sigma}$, which is only present in the gauge-preserving CSKR case. For the other profiles we cannot distinguish the contributions of different mediators in this experiment. For example, the $C2$ configuration is sensitive to both $(\boldsymbol{\sigma}_1 \cdot \mathbf{p})(\boldsymbol{\sigma}_2 \cdot \hat{\mathbf{r}})$ and $\boldsymbol{\sigma}_1 \cdot \boldsymbol{\sigma}_2$ dependences [124].

2.6 Partial conclusions

The investigated model describes an extra Abelian gauge boson, a sort of Abelian $Z^{0'}$, which appears as a massive excitation of a mixed $\{X_\mu, B_{\nu\kappa}\}$ system of fields, cf. Section 1.2. It may be originated from some sector of BSM physics, where the coupling between an Abelian field and the 2-form gauge potential in a SUGRA multiplet may yield the topologically massive spin-1 particle we considered. To have detectable macroscopic effect, this intermediate particle should have a small mass, of the order of meV, thus reaching experimentally accessible distances of $\sim$ mm. On the other side of the mass scale, short-range interactions may also be induced by heavy mediators[9] and may play a role in atomic and nuclear physics.

For the sake of concreteness, let us consider a (very) simplified hypothetical scenario where we could, in principle, distinguish between the two models. A possible experimental set-up could consist of a neutral and a polarized source (1 and 2, respectively). Suppose, furthermore, that the sources display all kinds of interactions (V, PV, T, etc). In this case, we must collect the terms proportional to the spin (polarization) of source 2 – we make $\langle\boldsymbol{\sigma}\rangle_2 \equiv \langle\boldsymbol{\sigma}\rangle$ – in the two scenarios.

In the case of the standard Proca mediator, we have

$$V^{\text{Proca}}_{\text{mon-dip}} = -\frac{g^2}{\mu}\frac{e^{-m_0 r}}{r}\mathbf{p}\cdot\langle\boldsymbol{\sigma}\rangle \tag{2.36}$$

whereas for the topological model we have

$$\begin{aligned} V^{\{X,B\}}_{\text{mon-dip}} &= -\frac{g^2}{\mu}\frac{e^{-m_0 r}}{r}\mathbf{p}\cdot\langle\boldsymbol{\sigma}\rangle - \frac{g^2}{m_1}\frac{(1+m_0 r)e^{-m_0 r}}{r^2}\hat{\mathbf{r}}\cdot\langle\boldsymbol{\sigma}\rangle \\ &+ \frac{g^2}{m_0}\frac{[1-(1+m_0 r)\,e^{-m_0 r}]}{r^2}\hat{\mathbf{r}}\cdot\langle\boldsymbol{\sigma}\rangle - \frac{g^2 m_0}{m_1 m_2}\frac{e^{-m_0 r}}{r}\mathbf{p}\cdot\langle\boldsymbol{\sigma}\rangle \\ &+ \frac{g^2}{\mu m_0}\frac{[1-(1+m_0 r)\,e^{-m_0 r}]}{r^3}\,(\mathbf{r}\times\mathbf{p})\cdot\langle\boldsymbol{\sigma}\rangle, \end{aligned} \tag{2.37}$$

[9] Maybe not even *that* heavy [125, 126].

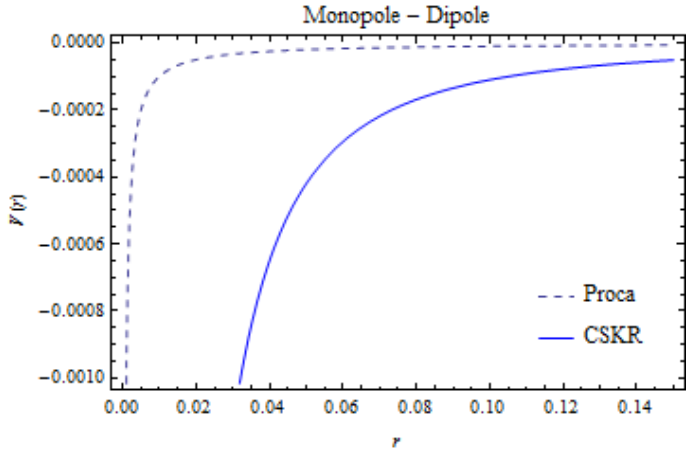

Figure 2.2: Monopole-dipole potentials with $m_1 = m_e = 10^5\,\text{eV}$, $m_0 = 10^{-3}\,\text{eV}$ and source 1 with velocity of order $v \simeq 10^{-6}$. Coupling constants not included for simplicity.

where, for simplicity, we have omitted the labels in the coupling constants. In the macroscopic limit, where large aggregates of particles constitute the sources, these would be effectively substituted by $g \to gN_i$, being N_i the (effective) number of interacting particles of type i in each source.

If we consider the case in which source 1 carries momentum so that $\mathbf{p} \parallel \langle \boldsymbol{\sigma} \rangle$, the last term in eq.(2.37) vanishes. Similarly, it is easy to see that the third term is essentially constant, while the fourth one is negligeable, since $m_0|\mathbf{p}|/m_1 m_2 \ll 1$ *par default*. In Fig. 2.2 we plot the profiles of the two resulting potentials.

It would then be possible, in principle, to determine which field representation, Proca or $\{X_\mu, B_{\nu\kappa}\}$, better describes the interaction at hand. It is worth mentioning that this difference is regulated by the $1/m_1$ factor in the second term of eq.(2.37), so that only the lightest fermions would contribute significantly.

The calculation we performed is based on the scattering amplitude in the NR limit and the potential obtained is also suitable to be introduced into the Schrödinger equation as a time-independent perturbation. This is a reasonable approach if these corrections are relatively small, which is expected given that the standard quantum mechanical/QED results are in good agreement with experiments.

If we take e.g. the second line of eq.(2.35) we notice a coupling of the angular momentum with the spin. Such a spin-orbit coupling is also found in the hydrogen atom, contributing to its fine structure. Supposing that the proton and electron are charged under the symmetries leading to the $\{X_\mu B_{\nu\kappa}\}$ fields, we can calculate a correction to the energy levels of their bound state due to $\langle X_\mu B_{\kappa\lambda} \rangle$ exchange to obtain a rough estimation for the $V - PT$ coupling constants.

Expanding the exponential in $1-(1+m_0 r)e^{-m_0 r}$ and keeping only the leading term, the spin-orbit term simplifies to

$$V^{\rm LS}_{\rm V-PT} \;=\; \frac{\sqrt{2} g_1^V g_2^{PT} m_0}{8\pi\mu}\frac{1}{r}\mathbf{L}\cdot\mathbf{S} \tag{2.38}$$

with $\mathbf{S}=\langle\boldsymbol{\sigma}\rangle/2$. Applying first-order perturbation theory to this potential gives a correction to the energy of

$$\Delta E^{\rm LS} = \frac{g_1^V g_2^{PT} m_0}{8\pi\sqrt{2}\mu(n^2 a_0)} X_l, \tag{2.39}$$

where $X_l = l$ for $j = l+1/2$ and $X_l = -(l+1)$ for $j = l-1/2$. As we are interested in a simple estimate, we take $|X_l|/n^2 \sim 1$. Given that the reduced mass and the Bohr radius are $\mu \simeq m_e = 5.11\times 10^5$ eV and $a_0 = 2.69\times 10^{-4}\,\mathrm{eV}^{-1}$, respectively, we can constrain[10] $\Delta E^{\rm LS}$ to be smaller than the current spectroscopic uncertainties of one part in 10^{14} [59]. We then obtain $|g^V g^{PT}| < 10^{-8}$, for a mass of order $m_0 \sim 10^{-2}$ eV.

In summary, we studied an alternative formulation for a massive spin-1 boson which mixes tensor and vector fields through a topological mass term (this is to be compared with the usual Proca case). The topological construction has an interesting feature, the automatic preservation of gauge invariance – this is not so in the typical Proca case. We discussed that, when the 2-rank field is coupled to a tensor current, the field redefinitions discussed in Section 1.3 are not applicable [85]. This indicates that, in the presence of pseudo-tensor or tensor sources, new interparticle potentials may arise. These have been explicitly treated in Section 2.5.

Our focus in Ref. [66] was not on setting experimental limits on the coupling constants and mass of possible new mediators[11], but rather on checking the effect of the extra off-shell d.o.f. from the topological CSKR system on the potential energy of fermionic sources, specially in the presence of a coupling between B and a tensor current. The first step in this direction was to extract the propagators (cf. Section 1.4), whereby we – not very surprisingly – observe that the CSKR system requires new generalized spin projectors (also the $S_{\mu\nu\alpha}$ operator) to close an algebra and allow the inversion of the wave operator. We found that the mixed propagator $\langle X_\mu B_{\nu\kappa}\rangle$ has a non-trivial dependence on the momentum transfer; this is ultimately responsible for the somewhat richer class of potentials between (pseudo-)vector and (pseudo-)tensor sources.

[10] This is naturally an overly optimistic statement; our goal here is simply to have an idea of possible applications rather than to extract precise upper limits on the couplings.

[11] The attempt performed in the last section in the context of the hydrogen atom was simply a brief application example. In principle all potentials would have to be taken into account.

In Sections 2.4 and 2.5 we explored the potentials generated when sources of different forms exchange either a Proca or CSKR boson and analysed the resulting spin- and velocity-dependence. When a pure vector gauge boson – be it A^μ or X^μ – is exchanged between vector currents, we obtain essentially the same results. This was expected and shows that it is the presence of the extra tensor gauge potential in the CSKR system that is responsible for the variety of potentials, specially when tensor sources are considered. This answers our initial question of whether the way we choose to represent the mediating particle is relevant despite of having the same on-shell properties, but conditioned to the form os the matter currents available to couple with the gauge potentials.

We found that monopole-monopole, monopole-dipole and dipole-dipole spin-interactions are generated and constitute long-range interactions (assuming light enough mediators). These are specially interesting in the presence of spin-polarized sources – experimentally this is still a tricky point once uniformly polarized macroscopic bodies are hard to attain [104, 105] – and the potentials found display clearly different profiles[12], therefore generating distinct spin-dependent forces that could be in principle experimentally detectable, as they may contrast with the usual standard electromagnetic and/or gravitational forces.

The study performed in Ref. [66] and discussed here in further detail has served as motivation to pursue a more thorough investigation of the role played by spin in interparticle interactions. Chapter 3 presents the summary of this effort (which was also published [67]) in the context of interactions between spin-1/2 and spin-1 sources, but mediated via "standard" scalar or Proca bosons. In order to better understand spin-dependent interactions, in the next chapter we also go beyond the NR approximation we used here (we use some nomenclature and concepts already introduced in this and in the previous chapters).

The content and results presented in this chapter stem from the cited references, parts of my own published work [66] – in collaboration with my Brazilian advisor, prof. José Abdalla Helayël-Neto, Leonardo Ospedal and Felipe Gomes Ferreira – and original independent modifications thereof. We have shared both writing and calculational work in Ref. [66]. This chapter also contains informations that will be used in the next chapter, which refers to my second publication [67]. Some of the topics presented here also stem from the material covered in lectures given by my Brazilian advisor at CBPF[13].

[12] As remarked in Section 2.5, a very distinctive contribution is the one $\sim \mathbf{L}\cdot\langle\boldsymbol{\sigma}\rangle$, which is exclusive to the CSKR system.

[13] Since 2008, most of the lectures given by members of our research group is recorded in video and is publicly available at the website: `www.professorglobal.com.br/fisica`.

Chapter 3

Spin-dependent potentials for spin-1/2 and spin-1 matter sources

This chapter is based upon the published work "Comparative aspects of spin-dependent interaction potentials for spin-1/2 and spin-1 matter fields" [67] whose content has been significantly expanded to help clarify the discussion. This work was done in collaboration with L.P.R. Ospedal, K. Veiga and J.A. Helayël-Neto (advisor), and we have shared both writing and calculational work.

3.1 Introduction

Back in 1950, Matthews and Salam [129] and subsequently Salam in 1952 [130, 131] clarified the quantum field-theoretical approach to the electrodynamics of (massive) charged scalar particles. Ever since, the problem of extending this investigation to include the case of charged vector particles became mandatory in view of the theoretical evidence for the role of charged and neutral spin-1 particles that couple to charged and neutral currents. The later experimental discovery of the $W^{\pm}$ and Z^0 bosons enforced this even further [2].

From 1960, Komar and Salam [132], Salam [133, 134], Lee and Yang [135] and Delbourgo and Salam [136], gave a push for the construction of a fundamental theory for the microscopic interaction between charged vector bosons and photons. Further works by Tzou [137], Aronson [138] and Velo and Zwanziger [139] summed up efforts to the previous papers and the final conclusion was that a consistent unitary and renormalizable quantum field-theoretical model would be possible only in a non-Abelian scenario with a Higgs sector that gives mass to the vector bosons, without spoiling the unitarity bounds for the cross section of the scattering of longitudinally polarized charged vector bosons [140]. Again, this is in line with the theoretical

expectations and experimental discovery of the non-Abelian gauge mediators and, more recently, also with the discovery of the Higgs boson in 2012 [15, 16].

We adopt the following framework: the electrodynamics of (massive) charged vector bosons with a non-minimal dipole-type term coupling to the gauge field. In the case of the massless photon, this ensures tree-level $g = 2$ for spin-1 particles. We should, however, point out that this dipole-type interaction is non-minimal from the viewpoint of an Abelian symmetry. If we take into account the local $SU(2)$ symmetry that backs up the plus- and minus-charged vector bosons, the dipole coupling in the action is actually a minimal $SU(2)$ interaction term after spontaneous symmetry breaking has taken place, cf. Section 3.2.2.

Here, our main effort consists in pursuing an investigation of the semi-classical aspects of the charge and spin interactions for massive charged matter of a vector nature. Our central purpose is to compare the features and specific profiles of the influence of the spin of the charge carriers on interaction potentials (electromagnetic or a more general $U(1)$ interaction) between two different categories of sources: fermionic (spin-1/2) and bosonic (spin-1).

At this point, we highlight that the literature in the topic is focused on the discussion of the structure of the electromagnetic current and electrodynamical aspects of spin-1 charged matter [141–150]. We pursue an investigation of an issue not considered in connection with spin-1 charged matter: the spin- and velocity-dependence of the interaction potential associated with (pseudo-)scalar sources and pseudo-vector currents that interact by exchanging scalar and vector mediators, respectively. For the spin-1, these specific cases have not been addressed in the literature. These extra sources may not necessarily be associated to the electromagnetic interaction in that they do not follow from the $U(1)$ symmetry of the electromagnetism.

Here we take the following point of view: we may be describing a new force between these extra sources/currents whose origin could be traced back to some more fundamental physics[1]. The case of the usual vector current is reassessed here and our results match with the ones in the literature. Here, as in Chapter 2, we assume that the non-vector currents (S, PS and PV) are conserved, so that longitudinal contributions such as the one from eq.(3.48) will not be considered in general. It is worth mentioning that fermionic sources/currents can display a wide range of spin-dependent interparticle potentials [66, 107, 113], and many of them are reconsidered in this chapter[2].

[1]Therefore some of the coupling constants may have a non-zero mass dimension.

[2]Some of the potentials obtained here, specially for spin-1/2 sources, are essentially equal to the ones found in Chapter 2. This is naturally no coincidence, for in the present chapter we have used currents in a higher order in v/c, therefore creating terms which are higher order in $1/r$.

The electrodynamics of ordinary fermionic matter is very well understood, from the macroscopic to the quantum level. However, charged scalar and vector bosons also experience a rich variety of interactions when coupled to the electromagnetic field. So far, most of the theoretical and experimental literature dealing with macroscopic interactions consider only spin-1/2 matter, i.e., fermionic sources [114, 116, 127]. This preference is natural: ordinary charges in matter are carried by electrons, which are readily available at low energies.

Elementary spin-1 charged particles are difficult to observe: the only known examples are the $W^{\pm}$, whose mass is too large (lifetime too short) to allow direct inspection [2]. Though not stable enough to be directly handled, spin-1 particles have, in principle, their own electrodynamics and it is of theoretical interest to study its deviations, or not, from its fermionic counterpart. This would tell us more about the effect of different spins in the interaction with the electromagnetic fields. On the other hand, at the atomic and nuclear level, it would be a good motivation to have a spin- and velocity-dependent expression for the electromagnetic potential between ionised spin-1 atoms and charged spin-1 nuclei or hypernuclei [152, 153].

We highlight here a particular feature of bosonic charge carriers as far as the electromagnetic interactions are concerned. From a purely macroscopic point of view, the Maxwell equations address the problem of determining field configurations from given charge and current densities and a number of duly specified boundary conditions. They do not take into account the microscopic nature of these sources (ρ and $\mathbf{j}$, respectively). If a microscopic description of charged matter in terms of classical fields is given (based on a local $U(1)$ symmetry), the particular aspects of the charge carriers become salient and London-type terms may arise [154]. We shall be more specific about this point at the final section of this chapter, where we render more evident the peculiarities of the spin of the charge carriers in the electromagnetic and general Abelian interactions.

This self-contained chapter is based upon the published work [67], though many parts have been extended by me. In Section 3.2 we review the concept of potential and conventions employed (similar to those of Chapters 1 and 2). In Section 3.3 we obtain the currents and respective potentials, discussing the similarities between spin-1/2 and spin-1 sources. We consider, in Section 3.4, another possible representation for the spin-1 charged carrier (rank-2 tensor) and work out the corresponding current-current potentials[3]. Finally, in Section 3.5 we present our conclusions. Appendix A summarizes the currents in their relativistic form.

[3]Section 3.4 was the focus of the PhD thesis from Kim Veiga, which was defended in 2015 at CBPF. For completeness, here I have shortened the discussion and just presented the main results.

3.2 Methodology

Since we are interested in comparing the low-energy behavior of spin-1/2 and spin-1 as interacting matter, it is convenient to work in the non-relativistic (NR) limit. For simplicity we work in the center of mass (CM) reference frame in which particle 1 has initial and final 3-momenta given by $\mathbf{P} = \mathbf{p} - \mathbf{q}/2$ and $\mathbf{P}' = \mathbf{p} + \mathbf{q}/2$, respectively. Here, $\mathbf{p}$ is the average momentum of particle 1, while $\mathbf{q}$ is the momentum transfer carried by the intermediate boson, cf. Fig. 2.1.

As in Chapter 2, the interparticle potential is calculated through the first Born approximation [118]. It is clear from the NR currents presented below that not only velocity-dependent terms will arise, but also spin-dependent ones[4]. This is due to our choice of keeping terms in the currents which go beyond the zeroth order (static) case. Furthermore, in the amplitude we will keep only terms up to second order in $|\mathbf{p}|/m_{1,2}$ and/or in $|\mathbf{q}|/m_{1,2}$ – note that in Section 2.3 we kept terms in the amplitude of only first order in these parameters. The main reason to do so was to determine whether new spin patterns would arise in the potentials if we go to higher orders.

The Feynman rules for the tree-level diagram are equivalent to taking $iJ_{1,2}$ as the interaction vertices, where $J_{1,2}$ are the NR matter currents associated with particles 1 and 2, respectively. The corresponding NR amplitudes may then be written as $\mathcal{A} = iJ_1\langle\text{prop.}\rangle J_2$, where $\langle\text{prop.}\rangle$ is the momentum-space propagator of the intermediate boson with adequate Lorentz indices as the case may be (cf. Section 2.4). In this chapter we are interested in interactions mediated by massive neutral scalars (Klein-Gordon-type) and spin-1 vector particles (Proca-type), whose momentum-space propagators are:

$$\langle\phi\phi\rangle = \frac{i}{q^2 - m_\phi^2} \tag{3.1}$$

$$\langle A_\mu A_\nu\rangle = \frac{-i}{q^2 - m_A^2}\left(\eta_{\mu\nu} - \frac{q_\mu q_\nu}{m_A^2}\right). \tag{3.2}$$

The currents J_1 and J_2, as representatives of the respective vertices, must translate the different possible couplings to the gauge sector: scalar, pseudo-scalar, vector and pseudo-vector. The vector currents are obtained from the Lagrangian through the Noether method, but, for the bosonic case, we consider only first order in the electromagnetic coupling constant e, since we wish to compute $\mathcal{A}$ to second order in e (we discuss this in more details in Section 3.2.2). The other currents are built based on the principle that they should be bilinear in the field and its complex conjugate and reflect the desired symmetry.

[4] As in Chapter 2, we have $q^0 = 0$, i.e., q is space-like: $q^2 = -\mathbf{q}^2$, and $\mathbf{p}\cdot\mathbf{q} = 0$.

Below we recall some properties from spin-1/2 and spin-1 fields. For the latter we start from the rest frame, where the essential degrees of freedom become apparent, and then Lorentz-boost it to the laboratory (LAB) frame. This will be important when we calculate the NR limit of each current and then apply them to extract the interparticle potential (cf. Appendix A). Here we choose to work the spin-1 in its vector-field representation, but, in Section 3.4 we briefly discuss it in its less usual tensor representation [147, 148, 155].

3.2.1 Spin-1/2

For the sake of completeness, we present the well-known properties of Dirac fermions. The Dirac equation for the positive-energy spinors is, in momentum-space,

$$[\gamma^\mu P_\mu - m]\, u(P) = 0 \tag{3.3}$$

with a corresponding equation for $\bar{u} \equiv u^\dagger \gamma^0$; here $\bar{u} = \bar{u}(P')$.

Manipulating eq.(3.3) and its conjugate we obtain the Gordon decomposition of the vector current (which is usually obtained via the Noether method [73])

$$\bar{u}\gamma^\mu u = \frac{p^\mu}{m}\,\bar{u}u + \frac{i}{m}\,q_\nu\,\bar{u}\,\Sigma^{\mu\nu}\,u \tag{3.4}$$

expressed in terms of $p \equiv (P + P')/2$, the average momentum, and $q \equiv P' - P$, the momentum transfer. The spin matrix is $\Sigma^{\mu\nu} \equiv \frac{i}{4}\,[\gamma^\mu, \gamma^\nu]$. Similar decompositions are possible for other bilinear forms, for example

$$q_\mu\,\bar{u}\gamma^\mu\gamma_5 u = 2m\,\bar{u}\gamma_5 u. \tag{3.5}$$

The Gordon decomposition of the vector current, eq.(3.4), yields a first term proportional to the field density $\sim |u|^2$ and a second one involving a coupling between momentum transfer and the spin matrix in a given representation [156]. This connection will be responsible for the zeroth-order magnetic dipole moment interaction of the fermion with gyromagnetic ratio $g = 2$ [73]. Interestingly enough, the structure found for the Gordon decomposition for the spin-1/2 will have a perfect analog in the spin-1 case if we correctly include a non-minimal coupling, cf. Section 3.2.2.

Our interparticle potentials are derived from an effective Lagrangian describing the interactions between the exchanged (scalar or vector) particles and the fermionic sources. The Lagrangian is

$$\mathcal{L}_{\rm int}^{s=1/2} = \bar{\psi}\left[\left(g_{\rm S} + g_{\rm PS} i\gamma_5\right)\phi + \left(g_{\rm V}\gamma^\mu + g_{\rm PV}\gamma^\mu\gamma_5\right)A_\mu\right]\psi, \tag{3.6}$$

where the different couplings are all dimensionless. Henceforth we denote the coupling constant $g_{\rm V} \equiv e$ whenever considering the electromagnetic interaction (massless mediator).

The scalar (S) and pseudo-scalar (PS) sources are not conserved and, since we are dealing with a massive Dirac field, we also have a non-conserved pseudo-vector (PV) current, cf. eq.(3.5). As pointed out by Boulware [157], the Proca-type field, whenever coupled to a conserved current, leads to a renormalizable model. In general, the Proca propagator is problematic, as already mentioned in Section 1.1, since, in the high-energy limit, it behaves like a constant (independent of momentum). At tree level this is fine whenever the massive boson is coupled to conserved currents, but when loops are considered, the associated momentum integrals are not quite compensated by the propagators, as it is in the case of QED – there the divergences are less severe – so the divergences here become stronger as the number of loops increases.

This divergent behavior is caused by the $\sim k_\alpha k_\beta/m^2$ piece of the Proca propagator and it would require an infinite number of counter-terms to eliminate all the divergences. This can be avoided, in the context of a Higgs mechanism, by adopting the 't Hooft gauge, which generates a QED-like propagator for the Proca field, thus behaving well in the $k \to \infty$ limit [158]. Incidentally, this was one of the compelling theoretical arguments in favor of the Higgs (mechanism) prior to its experimental discovery.

For this reason, we take the coupling between the PV current and Proca-type field as an effective interaction. The UV divergences do not harm our purposes here, since we are interested in the low-energy regime described by the interparticle potential. Actually, our external currents are tailored in the NR regime, meaning that we are working way below the scale where UV divergences may show up.

3.2.2 Spin-1

We have reviewed some basic aspects concerning spin-1/2 particles above. Here, we would like to follow up with a similar discussion for massive charged spin-1 particles. We start off by discussing the vector field representation for a massive charged spin-1 particle, whose dynamics can be obtained from the following Lagrangian:

$$\mathcal{L}_{\rm vec.} = -\frac{1}{2}\,\mathcal{W}^*_{\mu\nu}\mathcal{W}^{\mu\nu} + m^2\,W^*_\mu W^\mu + ie(g-1)W^*_\mu W_\nu F^{\mu\nu} \tag{3.7}$$

where m is the mass and $\mathcal{W}_{\mu\nu}$ is the gauge-covariant field-strength tensor given by $D_\mu W_\nu - D_\nu W_\mu$ with $D_\mu = \partial_\mu + ieA_\mu$ being the covariant derivative.

One can see that the Lagrangian above is invariant under $U(1)$ gauge transformations on the spin-1 matter fields: $W_\mu(x) \to W'_\mu(x) = e^{-i\alpha(x)}W_\mu(x)$, with $\alpha(x)$ being related to the gauge transformation of A_μ via $A_\mu(x) \to A'_\mu(x) = A_\mu(x) + \partial_\mu\alpha(x)$. Though gauge invariant, it is clear that the last term in $\mathcal{L}_{\text{vec.}}$ is not minimal in the usual sense (i.e., the electromagnetic interaction is not via the gauge potentials, but rather the field-strength tensors themselves).

This last term is said to be a *non-minimal* coupling between the bosonic matter fields and the field strength of the interaction mediator. It asserts that $g = 2$ at tree level for the spin-1 particle [159–161]. This can be shown by considering the NR limit of the equations of motion for W_μ, where it becomes visible that the extra term in eq.(3.7) is responsible for correcting the value of the gyromagnetic factor. Actually, without it we would find $g = 1$, which is just half of the *allegedly* correct tree-level value, as we argue below.

A brief comment on the minimal or non-minimal character of the g-dependent term in $\mathcal{L}_{\text{vec.}}$ is in order, but, for this, let us consider the larger picture: the $SU(2)_L \otimes U(1)_Y$ Standard Model [4], where charged massive spin-1 bosons naturally live. Due to the non-Abelian character of the symmetry group, the field-strength tensor for the associated gauge bosons is modified and reads $F_a^{\mu\nu} = \partial^\mu W_a^\nu - \partial^\nu W_a^\mu + g_L\epsilon_{abc}W_b^\mu W_c^\nu$, where g_L is the $SU(2)_L$ coupling constant and a, b, c represent generator indices.[5]. It must be noted that this is the generalization of the Abelian field strength and this is necessary in order to account for the more complicated transformation properties of the fields themselves.

In the general Lagrangian of the SM one finds, among the contributions from the Higgs, pure leptons, etc, the pure kinetic part for the gauge bosons, $\mathcal{L}_B = -\frac{1}{4}F_a^{\mu\nu}F^a_{\mu\nu} - \frac{1}{4}Y^{\mu\nu}Y_{\mu\nu}$, where the second term is for the gauge boson associated with the (weak) hypercharge. More specifically, one finds an interesting term, namely,

$$\mathcal{L}_B \supset g_L\epsilon_{abc}W_\mu^a W_\nu^b \partial^\mu W_c^\nu,$$

which, if we use the usual definitions of the $W_\mu^\pm$ fields in terms of the $W_\mu^{1,2}$ and that $W_\mu^3 \sim \sin\theta_W A_\mu$, may be re-written as

$$\mathcal{L}_B \supset ig_L \sin\theta_W W_\mu^+ W_\nu^- F^{\mu\nu} + \cdots, \tag{3.8}$$

where $F^{\mu\nu} = \partial^\mu A^\nu - \partial^\nu A^\mu$ is the field-strength tensor of the usual photon and the ellipsis denotes the other terms which do not interest us here.

[5]Remember that $SU(2)$ has three generators, which, in the adjoint representation, are given by $(\tau_a)_{bc} = -i\epsilon_{abc}$.

What can we learn from eq.(3.8)? First of all, if we use that $g_L \sin\theta_W \equiv e$ [4], we obtain $\mathcal{L}_B \supset ieW^+_\mu W^-_\nu F^{\mu\nu}$, which is exactly what we had in eq.(3.7) for our (Abelian) spin-1 bosons. This result only comes about after spontaneous symmetry breaking has taken place, so we see that this term, which seems a bit alien in the Abelian context, is completely natural in the non-Abelian scenario. This justifies our previous statement, since, in an Abelian formulation, this contribution is definitely non-minimal, but, if we search for its $SU(2)_L$ roots, we see that it is actually a minimal coupling, but from a non-Abelian perspective.

After this short detour, let us get back on track. The field $W^\mu = (W^0, \mathbf{W})$ has, in principle, four degrees of freedom (see below). The equations of motion read

$$D_\mu \mathcal{W}^{\mu\nu} + m^2 W^\nu - ie(g-1)W_\mu F^{\mu\nu} = 0 \tag{3.9}$$

with analogue ones for the complex conjugated field.

Our goal is to characterize the interaction potentials between spin-1 sources exchanging scalar or vector fields, so the asymptotic states are the (free) particle states composed only of W fields. Therefore, we use the free-field equations, which reduce to $\partial_\mu W^{\mu\nu} + m^2 W^\nu = 0$.

In this situation the covariant derivatives reduce to the ordinary ones and, applying ∂_ν to the equations of motion and using the anti-symmetry of the field-strength tensor, we obtain the subsidiary condition $\partial_\mu W^\mu = 0$. This constraint is better seen in momentum space

$$W^0 = \frac{1}{E}\mathbf{P}\cdot\mathbf{W}, \tag{3.10}$$

where we have used the same symbol to denote the field in position and momentum spaces. This equation relates different components of W and reduces the number of degrees of freedom from four to three. The time component is proportional to the longitudinal projection of $\mathbf{W}$. It is first order in $\boldsymbol{\beta} = \mathbf{P}/E$, thus playing the role of a "small" component similar to the spin-1/2 case.

It also allows us to write W^μ in its rest frame as $W^\mu_{\text{rest}} = N_W\,(0, \boldsymbol{\epsilon})$, where $\boldsymbol{\epsilon}$ stands for the dimensionless polarization 3-vector and N_W is a normalization constant. The next step is to bring the system from rest into motion (i.e., to the LAB frame) via an appropriate Lorentz transformation. In doing so, we obtain[6]

$$W^\mu_{\text{lab}} = N_W \left[\frac{1}{m}(\mathbf{P}\cdot\boldsymbol{\epsilon})\ ,\ \boldsymbol{\epsilon} + \frac{1}{m(E+m)}(\mathbf{P}\cdot\boldsymbol{\epsilon})\mathbf{P}\right] \tag{3.11}$$

and with this, two comments are in order:

[6]It is easy to see that eq.(3.11) satisfies the subsidiary condition, eq.(3.10).

- Eq.(3.10) tells us that, in the rest frame (where $\mathbf{P} = 0$), all the information about the vector field is contained in its spatial part. In this frame the only 3-vector available is the polarization, i.e., its spin, which again enforces the vector character of the field.

- The normalization constant is given[7] by $N_W = 1$.

Let us now make some considerations on the vector currents, both global and local, associated with eq.(3.7). At the global level, i.e., prior to the gauging of the $U(1)$ symmetry, the Noether current (in configuration space) reads

$$J^{\mu}_{\text{global}} = ie\left(W^{*\mu\nu}W_{\nu} - W^{\mu\nu}W^{*}_{\nu}\right), \tag{3.12}$$

where no covariant derivative is involved. Upon the gauging of the symmetry, and by including the non-minimal coupling, the current changes into

$$J^{\mu}_{\text{V}} = ie\left(\mathcal{W}^{*\mu\nu}W_{\nu} - \mathcal{W}^{\mu\nu}W^{*}_{\nu}\right) + ie(g-1)\partial_{\nu}\left(W^{\nu}W^{*\mu} - W^{*\nu}W^{\mu}\right). \tag{3.13}$$

To calculate the current-current potential at tree level (one-boson exchange), we actually only consider the current to the first order in the coupling constant, e. This amounts to neglecting the terms in the gauge potential present in the current in eq.(3.13). In other words: to calculate the potential to order e^2, we consider the current only up to order e. Therefore, to the desired order in e, the vector current is globally conserved plus the non-minimal g-term. The consequences of the e^2-terms are only seen when two-photon exchange is included.

At the approximation level we are working with (matter currents contain no gauge fields), the current J^{μ}_{V} is given by the global and non-minimal terms, as displayed in the second line of eq.(3.14) below:

$$\begin{aligned}
\mathcal{L}^{s=1}_{\text{int}} &= \left[g_{\text{S}}W^{*}_{\mu}W^{\mu} + g_{\text{PS}}W^{*}_{\mu\nu}\tilde{W}^{\mu\nu}\right]\phi + \\
&+ ig_{\text{V}}\left[W^{*\,\mu\nu}W_{\nu} - W^{\mu\nu}W^{*}_{\nu} + (g-1)\partial_{\nu}\left(W^{\nu}W^{*\mu} - W^{*\nu}W^{\mu}\right)\right]A_{\mu} + \\
&+ ig_{\text{PV}}\left[\tilde{W}^{*\,\mu\nu}W_{\nu} - \tilde{W}^{\mu\nu}W^{*}_{\nu}\right]A_{\mu},
\end{aligned} \tag{3.14}$$

where the coupling constants have the following mass dimensions: $[g_{\text{S}}] = -[g_{\text{PS}}] = 1$ and $[g_{\text{V}}] = [g_{\text{PV}}] = 0$. We denote the dual of $W_{\mu\nu}$ by $\tilde{W}_{\mu\nu} \equiv \frac{1}{2}\,\epsilon_{\mu\nu\alpha\beta}W^{\alpha\beta}$. We also note that the (global) PV bosonic current is conserved in a topological sense, i.e., without making use of either the equations of motion or the symmetries of the Lagrangian.

[7] Note that this differs from the normalization for the tensor representation (cf. Section 3.4).

This is not so for the fermionic PV current and this will lead to extra *longitudinal* terms in the potentials involving two PV spin-1/2 sources, as will be seen in Section 3.3.3 (this was also mentioned in Section 2.4). As in the case of spin-1/2, the S and PS sources for spin-1 are equally not conserved, but in this case there is obviously no longitudinal contribution, since we are dealing with scalar mediators. In general, though, we are assuming that these "non-vector" currents stem from symmetries present in some high-energy scale, whereby they are exactly conserved and we shall mostly ignore possible longitudinal contributions.

The vector current may be written in terms of the fields W^μ and the variables $\{p, q\}$. For this, let us introduce the generators $(\Sigma_{\rm V}^{\mu\nu})_{\alpha\beta} \equiv -i\left(\delta^\mu_\alpha\delta^\nu_\beta - \delta^\nu_\alpha\delta^\mu_\beta\right)$, which may be related to the spin operators via $\Sigma_{ij} = \epsilon_{ijk}S_k$, with $(S_i)_{jk} = -i\epsilon_{ijk}$. Now, by using the equations of motion and the (free) subsidiary condition, we may re-write the vector current in momentum space as

$$J^\mu_{\rm V}(p,q) = 2ep^\mu W^*_\nu W^\nu + iegq_\nu W^{*\,\alpha}\,(\Sigma_{\rm V}^{\mu\nu})_{\alpha\beta}\,W^\beta \tag{3.15}$$

in which, as for the spin-1/2 case, we have set $g_V \equiv e$.

In the equation above we left the g-factor explicit but in the NR limits we shall use its tree-level value, $g = 2$. Equation (3.15) is nothing but the Gordon decomposition for the vector field representation of a massive and charged spin-1 and the similarity with the spin-1/2 case, eq.(3.4), is remarkable. This Gordon decomposition for spin-1 particles was found independently and agrees with the results of Delgado-Acosta *et al.* [147].

3.3 Non-relativistic currents and potentials

Following the indications above, we present below the NR limit of the currents, which may be extracted (in configuration space) from Lagrangians (3.6) and (3.14) as $J\phi$ or $J_\mu A^\mu$, as the case may be. In the following, the fields are already normalized[8].

We point out that the matter sources developed in this section are for "particle 1", i.e., the left vertex in Fig. 2.1. The second current may be obtained by taking $\mathbf{q} \to -\mathbf{q}$, $\mathbf{p} \to -\mathbf{p}$ in the first one. Also, in the fermionic case, we shall denote the expectation value of its spin, σ_i, by contracting the basic spinors ξ with the Pauli matrices, namely, $\langle\sigma_i\rangle \equiv \xi^\dagger\sigma_i\xi$. Similarly, in the bosonic case, the spin matrix of the particle is $(S_i)_{jk} = -i\epsilon_{ijk}$ and its expectation value is given by $\langle S_i\rangle \equiv \boldsymbol{\epsilon}^*_j\,(S_i)_{jk}\,\boldsymbol{\epsilon}_k$.

[8]From now on, for the sake of clarity, we shall adopt the variables $\{p, q\}$ instead of $\{P, P'\}$, so $u(P) = u(p - q/2)$ and $\bar{u}(P') = \bar{u}(p + q/2)$; similar definitions hold for $W_\mu(P)$ and $W^*_\mu(P')$.

A remark about our notation: in the process of calculating the amplitude factors, the objects $\xi^\dagger\xi \equiv \delta_i$ and $\boldsymbol{\epsilon}^* \cdot \boldsymbol{\epsilon} \equiv \delta_i$, with $i = 1, 2$ labelling the particle, will appear frequently. These indicate a possible spin flip between initial and final states[9], and we shall leave the δ_i explicit in the final expressions. As we shall see, the simplest monopole-monopole terms usually contain the product $\delta_1\delta_2$, but higher-order terms may contain just one δ_i.

3.3.1 On the normalizations in the non-relativistic limit

In Chapter 2 we pursued a similar analysis as in the present chapter to compare interparticle potentials in the low-energy limit, but with different focuses. There we worked in first order in the expansion parameter ($|\mathbf{p}|/m$) and this was enough to produce interesting spin and velocity effects. Also, in Chapter 2 we indicated that the normalization factor for fermions was given by $N_f \approx \sqrt{2m}$, so that, taking the NR correspondence between the Feynman amplitudes (cf. eq.(2.20)) into account, we had a pre-factor cancellation.

This is only possible if we ignore terms of $\mathcal{O}\left(|\mathbf{p}|^2/m^2\right)$, but in the present chapter we wish to go one step further and keep exactly these terms. This will affect the potentials, as the normalization factors will no longer cancel the energy pre-factors from eq.(2.20) – this is specially true for the case of spin-1/2 sources due to $N_f = \sqrt{E+m}$. In our published work [67] we inadvertently neglected this issue and assumed a static normalization; a few corrections had to be included (they are published as a *corrigendum* [68]). In the remainder of this chapter we discuss the updated results already taking these corrections into account. For the fully relativistic currents, please refer to Appendix A.

The need for the aforementioned corrections became clear when we looked at spin-1/2 fermions and the amplitudes built with them. As mentioned before, in Chapter 2, and in Ref. [66], we had an "accidental" cancellation, namely, $\frac{N_{f_1}^2 N_{f_2}^2}{2E_1 2E_2} \approx 1 + \mathcal{O}\left(|\mathbf{p}|^2/m^2\right)$, and this led us to inadvertently use the same result in Ref. [67]. It is clear that the second-order effects will induce new patterns of momentum dependence whenever they are multiplied by $\mathcal{O}(1)$ factors in the "uncorrected" amplitudes.

In order to correctly account for the transition from fully relativistic to non-relativistic, one has to first obtain the relativistic currents (i.e., with no approximations), then use eq.(2.20) to include the correction for the NR normalization – in this step appropriate NR approximations may be made. The first step is done and the relativistic currents are listed in Appendix A, while the second and most crucial

[9] Nevertheless, in general, low-energy interactions do not induce a change in the spin orientation of the particles involved.

step is fulfilled employing the following prescription:

$$J^{\rm NR} \;=\; \frac{1}{\sqrt{2E}\sqrt{2E'}} J^{\rm relat.} = \frac{1}{2E} J^{\rm relat.}, \tag{3.16}$$

where we used that $E' = E = \sqrt{\mathbf{P}^2 + m^2}$ for elastic collisions ($q^0 = 0$ and $\mathbf{P}^2 = \mathbf{P'}^2$). The NR amplitudes may then be read directly from

$$\mathcal{A} = i J_1^{\rm NR} \langle {\rm prop.} \rangle J_2^{\rm NR}, \tag{3.17}$$

and below we list the NR currents for the cases discussed in this section, namely, spin-1/2 and spin-1 in its vector representation.

Spin-1/2

In Section 2.2.1 we separated the bispinor from its energy-dependent normalization. Here we do the same: we start from the relativistic currents as explicitly stated in Section A.2.1, i.e., with the normalization factor, $N_f = \sqrt{E+m}$, kept out.

Now we include this factor, as well as the energy factors in the denominator, so the overall correction factor for these currents is

$$\begin{aligned} C_{\rm (s=1/2)} \;&=\; \frac{N_{f'} N_f}{\sqrt{2E}\sqrt{2E'}} = \frac{E+m}{2E} \\ &=\; 1 - \frac{1}{4m^2}\left(\mathbf{p}^2 + \frac{\mathbf{q}^2}{4}\right) + \mathcal{O}\left(|\mathbf{p}|^4/m^4\right), \end{aligned} \tag{3.18}$$

and we are now also free to assume $E + m \approx 2m$ in the denominator of momentum-dependent terms, as these will not be affected by the parts of the correction above which are $\mathcal{O}\left(|\mathbf{p}|^2/m^2\right)$, as this would go beyond our approximation level.

Below we list the NR currents with their basic wave functions already normalized and NR energy-dependent pre-factors already included à la eq.(3.16). The coupling constants are not explicitly given for the sake of clarity.

1) Scalar current (S):

$$\bar{u}(p+q/2)\, u(p-q/2) = \delta\left(1 - \frac{\mathbf{p}^2}{2m^2}\right) - \frac{i}{4m^2}\mathbf{q}\cdot(\mathbf{p}\times\langle\boldsymbol{\sigma}\rangle) \tag{3.19}$$

2) Pseudo-scalar current (PS):

$$\bar{u}(p+q/2)\, i\gamma_5\, u(p-q/2) = -\frac{i}{2m}\,\mathbf{q}\cdot\langle\boldsymbol{\sigma}\rangle \tag{3.20}$$

3) Vector current (V):

$$\bar{u}(p+q/2)\,\gamma^{\mu}\,u(p-q/2), \tag{3.21}$$

3i) For $\mu = 0$,

$$\bar{u}(p+q/2)\,\gamma^{0}\,u(p-q/2) = \delta\left(1-\frac{\mathbf{q}^2}{8m^2}\right)+\frac{i}{4m^2}\,(\mathbf{q}\times\mathbf{p})\cdot\langle\boldsymbol{\sigma}\rangle \tag{3.22}$$

3ii) For $\mu = i$,

$$\bar{u}(p+q/2)\,\gamma^{i}\,u(p-q/2) = \frac{\delta}{m}\mathbf{p}_i - \frac{i}{2m}\epsilon_{ijk}\mathbf{q}_j\langle\boldsymbol{\sigma}_k\rangle \tag{3.23}$$

4) Pseudo-vector current (PV):

$$\bar{u}(p+q/2)\gamma^{\mu}\gamma_5 u(p-q/2) \tag{3.24}$$

4i) For $\mu = 0$,

$$\bar{u}(p+q/2)\,\gamma^{0}\,\gamma_5\,u(p-q/2) = \frac{1}{m}\,\langle\boldsymbol{\sigma}\rangle\cdot\mathbf{p} \tag{3.25}$$

4ii) For $\mu = i$,

$$\begin{aligned}\bar{u}(p+q/2)\,\gamma^{i}\,\gamma_5\,u(p-q/2) &= \left(1-\frac{\mathbf{p}^2}{2m^2}\right)\langle\boldsymbol{\sigma}_i\rangle + \\ &- \frac{i\delta}{4m^2}\,(\mathbf{q}\times\mathbf{p})_i + \\ &+ \frac{1}{2m^2}\left[(\mathbf{p}\cdot\langle\boldsymbol{\sigma}\rangle)\,\mathbf{p}_i - \frac{1}{4}\,(\mathbf{q}\cdot\langle\boldsymbol{\sigma}\rangle)\,\mathbf{q}_i\right]\end{aligned} \tag{3.26}$$

Spin-1 (vec. rep.)

Similarly as done for the spin-1/2, here we include the following correction:

$$\begin{aligned}C_{(\mathrm{s}=1)} &= \frac{1}{\sqrt{2E}\sqrt{2E'}} = \frac{1}{2E} \\ &= \frac{1}{2m}\left[1-\frac{1}{2m^2}\left(\mathbf{p}^2-\frac{\mathbf{q}^2}{4}\right)\right]+\mathcal{O}\left(|\mathbf{p}|^4/m^4\right),\end{aligned} \tag{3.27}$$

where we used $N_W = 1$. This correction factor is the same for both spin-1 representations. Below we apply $C_{(\mathrm{s}=1)}$ and use $E + m \approx 2m$ in the denominator of the momentum-dependent terms.

1) Scalar current (S):

$$W^*_\mu(p+q/2)\,W^\mu(p-q/2) \;\simeq\; -\frac{1}{2m}\Bigg\{\delta\left[1-\frac{1}{2m^2}\left(\mathbf{p}^2+\frac{\mathbf{q}^2}{4}\right)\right]+ \\ -\;\frac{1}{2m^2}\left[i\,(\mathbf{q}\times\mathbf{p})\cdot\langle\mathbf{S}\rangle-(\mathbf{q}\cdot\boldsymbol{\epsilon}^*)\,(\mathbf{q}\cdot\boldsymbol{\epsilon})\right]\Bigg\} \tag{3.28}$$

2) Pseudo-scalar current (PS):

$$W^*_{\mu\nu}(p+q/2)\,\tilde{W}^{\mu\nu}(p-q/2)\simeq -i\mathbf{q}\cdot\langle\mathbf{S}\rangle \tag{3.29}$$

3) Vector current (V):

$$J^\mu_{\rm V}(p,q)=2p^\mu W^*_\nu W^\nu+igq_\nu W^{*\,\alpha}\left(\Sigma^{\mu\nu}_{\rm V}\right)_{\alpha\beta}W^\beta \tag{3.30}$$

3i) For $\mu=0$,

$$J^0_{\rm V}(p,q) \;=\; -\delta-\frac{g-1}{2m^2}\left[i\,(\mathbf{q}\times\mathbf{p})\cdot\langle\mathbf{S}\rangle-(\mathbf{q}\cdot\boldsymbol{\epsilon}^*)\,(\mathbf{q}\cdot\boldsymbol{\epsilon})\right] \tag{3.31}$$

3ii) For $\mu=i$,

$$J^i_{\rm V}(p,q)=-\frac{\delta}{m}\mathbf{p}_i+\frac{ig}{2m}\epsilon_{ijk}\mathbf{q}_j\langle\mathbf{S}_k\rangle \tag{3.32}$$

4) Pseudo-vector current (PV):

$$J^\mu_{\rm PV}(p,q)=\frac{i}{2}g\epsilon^{\mu\nu\kappa\lambda}q_\kappa W^{*\,\alpha}\left(\Sigma^{\rm V}_{\nu\lambda}\right)_{\alpha\beta}W^\beta \tag{3.33}$$

4i) For $\mu=0$,

$$J^0_{\rm PV}(p,q)=-\frac{i}{2m}\mathbf{q}\cdot\langle\mathbf{S}\rangle \tag{3.34}$$

4ii) For $\mu=i$,

$$J^i_{\rm PV}(p,q) \;=\; -\frac{1}{2m^2}\Bigg\{\left[\left(\mathbf{p}-\frac{1}{2}\mathbf{q}\right)\cdot\boldsymbol{\epsilon}\right](\mathbf{q}\times\boldsymbol{\epsilon}^*)_i+ \\ -\;\left[\left(\mathbf{p}+\frac{1}{2}\mathbf{q}\right)\cdot\boldsymbol{\epsilon}^*\right](\mathbf{q}\times\boldsymbol{\epsilon})_i\Bigg\} \tag{3.35}$$

Despite the objective of Ref. [67] and the present chapter be a comparative study of interparticle potentials, we see that the similarities between spin-1/2 and spin-1 sources are already evident at the level of the currents. The most important examples are the vector currents and their respective Gordon decompositions, eqs.(3.4) and (3.15): in both cases we find a "density" term coupled to the average momentum and a spin-dependent term coupled to the momentum transfer.

By comparing the vector currents, we notice essentially an extra term in the bosonic case associated with the contribution of the polarization, $(\mathbf{q}\cdot\boldsymbol{\epsilon})(\mathbf{q}\cdot\boldsymbol{\epsilon}^*)$. The PV currents display more remarkable differences. For example, for the $\mu = 0$ component we observe that the spin of the fermion couples to the average momentum $\mathbf{p}$, while for the bosons the spin couples to the momentum transfer $\mathbf{q}$. For the $\mu = i$ components we have many differences due to the spin terms. These special features will be responsible for the different behaviors of the bosonic and fermionic interparticle potentials.

Unlike the spin-1/2 V and PV currents, the V and PV currents for spin-1, as defined in Lagrangian (3.14) (marked by the V and PV coupling constants), always carry an explicit derivative. This is due to the presence of the field-strength tensors. At high energies, the extra derivatives (i.e., momentum factors) must dominate, but not in the NR limit.

The reader should be aware that the currents quoted in this thesis differ from those listed in Ref. [67], as already stressed above. The interparticle potentials presented in the following sections are the ones already corrected by the use of the NR currents above and match the results quoted in the *corrigendum* [68]. This thesis is therefore a more complete and organized guide to our potentials [67, 68].

3.3.2 Scalar (Klein-Gordon type) exchange

By means of the previous results we can carry out the calculations for the processes where scalar and/or pseudo-scalar currents exchange a massive Klein-Gordon-like mediator. Let us explicitly calculate the particular case of the $S-S$ interaction for both $s = 1$ and $s = 1/2$ sources.

We start with the fermionic case, for which the amplitude reads

$$\mathcal{A}_{\mathrm{S-S}} = \frac{1}{\mathbf{q}^2 + m_\phi^2}\, J_1^{\mathrm{NR}}\, J_2^{\mathrm{NR}}, \tag{3.36}$$

where we used eq.(3.2) with $q^0 = 0$. With the momentum assignments of Fig. 2.1, the NR current for particle 2 may be read from that for particle 1, eq.(3.19), by making $\mathbf{p} \to -\mathbf{p}$ and $\mathbf{q} \to -\mathbf{q}$.

Finally, the NR amplitude is obtained and reads

$$\begin{aligned}\mathcal{A}^{s=1/2}_{\rm S-S} &\simeq \frac{g^1_{\rm S} g^2_{\rm S}}{\mathbf{q}^2+m_\phi^2}\Bigg\{\delta_1\delta_2\left[1-\frac{1}{2}\left(\frac{1}{m_1^2}+\frac{1}{m_2^2}\right)\mathbf{p}^2\right]+\\ &- \frac{i}{4}\left(\mathbf{q}\times\mathbf{p}\right)\cdot\left[\frac{\delta_1\langle\boldsymbol{\sigma}\rangle_2}{m_2^2}+\frac{\delta_2\langle\boldsymbol{\sigma}\rangle_1}{m_1^2}\right]\Bigg\}\end{aligned} \tag{3.37}$$

and the Fourier transform yields the potential (cf. Section A.3):

$$\begin{aligned}V^{s=1/2}_{\rm S-S} &= -\frac{g^1_{\rm S} g^2_{\rm S}}{4\pi}\frac{e^{-m_\phi r}}{r}\Bigg\{\delta_1\delta_2\left[1-\frac{1}{2}\left(\frac{1}{m_1^2}+\frac{1}{m_2^2}\right)\mathbf{p}^2\right]+\\ &+ \frac{(1+m_\phi r)}{4r^2}\mathbf{L}\cdot\left(\frac{\delta_1\langle\boldsymbol{\sigma}\rangle_2}{m_2^2}+\frac{\delta_2\langle\boldsymbol{\sigma}\rangle_1}{m_1^2}\right)\Bigg\},\end{aligned} \tag{3.38}$$

where, as in Chapter 2, we defined $\mathbf{L}=\mathbf{r}\times\mathbf{p}$. Notice that, as previously advertised, single factors of δ_i have appeared, thus showing that the potential is not identically zero unless both δ_i are zero.

A similar approach can be used to obtain the NR amplitude for the case of spin-1 scalar sources, so that, following the same program, i.e., by using the NR limit of the bosonic scalar source, eq.(3.28), we obtain

$$\begin{aligned}\mathcal{A}^{s=1}_{\rm S-S} &\simeq \frac{g^1_{\rm S} g^2_{\rm S}}{4m_1m_2\left(\mathbf{q}^2+m_\phi^2\right)}\Bigg\{\delta_1\delta_2\left[1-\frac{1}{2}\left(\frac{1}{m_1^2}+\frac{1}{m_2^2}\right)\left(\mathbf{p}^2+\frac{\mathbf{q}^2}{4}\right)\right]+\\ &+ \left[\frac{\delta_1}{2m_2^2}\left[-i\left(\mathbf{q}\times\mathbf{p}\right)\cdot\langle\mathbf{S}\rangle_2+\left(\mathbf{q}\cdot\boldsymbol{\epsilon}_2^*\right)\left(\mathbf{q}\cdot\boldsymbol{\epsilon}_2\right)\right]+1\leftrightarrow 2\right]\Bigg\}\end{aligned}$$

and, performing the Fourier integral (cf. Section A.3), we get

$$\begin{aligned}V^{s=1}_{\rm S-S} &= -\frac{g^1_{\rm S} g^2_{\rm S}}{16\pi m_1m_2}\frac{e^{-m_\phi r}}{r}\Bigg\{\delta_1\delta_2\left[1-\frac{1}{2}\left(\frac{1}{m_1^2}+\frac{1}{m_2^2}\right)\left(\mathbf{p}^2-\frac{m_\phi^2}{4}\right)\right]+\\ &+ \frac{(1+m_\phi r)}{2r^2}\mathbf{L}\cdot\left(\frac{\delta_1\langle\mathbf{S}\rangle_2}{m_2^2}+\frac{\delta_2\langle\mathbf{S}\rangle_1}{m_1^2}\right)+\\ &+ \zeta\left[\frac{\delta_1}{2m_2^2r^2}\left[\delta_2(1+m_\phi r)-\left(\hat{\mathbf{r}}\cdot\boldsymbol{\epsilon}_2\right)\left(\hat{\mathbf{r}}\cdot\boldsymbol{\epsilon}_2^*\right)\left(3+3m_\phi r+m_\phi^2r^2\right)\right]+\ 1\leftrightarrow 2\right]\Bigg\}\\ &- \frac{g^1_{\rm S} g^2_{\rm S}}{96m_1m_2}\delta_1\delta_2\left(\frac{1}{m_1^2}+\frac{1}{m_2^2}\right)\delta^3(\mathbf{r}),\end{aligned} \tag{3.39}$$

where the parameter ζ in the last term may assume the values $\zeta=\pm1$. In eq.(3.39) its value is $\zeta=1$, but, in Section 3.4 the potential (3.39) also appears, but with $\zeta=-1$.

Here we notice that this potential describes the same interactions as in the fermionic case, namely, the Yukawa factor and a spin-orbit term, but it also displays a "polarization-polarization" interaction term, as well as a momentum- and spin-independent contact term.

Below, we quote the results for the other bosonic potentials:

$$V^{s=1}_{\mathrm{S-PS}} = -\frac{g^1_{\mathrm{S}} g^2_{\mathrm{PS}} \delta_1}{8\pi m_1} \frac{(1+m_\phi r) e^{-m_\phi r}}{r^2} \hat{\mathbf{r}} \cdot \langle \mathbf{S} \rangle_2 \tag{3.40}$$

$$\begin{aligned} V^{s=1}_{\mathrm{PS-PS}} &= \frac{g^1_{\mathrm{PS}} g^2_{\mathrm{PS}}}{4\pi} \frac{e^{-m_\phi r}}{r} \left\{ \left(m_\phi^2 + \frac{3m_\phi}{r} + \frac{3}{r^2} \right) (\hat{\mathbf{r}} \cdot \langle \mathbf{S} \rangle_1) (\hat{\mathbf{r}} \cdot \langle \mathbf{S} \rangle_2) + \right. \\ &- \left. \left(\frac{m_\phi}{r} + \frac{1}{r^2} \right) \langle \mathbf{S} \rangle_1 \cdot \langle \mathbf{S} \rangle_2 \right\} - \frac{g^1_{\mathrm{PS}} g^2_{\mathrm{PS}}}{3} \left(\langle \mathbf{S} \rangle_1 \cdot \langle \mathbf{S} \rangle_2 \right) \delta^3(\mathbf{r}), \end{aligned} \tag{3.41}$$

and we indicate that the fermionic $S-PS$ and $PS-PS$ potentials have the same functional form as the bosonic ones above. Apart from a global sign (for $PS-PS$), the results for $s=1$ above are very similar to those obtained by Moody and Wilczek in the context of fermionic sources exchanging pseudo-scalar bosons (axions) [107]. Indeed, they differ mainly by mass factors due the canonical mass dimension of our coupling constants.

3.3.3 Massive vector (Proca type) exchange

Let us now discuss the potentials involving V and PV currents mediated by a Proca-type particle. As already done previously, we exemplify the calculation through a particular configuration and then quote the final results. We choose to calculate one of the simplest cases explicitly: the interaction potential between vector and pseudo-vector spin-1 currents.

The amplitude is given by $\mathcal{A}^{s=1}_{\mathrm{V-PV}} = -\frac{1}{\mathbf{q}^2+m_A^2} J_1^{\mathrm{NR}\,\mu} J^{\mathrm{NR}}_{2\mu}$, where we have used current conservation to eliminate the longitudinal contribution of the Proca-type propagator, eq.(3.2). We need therefore to simplify the contraction $J_1^\mu J_{2\mu}$. According to our assumptions, only the $J_1^0 J_{2\,0}$ piece will contribute in the NR limit, so we get

$$\mathcal{A}^{s=1}_{\mathrm{V-PV}} \simeq i \frac{e_1 g^2_{\mathrm{PV}} \delta_1}{2m_2} \frac{\mathbf{q} \cdot \langle \mathbf{S} \rangle_2}{\mathbf{q}^2 + m_A^2}, \tag{3.42}$$

and we may finally calculate the Fourier integral (cf. Section A.3), which gives

$$V^{s=1}_{\mathrm{V-PV}} = \frac{e_1 g^2_{\mathrm{PV}} \delta_1}{8\pi m_2} \frac{(1+m_A r) e^{-m_A r}}{r^2} \hat{\mathbf{r}} \cdot \langle \mathbf{S} \rangle_2. \tag{3.43}$$

In a similar way, the case with spin-1/2 currents leads to

$$V_{\rm V-PV}^{s=1/2}=-\frac{e_1g_{\rm PV}^2}{4\pi}\,\frac{e^{-m_Ar}}{r}\left\{\delta_1\left(\frac{1}{m_1}+\frac{1}{m_2}\right)\mathbf{p}\cdot\langle\boldsymbol{\sigma}\rangle_2+\frac{(1+m_Ar)}{2m_1r}[\langle\boldsymbol{\sigma}\rangle_1\times\langle\boldsymbol{\sigma}\rangle_2]\cdot\hat{\mathbf{r}}\right\} \tag{3.44}$$

and here the PV current is not conserved. However, the conservation of the V current ensures that the longitudinal part of the Proca propagator drops out.

As we have already seen in the discussion of the currents, the PV currents of $s=1/2$ and $s=1$ exhibit remarkable differences and these explain why the potentials behave so differently. We anticipate that only this fermionic case yields the interaction with the $\mathbf{p}\cdot\langle\boldsymbol{\sigma}\rangle$ dependence and the spin-spin contribution of the form $\langle\boldsymbol{\sigma}\rangle_1\times\langle\boldsymbol{\sigma}\rangle_2$. In the bosonic case, we have the $\hat{\mathbf{r}}\cdot\langle\mathbf{S}\rangle$ dependence, but this is not exclusive of the $V-PV$ interaction, as it also appears in the $S-PS$ bosonic potential. The other potentials, $V-V$ and $PV-PV$, are listed below.

First we consider the case of the $V-V$ interaction between spin-1/2 sources:

$$\begin{aligned}
V_{\rm V-V}^{s=1/2} &= \frac{e_1e_2}{4\pi}\,\frac{e^{-m_Ar}}{r}\left\{\delta_1\delta_2\left[1+\frac{\mathbf{p}^2}{m_1m_2}+\frac{m_A^2}{8}\left(\frac{1}{m_1^2}+\frac{1}{m_2^2}\right)\right]+\right.\\
&- \frac{(1+m_Ar)}{2r^2}\mathbf{L}\cdot\left[\left(\frac{\delta_1\langle\boldsymbol{\sigma}\rangle_2}{2m_2^2}+\frac{\delta_2\langle\boldsymbol{\sigma}\rangle_1}{2m_1^2}\right)+\left(\frac{\delta_1\langle\boldsymbol{\sigma}\rangle_2}{m_1m_2}+\frac{\delta_2\langle\boldsymbol{\sigma}\rangle_1}{m_1m_2}\right)\right]+\\
&+ \frac{1}{4m_1m_2r^2}\langle\boldsymbol{\sigma}\rangle_1\cdot\langle\boldsymbol{\sigma}\rangle_2\left(1+m_Ar+m_A^2r^2\right)+\\
&- \left.\frac{1}{4m_1m_2r^2}\left(\langle\boldsymbol{\sigma}\rangle_1\cdot\hat{\mathbf{r}}\right)\left(\langle\boldsymbol{\sigma}\rangle_2\cdot\hat{\mathbf{r}}\right)\left(3+3m_Ar+m_A^2r^2\right)\right\}+\\
&- \frac{e_1e_2}{8}\left[\delta_1\delta_2\left(\frac{1}{m_1^2}+\frac{1}{m_2^2}\right)+\frac{4}{3m_1m_2}\langle\boldsymbol{\sigma}\rangle_1\cdot\langle\boldsymbol{\sigma}\rangle_2\right]\delta^3(\mathbf{r}),
\end{aligned} \tag{3.45}$$

where, as previously conventioned, $e_{1,2}$ stand for the electric charges of the particles (sources). The electromagnetic potential may be obtained as the limit of massless mediators. By setting $m_A=0$ we then find

$$\begin{aligned}
V_{\rm V-V}^{s=1/2}\Big|_{\rm EM} &= \frac{e_1e_2}{4\pi r}\left\{\delta_1\delta_2\left(1+\frac{\mathbf{p}^2}{m_1m_2}\right)+\right.\\
&- \frac{1}{2r^2}\mathbf{L}\cdot\left[\left(\frac{\delta_1\langle\boldsymbol{\sigma}\rangle_2}{2m_2^2}+\frac{\delta_2\langle\boldsymbol{\sigma}\rangle_1}{2m_1^2}\right)+\left(\frac{\delta_1\langle\boldsymbol{\sigma}\rangle_2}{m_1m_2}+\frac{\delta_2\langle\boldsymbol{\sigma}\rangle_1}{m_1m_2}\right)\right]+\\
&+ \left.\frac{1}{4m_1m_2r^2}\left[\langle\boldsymbol{\sigma}\rangle_1\cdot\langle\boldsymbol{\sigma}\rangle_2-3\left(\langle\boldsymbol{\sigma}\rangle_1\cdot\hat{\mathbf{r}}\right)\left(\langle\boldsymbol{\sigma}\rangle_2\cdot\hat{\mathbf{r}}\right)\right]\right\}+\\
&- \frac{e_1e_2}{8}\left[\delta_1\delta_2\left(\frac{1}{m_1^2}+\frac{1}{m_2^2}\right)+\frac{4}{3m_1m_2}\langle\boldsymbol{\sigma}\rangle_1\cdot\langle\boldsymbol{\sigma}\rangle_2\right]\delta^3(\mathbf{r}).
\end{aligned} \tag{3.46}$$

This reproduces the result from Holstein [119], with the exception of the $\sim \mathbf{p}^2/m_1 m_2$ monopole term (neglected in his NR approximation) and the contact terms (his focus is on long-range interactions). The contact terms, specially the spin-spin one, play an important role in multi-electron systems [162] and such short-range interactions will appear often in what follows.

For the $PV - PV$ case we obtain

$$\begin{aligned} V^{s=1/2}_{\mathrm{PV-PV}} &= -\frac{g^1_{\mathrm{PV}} g^2_{\mathrm{PV}}}{4\pi}\,\frac{e^{-m_A r}}{r}\left\{\langle\boldsymbol{\sigma}\rangle_1\cdot\langle\boldsymbol{\sigma}\rangle_2\left[1-\frac{1}{2}\left(\frac{1}{m_1^2}+\frac{1}{m_2^2}\right)\left(\mathbf{p}^2+\frac{m_A}{4r}+\frac{1}{4r^2}\right)\right]+\right. \\ &+ \left(\langle\boldsymbol{\sigma}\rangle_1\cdot\mathbf{p}\right)\left(\langle\boldsymbol{\sigma}\rangle_2\cdot\mathbf{p}\right)\left(\frac{1}{m_1 m_2}+\frac{1}{2m_1^2}+\frac{1}{2m_2^2}\right)+ \\ &+ \frac{(1+m_A r)}{4r^2}\mathbf{L}\cdot\left(\frac{\delta_2\langle\boldsymbol{\sigma}\rangle_1}{m_2^2}+\frac{\delta_1\langle\boldsymbol{\sigma}\rangle_2}{m_1^2}\right)+ \\ &+ \left.\frac{1}{8r^2}\left(\langle\boldsymbol{\sigma}\rangle_1\cdot\hat{\mathbf{r}}\right)\left(\langle\boldsymbol{\sigma}\rangle_2\cdot\hat{\mathbf{r}}\right)\left(\frac{1}{m_1^2}+\frac{1}{m_2^2}\right)\left(3+3m_A r+m_A^2 r^2\right)\right\}+ \\ &+ \frac{g^1_{\mathrm{PV}} g^2_{\mathrm{PV}}}{24}\left(\frac{1}{m_1^2}+\frac{1}{m_2^2}\right)\langle\boldsymbol{\sigma}\rangle_1\cdot\langle\boldsymbol{\sigma}\rangle_2\,\delta^3(\mathbf{r})+V^{s=1/2}_{\mathrm{PV-PV-LONG}}\,, \end{aligned} \tag{3.47}$$

where

$$\begin{aligned} V^{s=1/2}_{\mathrm{PV-PV-LONG}} &\equiv \frac{g^1_{\mathrm{PV}} g^2_{\mathrm{PV}}}{4\pi}\,\frac{e^{-m_A r}}{r}\left\{\left(\frac{3}{m_A^2 r^2}+\frac{3}{m_A r}+1\right)\left(\hat{\mathbf{r}}\cdot\langle\boldsymbol{\sigma}\rangle_1\right)\left(\hat{\mathbf{r}}\cdot\langle\boldsymbol{\sigma}\rangle_2\right)+\right. \\ &- \left.\left(\frac{1}{m_A^2 r^2}+\frac{1}{m_A r}\right)\langle\boldsymbol{\sigma}\rangle_1\cdot\langle\boldsymbol{\sigma}\rangle_2\right\}-\frac{g^1_{\mathrm{PV}} g^2_{\mathrm{PV}}}{3m_A^2}\langle\boldsymbol{\sigma}\rangle_1\cdot\langle\boldsymbol{\sigma}\rangle_2\delta^3(\mathbf{r}). \end{aligned} \tag{3.48}$$

The fermionic $PV - PV$ potential presents some peculiar aspects as an inheritance of the non-conserved PV currents, as we had to take into account the longitudinal part of the Proca propagator. By doing that we obtain eq.(3.48) and this potential is not well defined for $m_A \to 0$ (the excitation of the unphysical spin-0 component of the $s = 1$ mediator jeopardises unitarity).

To give a consistent interpretation we propose the following scenario: the mediator is relatively heavy ($m_1, m_2 > m_A \gg |\mathbf{q}|$) and we are working at energy and momentum-transfer scales much below m_A. With this we are far under the threshold for the excitation of the unphysical longitudinal mode of A_μ. We highlight two aspects concerning eqs.(3.47) and (3.48):

- We consider low momentum transfer and interaction ranges $r \sim |\mathbf{q}|^{-1}$. With the above hierarchy we have $r > \frac{1}{m_A} > \frac{1}{m_{1,2}}$, which ensures that we are considering the potential for distances larger than the Compton wavelengths of the ($s = 1$) sources. This is consistent with the fact that the potential is a meaningful quantity for macroscopically large distances.

- Though our non-conserved PV current couples to a massive vector boson, since we are working in a low-energy regime (heavy $m_{1,2}$) we are safe from the danger of non-unitarity, which shows up in the high-energy domain ($E \gg m_A$).

Let us move on to the spin-1 potentials. The $V-V$ potential has the form:

$$\begin{aligned}
V^{s=1}_{\mathrm{V-V}} &= \frac{e_1e_2}{4\pi}\frac{e^{-m_Ar}}{r}\Bigg\{\delta_1\delta_2\left(1+\frac{\mathbf{p}^2}{m_1m_2}\right)+ \\
&- \frac{(1+m_Ar)}{r^2}\mathbf{L}\cdot\left[\frac{1}{m_1m_2}\left(\delta_1\langle\mathbf{S}\rangle_2+\delta_2\langle\mathbf{S}\rangle_1\right)+\left(\frac{\delta_1}{2m_2^2}\langle\mathbf{S}\rangle_2+\frac{\delta_2}{2m_1^2}\langle\mathbf{S}\rangle_1\right)\right]+ \\
&+ \frac{1}{m_1m_2r^2}\left[\langle\mathbf{S}\rangle_1\cdot\langle\mathbf{S}\rangle_2\left(1+m_Ar+m_A^2r^2\right)-\left(\hat{\mathbf{r}}\cdot\langle\mathbf{S}\rangle_1\right)\left(\hat{\mathbf{r}}\cdot\langle\mathbf{S}\rangle_2\right)\left(3+3m_Ar+m_A^2r^2\right)\right]+ \\
&- \zeta\left[\frac{\delta_1}{2m_2^2r^2}\left(\delta_2\left(1+m_Ar\right)-\left(3+3m_Ar+m_A^2r^2\right)\left(\hat{\mathbf{r}}\cdot\boldsymbol{\epsilon}_2\right)\left(\hat{\mathbf{r}}\cdot\boldsymbol{\epsilon}_2^*\right)\right)+1\leftrightarrow 2\right]\Bigg\}+ \\
&- \frac{e_1e_2}{6}\left[\delta_1\delta_2\left(\frac{1}{m_1^2}+\frac{1}{m_2^2}\right)+\frac{4}{m_1m_2}\langle\mathbf{S}\rangle_1\cdot\langle\mathbf{S}\rangle_2\right]\delta^3(\mathbf{r}), \qquad (3.49)
\end{aligned}$$

where, as in $V^{s=1}_{\mathrm{S-S}}$, eq.(3.39), we introduced the parameter $\zeta = \pm 1$ for the vector or tensor representation, respectively. The electromagnetic potential for the spin-1 sources ($m_A = 0$) is

$$\begin{aligned}
V^{s=1}_{\mathrm{V-V}}\Big|^{\mathrm{vector}}_{\mathrm{EM}} &= \frac{e_1e_2}{4\pi r}\Bigg\{\delta_1\delta_2\left(1+\frac{\mathbf{p}^2}{m_1m_2}\right)+ \\
&- \frac{1}{r^2}\mathbf{L}\cdot\left[\left(\frac{\delta_1\langle\mathbf{S}\rangle_2}{2m_2^2}+\frac{\delta_2\langle\mathbf{S}\rangle_1}{2m_1^2}\right)+\left(\frac{\delta_1\langle\mathbf{S}\rangle_2}{m_1m_2}+\frac{\delta_2\langle\mathbf{S}\rangle_1}{m_1m_2}\right)\right]+ \\
&+ \frac{1}{m_1m_2r^2}\left[\langle\mathbf{S}\rangle_1\cdot\langle\mathbf{S}\rangle_2-3\left(\hat{\mathbf{r}}\cdot\langle\mathbf{S}\rangle_1\right)\left(\hat{\mathbf{r}}\cdot\langle\mathbf{S}\rangle_2\right)\right]+ \\
&- \frac{\zeta}{2r^2}\left[\delta_1\delta_2\left(\frac{1}{m_1^2}+\frac{1}{m_2^2}\right)-3\left(\frac{\delta_2}{m_1^2}\left(\hat{\mathbf{r}}\cdot\boldsymbol{\epsilon}_1^*\right)\left(\hat{\mathbf{r}}\cdot\boldsymbol{\epsilon}_1\right)+\frac{\delta_1}{m_2^2}\left(\hat{\mathbf{r}}\cdot\boldsymbol{\epsilon}_2^*\right)\left(\hat{\mathbf{r}}\cdot\boldsymbol{\epsilon}_2\right)\right)\right]\Bigg\}+ \\
&- \frac{e_1e_2}{6}\left[\delta_1\delta_2\left(\frac{1}{m_1^2}+\frac{1}{m_2^2}\right)+\frac{4}{m_1m_2}\langle\mathbf{S}\rangle_1\cdot\langle\mathbf{S}\rangle_2\right]\delta^3(\mathbf{r}). \qquad (3.50)
\end{aligned}$$

Finally, the bosonic $PV-PV$ potential

$$\begin{aligned}
V^{s=1}_{\mathrm{PV-PV}} &= -\frac{g^1_{\mathrm{PV}}g^2_{\mathrm{PV}}}{16\pi m_1m_2}\frac{e^{-m_Ar}}{r^3}\Bigg\{\left(3+3m_Ar+m_A^2r^2\right)\left(\hat{\mathbf{r}}\cdot\langle\mathbf{S}\rangle_1\right)\left(\hat{\mathbf{r}}\cdot\langle\mathbf{S}\rangle_2\right)+ \\
&- \left(1+m_Ar\right)\langle\mathbf{S}\rangle_1\cdot\langle\mathbf{S}\rangle_2\Bigg\}+\frac{g^1_{\mathrm{PV}}g^2_{\mathrm{PV}}}{12m_1m_2}\langle\mathbf{S}\rangle_1\cdot\langle\mathbf{S}\rangle_2\,\delta^3(\mathbf{r}) \qquad (3.51)
\end{aligned}$$

and we recall that, opposed to the $s = 1/2$ case, the PV current for $s = 1$ is conserved, so this potential does not present the problems of its fermionic counterpart.

By comparing the results, we notice very similar spin dependence in both $V-V$ potentials, such as spin-orbit and spin-spin interactions. However, the bosonic case has additional terms with monopole-monopole and polarization-polarization interactions. From the fermionic $PV-PV$ potential we observe an exclusive spin-spin interaction with a $(\langle\boldsymbol{\sigma}\rangle_1\cdot\mathbf{p})(\langle\boldsymbol{\sigma}\rangle_2\cdot\mathbf{p})$ dependence. The bosonic case does not present such contributions and it reveals the same functional spin-dependence of the $PS-PS$ potential, eq.(3.41).

To conclude this section, in possession of the potentials we have calculated for spin-1 charged sources, we point out the possibility to apply our results to the study of the recently discovered heavy hyperhydrogen [152] and hyperhelium [153]. To study the spectroscopy of the excited spin-1 states of $\Lambda-$hypernuclei, systems where a Λ baryon is introduced into the nucleus, a careful analysis of the spin dependence of the potentials is needed [163].

3.4 Tensor representation

We discussed the spin-1 particle in terms of the vector representation, but this is not the only possibility [147, 155]. On-shell, a massive spin-1 particle may be described by a complex 2-form via

$$\mathcal{L}_{tens.}=-\frac{1}{6}\mathcal{G}^{*\mu\nu\kappa}\mathcal{G}_{\mu\nu\kappa}+\frac{1}{2}\,m^2B^{*\nu\kappa}B_{\nu\kappa}+ie(g-1)F_\nu{}^\mu B_{\mu\kappa}B^{*\nu\kappa}, \tag{3.52}$$

with $\mathcal{G}_{\mu\nu\kappa}=D_\mu B_{\nu\kappa}+D_\kappa B_{\mu\nu}+D_\nu B_{\kappa\mu}$. The equations of motion are

$$D^\mu\mathcal{G}_{\mu\nu\kappa}+m^2B_{\nu\kappa}+ie(g-1)B_{\mu\kappa}F_\nu{}^\mu+ie(g-1)B_{\nu\mu}F_\kappa{}^\mu=0. \tag{3.53}$$

Following similar arguments as in Section 3.2, in the rest frame, we have $B^{0i}_{\rm rest}=0$ and $B^{ij}_{\rm rest}=N_B\epsilon_{ijk}\boldsymbol{\epsilon}_k$, where $\boldsymbol{\epsilon}$ is the polarization 3-vector. By suitably applying a Lorentz boost we obtain the final form for $B^{\mu\nu}$ in the LAB frame:

$$B^{0i}(P) = \frac{N_B}{m}\epsilon_{ijk}\boldsymbol{\epsilon}_j\mathbf{P}_k \tag{3.54}$$

$$B^{ij}(P) = N_B\left\{\epsilon_{ijk}\boldsymbol{\epsilon}_k+\frac{1}{m(E+m)}\left[\mathbf{P}_i(\boldsymbol{\epsilon}\times\mathbf{P})_j-\mathbf{P}_j(\boldsymbol{\epsilon}\times\mathbf{P})_i\right]\right\}, \tag{3.55}$$

where $N_B=1/\sqrt{2}$. The subsidiary condition, $\partial_\mu B^{\mu\nu}=0$, is also fulfiled.

It is worthwhile noticing that, despite seemingly different, the vector and tensor representations share some interesting similarities. For example, both W^0 and B^{0i} involve a product of polarization and 3-momentum: $W^0\sim\mathbf{P}\cdot\boldsymbol{\epsilon}$ and $B^{0i}\sim(\mathbf{P}\times\boldsymbol{\epsilon})_i$.

On the other hand, the spatial part of W^μ, eq.(3.11), resembles B^{ij}, but not quite. The parallel can be better seen by considering a specific direction (say z). We then have $W^z \sim \boldsymbol{\epsilon}_z + \frac{1}{m(E+m)}\mathbf{P}_z\,(\boldsymbol{\epsilon}\cdot\mathbf{P})$, while the B^{xy} component is

$$\begin{aligned} B^{xy} &\sim \boldsymbol{\epsilon}_z + \frac{1}{m(E+m)}\left[\mathbf{P}_x(\boldsymbol{\epsilon}\times\mathbf{P})_y - \mathbf{P}_y(\boldsymbol{\epsilon}\times\mathbf{P})_x\right] \\ &= \boldsymbol{\epsilon}_z + \frac{1}{m(E+m)}\left[-\mathbf{P}_z\left(\boldsymbol{\epsilon}_x\mathbf{P}_x + \boldsymbol{\epsilon}_y\mathbf{P}_y\right) + \boldsymbol{\epsilon}_z\left(\mathbf{P}_x^2 + \mathbf{P}_y^2\right)\right] \\ &= \boldsymbol{\epsilon}_z + \frac{1}{m(E+m)}\left[-\mathbf{P}_z\left(\boldsymbol{\epsilon}\cdot\mathbf{P} - \boldsymbol{\epsilon}_z\mathbf{P}_z\right) + \boldsymbol{\epsilon}_z\left(\mathbf{P}^2 - \mathbf{P}_z^2\right)\right] \\ &= \boldsymbol{\epsilon}_z + \frac{1}{m(E+m)}\left[-\mathbf{P}_z\left(\boldsymbol{\epsilon}\cdot\mathbf{P}\right) + \boldsymbol{\epsilon}_z\left(\mathbf{P}^2\right)\right] \\ &= \left(\frac{E}{m}\right)\boldsymbol{\epsilon}_z - \frac{1}{m(E+m)}\mathbf{P}_z\,(\boldsymbol{\epsilon}\cdot\mathbf{P})\,, \end{aligned} \tag{3.56}$$

which is structurally very similar to W^z, eq.(3.11).

To study the currents in this representation, we state below the interaction Lagrangian that contemplates all the couplings we are interested in:

$$\begin{aligned} \mathcal{L}_{int}^{s=1} &= \left[g_{\rm S}B^*_{\mu\nu}B^{\mu\nu} + g_{\rm PS}B^*_{\mu\nu}\tilde{B}^{\mu\nu}\right]\phi + \\ &+ ig_{\rm V}\left[G^{*\,\mu\nu\kappa}B_{\nu\kappa} - G^{\mu\nu\kappa}B^*_{\nu\kappa} + (g-1)\partial^\nu\left(B_{\nu\alpha}B^{*\,\mu\alpha} - B^*_{\nu\alpha}B^{\mu\alpha}\right)\right]A_\mu + \\ &+ ig_{\rm PV}\left[G^{*\mu\nu\kappa}\tilde{B}_{\nu\kappa} - G^{\mu\nu\kappa}\tilde{B}^*_{\nu\kappa}\right]A_\mu, \end{aligned} \tag{3.57}$$

where the coupling constants have the following mass dimensions: $[g_{\rm S}] = [g_{\rm PS}] = 1$ and $[g_{\rm V}] = [g_{\rm PV}] = 0$. The field strength $G_{\mu\nu\kappa}$ does not include covariant derivatives. As previously discussed in connection with the gauge current in the vector representation, the vector current is the one to order e upon use of the subsidiary condition (with ordinary derivatives), i.e., the free subsidiary condition, which is compatible with our procedure to get the potential to order e^2.

Much like the Gordon decomposition for spin-1/2 fermions, eq.(3.4), we may massage the equations of motion for $B^{\mu\nu}$ to write the vector current in terms of a density term proportional to the field squared and another term involving the spin matrix. Following this prescription, we obtain

$$\mathcal{J}^\mu_{\rm V}(p,q) = 2ep^\mu B^*_{\alpha\beta}B^{\alpha\beta} + iegq_\sigma B^{*\,\lambda\kappa}\left(\Sigma^{\mu\sigma}_{\rm T}\right)_{\lambda\kappa,\alpha\beta}B^{\alpha\beta}, \tag{3.58}$$

where $\left(\Sigma^{\kappa\sigma}_{\rm T}\right)_{\mu\nu,\alpha\beta} = \frac{1}{2}\left[\eta_{\mu\alpha}\left(\Sigma^{\kappa\sigma}_{\rm V}\right)_{\nu\beta} - \eta_{\nu\alpha}\left(\Sigma^{\kappa\sigma}_{\rm V}\right)_{\mu\beta} + \eta_{\nu\beta}\left(\Sigma^{\kappa\sigma}_{\rm V}\right)_{\mu\alpha} - \eta_{\mu\beta}\left(\Sigma^{\kappa\sigma}_{\rm V}\right)_{\nu\alpha}\right]$ is the spin generator in the tensor representation[10] and, from now on, the symbol $\mathcal{J}$ de-

[10] By construction, this generator is anti-symmetric in the pairs (μ,ν) and (α,β).

notes the momentum-space currents in the tensor representation. The same result was independently found by Delgado-Acosta *et al.* [147].

Despite of focusing on the tensor representation, $(\Sigma_{\rm T}^{\kappa\sigma})_{\mu\nu,\alpha\beta}$ is built from $(\Sigma_{\rm V}^{\mu\nu})_{\alpha\beta}$, and we keep the notation from the vector representation and denote $\langle S_i\rangle = \boldsymbol{\epsilon}_j^*\,(S_i)_{jk}\,\boldsymbol{\epsilon}_k$, with $(S_i)_{jk} = -i\epsilon_{ijk}$. The currents are decomposed in terms of $\{\mathbf{p},\mathbf{q}\}$ in Appendix A. Taking the NR limit and including eq.(3.27), we find:

1) Scalar current (S):

$$\begin{aligned} B^*_{\mu\nu}(p+q/2)B^{\mu\nu}(p-q/2) \;\simeq\; & \frac{\delta}{2m}\left[1-\frac{1}{2m^2}\left(\mathbf{p}^2+\frac{\mathbf{q}^2}{4}\right)\right]+ \\ - \;& \frac{1}{4m^3}\Big[i\,(\mathbf{q}\times\mathbf{p})\cdot\langle\mathbf{S}\rangle-\delta\mathbf{q}^2+(\mathbf{q}\cdot\boldsymbol{\epsilon}^*)(\mathbf{q}\cdot\boldsymbol{\epsilon})\Big] \end{aligned} \tag{3.59}$$

2) Pseudo-scalar current (PS):

$$B^*_{\mu\nu}(p+q/2)\,\tilde{B}^{\mu\nu}(p-q/2)) \simeq \frac{i}{m}\,(\mathbf{q}\cdot\langle\mathbf{S}\rangle) \tag{3.60}$$

3) Vector current (V):

$$J^{\mu}_{\rm V}(p,q) = 2p^{\mu}B^*_{\lambda\nu}B^{\lambda\nu} + igq_{\nu}B^{*\,\alpha\beta}\,(\Sigma_{\rm T}^{\mu\nu})_{\alpha\beta\,,\,\sigma\rho}\,B^{\sigma\rho} \tag{3.61}$$

3i) For $\mu = 0$,

$$\mathcal{J}^0_{\rm V}(p,q) = \delta + \frac{g-1}{2m^2}\left[i\,(\mathbf{q}\times\mathbf{p})\cdot\langle\mathbf{S}\rangle - \delta\mathbf{q}^2 + (\mathbf{q}\cdot\boldsymbol{\epsilon}^*)\,(\mathbf{q}\cdot\boldsymbol{\epsilon})\right] \tag{3.62}$$

3ii) For $\mu = i$,

$$\mathcal{J}^i_{\rm V}(p,q) = \frac{\delta}{m}\mathbf{p}_i - \frac{ig}{2m}\epsilon_{ijk}\mathbf{q}_j\langle\mathbf{S}_k\rangle \tag{3.63}$$

4) Pseudo-vector current (PV):

$$\begin{aligned} \mathcal{J}^{\mu}_{\rm PV}(p,q) \;=\; & 2p^{\mu}\tilde{B}^*_{\alpha\beta}B^{\alpha\beta} - i\,(\Sigma_{\rm T}^{\mu\nu})_{\alpha\beta\,,\,\lambda\kappa}\Bigg[p_{\nu}\left(\tilde{B}^{*\,\alpha\beta}B^{\lambda\kappa}+\tilde{B}^{\alpha\beta}B^{*\,\lambda\kappa}\right)+ \\ - \;& \frac{1}{2}q_{\nu}\left(\tilde{B}^{*\,\alpha\beta}B^{\lambda\kappa}-\tilde{B}^{\alpha\beta}B^{*\,\lambda\kappa}\right)\Bigg] \end{aligned} \tag{3.64}$$

4i) For $\mu = 0$,

$$\mathcal{J}^0_{\rm PV}(p,q) = \frac{i}{2m}\mathbf{q}\cdot\langle\mathbf{S}\rangle \tag{3.65}$$

4ii) For $\mu = i$,

$$\begin{aligned}\mathcal{J}^i_{\rm PV}(p,q) &= \frac{i}{2m^2}\left[\mathbf{p}_i\left(\mathbf{q}\cdot\langle\mathbf{S}\rangle\right)+\mathbf{q}_i\left(\mathbf{p}\cdot\langle\mathbf{S}\rangle\right)\right]+\\ &+ \frac{1}{2m^2}\left\{\left[\left(\mathbf{p}-\frac{1}{2}\mathbf{q}\right)\cdot\boldsymbol{\epsilon}\right]\left(\mathbf{q}\times\boldsymbol{\epsilon}^*\right)_i+\right.\\ &+ \left.\left[\left(\mathbf{p}+\frac{1}{2}\mathbf{q}\right)\cdot\boldsymbol{\epsilon}^*\right]\left(\mathbf{q}\times\boldsymbol{\epsilon}\right)_i\right\} \qquad (3.66)\end{aligned}$$

The currents in the different spin-1 representations are very similar in general[11] basically, a global sign distinguishes one from the other – compare eq.(3.28) with eq.(3.59), eq.(3.29) with eq.(3.60), eq.(3.31) with eq.(3.62), eq.(3.32) with eq.(3.63) and eq.(3.34) with eq.(3.65). The main exception is the spatial component of the PV currents, where we notice some differences in the functional form. For practical matters this detail is irrelevant, as its contribution to the $PV-PV$ or $V-PV$ potentials leads to higher-order terms, which we are ignoring in our calculations.

The most remarkable differences appear in the polarization sector of the scalar source and time component of the vector current. In the vector representation, eqs.(3.28) and (3.31), we obtained the following polarization dependences:

$$(\mathbf{q}\cdot\boldsymbol{\epsilon})(\mathbf{q}\cdot\boldsymbol{\epsilon}^*)=\mathbf{q}^2\left(\frac{\mathbf{q}_i\mathbf{q}_j}{\mathbf{q}^2}\right)\boldsymbol{\epsilon}_i\boldsymbol{\epsilon}^*_j\,, \qquad (3.67)$$

while in the tensor case, eqs.(3.59) and (3.62), we have

$$\delta\mathbf{q}^2-(\mathbf{q}\cdot\boldsymbol{\epsilon})(\mathbf{q}\cdot\boldsymbol{\epsilon}^*)=\mathbf{q}^2\left(\delta_{ij}-\frac{\mathbf{q}_i\mathbf{q}_j}{\mathbf{q}^2}\right)\boldsymbol{\epsilon}_i\boldsymbol{\epsilon}^*_j\,. \qquad (3.68)$$

According to these results, the two representations differ also due to opposite projections in the contribution coming from the polarization; this could be associated with the particular representation of the spin-1 we are dealing with. In order to evaluate the NR limit of these particular cases, we had to take into account the "weak" contributions (those with momenta) of the fields, such as $W^0\sim\mathbf{P}\cdot\boldsymbol{\epsilon}$ and $B^{0i}\sim(\mathbf{P}\times\boldsymbol{\epsilon})_i$, eqs.(3.11) and (3.55), and the analogues present in $\mathbf{W}$ and B^{ij}. These different couplings between momenta and polarization, $\mathbf{p}\cdot\boldsymbol{\epsilon}$ and $\mathbf{p}\times\boldsymbol{\epsilon}$, arise due to the Lorentz boost to the LAB frame and produce the observed longitudinal and transverse projections appearing in eqs.(3.67) and (3.68) above.

Equations (3.67) and (3.68) raise a question concerning the vector or axial character of the spin-1 particle. In the W^μ-case, we assume a vector-like particle. In the tensor representation, let us take the components as $B^{0i}=-B_{0i}\equiv\mathbf{X}_i$ and

[11] Except for eventual factors of $\sim\delta\mathbf{q}^2$ in the S and V currents; see discussion below.

$B^{ij} = B_{ij} \equiv \epsilon_{ijk}\mathbf{Y}_k$. On shell and in the rest frame, all the degrees of freedom (d.o.f.) are carried by $\mathbf{Y}$, since $\mathbf{X} \sim \mathbf{P} = 0$. Going over to the LAB-frame the tensor representation gives $\mathbf{X} \sim \mathbf{P} \times \mathbf{Y}$, i.e., in a frame-independent way, the on-shell d.o.f. actually reside in $\mathbf{Y}$. The form of the vector current is insensitive to the vector or axial behavior of $\mathbf{Y}$, as we may conclude by inspecting $\mathcal{J}^\mu$ expressed in terms of $\mathbf{X}$ and $\mathbf{Y}$. If $\mathbf{Y}$ is vector-like, then $\mathbf{X}$ must be axial, and *vice-versa*. Therefore, the sign difference highlighted above is always present as a consequence of the choice of representation, regardless of whether the particle is vector- or axial-like.

Let us now return to the main problem of determining the potentials for the tensor representation of the spin-1 sources. As in Section 3.3, it can be shown that the $V-PV$ and $PV-PV$ potentials are identical to the ones obtained in the vector representation, eqs.(3.43) and (3.51), also including the contact terms. The $S-PS$ potentials differ by global mass factors, while the $PS-PS$ potentials differ by global mass and numerical factors.

The remaining potentials, $S-S$ and $V-V$, have the following profiles:

$$\begin{aligned}
V^{s=1}_{\mathrm{S-S}} &= -\frac{g^1_{\mathrm{S}} g^2_{\mathrm{S}}}{16\pi m_1 m_2}\frac{e^{-m_\phi r}}{r}\Bigg\{\delta_1\delta_2\left[1-\frac{1}{2}\left(\frac{1}{m_1^2}+\frac{1}{m_2^2}\right)\left(\mathbf{p}^2+\frac{3m_\phi^2}{4}\right)\right]+ \\
&+ \frac{(1+m_\phi r)}{2r^2}\mathbf{L}\cdot\left(\frac{\delta_1\langle\mathbf{S}\rangle_2}{m_2^2}+\frac{\delta_2\langle\mathbf{S}\rangle_1}{m_1^2}\right)+ \\
&+ \zeta\left[\frac{\delta_1}{2m_2^2 r^2}\left[\delta_2(1+m_\phi r)-(\hat{\mathbf{r}}\cdot\boldsymbol{\epsilon}_2)\,(\hat{\mathbf{r}}\cdot\boldsymbol{\epsilon}_2^*)\left(3+3m_\phi r+m_\phi^2 r^2\right)\right]+\ 1\leftrightarrow 2\right]\Bigg\} \\
&- \frac{5g^1_{\mathrm{S}} g^2_{\mathrm{S}}}{96 m_1 m_2}\delta_1\delta_2\left(\frac{1}{m_1^2}+\frac{1}{m_2^2}\right)\delta^3(\mathbf{r}),
\end{aligned} \tag{3.69}$$

and

$$\begin{aligned}
V^{s=1}_{\mathrm{V-V}} &= \frac{e_1 e_2}{4\pi}\frac{e^{-m_A r}}{r}\Bigg\{\delta_1\delta_2\left[1+\frac{\mathbf{p}^2}{m_1 m_2}+\frac{m_A^2}{2}\left(\frac{1}{m_1^2}+\frac{1}{m_2^2}\right)\right]+ \\
&- \frac{(1+m_A r)}{r^2}\mathbf{L}\cdot\left[\frac{1}{m_1 m_2}\left(\delta_1\langle\mathbf{S}\rangle_2+\delta_2\langle\mathbf{S}\rangle_1\right)+\left(\frac{\delta_1}{2m_2^2}\langle\mathbf{S}\rangle_2+\frac{\delta_2}{2m_1^2}\langle\mathbf{S}\rangle_1\right)\right]+ \\
&+ \frac{1}{m_1 m_2 r^2}\left[\langle\mathbf{S}\rangle_1\cdot\langle\mathbf{S}\rangle_2\left(1+m_A r+m_A^2 r^2\right)-(\hat{\mathbf{r}}\cdot\langle\mathbf{S}\rangle_1)\,(\hat{\mathbf{r}}\cdot\langle\mathbf{S}\rangle_2)\left(3+3m_A r+m_A^2 r^2\right)\right]+ \\
&- \zeta\left[\frac{\delta_1}{2m_2^2 r^2}\left(\delta_2\left(1+m_A r\right)-\left(3+3m_A r+m_A^2 r^2\right)\,(\hat{\mathbf{r}}\cdot\boldsymbol{\epsilon}_2)\,(\hat{\mathbf{r}}\cdot\boldsymbol{\epsilon}_2^*)\right)+\ 1\leftrightarrow 2\right]\Bigg\}+ \\
&- \frac{e_1 e_2}{3}\left[\delta_1\delta_2\left(\frac{1}{m_1^2}+\frac{1}{m_2^2}\right)+\frac{2}{m_1 m_2}\langle\mathbf{S}\rangle_1\cdot\langle\mathbf{S}\rangle_2\right]\delta^3(\mathbf{r}),
\end{aligned} \tag{3.70}$$

whose electromagnetic limit reads

$$
\begin{aligned}
V^{s=1}_{\mathrm{V-V}}\Big|^{\mathrm{tensor}}_{\mathrm{EM}} &= \frac{e_1 e_2}{4\pi r}\Bigg\{\delta_1\delta_2\left(1+\frac{\mathbf{p}^2}{m_1 m_2}\right)+ \\
&- \frac{1}{r^2}\mathbf{L}\cdot\left[\frac{1}{m_1 m_2}\left(\delta_1\langle\mathbf{S}\rangle_2+\delta_2\langle\mathbf{S}\rangle_1\right)+\left(\frac{\delta_1}{2m_2^2}\langle\mathbf{S}\rangle_2+\frac{\delta_2}{2m_1^2}\langle\mathbf{S}\rangle_1\right)\right]+ \\
&+ \frac{1}{m_1 m_2 r^2}\left[\langle\mathbf{S}\rangle_1\cdot\langle\mathbf{S}\rangle_2-3\left(\hat{\mathbf{r}}\cdot\langle\mathbf{S}\rangle_1\right)\left(\hat{\mathbf{r}}\cdot\langle\mathbf{S}\rangle_2\right)\right]+ \\
&- \frac{\zeta}{2r^2}\left[\delta_1\delta_2\left(\frac{1}{m_1^2}+\frac{1}{m_2^2}\right)-3\left[\frac{\delta_2}{m_1^2}\left(\hat{\mathbf{r}}\cdot\boldsymbol{\epsilon}_1^*\right)\left(\hat{\mathbf{r}}\cdot\boldsymbol{\epsilon}_1\right)+\frac{\delta_1}{m_2^2}\left(\hat{\mathbf{r}}\cdot\boldsymbol{\epsilon}_2^*\right)\left(\hat{\mathbf{r}}\cdot\boldsymbol{\epsilon}_2\right)\right)\right]\Bigg\}+ \\
&- \frac{e_1 e_2}{3}\left[\delta_1\delta_2\left(\frac{1}{m_1^2}+\frac{1}{m_2^2}\right)+\frac{2}{m_1 m_2}\langle\mathbf{S}\rangle_1\cdot\langle\mathbf{S}\rangle_2\right]\delta^3(\mathbf{r}). \qquad (3.71)
\end{aligned}
$$

These potentials share some similarities with their counterparts in the vector representation (cf. eqs.(3.39) and (3.49)). In case of the $S-S$ potentials, the two representations have the same monopole-monopole and spin-orbit terms; whereas for the $V-V$ potentials, the similarities include the spin-orbit and spin-spin terms. As for the differences, in both $S-S$ and $V-V$ potentials the tensor representation introduces extra monopole-monopole and contact terms: this is due to the extra $\sim \delta\mathbf{q}^2$, as we have seen in the discussion above about the scalar source and time component of the vector current. Besides, in the polarization-polarization sector we have $\zeta = \pm 1$ in the vector and tensor representations, respectively.

In general, we cannot distinguish between the vector and tensor representations by only considering the spin-dependent sector of the potentials. We emphasize that the differences are suppressed as they only show up in $\mathcal{O}(v^2)$ in the amplitude. This is so because we consider only dipole contributions. If we extend our calculations to include quadrupole effects, differences in the $V-V$ potentials for the vector and tensor representation might become evident, as we could expect from studies reported elsewhere [147].

3.5 Partial conclusions

In this chapter we focused on the spin dependence of current-current interaction potentials in the NR limit for spin-1 and spin-1/2 charged matter. Our results indicate some universalities between bosons and fermions when exchanging scalar and vector particles. Essentially, we observe very similar contributions in the spin sector of the $S-S$, $S-PS$, $PS-PS$ and $V-V$ potentials. The main differences appear in connection with PV currents.

We highlight here a result presented in Section 3.4: the non-trivial consequences of choosing a particular field representation for the spin-1 particle, as indicated by the parameter $\zeta = \pm 1$. Even if the vector and tensor representations are equivalent on shell (and the particles in the sources are indeed on shell), the results for the $S-S$ and $V-V$ potentials do differ. Furthermore, we would like to point out that these polarization-polarization terms were also reported – though mostly ignored – in Ref. [119] in the treatment of spin-0 - spin-1 scattering.

It is important to mention the results from this chapter in the context of pure electromagnetic (EM) interactions, i.e., when the mediator is massless. In Section 3.3.3 we made this discussion explicit for the case of (vector) spin-1/2 sources, whereby we recovered well-known results [119]. Similarly, for the two spin-1 representations we have found eqs.(3.50) and (3.71). If we compare the two, it becomes clear that the respective EM potentials exhibit a great deal of similarities:

$$
\begin{aligned}
V_{\mathrm{V-V}}^{\mathrm{s=1/2\,,\,s=1}}\Big|_{\mathrm{EM}} &= \frac{e_1 e_2}{4\pi r}\Bigg\{\delta_1\delta_2\left(1+\frac{\mathbf{p}^{\,2}}{m_1 m_2}\right)+ \\
&- \frac{1}{r^2}\mathbf{L}\cdot\left[\left(\frac{\delta_1\langle\mathbf{S}\rangle_2}{2m_2^2}+\frac{\delta_2\langle\mathbf{S}\rangle_1}{2m_1^2}\right)+\left(\frac{\delta_1\langle\mathbf{S}\rangle_2}{m_1 m_2}+\frac{\delta_2\langle\mathbf{S}\rangle_1}{m_1 m_2}\right)\right]+ \\
&+ \frac{1}{m_1 m_2 r^2}\left[\langle\mathbf{S}\rangle_1\cdot\langle\mathbf{S}\rangle_2-3\left(\langle\mathbf{S}\rangle_1\cdot\hat{\mathbf{r}}\right)\left(\langle\mathbf{S}\rangle_2\cdot\hat{\mathbf{r}}\right)\right]\Bigg\}+ \\
&- \frac{2e_1 e_2}{3m_1 m_2}\langle\mathbf{S}\rangle_1\cdot\langle\mathbf{S}\rangle_2\,\delta^3(\mathbf{r}),
\end{aligned}
\tag{3.72}
$$

where $\langle\mathbf{S}\rangle$ is the spin operator for each case; $\langle\mathbf{S}\rangle = \langle\boldsymbol{\sigma}\rangle/2$ for fermions.

Here and in other interparticle potentials we notice the presence of Dirac deltas, i.e., contact terms. Quantum mechanically, in the context of hydrogen-like atoms, these terms only affect s-waves ($\ell = 0$), for these are the only wave functions not zero at the origin. In macroscopic contexts, where sources are localized objects placed at considerable distances apart (i.e., no "quantum overlap"), these terms do not contribute. The calculational origin of these contact interactions is shown in Section A.3.

Apart from the aforementioned opposite signs for the polarization-polarization terms, spin-1/2 and spin-1 (also between representations) also differ by a spin-independent contact term. Despite of these punctual differences, we see that the EM interaction has a general, *universal* profile common to both spin-1/2 and spin-1 particles. This goes way beyond the expected static monopole (Coulomb) contribution and includes also spin-orbit terms, as well as the spin-spin dipolar interaction. This means that, to a large extent, the EM interactions of massive charged particles, either spin-1/2 or spin-1, is universal and cannot be distinguished by spin-spin

contributions, as one would expect.

To close this chapter, we point out a question that might be addressed to with the help of our results on the comparison between the interaction potentials between spin-1/2 and spin-1 matter sources. For the fermionic case, the electromagnetic potential does not couple to the particle density, as it happens instead for spin-0 and spin-1 charged matter.

In fact, if a charged spin-1 field W^μ is non-minimally coupled (cf. eq.(3.7)) to the electromagnetic field, we have

$$\partial_\mu F^{\mu\nu} - 2e^2 \left(W^*_\mu W^\mu\right) A^\nu + e^2 \left[W^{*\nu} \left(W_\mu A^\mu\right) + W^\nu \left(W^*_\mu A^\mu\right)\right] =$$

$$= J^\nu_{\text{global}} + ie\partial_\mu \left(W^\mu W^{*\nu} - W^{*\mu} W^\nu\right) \tag{3.73}$$

where $J^\nu_{\text{global}} = -ie\left(W^*_\mu W^{\nu\mu} - W^{*\nu\mu} W_\mu\right)$ and $W_{\nu\mu} \equiv \partial_\nu W_\mu - \partial_\mu W_\nu$. The second term in the right-hand side stems from the non-minimal coupling ($g = 2$), eq.(3.7).

From eq.(3.73) two interesting properties of the electromagnetic interactions of spin-1 fields are made explicit: the London-like term that couples A^μ to the density of charge carriers, and the interaction between the photon and the charged spin-1 through their polarization vectors. These aspects are expected to influence the interparticle potentials only if we take two-photon exchange effects ($\sim e^4 \sim \alpha^2$, i.e., go beyond tree level) into account.

However, the e^2-terms in eq.(3.73) introduce singularities associated to the point-like idealization of spin-1 charged particles. Indeed, by writing the equations of motion for the EM fields generated by point-like spin-1 sources one finds[12] $\boldsymbol{\nabla} \cdot \mathbf{E}(\mathbf{x}) \sim e^2 W^*_\mu W^\mu A^0(\mathbf{x}) \sim e^2 \delta^3(\mathbf{x} - \mathbf{x}_0) A^0(\mathbf{x})$, which is singular since $A^0(\mathbf{x}) \sim 1/|\mathbf{x} - \mathbf{x}_0|$. This tells us that, maybe, localized bosonic sources $\sim \delta^3(\mathbf{x} - \mathbf{x}_0)$ are too much of an idealization and one must consider extended charge distributions. The 1962 paper by Dirac[13] [164] and the recent works by Fabbri [165] and Dain [166] address the issue of extensibility in connection with charged particles.

Here we do not calculate classical field configurations generated by spin-1 currents. Instead, we built interaction potentials by means of a semi-classical calculation – the Born approximation with NR sources at tree level – so we do not run into the complications yielded by the singularities mentioned above. It would be nevertheless worthwhile to analyse the details of the connection between particle extension, mass, charge and spin. The electrodynamics of bosonic carriers seems to suggest that the point-like idealization of charged (bosonic) particles is indeed too

[12] This is to be contrasted with Gauss' law for point-like fermions, $\boldsymbol{\nabla} \cdot \mathbf{E}(\mathbf{x}) \sim e\delta^3(\mathbf{x} - \mathbf{x}_0)$.

[13] This paper is quite interesting as there Dirac tries to explain the recenty measured mass of the muon by treating the latter as a form of radial excitation of the electron.

restrictive.

In this first part we have worked out potentials between particles with different spins and with interactions mediated through different force carriers. In Chapter 2 we considered a new (heavy) mediator, the rank-2 tensor coupled with a 4-vector via a Chern-Simons-like topological term (CSKR system). In this chapter we undertook a more thorough comparison between the spin-dependent interaction potentials from sources with different spins, but exchanging rather standard mediators.

The main motivation in Part I is to determine how possible BSM scenarios can be addressed when new particles work as interaction mediators – this is particularly important in Chapter 2. In this first part we did not try to extract new limits on parameters (typically mass and coupling) of new forces and their carriers, but rather worked out how different sources would interact – especially in terms of spin interactions – in their presence.

In Part II we depart from this path and seek to establish limits on the parameters of a novel (BSM) particle by cross-examining theoretical predictions against experimental data. There we consider so-called axion-like particles (ALPs), which appear in many string theory-based models, and may be coupled exclusively to photons. Our main interest is not on the explicit role of ALPs as mediators[14], but rather as sources to a non-standard gamma-ray signal that could be detected after these (heavy) particles are produced during the core collapse leading to a type-II supernova.

We take the concrete case of SN 1987A and the subsequent non-observation of such a gamma-ray flux to set robust constraints on the parameter space of heavy ALPs. Furthermore, we use Betelgeuse to project how these bounds would improve if it exploded in a supernova event. Due to its proximity, Betelgeuse's explosion would in principle produce a much larger flux of ALP-originated radiation that could be detected by more sensitive instruments in the future.

The content and results of this chapter stem from the cited references, parts of my own published work [67, 68] – in collaboration with my Brazilian advisor, prof. José Abdalla Helayël-Neto, Leonardo Ospedal and Kim Veiga – and original independent modifications thereof. The calculational and writing efforts in Refs. [67, 68] were equally shared. Some of the topics presented here also stem from material covered in lectures given by my Brazilian advisor at CBPF[15].

[14] If we consider couplings exclusively to two photons, ALPs could mediate e.g. light-by-light scattering [167].

[15] Since 2008, most of the lectures given by members of our research group is recorded in video and is publicly available at the website: `www.professorglobal.com.br/fisica`.

Part II

Chapter 4

Axions and axion-like particles

4.1 Introduction

In the Presentation we have argued that BSM scenarios are generally populated by a variety of novel particles which may serve as mediators to new interactions [168]. Axion-like particles (ALPs) are generic pseudo-scalar fields predicted by such models that could impact our low-energy world. As the name says, ALPs are cousins of axions – also referred to as QCD axions – which are neutral (possibly massive) particles that are supposed to solve the so-called strong CP problem. In this chapter we give a brief and general introduction to the physics of axions to prepare the ground for the discussion on ALPs in the next chapter.

Quantum chromodynamics (QCD) is the theory that describes the strong interaction between quarks (and agglomerations thereof) through the mediation of gluons. Unlike quantum electrodynamics, QCD is a gauge theory invariant under $SU(3)_{\rm C}$, where C stands for color. The Lagrangian for QCD is

$$\mathcal{L}_{\rm QCD} = \sum_{q=u,d,\cdots} \bar{q}\left[i\not{D} - m_q\right] q - \frac{1}{4} G_a^{\mu\nu} G_{a\,\mu\nu}, \tag{4.1}$$

where[1] $D_\mu = \partial_\mu - i g_s G_\mu^a \lambda^a/2$ and m_q are the quark masses[2].

A distinctive feature of QCD is that, due to its non-Abelian character, the field-strength tensors are given by $G_a^{\mu\nu} = \partial^\mu G_a^\nu - \partial^\nu G_a^\mu + g_s f_{abc} G_b^\mu G_c^\nu$, where f_{abc} is the structure constant. These more complicated tensors (relative to QED) give rise to triple and quartic vertices, meaning that the gluons can interact with each other. This self interaction is also responsible for an important feature of QCD: asymptotic

[1] Here λ^a are the generators and G_μ^a represent the gluons ($a = 1, \cdots, 8$).

[2] The values of the masses are the following (in MeV): $m_u = 2.2$, $m_d = 4.7$, $m_s = 96$, $m_c = 127$, $m_b \approx 430$ and $m_t \approx 170000$ with progressively larger experimental uncertainties [2].

freedom, i.e., the fact that, as the distance between two quarks decreases (momentum increases) the gluon fields connecting them become less tense (the interaction becomes weaker)[3]. This is the opposite of what happens in QED, where the interaction between two electric charges increases for shorter distances.

Lagrangian (4.1) possesses a number of symmetries, such as Lorentz and gauge symmetries, as well as invariance under parity and time reversal transformations. These invariances are all supported by experiment [169]. Besides these, there is a number of other continuous symmetries, such as a global $U(1)_u \otimes \cdots \otimes U(1)_t$, which reflects conservation of individual flavor.

Since m_u, $m_d \ll \Lambda_{\rm QCD} \sim 200\,{\rm MeV}$, we may take the two lightest quarks to be approximately massless. In this case the symmetries of $\mathcal{L}_{\rm QCD}$ are enlarged and we have also a global $U(2)_V \otimes U(2)_A$, where the former gives rise to a conserved vector current and the latter to a conserved axial-vector current. Each $U(2)$ can be decomposed into $SU(2) \otimes U(1)$, and we find that the symmetry group of QCD ($m_q = 0$) is $SU(2)_I \otimes U(1)_B \otimes SU(2)_A \otimes U(1)_A$. The $SU(2)_I \otimes U(1)_B$ stands for isospin and baryon number, and it is a good (approximate) symmetry, as the pions are an isospin triplet with almost equal masses, and baryon number is overall conserved.

The axial subgroup $U(2)_A = SU(2)_A \otimes U(1)_A$ is different. Isospin and baryon symmetry are realized, so one may say that the $U(2)_A$ is spontaneously broken, giving rise to four Goldstone bosons. Given that the quarks are not exactly massless, one would expect that the symmetry is only approximate, so the modes produced by its spontaneous breakdown are pseudo-Nambu-Goldstone bosons (pNGB) and are in fact massive. The π^0, $\pi^\pm$ mesons ($m_\pi \approx 130$ MeV) would serve as pNGB for the $SU(2)_A$ piece of the $U(2)_A$. Weinberg estimated that the mass of the pNGB for the broken $U(1)_A$ should be $m_A \lesssim \sqrt{3} m_\pi$, but there were no adequate, i.e., sufficiently light, candidates. This became known as the $U(1)$ problem [170–173].

The $U(1)$ problem consists in the fact that a light pNGB connected with the $U(1)_A$ is not observed. In the massless limit, a chiral transformation[4], $q \to q' = e^{i\alpha\gamma_5} q$, leaves the (classical) Lagrangian (4.1) unchanged, but not the integration measure in the quantum path-integral formalism. This leads to the so-called axial anomaly[5] [174–177]

$$\partial_\mu J^\mu_A = \frac{g_s^2}{32\pi^2} \epsilon_{\mu\nu\lambda\kappa} G^{\mu\nu}_a G^{\lambda\kappa}_a . \tag{4.2}$$

[3]Also important is confinement, which comes from the observation that no colored hadrons exist, even though its constituents – quarks and gluons – are themselves colored.

[4]Here γ_5 makes the left and right components of the quark field transform with opposite phases.

[5]In the classical theory eq.(4.1) the chiral transformations $\sim \exp(i\alpha\gamma_5)$ leave $\mathcal{L}_{\rm QCD}$ invariant. This is the reason why this is called an anomaly: the classical theory exhibits a symmetry which does not hold due to quantum effects. Besides, even without this quantum effect, the axial current is not conserved when the quarks are massive, cf. eq.(3.5).

The solution to this problem, found by 't Hooft, comes from non-trivial topological vacuum configurations (instantons) in $SU(3)$ theories [178–180]. These configurations make the contribution of the surface terms from space integrals involving eq.(4.2) (the RHS is a 4-divergence [170, 173]) not vanish at space infinity, thus leading to the non-conservation of the axial-vector current and the absence of any Goldstone boson [181]. In this sense, the $U(1)$ problem is solved due to the axial anomaly, but, as a matter of fact, the right-hand side of eq.(4.2) will surface back in the QCD Lagrangian with a (periodic) vacuum-dependent θ-coefficient,

$$\mathcal{L}_{\text{QCD}} = \sum_{q=u,d,\cdots} \bar{q}\left[i\not{D} - m_q\right] q - \frac{1}{4}F_a^{\mu\nu}F_{a\,\mu\nu} + \frac{\theta g_s^2}{32\pi^2}\epsilon_{\mu\nu\lambda\kappa}G_a^{\mu\nu}G_a^{\lambda\kappa}. \tag{4.3}$$

Contrary to the rest of $\mathcal{L}_{\text{QCD}}$, eq.(4.3), the θ-term breaks P and T, so it would be desirable to eliminate it. A chiral rotation in the quark fields would change θ in eq.(4.3) and could actually eliminate it if the quarks were massless. Since they are not, such a transformation would also have an effect on the quark masses. This is because, in the electroweak sector, the mass matrix is generally complex [173]. Therefore, to get real and positive masses, one has to diagonalize the mass matrix, what is done by applying chiral rotations. These add a contribution to the θ-term in eq.(4.3), so the final coefficient reads $\bar{\theta} = \theta + \arg(\det M)$, with M the complex quark mass matrix. We see that $\bar{\theta}$ is composed of two different and unrelated parts, the first coming from the QCD vacuum and the second from the quark masses.

Experimentally, this term would result in an (unobserved) electric dipole moment for the neutron. This null result can be converted into the upper limit [182]

$$|\bar{\theta}| \lesssim 10^{-10}, \tag{4.4}$$

and now we have another problem: why is $\bar{\theta}$, which is arbitrary, so small with $g_s \sim \mathcal{O}(1)$ and no reason to set $\bar{\theta}$ so small by hand? The smallness of $\bar{\theta}$ is a matter of fine tuning and gives rise to the so-called strong CP problem.

4.2 The Peccei-Quinn solution: the axion

We have seen that, in order to solve the $U(1)$ problem, another was created. In the larger context of the SM, where CP violation is allowed through the weak interactions, a term such as

$$\mathcal{L}_{\bar{\theta}} \supset \frac{\bar{\theta} g_s^2}{32\pi^2}\epsilon_{\mu\nu\lambda\kappa}G_a^{\mu\nu}G_a^{\lambda\kappa} \tag{4.5}$$

is not forbidden, though no CP violation in QCD has been observed. For QCD, this term is important; without it, the $U(1)$ problem returns (in this sense, QCD is dependent on $\bar{\theta}$), so the question is[6] how can we explain the smallness of $\bar{\theta}$?

Peccei and Quinn suggested that the solution would be to make the $\bar{\theta}$-parameter dynamic by introducing another spontaneously broken chiral symmetry, $U(1)_{\rm PQ}$ [183], which produces a Goldstone boson, the axion [184, 185]. Due to the axial anomaly, the $U(1)_{\rm PQ}$ is not exact and the axion is a pNGB with a finite mass. The mechanism is based on the following Lagrangian [173, 183]

$$\mathcal{L}_{\rm a} = \frac{1}{2}\left(\partial_\mu a\right)^2 + \left(\bar{\theta} + \frac{a}{f_a}\right)\frac{g_s^2}{32\pi^2}\epsilon_{\mu\nu\lambda\kappa}G_a^{\mu\nu}G_a^{\lambda\kappa}, \tag{4.6}$$

where $a(x)$ is the axion field and f_a a dimensionful constant related to the scale of spontaneous breaking of $U(1)_{\rm PQ}$.

It can be shown that the last term in eq.(4.6) represents a periodic potential for the axion [179, 186, 187] whose minimum lies at $\langle a\rangle = -f_a\bar{\theta}$. This shows that the PQ symmetry is broken at a scale $\sim f_a$ [173, 183]. Defining the physical field as $\tilde{a} = a - \langle a\rangle$ we are able to eliminate $\bar{\theta}$ and, when $\tilde{a}$ relaxes to the minimum of its potential – where it is zero – there is no more CP violation in QCD. This comes at the expense of introducing the axion directly coupled to the gluons.

Since the aforementioned potential has a minimum at zero, we have $V(0) \leq V(\theta)$, which means that the effective potential is not flat and the axion acquires a small non-zero mass[7]. The mass is given by $m_a = \frac{\sqrt{z}}{1+z}\frac{f_\pi}{f_a}m_\pi$, where $z = m_u/m_d \simeq 0.56$, $m_\pi = 135$ MeV and $f_\pi = 92$ MeV, within a $\mathcal{O}(1)$ model-dependent factor [188–190]. With these values, we have

$$m_a = 6\times 10^{-3}\left(\frac{10^9\,\text{GeV}}{f_a}\right)\text{ eV}, \tag{4.7}$$

which shows that m_a is essentially determined by f_a.

Furthermore, the axions may interact with fermions via $\mathcal{L}_{a\psi} = g_{a\psi}\partial_\mu a\bar{\psi}\gamma^\mu\gamma_5\psi$, which in turn allows for a coupling of the axion to two photons, $g_{a\gamma}$. This coupling is also a function of the axion decay constant, $g_{a\gamma} = 10^{-13}\,\text{GeV}^{-1}\,(10^{10}\,\text{GeV}/f_a)$, also up to a $\mathcal{O}(1)$ model-dependent factor. This shows that both m_a and $g_{a\gamma}$ depend crucially on f_a and are therefore not independent variables. As a matter of fact, all axion couplings (to matter and gauge fields) are $\sim f_a^{-1}$.

[6] In the words of Peccei: "It might be possible that, as a result of some anthropic reasons $\bar{\theta}$ just turns out to be of $\mathcal{O}(10^{-10})$ but I doubt it, as a Universe where CP is violated strongly seems as viable as one where it is not" [173].

[7] It may be ultimately traced back to its mixing with the neutral pion.

The implementation of the Peccei-Quinn mechanism depends on the introduction of a non-standard particle. In this sense, it is necessary to extend the SM and that is where the aforementioned model-dependent factors determining m_a and $g_{a\gamma}$ come from. The original proposal from Peccei, Quinn, Weinberg and Wilczek (PQWW) links the PQ scale to that of electroweak breakdown, $v_{\text{Fermi}} \approx 247$ GeV, implying that $m_a \sim 100$ keV (cf. eq.(4.7)), which is way too heavy. This massive axion would also be (relatively) strongly coupled to standard matter and gauge bosons. Because of this, the PQWW model was soon – after a decade or so – ruled out by experiments. For a review, see e.g. Refs. [191, 192].

The PQWW axion was too obvious to escape observation and this led to the so-called invisible axion models. As discussed above, the problem in the PQWW proposal was the relation $f_a \sim v_{\text{Fermi}}$, which made masses and couplings too large. Other models were then proposed in which the PQ scale is way larger than the electroweak one, so that both mass and coupling are correspondingly smaller, thus making its axions "invisible".

The most important examples in this category are the KSVZ [193, 194] and DFSZ [195, 196] models, whereby, similar to the PQWW model, the axion is introduced in connection with the Higgs sector[8]. The trick is to assign the axion to the (neutral) angular component of the (complex) Higgs field which undergoes spontaneous symmetry breaking at a scale $f_a \gg v_{\text{Fermi}}$, thus forcing down both mass and coupling. We shall not go into the specifics of these models, as this is beyond the scope of this thesis, but we see that there are possible realizations of axion models that may be compatible with observations.

4.2.1 Axions as dark matter candidates

Besides offering a solution to the strong CP problem, the (invisible) axion is attractive for yet another reason: it serves as a dark matter candidate.

Dark matter is a non-standard form of matter that is supposed to compose a large portion ($\sim 23\%$ in contrast to $\sim 4\%$ baryonic matter) of the Universe. The acknowledgement of its existence can be traced back to 1933, when Zwicky noticed a very large mass-to-light ratio[9] in the Coma cluster [197]. Some time

[8]There is generally an extended Higgs sector with more than one Higgs field. In the KSVZ model there is the usual SM Higgs doublet and an extra singlet, whose phase is the axion. For the DFSZ model there are two Higgs doublets and also another scalar. In both models fermions may have PQ charges.

[9]This refers to the difference in mass as calculated via luminosity measurements and dynamical properties of the clusters or nebulae. In Ref. [197] Zwicky found that there were more than 400 times more matter than what was observed as coming from luminous sources. Though this value was an overestimation, there is still a significant discrepancy which points to the existence of

later, measurements of the rotation velocity from Andromeda showed that there is some kind of *hidden* mass at larger distances from the galactic center [198]. This was observed in several other galaxies and clusters afterwards, as well as in other instances (e.g. gravitational lensing [199]). For reviews, see Refs. [200–202].

In all the instances mentioned above, the fact is that the visible matter cannot account for the observations. To solve this problem a few proposals have been made, such as modified models of gravity, where the aforementioned discrepancies are tentatively solved by modifying Newtonian dynamics[10] (for reviews, see e.g. Ref. [204, 205] and Ref. [206]). However, the most prominent explanation to the "mass deficit" in the Universe seems to be the existence of a new form of matter, which is dark, i.e., non-electromagnetic, and interacts with the known particles only gravitationally (or at least very weakly otherwise).

As we saw earlier, the coupling constant of the (invisible) axion is in principle very small, so its interaction with other particles from the SM is very weak: all couplings, be it with electrons, photons, gluons, etc are proportional to $1/f_a$. Even though possibly extremely light (cf. eq.(4.7)), axions may be produced in such a way as to be non-relativistic[11], so it can serve as *cold* dark matter. Furthermore, the only long-range interaction is gravitational (the axion must therefore be neutral to avoid electromagnetic interactions). The points addressed above are only a part of the requirements that have to be fulfilled by any dark matter candidate, but the axion seems to do the job[12] [209, 210].

4.3 Partial conclusions

In this chapter we have briefly addressed a novel hypothetical pseudo-scalar particle, the axion, which appears as a solution to the strong CP problem in QCD.

As we saw in Section 4.1, a sector of the classical symmetries in QCD is not realized due to quantum effects, thus creating the so-called $U(1)$ problem. This in turn led to the introduction of the θ-term (connected to the vacuum structure of QCD), which produces a CP-violating contribution to the otherwise CP-conserving QCD – this is the strong CP problem.

---

non-luminous matter.

[10] It can also be argued that, due to the variety of observational constraints, modified theories of gravitation may not be a substitute of dark matter, but they may nonetheless act as a source for it due to extra degrees of freedom [203].

[11] Even though the axion is allegedly light, it can be produced with non-relativistic velocities, mostly due to its extremely weak coupling to SM fields (it does not interact strongly enough to be in thermal equilibrium). See e.g. Refs. [207, 208] for discussions on possible production mechanisms.

[12] It is a good candidate, but not the only one. For an overview, see e.g. Refs. [2, 209].

Peccei and Quinn proposed a solution to this puzzle by allowing the $\bar{\theta}$-coefficient to be dynamical. When it relaxes to the lowest energy state of its effective potential, it eliminates the CP-breaking factor (justifying the smallness of the electric dipole moment of the neutron, cf. eq.(4.4)). Furthermore, the axion is generically fit as a dark matter candidate, so its discovery could actually kill two birds with one stone.

In general, the axion can couple to photons, gluons and fermions à la [32]

$$\mathcal{L}_{\rm a} = \frac{1}{2}\left(\partial_\mu a\right)^2 - \frac{m_a^2}{2}a^2 - \frac{1}{4}g_{{\rm a}\gamma}aF_{\mu\nu}\tilde{F}^{\mu\nu} + g_{{\rm a}\psi}\bar{\psi}\gamma^\mu\gamma_5\psi\partial_\mu a + \frac{a}{f_a}\frac{g_s^2}{32\pi^2}G_a^{\mu\nu}\tilde{G}_{a\,\mu\nu}, \quad (4.8)$$

and it can be searched for specially through its coupling to two photons. In practice, since no detection has ever been reported, only (upper) limits on the couplings can be drawn. Having in mind that m_a, $g_{a\gamma}$, $g_{a\psi} \sim f_a^{-1}$, the experimental bounds are converted into bounds on f_a.

A number of experiments and observations have been used – or are being currently explored or planned – to constrain the axion parameter space (see Refs. [2, 39, 65]). Laboratory searches are largely focused on the axion coupling to photons. For example, in accelerators (e.g. LEP and LHC), weakly coupled and/or light axions may leave a trace in the form of mono-γ/jet + missing energy in processes such as $f + \bar{f} \to \gamma + a$ or, if they not so weakly coupled and/or heavier, also $f + \bar{f} \to 3\,\gamma$. The analyses presented in Ref. [54] show that, in this way, an upper bound $g_{a\gamma} \lesssim 10^{-3}\,\mathrm{GeV}^{-1}$ for $50\,\mathrm{GeV} \lesssim m_a \lesssim 1000\,\mathrm{GeV}$ can be obtained.

Another interesting experimental set-up to test the axion-photon coupling is the so-called light shining through walls (LSW) experiment. The basic mechanism behind it is the Primakoff process $\gamma + Ze \to a + Ze$, whereby an axion is created in the presence of an external electromagnetic field[13] [211, 212]. In fact, this can be seen as an axion-photon oscillation.

The idea behind LSW experiments is to shoot a laser onto an opaque wall and, before it, expose the laser to a transverse magnetic field. This should cause the photons to convert into axions[14] and, since the coupling to matter is feeble, the axions would be able to pass through the wall. After crossing it, they could oscillate back into photons in the presence of another external magnetic field[15] [213]. Since no signal has been found, the current best bound is $g_{a\gamma} < 3.5 \times 10^{-8}\,\mathrm{GeV}^{-1}$ for $m_a \lesssim 0.3$ meV [2, 214].

[13] This process is the main production mechanism for ALPs to be explored in the next chapter, where we discuss ALPs produced in the dense – and ion-rich – core of an exploding supernova.

[14] It may also be used to search for e.g. hidden photons [65, 213].

[15] The regeneration probability is $P(\gamma \to a \to \gamma) \sim (g_{a\gamma}BL)^4$, where B and L are the transverse magnetic field and its length, respectively [2].

On the other hand, away from laboratories, astrophysics also provides means to test axion physics. The fact that axions may be produced via the Primakoff process in the dense core of stars gives rise to a cooling mechanism that could modify the life time of the star [191, 215].

For example, horizontal-branch stars have a well-known helium burning rate (and energy release) which would be increased if axions exist. Given that photons are scattered multiple times before leaving the star, novel weakly coupled particles would represent an efficient channel for energy loss. Once this possibility is included, the life time of the star is shortened [216]. By analysing the population of such stars in globular clusters it was found that $g_{a\gamma} < 6.6 \times 10^{-11}\,\mathrm{GeV}^{-1}$, i.e., $f_a \gtrsim 10^7$ GeV for $m_a \lesssim 0.1$ eV [217]. Moreover, bounds on g_{ae} can be found through a (non-observed) increase in brightness due to accelerated helium ignition in red-giant branch stars, giving $g_{ae} < 4.3 \times 10^{-13}$ [218]. Further bounds can be found in Refs. [2, 39].

In summary, the QCD axion is an interesting by-product of the Peccei-Quinn solution to the strong CP problem. Its couplings to both matter and gauge bosons offer opportunities for detection, which have all come empty handed thus far.

In the Presentation we discussed that beyond the SM scenarios provide a multitude of (pseudo-)scalar particles that are generically similar to the QCD axion. These arise as a result of compactifying the unobserved extra dimensions into small spatial regions to evade experimental constraints [168]. These axion-like particles – our main interest in this part of the thesis and focus of Chapter 5 – are low-energy modes remanent of the possible compactifications. They are described by effective, low-energy Lagrangians such as ($g_{\mathrm{a}\gamma\gamma}$ is dimensionful: $[g_{\mathrm{a}\gamma\gamma}] = \mathrm{mass}^{-1}$)

$$\mathcal{L}_{\mathrm{ALP}} = \frac{1}{2}\left(\partial_\mu a\right)^2 - \frac{m_a^2}{2}a^2 - \frac{1}{4}g_{\mathrm{a}\gamma\gamma}aF_{\mu\nu}\tilde{F}^{\mu\nu}. \tag{4.9}$$

As we saw before, the QCD axion starts with a coupling to gluons $\sim (a/f_a)\, G\tilde{G}$ which generates an effective (non-flat) potential. This in turn generates a non-zero mass m_a, which is also a function of f_a. Therefore, m_a and couplings are connected by f_a and axion models are intrinsically limited in terms of mass range.

Contrary to the QCD axion, the ALP mass m_a and (particularly) its coupling to two photons $g_{\mathrm{a}\gamma\gamma}$ are not connected via an underlying energy scale: these parameters are independent. Nevertheless, the coupling of either axions or ALPs to two photons is functionally the same ($\sim \mathbf{E}\cdot\mathbf{B}$), so many of the bounds obtained for invisible axions are also valid for ALPs (for recent reviews, see e.g. Refs. [2, 219, 223]). Incidentally, because of this independence, ALPs are relatively more "flexible" than axions, thus creating a much vaster parameter space.

ALPs will be the focus of the next chapter in the astrophysical context of their production in the dense core of exploding supernovae. The essential idea is that these particles would be copiously produced via the Primakoff effect and, being very weakly coupled, they would escape the progenitor star. We are interested in heavy ALPs, which means that they may *decay* in two photons on the way to Earth. These high-energy photons could, in principle, be detected with a certain (time) delay after the supernova explosion is recorded.

The supernova from 1987, which is so far the best studied event of its kind, offered a concrete opportunity to look for ALPs. Through a state-of-the-art simulation of the ALP production in the core of the progenitor star it is possible to determine (in terms of $g_{a\gamma\gamma}$) the ALP emission spectrum, with the ALPs assumedly able to leave the influence of the star. Very light ALPs ($m_a \lesssim 10^{-10}$ eV) may efficiently convert back and forth into photons in the magnetic field of the galaxy, so there is a fraction of the initial flux that might have arrived as gamma rays on Earth [56].

Unfortunately, gamma-ray detectors did not capture any excess of radiation that could be attributed to photon conversion, thus allowing the authors of Ref. [56] to set constraints on the parameter space for very light ALPs. In the next chapter we exploit the other side of the mass scale, i.e., heavy ALPs, where ALP-photon regeneration in an external magnetic field is not efficient. In this case, the ALPs may decay in a pair of photons – usually gamma rays – which could then have reached Earth. The non-zero mass causes the hypothetical ALP-originated photon signal to suffer some interesting effects, such as a time delay and a smearing in the direction of arrival relative to the supernova.

Again, given that no unexpected signal reached the detectors at the time, we are able to exclude a region in the $m_a - g_{a\gamma\gamma}$ plane for heavy ($10\,\text{keV} \lesssim m_a \lesssim 100\,\text{MeV}$) ALPs. Furthermore, we estimate the projected improvement in the bounds in case Betelgeuse, a red supergiant star that is much closer than SN 1987A, explodes in a supernova event in the near future [69]. In the next chapter we get into the details of this analysis and present our results.

Chapter 5

Limits on heavy ALPs: an analysis of SN 1987A

This chapter is based upon the (soon to be published) work "Decay photons from the ALP burst of type-II supernovae" [69] whose content has been significantly expanded to help clarify the discussion. This work was done in collaboration with J. Redondo and J. Jäckel (advisor), and I have done most of the writing and calculational work, as well as simulations and plots.

5.1 Introduction

Many beyond the Standard Model scenarios include new massive (pseudo-)scalars – dubbed *axion-like particles* (ALPs) – among their particle spectrum (see e.g. Refs. [65, 168, 220–223] for reviews). The name originates from their similarity to the axion of the Peccei-Quinn solution to the strong CP problem, cf. Chapter 4. Contrary to the QCD axion, that also couples to gluons and fermions, ALPs may solely interact with two photons via

$$\mathcal{L}_{\text{int}} \supset \frac{g_{a\gamma\gamma}}{4} a F_{\mu\nu} \tilde{F}^{\mu\nu}, \tag{5.1}$$

where a denotes the ALP and $g_{a\gamma\gamma}$ is its coupling constant with dimension of inverse energy, often linked to an underlying scale of new physics[1] f_a via $g_{a\gamma\gamma} \sim \frac{\alpha}{2\pi}\frac{1}{f_a}$. In contrast to the Peccei-Quinn axion (cf. eq.(4.7)), in the more general case of generic ALPs there is no fixed relation between mass and coupling: these are henceforth taken as completely independent parameters.

[1] Similar to the case of PQ axions discussed in the previous chapter, ALPs may be produced as pNGB of some $U(1)$ symmetry from a high-energy theory that is spontaneously broken at $f_a \gg v_{\text{Fermi}}$.

In this chapter we focus on ALPs purely coupled to photons as given by eq.(5.1). The aim is to determine which regions in the $g_{a\gamma\gamma} - m_a$ space are allowed (or not) by considering supernovae-originated ALPs. Since we have very weakly coupled ALPs in mind, these may be produced in hot and dense stellar cores through the Primakoff process in such a way that their voluminous production is not sufficient to affect the collapse itself (e.g., its duration[2]). However, the emission of heavy ALPs may produce a large enough flux of ALP-originated gamma rays from their decay to two photons. The general strategy is to use the non-observation of any radiation excess in measurements performed directly after the supernova explosion – in our concrete case, SN 1987A – to impose limits on the mass and coupling of ALPs.

SN 1987A has been widely exploited to test not only models of supernova core collapse and the nuclear processes taking part in it, but also as means to constrain new physics (e.g., heavy neutrinos [224], unparticles [225] and supersymmetric particles [226]). Also ALPs, our main interest, have been constrained. The perhaps simplest bounds can be obtained via the energy loss caused by ALP emission, which would cause a reduction in the duration of the neutrino burst [215, 227]. For very light ALPs with masses below $m_a < \text{few} \times 10^{-10}\,\text{eV}$ a better limit can be obtained by taking into account that light ALPs emitted from the supernova can be reconverted into photons in the magnetic field of the galaxy [228, 229], which can then be detected by gamma-ray detectors [230, 231] (see also Refs. [232–234]). For heavier ALPs this does not work because the reconversion into photons is strongly suppressed[3].

For sufficiently heavy ALPs with masses in the 10 keV - 100 MeV region however, another ALP-photon conversion process becomes possible: ALP decay into two photons. This has already been considered in Ref. [235], but they assume a coupling of the ALP to nucleons (they assumed the production to occur by emission from nucleons). Our analysis extends this to the case of pure photon couplings as given by eq.(5.1), which is responsible for both production and decay (in this sense our analysis is less model dependent than that of Ref. [235]).

In the following we discuss how geometrical effects in the ALP propagation and decay play an important role in the case of heavy ALPs. This is because the by-products of a heavy parent particle are generally not collinearly emitted, which results in a "triangular" trajectory, cf. Fig. 5.1. This leads to longer times of flight and correspondingly larger time delays. Furthermore, since the ALP-originated photons will not come exactly from the direction of line of sight to the supernova,

[2]The extra outwards energy flux would cool the core and steal energy from the standard neutrino burst, also causing to shorten it (this was also not observed).

[3]In fact, this conversion is only effective for very small masses ($m_a \lesssim 10^{-9}$ eV [231]). For $m_a \lesssim 10^{-11}$ eV the authors of Ref. [56] quote a conversion probability of $\sim 10^{-1}$.

we can expect not a single point detection, but a somewhat sparse *halo* of gamma-ray photons from the explosion. With these points in mind we produce a realistic estimate of the number of ALP-originated photons that reach Earth by employing a numerical simulation of the time delay and angular distributions.

As we will detail in Section 5.2, the process is most effective in the 10 keV - 100 MeV mass range, since the ALP production rate is largest around some tens MeV (this is also the effective temperature of the core of the progenitor prior to core collapse). As can be seen from our result, Fig. 5.11, in this region supernovae provide better limits than existing laboratory and astrophysical constraints. While cosmological limits are better, they depend on a sufficiently high reheating temperature and can be circumvented [236] (cf. Section 5.5). Our analysis serves as an independent confirmation.

In addition to SN 1987A we also consider the possibility of future supernovae events. For concreteness, and also because it may produce the most spectacular effects, we entertain the possibility that the red supergiant Betelgeuse explodes in a supernova event in the near future. This is particularly interesting since its distance to Earth is only ~ 200 pc (~ 650 ly), much closer than SN 1987A (at 51.4 kpc $\sim$ 170000 ly)[4].

This self-contained chapter is based upon Ref. [69], though many parts have been extended by me. In Section 5.2 we discuss the basics of the production mechanism, the subsequent decay and the relevant geometrical features. In Section 5.3 we describe our numerical simulation and the results obtained for the detectable fraction of signal photons as well as their distribution in time and angle. In Section 5.4 we use SN 1987A to obtain concrete limits and discuss the potential sensitivity if Betelgeuse goes supernova. A brief conclusion is presented in Section 5.5.

5.2 Setting up the analysis

ALPs are produced in the core of the supernova (SN) via the Primakoff process, where a thermal photon is converted to an ALP in the presence of the external electromagnetic field provided by the charged particles in the plasma. The typical energies of the produced ALPs are of the order of the core temperature and are in the $\sim 100\,\mathrm{MeV}$ range. The associated energy spectrum has been recently calculated in Ref. [56] with detailed account of the production process in core-collapse SNe and we will use the ensuing ALP production rate to estimate the ALP-originated photon *fluence*, i.e., the number of photons per unit area, on Earth.

[4]For future convenience: $1\,\mathrm{ly} = 9.46 \times 10^{15}$ m and $1\,\mathrm{pc} = 3.09 \times 10^{16}$ m.

Despite the core being extremely dense ($\sim 10^{14}\,\mathrm{g/cm^3}$), due to the smallness of the coupling to two photons, the ALPs escape the core of the progenitor essentially unimpeded[5] and are emitted isotropically. However, the ALPs we are interested in are massive, thus having a finite life time. The associated decay rate is [2]

$$\Gamma_{a\gamma\gamma} = \frac{g_{a\gamma\gamma}^2 m_a^3}{64\pi}. \tag{5.2}$$

Given that this is calculated for an ALP at rest, the proper life time is $\Gamma_{a\gamma\gamma}^{-1}$. The life time in the frame where the ALP has velocity β and Lorentz factor $\gamma = (1-\beta^2)^{-1/2}$ suffers Lorentz dilatation and becomes $t_a = \gamma\Gamma_{a\gamma\gamma}^{-1}$. The distance covered by the ALP in the time frame of its life time is its decay length, which reads

$$\begin{aligned}
\ell_{\mathrm{ALP}} = \frac{\gamma\beta}{\Gamma_{a\gamma\gamma}} &= \frac{E_a}{m_a}\sqrt{1-\frac{m_a^2}{E_a^2}}\frac{64\pi}{g_{a\gamma\gamma}^2 m_a^3} \\
&\approx 4\times 10^{13}\,\mathrm{m}\left(\frac{E_a}{100\,\mathrm{MeV}}\right)\left(\frac{10\,\mathrm{MeV}}{m_a}\right)^4\left(\frac{10^{-10}\,\mathrm{GeV}^{-1}}{g_{a\gamma\gamma}}\right)^2 \\
&\approx 1.3\times 10^{-3}\,\mathrm{pc}\left(\frac{E_a}{100\,\mathrm{MeV}}\right)\left(\frac{10\,\mathrm{MeV}}{m_a}\right)^4\left(\frac{10^{-10}\,\mathrm{GeV}^{-1}}{g_{a\gamma\gamma}}\right)^2.
\end{aligned} \tag{5.3}$$

In the parameter range we are interested in the decay length is large, but at the same time mostly smaller than $d_{\mathrm{SN}} \sim 50\,\mathrm{kpc}$ (for SN 1987A). This means that a sizeable number of ALPs will decay before reaching Earth. Therefore, ALP decay is a relevant gamma-ray production mechanism to be considered and a flux of ALP-originated photons on Earth is expected. The observable quantity we wish to obtain is the time-integrated flux, i.e., the fluence. It can be obtained once we have the ALP production rate, which must be convoluted (folded) with the decay probability, thus giving the number of ALP-originated photons per unit (effective) area on the detector. By obtaining upper limits on the gamma-ray fluence shortly after the observation of SN 1987A we may constrain $g_{a\gamma\gamma}$ and m_a by demanding that the number of ALP-originated photons arriving at the detector does not exceed what was observed [57, 237].

An important point to be considered is that, having significant masses and being produced with energies of some ten MeV, ALPs emitted from the SN core have appreciable – but not enormous – Lorentz boost factors ($\gamma = E_a/m_a$): for $E_a \sim 100$ MeV and $m_a \sim 1$ MeV we have $\gamma = 100$. This has two specially important consequences.

[5]The distance it has to cover to be free is not just the ~ 50 km of the core radius, but a substantially larger one. See discussion around eq.(5.18).

Firstly, let us consider the ALP in its rest frame. Since its a spinless particle, in this frame its decay is isotropic, i.e., the decay angle is evenly distributed. The 4-momenta are[6] $P_a^\mu = (m_a, \mathbf{0})$, $P_{\gamma_1}^\mu = \frac{m_a}{2}(1, \mathbf{u}_0)$ and $P_{\gamma_2}^\mu = \frac{m_a}{2}(1, -\mathbf{u}_0)$, with $\mathbf{u}_0 = (\cos\alpha_0, \sin\alpha_0)$. Here $\alpha_0 \in [0, \pi]$ is the decay angle in the rest frame.

In practice, however, our ALPs are not at rest and we have to express the 4-momenta above in the frame where they are boosted. We take the boost along the x-direction, so that only this and the zeroth (energy) components will be Lorentz transformed. With this we obtain

$$P_{\gamma_1}^\mu = \gamma\frac{m_a}{2}\left[1 + \beta\cos\alpha_0,\ \beta + \cos\alpha_0,\ \gamma^{-1}\sin\alpha_0\right] \tag{5.4}$$

$$P_{\gamma_2}^\mu = \gamma\frac{m_a}{2}\left[1 - \beta\cos\alpha_0,\ \beta - \cos\alpha_0,\ -\gamma^{-1}\sin\alpha_0\right], \tag{5.5}$$

which correctly reduces to the rest frame results if $\beta = 0$ and $\gamma = 1$. With this we see that the decay angles (relative to the original ALP direction) are

$$\cos\alpha_1 = \frac{\beta + \cos\alpha_0}{1 + \beta\cos\alpha_0} \tag{5.6}$$

$$\cos\alpha_2 = \frac{\beta - \cos\alpha_0}{1 - \beta\cos\alpha_0}, \tag{5.7}$$

where it becomes clear that the role of the boost is to focus the decays in the "forward" direction: for $\beta \to 1$ we have both $\alpha_{1,2} \to 0$.

Importantly, we see that the angle between the two photons – and hence also between the original propagation direction of the parent ALP – is non-vanishing. In fact, the decay angle for an ALP-originated photon can then be written as

$$\sin\alpha \sim \gamma^{-1} \tag{5.8}$$

and this implies that, for heavy ALPs, the ensuing photons that reach Earth from the SN are not necessarily emitted along the SN-Earth direction, but rather at an angle. This is schematically shown in Fig. 5.1. Conversely, this implies that on Earth we would see the photons as if they were coming from a direction somewhat off the location of the SN, i.e., the signal is effectively smeared out over a halo[7].

Crucially, there is yet another important effect from the non-trivial geometry. The combined length traversed by the ALP and the ensuing photons is larger than the distance between Earth and the SN $d_{\rm SN}$. Moreover, massive ALPs have a ve-

[6] Using energy-momentum conservation we find that the two photons have the same energy fixed by the ALP's mass. Moreover, we are considering the components in the $x - y$ plane.

[7] As we shall see in Sections 5.3.3 and 5.4, this halo is typically not extremely broad, but it is nonetheless finite.

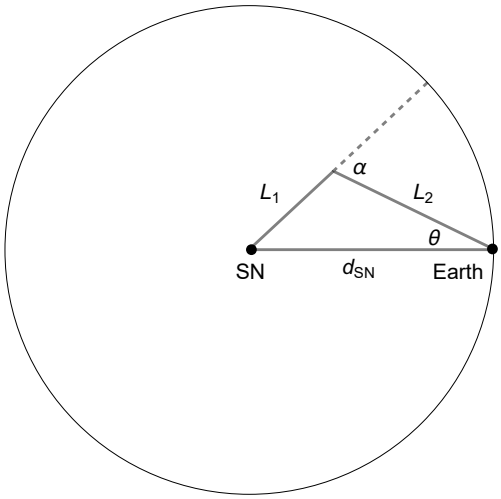

Figure 5.1: The ALP is produced at the SN, travels a length L_1 until decay with an angle α. The photon propagates a distance L_2 until Earth, where it is detected under an angle θ.

locity $\beta < 1$. This leads to a time delay, which, considering the distances involved, can be of the order of years even if the decay angles are not very large. Instead of a signal that lasts as long as the duration of the SN explosion and associated neutrino burst (~ 10 s) – as was the case for massless ALPs in Ref. [56] for SN 1987A – the signal from massive ALPs may be spread out over much longer time scales.

5.2.1 Flux of massive ALPs

A supernova explosion is an extremely violent event that takes place in the later stages of stellar evolution. Essentially, the life of any star is based upon the constant struggle to balance compression due to its own gravitating mass and the outward pressure generated by the nuclear reactions in its interior. Though the exact fate of a star depends on its mass (it can become a white dwarf, neutron star, black hole, etc[8]), for $M_{\rm star} \gtrsim 8M_\odot$ the final evolutionary stages will include a supernova explosion [238, 239].

The internal pressure that counter-balances gravity is generated through the fusion of lighter elements into heavier ones (nucleosynthesis). The process starts with hydrogen fusing to form helium and then helium to carbon and oxygen, whereby binding energy is released, thus powering the outwards thermonuclear pressure. If the star has a mass smaller than about eight solar masses it will not be possible to fuse carbon and instabilities cause a large mass loss, thus leaving a very compact and hot carbon-oxygen core: this is a white dwarf.

[8]These are all compact objects, not really stars (they are sometimes called stellar *corpses*).

For heavier stars light elements will fuse until we arrive at iron[9], beyond which there is no more energy release – it actually consumes energy. The heavy and hot iron core is crushed by its gravitational pull until the point where no contraction is possible, as degeneracy pressure sets in[10]. This marks the onset of the supernova explosion, as the collapsing outer layers bounce off the surface of the almost incompressible core and an outwards shock wave is created (at this moment also a large amount of neutrinos is produced), thus releasing enough energy to eject the outer stellar material – this is essentially a supernova.

The quantitative treatment of the physical processes leading to core-collapse SNe is an extremely difficult task and is the subject of on-going research. The subtleties of the core collapse of a progenitor star of mass around $\sim 18 M_\odot$ – the case of SN 1987A – and the associated ALP production in its interior have been thoroughly analysed in Ref. [56]. In what follows we shall adopt their results.

Massless spectrum

The production rate of massless ALPs for $g_{a\gamma\gamma} = 10^{-10}\,\mathrm{GeV}^{-1}$ can be fitted[11] by

$$\frac{d\dot{N}_a}{dE_a} = a(t) E_a^{b(t)} \exp\left[-c(t) E_a\right] \tag{5.9}$$

in overall units of $10^{50}\,\mathrm{MeV}^{-1}\mathrm{s}^{-1}$. The total ALP spectrum can be obtained by integrating this function over the time of the core collapse (~ 10 s), i.e.,

$$\frac{dN_a}{dE_a} = \int_0^{10\,\mathrm{s}} dt\, \frac{d\dot{N}_a}{dE_a}, \tag{5.10}$$

which is also as far as the detailed analysis from Ref. [56] goes. Equation (5.10) gives us the energy distribution (spectrum) of nearly massless ALPs produced during core collapse and this is the central ingredient needed to our analysis.

[9] Actually, contractions take place at the end of each burning stage (hydrogen to helium, helium to carbon and oxygen, etc), after which a new hydrodynamical equilibrium is found. During these stable phases there is usually no further compression.

[10] This is a quantum-mechanical effect that takes place when densities are so large that protons and/or electrons, which are spin-1/2 fermions, are compressed in distances of the order of their Compton wavelength. In this stage the core reaches extreme densities, in excess of nuclear matter densities of $\sim 10^{14}\,\mathrm{g/cm}^3$ and the particles have a high average momentum (due to Heisemberg's uncertainty principle). Furthermore, due to Pauli's exclusion principle, to add an extra fermion, the existing one must raise its energy – and momentum – thus creating a pressure that prevents further compression. In neutron stars electrons and protons fuse to form neutrons and the neutron-rich matter exerts the necessary (degeneracy) pressure to balance the gravitational pressure.

[11] The time-dependent coefficients, with adequate dimensions, are found to be $a(t) = 0.0054 - 0.001\,t + 5.77 \times 10^{-5}\,t^2$, $b(t) = 2.10 + 0.067\,t - 0.004\,t^2$ and $c(t) = 0.03 + 0.0003\,t + 1.78 \times 10^{-5}\,t^2$, with t in seconds and E_a in MeV.

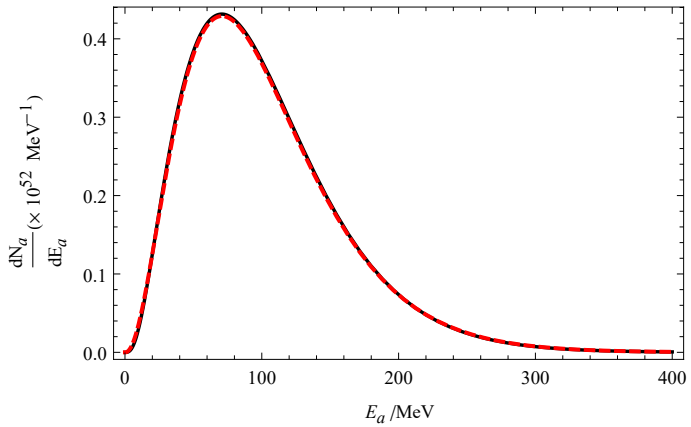

Figure 5.2: Energy distributions from eq.(5.10) (solid black) and eq.(5.11)(dashed red).

The production rate above was obtained in Ref. [56] for almost massless ALPs ($m_a \lesssim 10^{-11}$ eV), but here we are interested in the opposite side of the mass scale. To facilitate the extension of the production to non-negligible ALP masses we parametrize eq.(5.10) as

$$\left.\frac{dN_a}{dE_a}\right|_{\text{approx}} = C\frac{E_a^2}{\exp(E_a/T)-1}\sigma_0(E_a), \tag{5.11}$$

where C is a constant with dimension of inverse energy and, from now on, we are assuming that the ALP production is essentially instantaneous.

Here $\sigma_0(E_a)$ is the Primakoff production cross section [211] for massless ALPs

$$\sigma_0(E_a) = \frac{\alpha g_{a\gamma\gamma}^2}{8}\left[\left(1+\frac{k_s^2}{4E_a^2}\right)\log\left(1+\frac{4E_a^2}{k_s^2}\right)-1\right], \tag{5.12}$$

where it has been assumed that the ions in the plasma – essentially non-relativistic protons – are heavier than the ALPs produced, so that the ALP carries effectively the energy of the initial photon (i.e., $\omega \simeq E_a \geq m_a$). The variable k_s represents the Debye screening scale, which reflects the short-range character of the Coulomb interaction in a plasma[12]. In fact, the cross section above is reduced as k_s increases, showing that stronger screening reduces the reaction rate (the opposite happens for increasing temperature).

[12]More precisely, the origin of the screening (or shielding) is that the particle density of the constituents of the plasma is given by $n(r) = n_0 e^{-q\phi(r)/T}$, where q is the electric charge, $\phi(r)$ is the electric potential to which the charge is exposed and T is the temperature. Since the (charge) density is $\rho = qn(r)$, the Poisson equation reads $-\nabla^2\phi = \rho = qn_0 e^{-q\phi(r)/T}$, whose (linearised) solution is $\phi(r) \sim e^{-r/\lambda_s}/r$. It shows that a test charge would not feel the full Coulomb potential, but rather a shielded Yukawa potential. Here $\lambda_s = \sqrt{T/n_0 q^2}$ is the Debye screening length, which can be related to k_s by $k_s = \lambda_s^{-1}$.

We use eq.(5.11) to fit eq.(5.10) (with eq.(5.9)) and we find that $C = 2.54 \times 10^{77}\,\mathrm{MeV}^{-1}$, with $[g_{a\gamma\gamma}] = \mathrm{MeV}^{-1}$, $T = 30.6$ MeV and $k_s = 16.8$ MeV. These are *effective* values for the temperature of the core T and the Debye screening scale k_s. The two spectra, the one stemming from Ref. [56], eq.(5.10), and the other obtained via eq.(5.11), are shown in Fig. 5.2 and are in good agreement. This gives us confidence that our fit values are close to the relevant physical time and space averages.

Massive spectrum

So far we have only considered the production and spectrum of massless ALPs, but using the effective temperature and Debye scale quoted above it is possible to obtain estimates also for the massive case. When the mass of the ALP becomes of the order of the effective Debye scale k_s, the cross section for ALP production is modified and reads

$$\begin{aligned}\sigma(E_a) &= \frac{\alpha g_{a\gamma\gamma}^2}{8}\Bigg\{\left(1+\frac{k_s^2}{4E_a^2}-\frac{m_a^2}{2E_a^2}\right)\log\left[\frac{2E_a^2(1+\beta)+k_s^2-m_a^2}{2E_a^2(1-\beta)+k_s^2-m_a^2}\right]-\beta \\ &- \frac{m_a^4}{4k_s^2E_a^2}\log\left[\frac{m_a^4+k_s^2\left(2E_a^2(1+\beta)-m_a^2\right)}{m_a^4+k_s^2\left(2E_a^2(1-\beta)-m_a^2\right)}\right]\Bigg\},\end{aligned} \tag{5.13}$$

where $\beta = \sqrt{E_a^2 - m_a^2}/E_a$ is the ALP velocity. This expression correctly reduces to eq.(5.12) when $m_a \to 0$ ($\beta \to 1$).

Using the effective temperature and Debeye scale that provide a good fit to the massless ALP spectrum (cf. eq.(5.11)), we can now estimate the flux with the massive cross section, eq.(5.13). To get an impression of the effect of non-vanishing masses we compare the total fluxes calculated with the massless and the massive cross sections to determine an energy-averaged suppression factor:

$$\mathcal{S}(m_a) = \frac{\int \frac{d^3k}{(2\pi)^3}\frac{1}{\exp(\omega/T)-1}\sigma(\omega, m_a)}{\int \frac{d^3k}{(2\pi)^3}\frac{1}{\exp(\omega/T)-1}\sigma_0(\omega)}. \tag{5.14}$$

This is shown in Fig. 5.3 and, in the end, we have to rescale the observable flux by this factor (this is done numerically). We note that the corresponding correction is only appreciable for quite large masses, $m_a \gtrsim \sqrt{k_s E_a} \sim 20\,\mathrm{MeV}$ (cf. eq.(5.13)). At this point we expect a suppression of the massive ALP production – and flux of ALP-originated photons – relative to the massless case. The reason is essentially that, for heavy ALPs, part of the initial energy available for the photon-ALP conversion is consumed in the "making" of the ALP's rest mass.

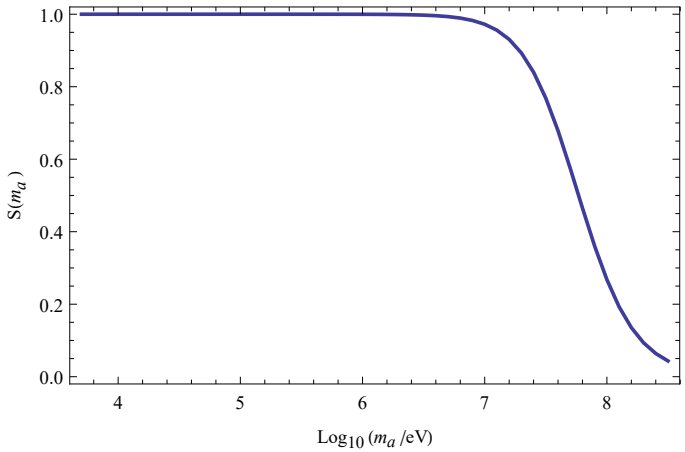

Figure 5.3: Suppression factor, eq.(5.14), as a function of ALP mass. We assume the effective values $T = 30.6\,\mathrm{MeV}$ and $k_s = 16.8\,\mathrm{MeV}$ for core temperature and Debye scale, respectively.

5.2.2 Number of photons at the detector

If all ALPs were to decay outside the SN, but before they reach Earth, the total fluence – number of photons per unit area – of ALP-originated photons on Earth would be

$$\mathcal{F}_\gamma^{\mathrm{naive}}\big|_{\mathrm{Earth}} = \frac{2}{4\pi d_{\mathrm{SN}}^2}\int dE_a \left(\frac{dN_a}{dE_a}\right), \tag{5.15}$$

where d_{SN} is the SN-Earth distance and the factor of two accounts for the two photons emitted per ALP decay. Here dN_a/dE_a, the ALP spectrum, is the result of integrating the production rate over the duration of the core collapse (~ 10 s).

For massless ALPs with instantaneous decay we would then have a naive fluence[13]

$$\mathcal{F}_\gamma^{\mathrm{naive}} = N_\gamma/\mathrm{cm}^2 = \left(3.3\times 10^6\,\gamma\cdot\mathrm{cm}^{-2}\right)\times\left(\frac{g_{a\gamma\gamma}}{10^{-10}\,\mathrm{GeV}^{-1}}\right)^2. \tag{5.16}$$

However, as already indicated above, for massive ALPs with a finite decay length we have to take a variety of additional effects into account. These are divided in essentially two sub-categories: the effect of mass in the production, i.e., the correction factor of eq.(5.14), and kinematic effects due to the non-zero decay angle (cf. eq.(5.8)). Therefore we correct the fluence to $\mathcal{F}_\gamma = \mathcal{F}_\gamma^{\mathrm{naive}} \times \mathcal{P}_{\mathrm{total}}$, where

$$\mathcal{P}_{\mathrm{total}} = \mathcal{S}(m_a)\mathcal{P}_{\mathrm{survival}}\mathcal{P}_{\mathrm{decay}}\mathcal{P}_{\mathrm{time}}\mathcal{P}_{\mathrm{acceptance}}. \tag{5.17}$$

[13]Here we used the distance to SN 1987A, $d_{\mathrm{SN}} = 51.4\,\mathrm{kpc} = 1.58\times 10^{23}\,\mathrm{cm}$ and assumed that all ALPs produced are successfully converted into detectable gamma rays.

The fluence $\mathcal{F}_\gamma$ as given above is not to be taken literally – it is a formal representation: the total probability cannot be factored out in general, as it is the result of convoluting the different factors with the ALP energy spectrum. The various contributions to $\mathcal{P}_{\text{total}}$ take into account additional effects that are important for a realistic estimate of the sensitivity.

- $\mathcal{S}(m_a)$ is the mass-dependent factor defined in eq.(5.14) which corrects eq.(5.11) for massive ALPs. It is responsible for the suppression of the production for heavy ALPs ($m_a \gtrsim 20$ MeV).

- $\mathcal{P}_{\text{survival}}$ gives the fraction of ALPs decaying outside the region effectively occupied by the progenitor star, since the photons originating inside this region may be absorbed or scattered. In our analysis we assumed that all ALP-originated photons decaying within a certain finite region are blocked (cf. eq.(5.18)).

- $\mathcal{P}_{\text{decay}}$ takes into account that the ALP-originated photons from a decay at a distance greater than d_{SN} typically do not reach the detector. Statistically, there is a small number of photons that are emitted essentially backwards with respect to the direction of the parent ALP and that could in principle reach the detector, even if the ALP decays after travelling beyond Earth. Nevertheless, their number is typically quite small and we neglect them in most of the discussion.

- $\mathcal{P}_{\text{time}}$ is the fraction of ALP-originated photons arriving within the measurement time of the detector. These are the only photons that can be effectively counted. In Ref. [56] the ALPs were essentially massless, so they should have arrived more or less at the same time as the neutrinos. This means that all detectable gamma rays from ALP-photon conversion would arrive within the observation time of ~ 10 s. For massive ALPs, on the other hand, the arrival of ALP-originated photons at the detector is not limited to the duration of the neutrino burst. Therefore one must consider the fraction of ALP-originated photons, $\mathcal{P}_{\text{time}}$, that arrive within a given (finite) observation time.

- $\mathcal{P}_{\text{acceptance}}$ accounts for the fact that some detectors may have a finite angular acceptance. Photons from ALP decays will arrive within a range of non-vanishing angles with respect to the SN (cf. Fig. 5.1). Therefore, a detector with finite angular acceptance will only see a fraction $\mathcal{P}_{\text{acceptance}}$ of all photons. Besides this, $\mathcal{P}_{\text{acceptance}}$ also covers the fact that detectors usually have specific energy ranges where their sensitivity is optimal. For SN 1987A we work with photons in the $25 - 100$ MeV energy range at the detector [57, 237].

These effects are collated to $\mathcal{P}_{\rm total} = \mathcal{P}_{\rm total}(m_a, g_{a\gamma\gamma})$, the probability for the photon to be counted at the detector. For a very light ALP this factor is practically constant and only ALP-photon oscillation in the magnetic field of the galaxy is relevant [56]. Here, on the other hand, $\mathcal{P}_{\rm total}$ depends on m_a and $g_{a\gamma\gamma}$ in a non-trivial way, also reflecting the relatively more complicated geometry shown in Fig. 5.1.

In Section 5.3 we will numerically determine the effects of $\mathcal{P}_{\rm total}$, but it is worthwhile to briefly address the essential factors. To simplify the discussion we will consider next a situation of an ALP with fixed energy and discuss the probability for the resulting photons to reach the detector. This assumption means that in what follows we do not consider the necessary convolution of the various factor with the energy distribution. Since we are interested in understanding the low-mass ($m_a \sim$ 10 keV - 1 MeV) behavior of the fluence, the mass dependence of the Primakoff cross section may be disregarded. In this sense, the suppression factor of eq.(5.14) is also disregarded in this discussion[14].

The probabilities for such a case will be denoted by P, in contrast with $\mathcal{P}$. We have already discussed $\mathcal{S}(m_a)$ earlier, so let us comment on the second effect, $\mathcal{P}_{\rm survival}$. This factor refers to the survival probability for the ALP to leave the influence of the progenitor star,

$$P_{\rm survival} = \exp\left(-\frac{R_\star}{\ell_{\rm ALP}}\right), \tag{5.18}$$

where $R_\star$, the effective radius, is much larger than the actual radius of the progenitor's core ($\sim$ 50 km for SN 1987A). It is actually the outer radius of the progenitor star[15] [240]. Following Ref. [241] we shall take

$$R_\star \sim 3 \times 10^{10}\,{\rm m}. \tag{5.19}$$

As can be seen from eq.(5.3), for masses above a few tens MeV and couplings larger than $\sim 10^{-10}\,{\rm GeV}^{-1}$, the decay length is typically smaller than the effective radius. For such large masses one expects that the bound weakens due to the loss in sensitivity, what is indeed observed in our simulations, cf. Fig. 5.8: on the upper-right corner, the region where $\ell_{\rm ALP} \lesssim R_*$, is not excluded. There the bound behaves as $g_{a\gamma\gamma} \sim m_a^{-2}$, which is compatible with eqs.(5.18) and (5.3). The effective radius and the fact that decays within $R_\star$ are blocked inside the progenitor also place an upper limit on the mass range available to our analysis.

[14] As already mentioned, the suppression factor will become important for masses comparable to the other (effective) parameters in the production, namely, the effective Debye screening scale and core temperature, where it will trigger a reduction of the ALP production and gamma-ray flux.

[15] We assume that the external layers of the collapsing star are still able to absorb and retain the ALP-originated photons.

The effect of the third and fourth factors – $\mathcal{P}_{\rm decay}$ and $\mathcal{P}_{\rm time}$ – are somewhat entangled, so let us treat them together. For this we shall consider the typical time delay of an ALP-originated photon. As shown in Fig. 5.1, due to the non-zero decay angle, together, the ALP and the ensuing photon cover a combined distance greater than the line-of-sight distance $d_{\rm SN}$.

Additionally, the ALP is massive and has a velocity $\beta < 1$, so that, to cover a distance L_1 it needs a time given by $\Delta t_a = L_1/\beta$. Similarly, the ensuing photons cover a distance L_2 in $\Delta t_\gamma = L_2$, cf. Fig. 5.1. The total time of travel is then given by $\Delta t_a + \Delta t_\gamma$. However, it is more interesting to measure the time starting from the first signal of the SN event[16], which is the experimental quantity most easily available. We would therefore observe a time delay

$$\Delta t = \frac{L_1}{\beta} + L_2 - d_{\rm SN}, \tag{5.20}$$

which measures the arrival time of the ALP-originated gamma rays relative to the arrival of the first indications of the SN event.

We wish to estimate the probability that the ALP decays before $d_{\rm SN}$ and is detected within a given time frame[17] δt. For simplicity we consider small masses ($m_a \lesssim$ MeV) and estimate the fraction of events occurring within a measurement time $\delta t \sim 100$ s as follows. To incur a time delay $\Delta t \lesssim \delta t$ the ALP must decay before a distance $L_{\rm max} = \delta t \frac{\beta}{(1-\beta)} \sim \delta t \gamma^2 = \delta t \frac{E_a^2}{m_a^2}$. As long as $L_{\rm max} \lesssim \ell_{\rm ALP}$, the probability of measuring ALPs with time delays $\Delta t \lesssim \delta t$ is $L_{\rm max}/\ell_{\rm ALP}$, i.e.,

$$P_{\rm decay} \times P_{\rm time} \approx \delta t E_a \, g_{a\gamma\gamma}^2 m_a^2. \tag{5.21}$$

Furthermore, having in mind that the ALP production cross section includes an extra factor of $g_{a\gamma\gamma}^2$ (cf. eq.(5.13)), we see that, for a given detection time, the ALP-originated fluence $\mathcal{F}_\gamma = \mathcal{F}_\gamma^{\rm naive} \times \mathcal{P}_{\rm total}$ behaves as $\sim g_{a\gamma\gamma}^4 m_a^2$, thus implying that the bound behaves as

$$g_{a\gamma\gamma} \sim m_a^{-1/2}, \tag{5.22}$$

which is the behavior we observe in our numerical results (cf. Section 5.4).

Finally, the gamma-ray detector that took the data for SN 1987A had half-sky field of view [57], so we may assume that the angular acceptance does not severely constrain $P_{\rm acceptance}$. However, the detector we are considering in connection to SN 1987A had three energy bands, $[4.1, 6.4]$ MeV, $[10, 25]$ MeV and $[25, 100]$ MeV. Looking at Fig. 5.2 we see that the ALP spectrum is peaked around $E_a \sim 80$ MeV.

[16] Via photons or massless neutrinos travelling directly the distance between the SN and Earth.
[17] From data provided in Ref. [57] we can extract limits for time intervals $\delta t \lesssim 223\,$s.

Considering that the ALP is relativistic for $m_a \ll E_a$ – a condition that is met for a large range of the mass scale we are considering – the two photons are strongly collimated along the direction of the ALP's motion and their energies are tightly distributed around $E_a/2 \sim 40$ MeV. This shows that the broadest energy band of the detector, $[25, 100]$ MeV, comprises the majority of the photons.

Using Fig. 5.2 we may estimate $P_{\text{acceptance}}$ as the normalized area under the curve within the aforementioned (optimal) energy band. By doing so we find $P_{\text{acceptance}} \sim 0.7$. As we shall see in Section 5.4.2, for Betelgeuse this factor is significantly smaller due to the energy range accessible to the Fermi-LAT detector that is slightly too high compared to the average energy of the ALPs (and their photons) produced at the supernova.

5.2.3 Angular and time distributions

The angular and time distributions are related. Due to the assumed isotropy of the SN explosion, the angular and time delay distributions will be the same at any point on a sphere with radius d_{SN} around the SN. Therefore, to obtain the aforementioned distributions, it is enough to look at the distribution in angle and time with which the photons hit the surface of this sphere[18].

Let us now look at the typical chain of events leading to detection on Earth. Following Fig. 5.1 we see that an ALP emitted from the SN will decay after covering a distance L_1. One of the photons – the argument is obviously valid for both – is emitted at an angle α and then, after travelling a distance L_2, hits the sphere of radius d_{SN}, i.e., it is detected. These quantities are related via $L_2^2 + 2\,(L_1 \cos\alpha)\, L_2 + L_1^2 - d_{\text{SN}}^2 = 0$, which can be solved for L_2, giving

$$L_2 = -L_1 \cos\alpha \pm \sqrt{d_{\text{SN}}^2 - \sin^2\alpha L_1^2}. \tag{5.23}$$

At this point it is important to differentiate between two regions in space: $0 \leq L_1 \leq d_{\text{SN}}$ and $L_1 > d_{\text{SN}}$. The first region corresponds to ALPs decaying between the SN and Earth. It is clear that, for $\alpha \leq \pi/2$, only the plus sign is physically meaningful, as the negative sign would result in a negative length. Now, for an obtuse decay angle, due to $L_1/d_{\text{SN}} \leq 1$, the plus sign is again the only choice. Both situations imply an incident photon in the "frontal" hemisphere of the detector (from now on we assume that the detector is aimed directly at the SN).

[18] In other words: if a photon originating from an ALP emitted in a certain direction hits this sphere, one can always find a rotation that puts Earth into the path of this particular photon. Hence, due to the isotropy assumption, emission of an ALP in this rotated direction has the same probability.

For the outer region, $L_1 > d_{\rm SN}$, a photon emitted with $\alpha \leq \pi/2$ will not be able to reach Earth. Since the ALPs are usually quite boosted, this is a relatively frequent situation. Therefore, in this region only backward decays ($\alpha > \pi/2$) are relevant, i.e., detectable in principle. In the latter scenario, both signs may result in acceptable solutions, but under the condition that $\sin\alpha \leq d_{\rm SN}/L_1$. This guarantees that the photon crosses the sphere with radius $d_{\rm SN}$ at least once: the plus (minus) sign indicates the first (second) intersection of the photon with the detector at $r = d_{\rm SN}$.

As already mentioned, the probability that a photon is emitted backwards is very small, since this can only happen if the parent ALP is not very boosted (either very heavy or low energetic) and, at the same time, travels beyond $r = d_{\rm SN}$. This is a highly unlikely scenario and most of the backward decays in the outer region do not reach Earth at all – these photons are therefore essentially lost.

Moreover, from the law of sines one finds that the incidence (detection, if we aim the detector at the SN) angle of the ALP-originated photon with respect to the line of sight is given by

$$\sin\theta = \frac{L_1}{d_{\rm SN}}\sin\alpha, \tag{5.24}$$

and we note that, for a large number of photons with this detection angle, the angular "halo" is $\Delta\phi = 2\theta$. As we shall see, the halo is usually small within the excluded region in the ALP parameter space, but may be sizeable outside of it, specially for MeV-scale ALPs (cf. Fig. 5.6).

To get an idea of the size of the effects discussed above, let us evaluate the time delay for an ALP with $m_a = 10\,\text{MeV}$ and $g_{a\gamma\gamma} = 10^{-10}\,\text{GeV}^{-1}$. If we take $E_a = 100\,\text{MeV}$ as a representative value for the energy, the photon is emitted under an angle $\alpha \simeq \sin^{-1}(\gamma^{-1}) \simeq 6$ deg. Using $d_{\rm SN} = 51.4\,\text{kpc}$ for SN 1987A and assuming that the ALP decays after a distance $L_1 \sim \ell_{\rm ALP} \simeq 0.13\,\text{kpc}$, eqs.5.23 and 5.24 show that the time delay would then be (cf. Fig. 5.5)

$$\Delta t \simeq 1.3 \times 10^3\,\text{s}, \tag{5.25}$$

showing that Δt can be significant, potentially spreading the signal over a much longer time period than the duration of the SN explosion ($\sim 10\,\text{s}$). In this case the angular halo would be $\Delta\phi \simeq 10^{-5}$ deg (cf. Fig. 5.7), which is due to the very short decay length.

Repeating this exercise for points in the *allowed* region in parameter space shown in Fig. 5.7 we would get even larger effects. For $m_a = 1$ MeV and $g_{a\gamma\gamma} = 10^{-12}\,\text{GeV}^{-1}$, we find that the time delay is $\Delta t \simeq 3 \times 10^8$ s, whereas the angular halo is $\Delta\phi \simeq 2$ deg (cf. Fig. 5.6).

So far we have assumed a fixed emission angle of the photon with respect to the original ALP direction. This assumption was based on the arguments around eq.(5.8), but let us now justify this in a different, more explicit way. Since the ALP is a spin-0 particle, in its rest frame photon decay is equally likely in any direction. The isotropy condition may be translated into

$$\frac{dN_{\gamma\gamma}}{d\cos\alpha_0} = \frac{1}{2}, \tag{5.26}$$

which is normalized to unity ($-1 \leq \cos\alpha_0 \leq 1$). Here $N_{\gamma\gamma}$ is the probability of finding the two photons when "photon 1" is emitted with α_0.

In the laboratory the ALP travels with finite speed $\beta \lesssim 1$ and the originally isotropic angular distribution is distorted into an anisotropic one. To see this explicitly we consider the angular distribution for the separation angle between the photons $\psi = \alpha_1 + \alpha_2$. By using $P_a^2 = (P_{\gamma_1} + P_{\gamma_2})^2$, we find that

$$\cos\psi = 1 - \frac{m_a^2}{2E_{\gamma_1}E_{\gamma_2}},$$

which gives the correct $\cos\psi = -1 \rightarrow \psi = \pi$ in the ALP's rest frame, where the energies of the photons are $E_{\gamma_{1,2}} = m_a/2$.

Now, using the chain rule, we have

$$\begin{aligned}\frac{dN_{\gamma\gamma}}{d\psi} &= \frac{dN_{\gamma\gamma}}{d\cos\alpha_0}\cdot\frac{d\cos\alpha_0}{d\psi} \\ &= \frac{1}{2}\left(\frac{d\cos\alpha_0}{d\psi}\right)\end{aligned}$$

and, using eq.(5.4), we may write $\cos\psi = \frac{\beta^2(2-\cos^2\alpha_0)-1}{1-\beta^2\cos^2\alpha_0}$, which can be inverted to express $\cos\alpha_0$ in terms of ψ. In doing so, we obtain

$$\frac{dN_{\gamma\gamma}}{d\psi} = \frac{1}{2\beta\gamma}\frac{\cos(\psi/2)}{\sin^2(\psi/2)}\frac{1}{\sqrt{\gamma^2\sin^2(\psi/2)-1}}, \tag{5.27}$$

which, for $\beta \neq 0$, is peaked at $\sin(\psi/2) = \gamma^{-1}$. It also becomes sharply peaked for $\beta \rightarrow 0$, what is sensible: for zero velocity the separation angle is fixed ($\psi = \pi$) and all photons go to this one value, thus saturating the distribution.

The smallness of the typical decay angle for both emitted photons is the reason why only a very small fraction of the photons from ALP decays outside the sphere of radius $d_{\rm SN}$ around the SN can reach Earth. Backward emissions are therefore very unlikely already for relatively slow ALPs, justifying the previous comments.

5.3 Simulation of the angular and time distributions

We have discussed the features of the ALP production and decay in order to obtain the observable quantity available to us, the fluence (photons per unit area at the detector). In Section 5.2.2 we considered some factors that arise due to the finite decay length of massive ALPs and we saw that, for ALPs with masses $m_a \lesssim 1$ MeV, the Primakoff cross section is effectively insensitive to the mass. Therefore only the kinetic (geometric) factors – $\mathcal{P}_{\rm survival}$, $\mathcal{P}_{\rm decay}$ and $\mathcal{P}_{\rm time}$ – determined the behavior of the ALP-originated fluence.

However, to arrive at eq.(5.22) we made the simplifying hypothesis that the ALPs were monoenergetic. This is clearly not the case and the various effects mentioned above are influenced by the energy distribution of the ALPs, cf. Fig. 5.2. To amend this and obtain a more realistic picture of the mass and coupling-dependent fluence of ALP-originated radiation we must convolute these factors with the actual ALP spectrum.

As we shall see, for the low-mass region ($m_a \sim 10\,\text{keV} - 10\,\text{MeV}$) this will not be determinant and the bound will follow our estimate, eq.(5.22). However, for larger masses ($m_a \sim 10\,\text{MeV} - 100\,\text{MeV}$) the Primakoff cross section is suppressed and we enter a region where the bound is less efficient. Therefore, in order to obtain the full mass and coupling dependence of the fluence, we perform a numerical simulation which takes all the aforementioned effects into account.

5.3.1 Description of the simulation

Approximate analytic results for the distribution in time have already been obtained[19] in Ref. [235]. We have instead used a full numerical simulation to account for the combined effect of the ALP production in the core of the SN, its motion out of the collapsing star and subsequent decay in two photons, as well as their path until arrival on Earth. Below we describe the simulation as well as the numerical results concerning the time-delay and angular distributions in the context of SN 1987A. We denote as "valid events" the events that pass all the cuts and reach Earth, that is, these are the detected photons.

[19] While we fully agree with the general approach taken in Ref. [235], we were unable to reproduce the resulting limits in their case. We think there are two reasons for that. 1) The approximation in their Eq. (2.10) requires $\frac{\Delta t}{d_{\rm SN}} \frac{1}{1-x\beta} \sim \frac{\Delta t}{d_{\rm SN}} \gamma^2 \ll 1$. For low masses and observation times several years later this does not seem to hold (in our case it does and we find a $g_{a\gamma\gamma} \sim m_a^{-1/2}$ behavior). 2) Emission with an effectively fixed temperature does take place only for a very small time frame ~ 10 s.

It is useful to have an overview of the different ingredients that come into the simulation in order to better understand which role they play. Below we list the variables and what we know about them.

- **ALP energy**: each ALP is produced in the core of the collapsing star with an energy E_a which follows a given distribution. This information will be relevant for a few reasons. First of all, this is what happens in Nature, so it would be a crude approximation not taking it into account. Secondly, the energy, together with the mass, determines the boost and this in turn fixes the kinematics of the decay (for a given angle α_0 in the rest frame). The ALP energies are distributed according to the spectrum from eq.(5.11) (corrected by the suppression factor incorporating the massive Primakoff cross section) which, when normalized, provides the probability distribution.

  In fact, the complicated functional dependence of the spectrum on the energy makes it difficult to implement the simple sampling procedure used to pick the decay distances (see below). To remedy this we employ the so-called acception/rejection (A/R) method[20]. Let us first concretely state our goal: generate random variables X which follow the desired PDF $f(x)$. In our case, $f(x)$ is the spectrum and $x = E_a$. The A/R method relies on choosing a function $t(x)$ that *majorizes* $f(x)$, that is, $t(x) \geq f(x)$ for every x with $t(x) \geq 0$. Since this function is rather arbitrary, it is not a *density* function, so we may normalize it to one and denote its normalized version as $T(x)$, now a proper density function. The A/R algorithm follows then as:

  - **Step 1**: generate a (random) number x following the density[21] $T(x)$
  - **Step 2**: generate u from an uniform distribution $U(0, 1)$
  - **Step 3**: *if* $u \leq f(x)/t(x)$, then accept x
  - **Step 4**: *else* reject x and go back to step 1

  In this fashion, the set of numbers $\{x\}$ that pass the test should follow the desired distribution $f(x)$. Very important is to find an adequate (i.e., simple) majoring density function $t(x)$ and we chose it to be the "height" of the normalized spectrum[22]. The normalized spectrum and the histogram of the sampled energies are shown in Fig. 5.4.

[20] Invented in 1951 by John von Neumann [242].

[21] Since we normalized it to unity, this is a uniform distribution $V(0, 1)$.

[22] Naturally this criterion is mass dependent, as the shape of the distribution changes for higher masses. We included this in the simulation by choosing different majoring functions for different mass ranges, so that the acceptance ratio remains roughly fixed – see Fig. 5.4. This choice is the simplest possible, but it comes at the cost of a relatively low efficiency ($\sim 30\%$ in our case).

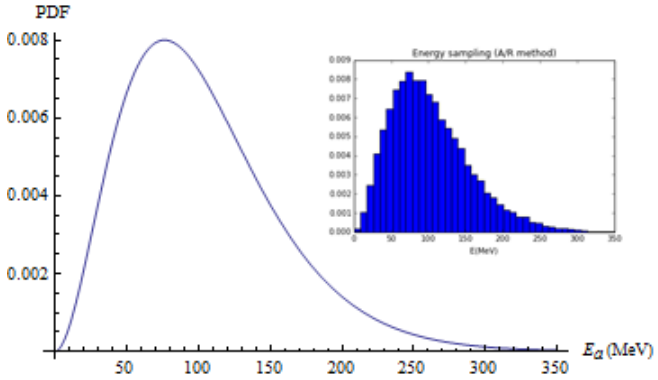

Figure 5.4: Normalized PDF and histogram of energies (acceptance rate: 30%).

- **Length covered by the ALP (L_1)**: apart from the radius of the star[23], the distance travelled by the ALP before decaying is statistically non-uniform, since (for a given fixed decay length) longer distances are less likely to happen than smaller ones.

  The distance travelled r is sampled from a distribution following the exponential decay/survival behavior typical of radioactive decays. The normalized *decay* probability density is given by $f_{\rm dec}(r) = \ell^{-1} e^{-r/\ell}$, so that the probability of decaying at $r \leq r_0$ is $P_{\rm dec}(r \leq r_0) = \int_0^{r_0} f_{\rm dec}(r) dr = 1 - e^{-r_0/\ell}$. With this the *survival* probability up to the distance r_0 is $P_{\rm surv}(r \leq r_0) = e^{-r_0/\ell}$, which is actually the cumulative distribution function (CDF) for the survival.

  We are interested in drawing sample distances from a distribution reflecting the survival chances of an ALP with a given decay length $\ell_{\rm ALP}$. This may be done using the "inversion" technique: $y(u) = {\rm CDF}^{-1}(u)$, where $u = [0, 1]$ is a uniformly distributed (random) number, such that the variable y is distributed as needed. In our case, we obtain

  $$y(u) = -\ell_{\rm ALP} \, \ln(u), \tag{5.28}$$

  which, due to the energy dependence of the decay length, is implemented in our simulation for each energy value sampled from the ALP spectrum as detailed above.

- **Decay angle in the rest frame (α_0)**: as already argued, the decay in the ALP's rest frame is isotropic. The angle α_0 may then be sampled from the uniformly distributed range $[0, \pi]$.

[23] According to the discussion around eq.(5.18), the ALP-originated photons will be completely blocked within a radius R_*.

- **Decay angles ($\alpha_{1,2}$)**: these angles are not isotropic any more, given that the ALP is boosted with parameter $\beta \lesssim 1$ (cf. eqs.(5.6) and (5.7)). Given the uniform distribution of the decay angle in the rest frame, we can plug these randomly sampled values to obtain a collection of $\{\cos\alpha_1, \cos\alpha_2\}$, which are functions of the uniformly distributed $\{\alpha_0\}$ and of the sampled energy like previously described.

With the discussion above the general "chronology" of the simulation is as follows. We first generate the ALP energy distribution for each $\{m_a, g_{a\gamma\gamma}\}$-pair based on the massive Primakoff cross section, eq.(5.13). For each $\{m_a, g_{a\gamma\gamma}\}$-pair we produce $\sim 10^7$ points, from which we extract (via the A/R method) roughly 0.3×10^7 energy values (our ALPs) following the production spectrum for the respective mass, naturally subject to $E_a \geq m_a$.

Next we make use of the geometry displayed in Fig. 5.1 and sample for each ALP a distance L_1 travelled by the ALP before it decays, which is exponentially distributed following $P_{\rm decay} = \exp\left(-L_1/\ell_{\rm ALP}\right)$. At this point we must impose the first physical cut by demanding that photons decaying inside the region $L_1 \leq R_*$ (cf. eq.(5.18)) are effectively absorbed and do not escape the SN, therefore not reaching the detector. This cut will only impact on relatively heavy and strongly coupled ALPs, not being relevant before a few tens MeV.

After covering the distance L_1, the ALP decays in two photons. In the ALP's rest frame the ALP-originated photons have equal energies, but, due to the boost, in our frame their energies are distributed with some spread around $E_a/2$. Since the detectors have in general a limited (optimal) energy acceptance, we impose here our second important physical cut by limiting the valid events in the simulation to boosted photons with energies in the range $[E_-, E_+]$. Here $E_\pm$ are determined by the specific detector under consideration. In the case of the original measurements from SN 1987A, the optimal energy range was for gamma rays in the interval $25 - 100$ MeV [56, 57]; see also discussion at the end of Section 5.2.2.

The simulations for time delay and angular distributions take the aforementioned aspects into account. We highlight again that, in our numerical simulation, the ALP production is taken as being instantaneous, i.e., all ALPs are produced at the same time in the core of the progenitor star. We will return to this point in Section 5.4. Below we present a few representative examples, as well as discuss their most important physical features.

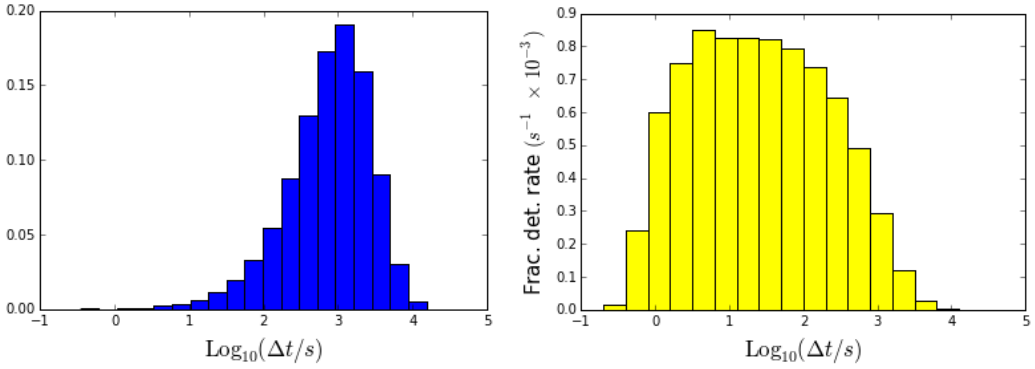

Figure 5.5: For ALPs with $m_a = 10$ MeV and $g_{a\gamma\gamma} = 10^{-10}\,\mathrm{GeV}^{-1}$: fraction (probability) histogram depicting the distribution of time delays (left) and fractional detection rates (right).

5.3.2 Time distribution

In Section 5.2.3 we discussed the path covered by the ALP and the ensuing photons, where we showed that the combined trajectory leads to time delays often longer than the ~ 10 s duration of the neutrino burst that announced SN 1987A [57]. As mentioned before, backwards photons reaching Earth are very rare, but these will be counted, despite of their relatively small contribution to the overall number of events.

The time-delay simulation follows the steps indicated in Section 5.3.1: a number of ALPs is generated with the energy distribution given in Fig. 5.2 and, after travelling a distance L_1, they decay into two photons that cover distances L_2 until detection. The respective time delays – two per ALP in general[24] – are then calculated according to eq.(5.20).

A typical example of a time distribution is shown on the left panel of Fig. 5.5, where we use a logarithmic time scale for convenience. Similarly, on the right panel we show the *fractional* detection rate (in units of $10^{-3}\,\mathrm{s}^{-1}$), i.e., the fraction of ALP-originated gamma rays arriving at the detector per unit time[25]. Note that this partially corrects the deformation introduced by the (convenient) logarithmic time scale and allows us to have a better idea of the time evolution of the signal.

More specifically, we see that the largest detection rates are observed until a time $\sim \Delta t$. Taking Fig. 5.5 as an example, for $m_a = 10$ MeV, $g_{a\gamma\gamma} = 10^{-10}\,\mathrm{GeV}^{-1}$ and $E_a \sim 100$ MeV, using eq.(5.20) we find $\Delta t \sim 10^3$ s, which indicates the beginning

[24] "In general" because, if the ALP decays after Earth, there is at most one photon that has the possibility of reaching the backward hemisphere of the detector.

[25] The height of each bin is given by the fraction of detections divided by the time length of that bin (note the logarithmic time scale).

of the reduction of the signal[26]. In this sense, Δt gives a good idea of the time period – starting from the "announcement" of the SN event – before which most of the ALP-originated gamma rays should arrive.

Finally, it is interesting to check the extreme points of the time-delay distribution for a given boost $\beta < 1$. If we only concentrate on detections in the forward direction of the detector[27], the shortest and longest time delays possible come from straight-line trajectories: the shortest time delay is obtained by a highly boosted ALP decaying collinearly after leaving R_*, so that the associated time delay is $\Delta t_{\rm short} = \frac{R_*}{c}\frac{1-\beta}{\beta} \simeq \frac{R_*}{c}\frac{m_a^2}{2E_a^2}$, where we used $R_* \ll d_{\rm SN}$.

On the other hand, the longest time delay is obtained when a very slow ALP decays backwards when it reaches $L_1 = d_{\rm SN}$. The corresponding time delay reads then $\Delta t_{\rm long} = \frac{d_{\rm SN}}{c}\frac{1+\beta}{\beta}$. Those limiting cases are nevertheless statistically rare and may not be realized in a finite numerical simulation.

5.3.3 Angular distribution

Given that the detection direction of the ALP-originated gamma rays does not in general coincide with the line of sight between Earth and the SN, it is expected that the signal at the detector exhibits an angular spreading, i.e., a halo around the position of the SN. According to eq.(5.24) and taking the energy distribution into account this halo should have an angular opening of $\Delta\phi \sim 2\theta$.

This halo could, in principle, cover a relatively large area of the sky. Considering the unconstrained angular distribution for a given $\{m_a, g_{a\gamma\gamma}\}$-pair we obtain distributions similar to the one in Fig. 5.6. This example shows that the majority of the detections would happen in the vicinities of the normal incidence. Furthermore, we see that it is possible to reach considerably large maximal angular openings, specially in the *non-excluded* region in parameter space. This is exactly the case shown in Fig. 5.6 – compare with Fig. 5.7 – where $\Delta\phi \sim 1^\circ$, which is about two times larger than the angular diameter of the Moon.

Since most of the photons arrive around $\theta = \theta_0 = 0$, it is interesting to consider a finite angular region centered at the SN that contains a certain fraction $f_{\rm ang}$ of the incident gamma rays. Moreover, when discussing angular distributions, we do not consider particular time intervals, but rather show the effective angular openings after *all* ALP-originated photons have been detected[28].

[26] In this case the angular halo would be $\Delta\phi \simeq 10^{-5}$ deg, cf. Fig. 5.7.

[27] For the backward hemisphere of the detector the largest time delay would be infinite.

[28] Looking at the typical time-delay distributions we expect the angular halo to grow until an instant $\sim \Delta t$ and, from this point on, to keep the aspect acquired until then (after all, at $\sim \Delta t$ most of the detectable photons would have already arrived).

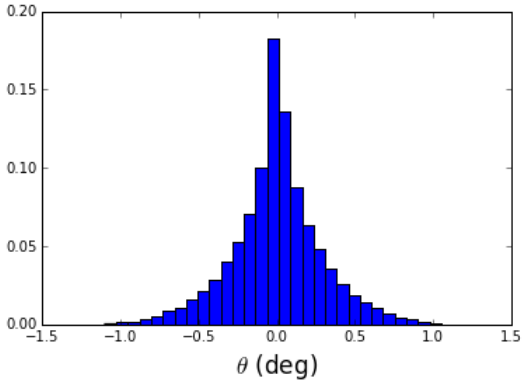

Figure 5.6: Distribution for the incidence angle for photons originated from ALPs with $m_a = 1\,\mathrm{MeV}$ and $g_{a\gamma\gamma} = 10^{-12}\,\mathrm{GeV}^{-1}$ emitted from SN 1987A. Here $\theta = \theta_0 = 0$ corresponds to the direct line-of-sight between Earth and the SN.

The fraction of events within the angular acceptance is relevant to determine the sensitivity. Therefore, we are looking for the angular windows $\Delta\phi$ such that the interval $[\theta_0 - \Delta\phi/2, \theta_0 + \Delta\phi/2]$ centered around θ_0 (here $\theta_0 = 0$ is taken as the direction of line-of-sight to the SN) contains the desired fraction of valid events. This is shown for SN 1987A in Fig. 5.7, where we present $\log_{10}(\Delta\phi/\mathrm{deg})$ in the $g_{a\gamma\gamma} - m_a$ plane for $f_{\mathrm{ang}} = 90\%$. Let us now address some features of Fig. 5.7.

The empty area on the left corner corresponds to small masses and couplings. It is not covered due to the extremely long decay lengths, $\ell_{\mathrm{ALP}} \gg d_{\mathrm{SN}}$, where few ALP-originated photons are able to reach the detector. However, for such small masses, the ALPs are typically very boosted ($\gamma \gg 1$), so it is unlikely that the detectable photons arrive at incidence angles close to $\theta = 0$, which in turn introduces a large spread in the angular distribution for such backward-emitted photons. In order to avoid introducing possibly misleadingly large angular windows (though poorly populated), we refrain from including backward decays in the simulation for the angular distribution. The lack of contour lines is not physically meaningful: it is actually an artifact due to the finite number of points in the simulation.

The opposite behavior is observed in the upper-right corner, where masses and couplings are large: the decay length is much smaller than d_{SN} and the great majority of events is effectively detected. Also important in this large-mass region is the fact that $\sin\theta \sim 1/m^3$ (cf. Eqs. (5.3) and (5.8)), so the angular windows are correspondingly tight. One must keep in mind, however, that in this region of the $m_a - g_{a\gamma\gamma}$ plane the decay length eventually shrinks below R_*, where the ALP-originated photons are trapped inside the stellar material and do not leave. This is indicated in the top-right part of Fig. 5.7, where the bound on the fluence is overlapped with the contour plot of the angular openings.

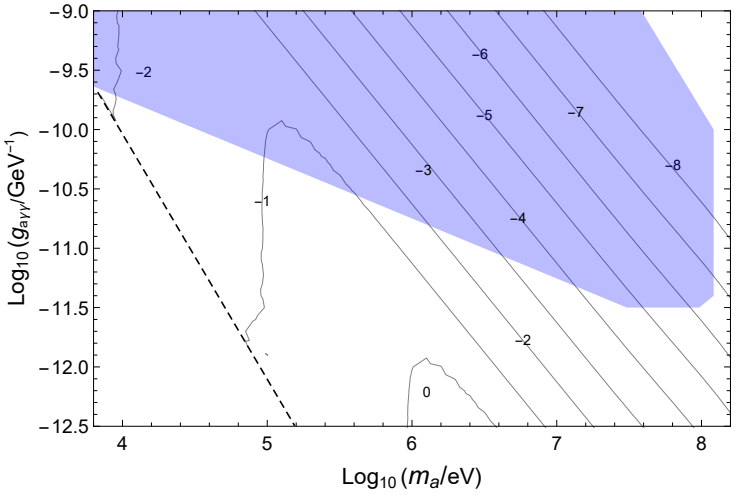

Figure 5.7: Angular windows for SN 1987A with contours corresponding to $f_{\rm ang} = 90\%$. The bound from Fig. 5.8 is shown in light blue.

The contours in Fig. 5.7 represent lines of constant detection angle. From eq.(5.24) we have $\sin\theta \simeq \ell_{\rm ALP} \sin\alpha$, which gives $g_{a\gamma\gamma} \sim m_a^{-3/2}$. It is noteworthy that, in the *allowed* regions (fluence below the experimental upper limit) one may find relatively broad angular windows for large masses and small couplings.

The (dashed) left border of the plot in Fig. 5.7 is not physical. In fact, it is an artifact of a finite numerical simulation. It is important to note that, as the decay length increases, the angular windows tend to get larger, but a considerable reduction in the overall number of events takes place. This is because, as $\ell_{\rm ALP} \to d_{\rm SN}$, the decay angle needs to be distributed over a larger range to ensure detection. This, in turn, demands lower boosts, what is only possible for large masses, but then the decay lengths are usually small. This "cycle" shows that we should expect a reduction in the number of detections in regions where $\ell_{\rm ALP} \gtrsim d_{\rm SN}$.

Also interesting is the presence of vertical lines in Fig. 5.7. To understand these, let us consider a fixed detection angle. For heavy ALPs, the decay angles may vary within a relatively large range and many different paths will end up having the same detection angle even though they have a variety of travelled distances ($L_1 \sim \ell_{\rm ALP}$) and decay angles ($\sin\alpha \sim \gamma^{-1}$). In a sense, the decay lengths may vary enough to "compensate" for the freedom in the decay angles.

As one goes to smaller masses, i.e, more boosted ALPs, the decay angles are quickly more constrained, thus leaving less room for the decay lengths to compensate. In this low-mass region, the detection angle is therefore dominated by the maximal decay angle $\sim \gamma^{-1}$, which is independent of the coupling constant, hence the vertical drop-off observed in Fig. 5.7.

5.4 Limits from supernovae

5.4.1 SN 1987A

The blue supergiant Sanduleak -69° 202 ($M_* \sim 18 M_\odot$ and $R_* \sim 3\times10^{10}$ m [237]), located at a distance of $d_{\rm SN} = 51.4$ kpc in the Large Magellanic Cloud, was the first supernova[29] of 1987 (23 February). Its observation in visible light was preceded by the detection of a 10.24 s-long neutrino burst containing 25 neutrinos [57], which were detected by three distinct experiments [243]-[245]. For a nice review, see Ref. [246] and references therein.

At the time of the event, the Gamma-Ray Spectrometer (GRS), which was sensitive in the $4.1 - 100$ MeV range with half-sky field of view, was mounted on the satellite-borne Solar Maximum Mission (SMM) [57]. The SSM was aimed at the Sun, not at Sanduleak -69° 202, but even then it was possible to extract data concerning the emissions from the direction of the SN – it was almost at 90° of the detector – during the time of the neutrino burst. The subsequent analysis showed that no excess of gamma-ray radiation reached the detector from the direction of the SN 1987A explosion during the neutrino burst[30]. This non-observation (null result) allowed only to set an upper limit on the gamma-ray fluence, namely, $\mathcal{F}_\gamma^{\rm exp}(10\,{\rm s}) < 0.6\,\gamma\cdot{\rm cm}^{-2}$ $(3\,\sigma)$, for photons in the energy range $25 - 100$ MeV. As already discussed in Section 5.2.2, this energy band is in fact the most interesting when looking for ALPs with $E_a \sim 80$ MeV or a bit higher, as the ensuing photons would have energies distributed around $E_a/2$.

As mentioned in Section 5.3.1, our simulation assumes that the ALP production happens instantaneously, so that all ALPs are produced in the core of the exploding progenitor at the same time. In practice, according to the analyses of Ref. [56], this process happens in a time frame of ~ 10 s. In contrast to Ref. [247], for massive ALPs the time-delay distributions may be quite broad, cf. Section 5.3.2.

It is therefore advantageous to use a longer time window after the first neutrino recorded. To do so we look at the full time window of Ref. [57], $\delta t \simeq 223$ s, and consider the $3\,\sigma$ statistical fluctuation on the fluence in this period. Since no excess number of events are recorded compared to the control region[31] we use the number of events $N = 1393$ and the estimate $\sigma = \sqrt{N}$. The upper bound on the fluence for the extended observation time is $\mathcal{F}_\gamma^{\rm exp}(223\,{\rm s}) \leq 3\times\sigma/A_{\rm eff} = 1.78\,\gamma\cdot{\rm cm}^{-2}$. Here we have used the effective area of the gamma-ray detector $A_{\rm eff} = 63\,{\rm cm}^2$ [57].

[29] It was the first SN to be visible with the naked eye since the one observed by Kepler in 1604.

[30] The original reason to search for this coincidence was to constrain the mass of neutrinos, which could then radiatively decay into gamma rays [57].

[31] That is the time range *before* the arrival of the first signal from SN 1987A.

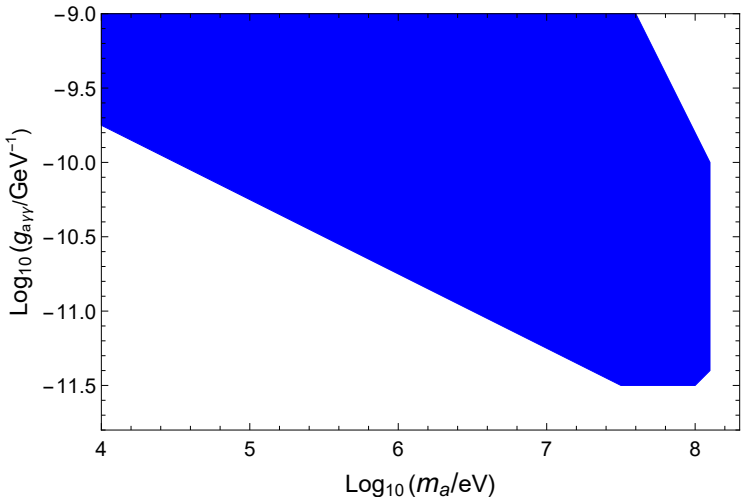

Figure 5.8: Bound based on the fluence for SN 1987A with $\mathcal{F}_\gamma^{\rm exp}(223\,{\rm s}) \leq 1.78\,\gamma\cdot{\rm cm}^{-2}$. The excluded region is displayed in blue.

With this we are able to derive the bound presented in Fig. 5.8. As mentioned in Section 5.2.2, the bound in the low-mass region behaves as $g_{a\gamma\gamma} \sim m_a^{-1/2}$. The non-excluded region increases as the mass decreases due to the decay length: as the masses get smaller, the ALPs are able to survive statistically longer, until the point where they decay predominantly behind Earth, so that, being extremely boosted, very few photons reach us on average, thus suppressing the bound.

The linear behavior is sustained until masses of $\mathcal{O}(10\,{\rm MeV})$ and then a turn up takes place. This was anticipated in the discussion of the suppression factor $\mathcal{S}(m_a)$ depicted in Fig. 5.3. This is attributed to the size of the physical parameters entering the (massive) Primakoff-based production, namely, the effective Debye screening scale and core temperature, both $\mathcal{O}(10\,{\rm MeV})$. This is the point where the production rate "feels" that the ALPs being produced are actually heavy, thus consuming a portion of the energy available and converting it into rest mass for the ALPs. This reduces the number of ALPs produced and the fluence is correspondingly suppressed, thus causing the bound to recede.

Another interesting feature is the impact of the effective radius, which is visible on the upper-right region of Fig. 5.8. This area in parameter space is characterized by very small decay lengths, which may be eventually smaller than R_*. When this happens, the ALP-originated photons are absorbed and cannot be detected on Earth – this explains the *allowed* region above the excluded area (cf. Section 5.2.2).

The energy range of the photons used to obtain the bound in Fig. 5.8 is $[25, 100]$ MeV and this is a somewhat optimal range. Since each ALP decays in two photons, the energy of each photon is distributed around $E_a/2$ and, given that the ALP spectrum achieves a maximum around $E_a \sim 80$ MeV, most of the ALP-originated

gamma rays will be produced with $E_\gamma \sim 40$ MeV. In this sense, the optimal energy range for gamma-ray detection should include this value – and possibly even lower ones – in order to cover the range where ALP production is largest.

5.4.2 Betelgeuse

Betelgeuse is a red supergiant located at the Orion constellation and is one of the brightest objects in the night sky. Its distance to Earth is around 200 pc (650 ly) and its mass is estimated to be $17 - 25\, M_\odot$. For simplicity, we shall assume that Betelgeuse is as massive as the progenitor from SN 1987A, $\sim 18 M_\odot$, which is not unreasonable [248]. Furthermore, since Betelgeuse is a red – not a blue – supergiant, its radius is larger than that of the progenitor for SN 1987A. This means that the associated effective radius[32] is roughly 20 times larger than the one from SN 1987A, i.e., $R_* \sim 6 \times 10^{11}$ m, so we expect a contraction, i.e., a worsening, of the bounds for large masses and couplings.

Betelgeuse has already finished burning H and is burning He. It is expected to continue its evolution through the C-, O-, Si- and Fe-burning phases and it has been estimated that in $\lesssim 10^5$ years it will reach its final evolutionary stages and go supernova [249]. Due to its proximity, should it transition to a supernova, the explosion would be very bright (also in X and gamma rays), though not dangerous to us [248]. More interestingly, the associated ALP-originated gamma-ray flux would be much more intense than the one from SN 1987A. Besides this, the gamma-ray instruments have improved in the last decades, so we expect the sensitivity to be significantly better, thus allowing us to set stronger bounds on the ALP parameter space.

One of the best detection possibilities currently would be the Fermi large-area telescope (Fermi-LAT) whose point source sensitivity after an observation time of one year is $3 \times 10^{-9}\, \gamma \cdot \mathrm{cm}^{-2} \cdot \mathrm{s}^{-1}$ for incident photons with energies $E_\gamma > 100\,\mathrm{MeV}$ [250]. Since we are interested in comparing the (projected) sensitivity for Betelgeuse to that for SN 1987A, we may wish to take a similar observation time frame $\delta t \simeq 223$ s.

However, for such a short period (compared to a full year $\sim 3 \times 10^7$ s), the very low fluence from Fermi-LAT cannot be directly used. For this time period, using the effective area of $A_{\mathrm{eff}} = 9500\,\mathrm{cm}^2$ [250], we find $N_\gamma \sim (3 \times 10^{-9}\, \gamma \cdot \mathrm{cm}^{-2} \cdot \mathrm{s}^{-1}) \times 220\,\mathrm{s} \times 9500\,\mathrm{cm}^2 \approx 6 \times 10^{-3}\, \gamma$, i.e., we would have less than one photon.

[32] This is a simplification since it has been established that Betelgeuse's surface radius varies (oscillates) in time [248]. In any case, the oscillation period (~ 100 days) is much larger than the collapse duration (~ 10 s), so we may take a fixed valued for R_*.

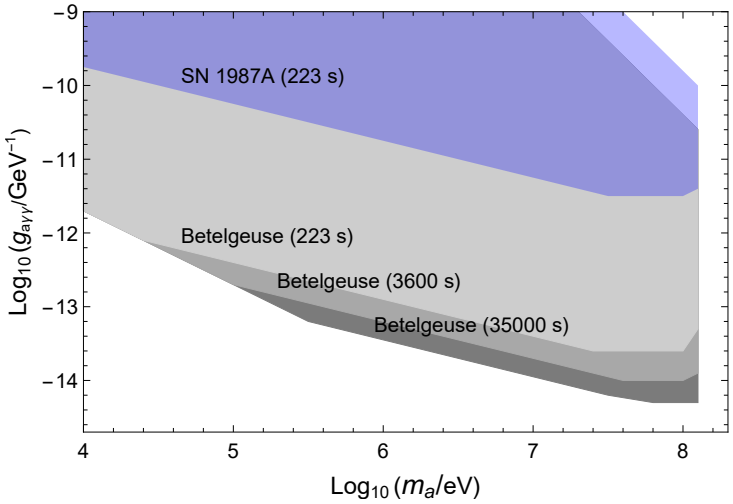

Figure 5.9: Projected sensitivity based on the 223 s, 3600 s and 35000 s observation times for Betelgeuse. The bound from SN 1987A is shown for comparison.

The argument above allows us to assume that, for observation times $\lesssim 3.5\times10^4$ s, the background for Fermi-LAT is expected to be zero (i.e., no photons). To obtain a more realistic upper limit on the fluence we may take a maximum of, say, three photons, so we end up with

$$\mathcal{F}_\gamma^{\rm eff} \lesssim \frac{N_\gamma}{A_{\rm eff}} = 3.2\times10^{-4}\,\gamma\cdot{\rm cm}^{-2}, \tag{5.29}$$

which is our upper limit on the ALP-originated fluence for $E_\gamma > 100$ MeV.

With this estimate of the maximal fluence for Fermi-LAT we may repeat the analysis leading to the results concerning SN 1987A, but now also including other larger observation times (one hour and $\sim$ 10 hours). With this we obtain the projected sensitivities displayed in Fig. 5.9. We see that for $m_a \sim 0.1-10$ MeV the contours behave as expected[33], cf. Section 5.2.2. However, for masses $\lesssim 1$ MeV, the $g_{a\gamma\gamma} \sim m_a^{-1/2}$ behavior changes to $g_{a\gamma\gamma} \sim m_a^{-1}$. This change is due to two intertwined factors: the shorter distance to Betelgeuse and the larger observation times.

To see how these factors contribute to the new behavior we have to consider that $\ell_{\rm ALP} \gg d_{\rm SN}$ for small masses and couplings. This means that only ALPs decaying very close to Earth ($L_1 \approx d_{\rm SN}$) result in detectable photons[34]. Therefore, the detection probability is dominated by $P_{\rm decay} = 1-\exp\left(-d_{\rm SN}/\ell_{\rm ALP}\right) \approx d_{\rm SN}/\ell_{\rm ALP}$. With eq.(5.3) and the extra $g_{a\gamma\gamma}^2$ from ALP production this leads to

$$\mathcal{F}_\gamma \sim g_{a\gamma\gamma}^4 m_a^4 \quad \rightarrow \quad g_{a\gamma\gamma} \sim m_a^{-1}. \tag{5.30}$$

[33]Notice the contraction of the contours due to the larger R_* for Betelgeuse.
[34]This is the smallest distances generated by the distribution of decays with such a large $\ell_{\rm ALP}$.

This is not the end of the story. From Fig. 5.9 we see that the sensitivity contours are affected by this effect at different points. Since the only difference between them is the respective observation times δt, we conclude that this is also a relevant aspect. First of all, we notice that the observations are assumed to be limited to a finite time period δt. Hence, only ALP-originated photons arriving within the interval $\Delta t \leq \delta t$ are effectively counted at the detector (cf. Section 5.3.2). In this sense, the maximal time delay useful for detection is fixed by the observation time.

Since $m_a \ll E_a$, according to eq.(5.8), we have very boosted ALPs and practically collinear ALP-originated photons. This means that the trajectories sketched in Fig. 5.1 are reduced to straight lines with the distance covered by the photons given by $L_2 \approx d_{\rm SN} - L_1$. With this we may write eq.(5.20) as

$$\Delta t \approx L_1 \frac{1-\beta}{\beta} \approx L_1 \frac{m_a^2}{2E_a^2}, \tag{5.31}$$

which can be cast in a more convenient form as

$$\Delta t \approx 5.2 \times 10^{-6}\,\mathrm{s} \left(\frac{m_a}{\mathrm{eV}}\right)^2 \left(\frac{L_1}{\mathrm{kpc}}\right) \left(\frac{100\,\mathrm{MeV}}{E_a}\right)^2. \tag{5.32}$$

As already mentioned, we are bound to time delays as large as or smaller than the observation time. Given that $\Delta t \sim L_1$, the largest time delay ($\Delta t = \delta t$) is only reached by the largest distance possible ($L_1 = d_{\rm SN}$). Plugging this into eq.(5.32) we have $\delta t \approx 5.2 \times 10^{-6}\,\mathrm{s} \left(\frac{m_a}{\mathrm{eV}}\right)^2 \left(\frac{d_{\rm SN}}{\mathrm{kpc}}\right) \left(\frac{100\,\mathrm{MeV}}{E_a}\right)^2$ and we are now able to find the "critical" mass $\tilde{m} = \tilde{m}\,(d_{\rm SN}, \delta t)$ that marks the transition between the two behaviors into the low-mass region. Inverting this expression we find

$$\tilde{m}\,(d_{\rm SN}, \delta t) \approx 4.4 \times 10^2\,\mathrm{eV} \left(\frac{E_a}{100\,\mathrm{MeV}}\right) \left(\frac{\mathrm{kpc}}{d_{\rm SN}}\right)^{1/2} \left(\frac{\delta t}{\mathrm{s}}\right)^{1/2}. \tag{5.33}$$

Looking at Fig. 5.9 we see that $\tilde{m}$, eq.(5.33), is able to approximately match the transition points for Betelgeuse. For SN 1987A, on the other hand, $\tilde{m} < 10$ keV and the low-mass behavior is not visible in our plots[35], but it would be there otherwise. The fact that $\tilde{m}$ increases with δt is reasonable, since heavier ALPs move slower, so longer observation times are sensitive to larger masses. One must note however that here E_a must be such that the photon energies satisfy the constraints of the detector, naturally accounting for the fact that for $E_a \gg m_a$ we have $E_a \approx 2E_\gamma$, which implies that the detector is sensitive to $E_a \sim [2E_-, 2E_+]$, cf. Section 5.3.1.

[35] Incidentally, this point also disagrees with the behavior shown in Ref. [235]. For 22 years later the change in behavior should happen for $\tilde{m} \sim 1$ MeV.

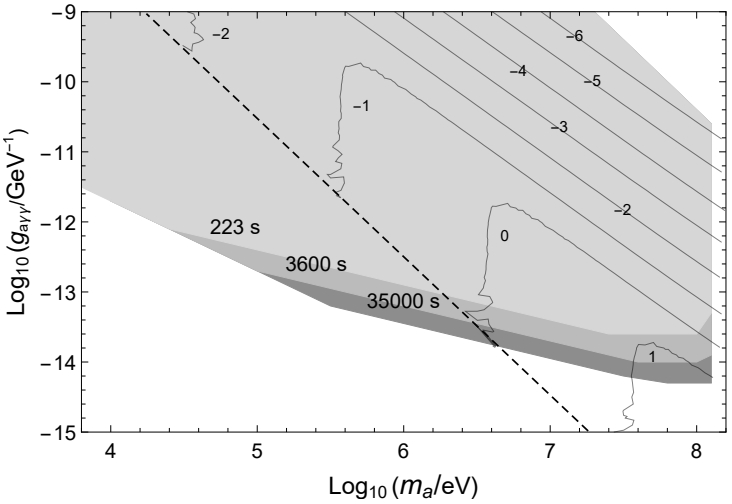

Figure 5.10: Angular windows for Betelgeuse. The contours correspond to the angular intervals containing 90% of the ALP-originated photons arriving on Earth. The sensitivities from Fig. 5.9 for the different observation times are shown in gray.

One may wonder why for very small masses an increased observation time does not lead to an improvement in the limit (cf. Fig. 5.9). The reason for this is rather simple. In this region the time delay is actually quite small and all photons that will ever arrive already do so in a time smaller than the smallest chosen observation time. In the present case the background is negligible and hence all observation times lead to the same result.

The projected improvements from Betelgeuse come from two factors. The first is the larger effective area of the detector, $9500\,\mathrm{cm}^2$ for Fermi-LAT [250] compared to $63\,\mathrm{cm}^2$ from the SMM [57], which leads to a lower upper limit on the fluence. The second is the shorter distance to Earth, $d_{\mathrm{SN}} = 0.2\,\mathrm{kpc}$ for Betelgeuse in comparison with $d_{\mathrm{SN}} = 51.4\,\mathrm{kpc}$ for SN 1987A, what helps increase the flux. Incidentally, this last factor is also responsible for the displacement[36] of the constant-angle contours shown in Fig. 5.10.

Lastly, the angular acceptance of the Fermi-LAT detector does not strongly constrain $P_{\mathrm{acceptance}}$. However, as mentioned in Section 5.2.2, this factor also takes the energy range of the detector into account: for Fermi-LAT we have $E_\gamma > 100$ MeV. Keeping in mind that $E_\gamma \sim E_a/2$, from Fig. 5.2 we see that $E_a \gtrsim 200$ MeV is far from the peak of the ALP production, thus causing the sensitivity to drop

[36]For a given $\{m_a, g_{a\gamma\gamma}\}$-pair, the angular windows for Betelgeuse are larger than for SN 1987A. One notices that the contours have receded relative to those in Fig. 5.7 and the reason is simple: since Betelgeuse is $\sim$ 250 times closer than SN 1987A, many of the ALPs which would have otherwise decayed *before* reaching Earth ($L_1 \leq 51.4$ kpc) – thus generating detectable photons – are now, for Betelgeuse, decaying *behind* Earth ($L_1 \geq 0.2$ kpc). This causes the reduction of the region in parameter space where detection of forward ALP-originated photons is possible.

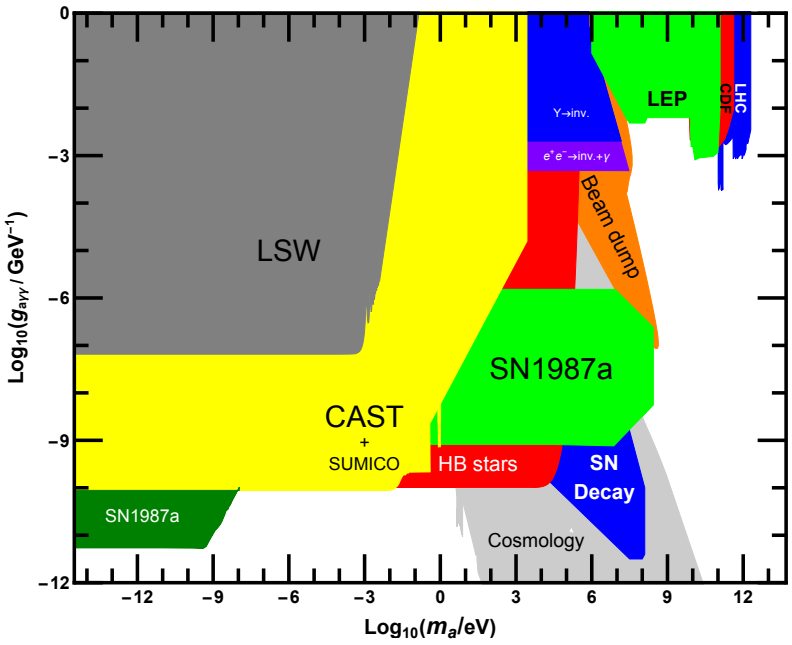

Figure 5.11: Excluded regions in ALP parameter space (figure adapted from [65, 254–256] with added limits from [54, 55, 236, 257–259]). Our bound is shown in dark blue ("SN decay"). The dark-green region is excluded based on ALP-photon conversion [56], whereas the light-green region is excluded based upon a nonobserved reduction in the duration of the neutrino burst [227].

by a factor of $P_{\text{acceptance}} \approx 0.06$. Future experiments like e-ASTROGAM [251], ComPair [252], or PANGU [253] will hopefully be able to improve on this aspect. Yet, even with this reduction, the ALP-originated gamma-ray flux from Betelgeuse would be significantly larger due to the closer distance.

5.5 Partial conclusions

In this chapter, which is based upon Ref. [69], we have considered the Primakoff-based production of ALPs purely coupled to two photons in the hot and dense core of the collapsing progenitor of SN 1987A. The subsequent decay in two photons would have generated a gamma-ray flux in excess of what has been observed, thus allowing us to extract new limits on heavy ALPs.

For ultra-light ALPs ($m_a < \text{eV}$) other limits are better, but in the 10 keV – 100 MeV mass range our limits – shown in dark blue in Fig. 5.11 ("SN decay") – improve upon existing laboratory and astrophysical ones. One also notices that our limit overlaps with the cosmological limits discussed in Refs. [236, 258], which are based upon the effects of the decay of early-universe relic ALPs on observables of the cosmic microwave background (CMB) and big-bang nucleosynthesis (BBN).

While cosmological limits from thermal production of ALPs in the early Universe are stronger, they are also model dependent. The grey region at the lower-right corner of Fig. 5.11 is excluded assuming that ALPs were in thermal equilibrium with the primordial plasma and that the later expansion of the universe was dominated by the relativistic degrees of freedom of the standard model.

These assumptions set the relic abundance of ALPs and require a sufficiently large (maximum) temperature of the Universe $T_{\rm RH} > T_{\rm fo} \sim 123\,{\rm GeV}\frac{\sqrt{g_*}}{g_q}\left(\frac{10^{-9}{\rm GeV}}{g_{a\gamma\gamma}}\right)^2$, where g_* and g_q are the energy and electric charge effective number of relativistic species, respectively [236]. Achieving such a large temperature strongly depends on the cosmological model considered. Many models feature smaller reheating temperatures, which would not be large enough to produce the thermal abundance assumed in the constraints. A very conservative lower limit is set by standard BBN, which requires $T_{\rm RH} \gtrsim 20$ MeV, implying that only for $g_{a\gamma\gamma} > 7 \times 10^{-8}$ GeV^{-1} the bounds are proven to be consistent. The constraints discussed in this paper, which reach even lower coupling constants, even if superficially weaker, do not suffer from this model dependence and imply a robust exclusion.

In summary, the massive ALPs we are interested in are produced during the core collapse leading to a supernova and, being very weakly coupled to photons, predominantly escape the influence of the star and propagate a certain mass- and coupling-dependent distance (determined by the decay length). Due to its massiveness, the ALP will then decay into two gamma-ray photons that may reach Earth, cf. Fig. 5.1. As initially pointed out in Ref. [235], due to non-zero decay angles, a considerable fraction of the signal arrives significantly delayed compared to the first neutrinos announcing the supernova event, cf. Fig. 5.5.

Indeed, depending on the parameter values, we found that the signal can be spread out over years (cf. eq.(5.25)). Although this dilutes the signal, it also provides opportunities as photons may be observed today or even in the near future with better instruments than were available in 1987. Furthermore, along with the time delay, the signal will also be spread in angles away from the line of sight, cf. Fig. 5.7. While this effect is not very large for SN 1987A, it can become important for future, closer supernovae which may be observed with gamma-ray instruments with better directional readiness and angular resolution.

As a realistic example we discussed the possibility of Betelgeuse going supernova in the *not too* distant future, leading to a significantly improved sensitivity, cf. Fig. 5.9. This is a good motivation to investigate potential improvements also in other SN 1987A-originated limits that could be extended by a future supernova observation.

This chapter is dedicated to a thorough study of the effects that heavy and very weakly coupled ALPs would have if produced during the core collapse of a type-II supernova. Similar to Part I, but in a more practical way, here we studied the low-energy phenomenology of a new particle that may be the remnant of some BSM scenario. In the next chapters (Part III) we do not consider any new particle, but rather discuss the possibility that, at very high energies, Lorentz symmetry itself is (spontaneously) broken. This could lead to all-pervading non-dynamic fields, i.e., backgrounds, that break spatial isotropy by pointing to a certain direction.

These backgrounds can in principle be coupled to all sectors of the SM (and gravity) and introduce minute – but important – modifications to the dynamics of the known particles and fields. In the next chapters we shall focus on Lorentz-symmetry violation (LSV) in QED, in particular in two sectors: the pure Maxwell sector via the Chern-Simons-like Carroll-Field-Jackiw term, and the electron-photon interaction, where we introduce a new LSV non-minimal coupling. The main idea is to use laboratory-based results on QED processes to constrain the respective background 4-vectors. In much the same way as with axion-like particles (cf. Presentation and this chapter), the upper limits we obtain are not only constraints on the LSV coefficients themselves, but also on the underlying physics that generate the new, non-standard effects behind them.

I would like to highlight that the contents and results presented in this chapter stem from the cited references, parts of my own work [69] – in collaboration with Javier Redondo and my German advisor, prof. Jörg Jäckel – and original independent modifications thereof. I have been responsible for most of the calculations and all simulations and plots. The writing efforts in Ref. [69] were more or less equally shared.

Part III

Chapter 6

Lorentz-symmetry violation

6.1 Introduction

Throughout the history of science there has always been some kind of guiding principle which helped scientists orient themselves towards progress. In the case of physics, it seems that this guiding principle has been the quest for unification. The XIX century saw the efforts of Faraday, Hertz, Maxwell, Lorentz, among others, to consistently unify the description of electricity and magnetism, thus giving birth to the electromagnetic theory. With the discovery of (special) relativity, Einstein further strengthened the unified character of electromagnetism by showing how electric and magnetic fields transform into each other under symmetry operations – the Lorentz transformations. Symmetry has been, for the whole XX century and until today, a valuable guide to progress[1].

In his elaboration of special relativity [260], Einstein states that the laws of physics must retain the same form in any inertial reference frame. By "laws of physics" he meant the equations of motion and, by "retain the same form", he meant that the functional form of these equations must remain the same for two observers sitting in inertial frames, which in turn are assumed to be equally good and valid standpoints for measurements. All this can be summarized by saying that the equations of motion must be invariant under Lorentz transformations.

Due to its extension – it covers the whole of classical mechanics and electromagnetism – the special theory of relativity (STR) provides high-velocity corrections to a broad realm of phenomena. Furthermore, the STR needs to be included in the description of the quantum world, as also there high velocities are possible. From the junction of quantum mechanics and STR it was born the quantum theory of relativistic fields, an extremely successful description of particle, atomic, molecular

[1]The electroweak theory from Weinberg, Glashow and Salam is a good example.

and optical physics. In this sense, the STR has been subjected to a wide variety of experimental tests; the most famous ones are those by Michelson and Morley [261] and Kennedy and Thorndike [262] (for reviews of recent tests, see Refs. [263, 264]). No long-lasting deviations from its predictions have been found[2].

It looks like the story is over, but not quite. As already mentioned in the Presentation and elsewhere in this thesis, the Standard Model (SM) of particle physics is not believed to be complete up to arbitrarily high energies – specially above the TeV scale where we are currently able to probe. In some of the candidates to supersede it, string theory for example[3] [44, 270], it is possible that Lorentz symmetry is indeed broken in its low-energy manifestations, but not by a huge amount, of course, as this would contradict the experimental evidence.

Among the possible effects caused by Lorentz-symmetry violation (LSV), we can list a few interesting ones, such as variation of the speed of light, modifications to the dispersion relations of fermions (e.g., neutrinos), generation of corrections to the gyromagnetic factor of leptons, etc. These and other effects will be briefly addressed in the next section when we present the general scope of LSV in the context of the SM. We highlight here that these effects are supposed to show up in the energy scales already available to us today, but their true origin lies in a much deeper and fundamental physical theory.

In the next section we shall get into the details of how Lorentz symmetry may be broken and where the signs of its breaking could show up.

6.2 Breaking Lorentz symmetry

In order to talk about breaking Lorentz symmetry, maybe it is didactic to first briefly go through the well-known process of spontaneous symmetry breaking (SSB) implemented via the Higgs mechanism [4]. V.A. Kostelecký and S. Samuel used roughly the same approach to investigate the possible origins of LSV in string theory [44, 271], but here we shall not go into the specifics of the latter and just make a general discussion.

As mentioned in Chapter 1, the goal of the Higgs mechanism is to generate mass to gauge bosons so that, when the symmetry is still exact, no gauge-breaking mass term exists and, after SSB, a mass term emerges and the gauge boson is massive

[2]This does not mean, however, that some experiments *never* claimed to have found discrepancies. One of the the latest – and most famous – was the Opera experiment [265] in Gran Sasso (Italy), where they claimed having seen superluminal neutrinos. This was later corrected and neutrinos are still consistent with special relativity [266].

[3]Also, e.g., in non-commutative field theories [267], quantum loop gravity [268] and spacetime foams [269].

(this is also the mass-generation mechanism for charged leptons). This happens at the expense of one degree of freedom from the Higgs field that is "eaten" by the vector boson, thus becoming its longitudinal part[4].

For concreteness, let us take the case of the SM with $SU(2) \otimes U(1)$ symmetry[5]. Let us further consider a scalar field ϕ – this is our Higgs – coupled to fermions in a Yukawa-like interaction,

$$\mathcal{L} \sim \phi\bar{\psi}\psi + \text{H.c.} + V(\phi). \tag{6.1}$$

We see that if ϕ transforms as a doublet under $SU(2)$, this Lagrangian is invariant under the gauge transformations. In higher energies, ϕ and $\langle\phi\rangle$, its vacuum expectation value (VEV), exhibit the usual $SU(2) \otimes U(1)$ symmetry, but, upon reaching the lowest energy level where the (Mexican-hat) potential $V(\phi)$ is minimized, a specific $\langle\phi\rangle_0$ is chosen and invariance is lost. One then says that the symmetry was spontaneously broken.

On a more general note, let us assume that our "Higgs" field – not necessarily a scalar – transforms under the Lorentz group via $\Phi \to \Phi' = e^{-\frac{i}{2}\omega_{\mu\nu}M^{\mu\nu}}\Phi$, where $M^{\mu\nu}$ are the generators and $\omega_{\mu\nu}$ are the parameters of the transformation. Suppose further that the latter are infinitesimal, i.e., $e^{-\frac{i}{2}\omega_{\mu\nu}M^{\mu\nu}} \simeq 1 - \frac{i}{2}\omega_{\mu\nu}M^{\mu\nu}$. In this case, we have

$$\langle\Phi'\rangle_0 \simeq \langle\Phi\rangle_0 - \frac{i}{2}\omega_{\mu\nu}M^{\mu\nu}\langle\Phi\rangle_0\,. \tag{6.2}$$

Within the SM, one of the most important requirements is that Lorentz symmetry be preserved, thus leaving the vacuum invariant. For this to happen, we must have $M^{\mu\nu} \equiv 0$, which means that $\langle\Phi\rangle_0$ transforms as a scalar, i.e., $\langle\Phi'\rangle_0 = \langle\Phi\rangle_0$. For this reason, the SM Higgs, $\Phi = \phi$, is a complex (Lorentz) scalar field [4].

However, if we assume that Φ is not a scalar, but rather transforms as a Lorentz *tensor*, the situation is different: $M^{\mu\nu} \neq 0$ and we are dealing with a nontrivial representation of the Lorentz group. In this scenario we have $\langle\Phi'\rangle_0 \neq \langle\Phi\rangle_0$, i.e., the vacuum is not invariant, and Lorentz symmetry is spontaneously broken[6]. In analogy to the SM Higgs mechanism, we may say that spacetime is filled with a tensor "condensate" which may violate e.g. rotational invariance.

[4]This is accomplished by means of a gauge transformation which, when acting upon the Higgs field, eliminates some of its degrees of freedom, while, when acting upon the gauge fields, transfers these degrees of freedom, thus generating a longitudinal component. This gauge choice is the the so-called unitary gauge [4].

[5]This argument is based on Ref. [271].

[6]As in the case of the Higgs mechanism, Nambu-Goldstone and massive modes should follow SSB. Here we do not touch these topics and the reader is encouraged to check Refs. [272–274] and references therein for further details.

In practice, we can take the example of the Yukawa coupling, which may be generalized to accommodate a Higgs-like tensor field Φ (with indices suppressed for clarity), that is [271]

$$\mathcal{L} \sim \frac{\lambda}{M_{\rm Pl}^k} \Phi \bar{\psi} \, \Gamma \, (i\partial)^k \, \psi + \text{H.c.} - V(\Phi), \tag{6.3}$$

where λ is a dimensionless coupling constant, k is an integer, $M_{\rm Pl}$ is the mass scale of new physics (possibly the Planck scale $\sim 10^{19}$ GeV) and Γ is a general gamma-matrix structure[7] with adequate Lorentz indices matching those of Φ.

If the Higgs-like tensor Φ has a potential with degenerate vacua, it may then undergo SSB and acquire a non-zero VEV $\langle \Phi \rangle_0 \neq 0$, so that

$$\mathcal{L}_{\rm LSV} \sim \frac{\lambda}{M_{\rm Pl}^k} \langle \Phi \rangle_0 \bar{\psi} \, \Gamma \, (i\partial)^k \, \psi + \text{H.c.} - V(\langle \Phi \rangle_0) \tag{6.4}$$

now contains a non-dynamical Lorentz tensor, i.e., not a *field*, $\langle \Phi \rangle_0$, as a leftover from SSB. A simple example [275] would be that of a hypothetical 3-vector, $\Phi = \mathbf{C}$, which has a "Higgs-like" potential, $V(\mathbf{C}) = (\mathbf{C}^2 - \chi^2)^2$, with $\chi > 0$. In this case, the state with lowest energy is $\mathbf{C} = \mathbf{C}_0 = \boldsymbol{\chi}$, with $|\boldsymbol{\chi}|^2 = \chi^2$. After SSB a (sample) Lagrangian involving such a vector would look like $\mathcal{L}_{\mathbf{C}} \sim \lambda \bar{\psi} \boldsymbol{\chi} \cdot \boldsymbol{\gamma} \psi$, thus introducing the non-dynamical 3-vector $\boldsymbol{\chi}$ into the model.

It is also worthwhile mentioning that, besides Lorentz symmetry, another important invariance is included in the SM: CPT. The joint transformations involving charge conjugation (C), parity inversion (P) and time reversal (T) are cornerstones of the SM, from both theoretical and experimental points of view [276]. The CPT theorem is valid for point-like particles (and local interactions) and this is precisely what strings are *not*, since they are extended objects. Besides, the CPT theorem uses Lorentz invariance as one of its fundamental predicates [277], so, it is possible that, in scenarios within string theories, Lorentz and CPT symmetries be broken in our low-energy world [278].

The claim that CPT violation implies the Lorentz violation (or/and vice versa) has been disputed in the literature; see e.g. Greenberg [279] and Chaichian *et al.* [280, 281]. The former showed, based on locality and time ordering of the fields in the Green functions, that CPT violation implies Lorentz violation, whereas the latter said otherwise. However, Chaichian used very pathological – manifestly non-local – cases, so Greenberg's conclusion remains valid. In the following we assume that it is possible to have LSV terms with CPT even and odd behaviors.

[7] This may be applied to other kinds of fields, e.g., instead of fermions, vector fields, *mutatis mutandis*.

6.3 Particle *vs* observer transformation

We have just seen that Lorentz symmetry may be spontaneously broken and it would be interesting to know how this violation could show up in practice. For this, let us consider rotations, which are simplest to visualize.

For the sake of clarity[8], let us take a spherical harmonic oscillator, whose Lagrangian is given by $\mathcal{L}_1 = \frac{1}{2}m\dot{\mathbf{r}}^2 - \frac{1}{2}\kappa\mathbf{r}^2$, with m and κ fixed (scalar) quantities. We now want to test the rotational properties of this system. This can be done in basically two ways by applying the following transformations:

- Observer transformations: a general rotation is applied to the coordinate system, i.e., all vectors (or tensors, in general) will be equally rotated. This amounts to a re-labelling of the axes, but the relative orientations of the constituent objects do not change.

- Particle transformations: rotations are applied to the individual vectors (or tensors, in general), thus leaving the reference frame untouched. This is attained through an *active* rotation of the physical system at hand.

We now apply a rotation to the oscillator and, as mentioned above, this can be done in two ways. If we apply an observer transformation, all vectors will be acted upon by a rotation matrix, $\mathcal{R}$, but we have only rotationally-invariant terms in $\mathcal{L}_1$, so the system would look just the same from a rotated coordinate system. We are equally free to apply a particle transformation, but again, if we rotate the parts of the system, due to its rotational symmetry, nothing changes. We are led to the conclusion that, in rotationally invariant systems, the two transformations (observer and particle) are equivalent, or at least can be made to coincide.

Let us choose a different physical system now. We take a magnetized system (with dipole moment $\boldsymbol{\mu}$) placed in the static magnetic field of the Earth, $\mathbf{B}$. The associated Lagrangian is given by $\mathcal{L}_2 \sim -\boldsymbol{\mu}\cdot\mathbf{B}$ and we can expect some sort of rotation-invariance violation as the dipole moment and the magnetic field are not related – one depends on the object under study, while the other is external. We first apply an observer transformation, which takes all vectors – $\boldsymbol{\mu}$ and $\mathbf{B}$ alike – into their rotated versions, $\boldsymbol{\mu}' = \mathcal{R}\boldsymbol{\mu}$ and $\mathbf{B}' = \mathcal{R}\mathbf{B}$. This leaves the system unchanged as a whole and the experimenters will find no observable that tells them that an actual transformation took place (except for possible harmless coordinate re-labellings).

Next, let us perform a particle transformation. In this case, only the magnetized object is rotated (e.g., mechanically by the experimenters) and has the orientation

[8]This and the following examples are based on Refs. [282, 283].

of its dipole moment relative to the reference frame of the laboratory modified. This time, the magnetic field of the Earth does not feel the action of $\mathcal{R}$, as it is an external, fixed *background*. The Lagrangian now reads $\mathcal{L}_2^{'} \sim -(\mathcal{R}\boldsymbol{\mu}) \cdot \mathbf{B}$ and it is clearly different from $\mathcal{L}_2$ and so will be the phenomena described by it (the equations of motion will change accordingly).

The conclusion: in the presence of an external background, the equivalence between observer and particle transformations is destroyed. We see that a background with different particle-transformation properties than the other ingredients of the theory is the key to break the aforementioned observer-particle equivalence – this is exactly the situation encountered in LSV models[9].

As we shall see in the following, the SM may be extended by including terms analogous to the Lorentz-preserving ones, but coupled to generic tensors which break Lorentz particle-transformation invariance à la eq.(6.4), while keeping other interesting symmetries intact, gauge invariance, for example. Also Lorentz observer-transformation invariance is maintained and, by the way, this is exactly why we may have Lorentz-violating Lagrangians which are themselves Lorentz scalars: all the dynamical fields, as well as the fixed LSV tensors, transform under *observer* transformations, so the Lagrangian is overall observer invariant.

6.4 The Sun-centered reference frame

We have already discussed that LSV coefficients transform differently under observer- and particle-Lorentz transformations and that they are taken as generic fixed background tensors. This is a frame-dependent statement and we must look for a convenient reference frame where the aforementioned coefficients are *truly* fixed.

It is clear that a frame fixed to Earth's surface will not suffice, as we are clearly a non-inertial (rotating) reference frame, so we cannot really expect an external background to be fixed from our point of view – in fact we should expect to see it rotating. The next, and perhaps most convenient, possibility is to use the Sun as a "reference" reference frame[10]. This is actually a good choice for a few reasons: it is approximately inertial over the time scale of most experiments[11], it is experimentally accessible, and may have its axes conveniently oriented relative to the Earth (cf. Fig. 6.1).

[9] Another neat example is that of a non-relativistic Lagrangian given by $\mathcal{L}_3 = m_{ij}\dot{r}_i\dot{r}_j - U(\mathbf{r})$, where m_{ij} transforms as a (symmetric) tensor under observer transformations, but as a scalar under particle transformations. This and other very interesting examples in LSV classical mechanics can be found in Ref. [284].

[10] Sorry for the cacophony!

[11] Its motion around the galaxy has a period of ~ 200 million years.

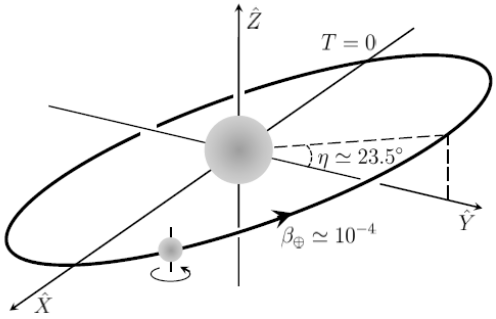

Figure 6.1: The canonical Sun-centered frame [285].

We, and the community around LSV, will then adopt the Sun-centered frame (SCF) as a standard reference frame where the background coefficients are constant, i.e., time-independent [58, 286]. Therefore, relative to an observer fixed on Earth, the background will seem to rotate, so that experimental signals affected by LSV effects should generally present time oscillations, specially with sidereal frequencies. Also important is to note that even isotropic backgrounds in the SCF will appear to be anisotropic in our frame because of both rotational and translational motions of the Earth relative to itself and to the Sun, respectively, which produce boosts. In this sense, rotation violations are a key signal for Lorentz violations in Earth-bound experiments (also in space-based experiments [285]).

According to Refs. [58, 285, 286], the axes in the SCF are defined such that the Z axis is directed north (parallel to Earth's rotational axis), X points from the Sun to the vernal equinox, while Y completes a right-handed system. The origin of time T is at the 2000 vernal equinox. Regarding the standard Earth-bound frame for a point in the northern hemisphere, the z axis is vertical from the surface (points to the local zenith), x points south and y points east. The local time $T_\oplus$ is related to the time in the SCF, T: the local sidereal time $T_\oplus$ is defined to be the time measured in the SCF from one of the moments when y lies along Y[12].

To see how we can make the passage from the LSV coefficients in the laboratory (LAB) frame, where they are usually time dependent, to the SCF, where they are fixed, we use a vector background, V^μ. The components of this vector in the two frames are connected via

$$V^\mu_{\rm LAB} = \Lambda^\mu{}_\nu V^\nu_{\rm SCF}, \tag{6.5}$$

with $\Lambda^\mu{}_\nu$ representing an observer-Lorentz transformation between Earth and the

[12]It can be shown that the exact relationship is $T_\oplus = T - 2\pi n/\omega_\oplus - \delta_T$, where $\delta_T \simeq 86164\,(0.18403 - \lambda/360)$ s; here λ is the longitude of the LAB. For the case of Kostelecky's workplace (Indiana University at $\lambda \simeq -86.52°$), we find $T_\oplus = T - 86164n - 36565$, with the times in second and n an integer to be conveniently chosen.

SCF. From now on, we represent the components of V in the LAB frame by $V^{0,x,y,z}_{\rm LAB}$, whereas those in the SCF are $V^{T,X,Y,Z}_{\rm SCF}$.

The explicit form of the (time-dependent) Lorentz transformation $\Lambda^{\mu}{}_{\nu}$ is [286]

$$\Lambda^0{}_T = 1, \quad \Lambda^0{}_I = -\boldsymbol{\beta}^I, \quad \Lambda^i{}_T = -(R\cdot\boldsymbol{\beta})^i, \quad \Lambda^i{}_I = R^{iI}, \tag{6.6}$$

where $\boldsymbol{\beta}$ is the velocity $(\mathbf{v}/c)$ of the LAB relative to the SCF and R^{iJ} is a spatial rotation. The boost is given by ($\eta \approx 23.4^\circ$ is the inclination of Earth's orbital plane)

$$\boldsymbol{\beta}^X = \beta_\oplus \sin\Omega_\oplus T - \beta_L \sin\omega_\oplus T_\oplus \tag{6.7}$$

$$\boldsymbol{\beta}^Y = -\beta_\oplus \cos\eta \cos\Omega_\oplus T + \beta_L \cos\omega_\oplus T_\oplus \tag{6.8}$$

$$\boldsymbol{\beta}^Z = -\beta_\oplus \sin\eta \cos\Omega_\oplus T \tag{6.9}$$

and, defining $\sin\chi \equiv s_\chi$, $\cos\chi \equiv c_\chi$; $\sin\omega_\oplus T_\oplus \equiv s_\oplus$, $\cos\omega_\oplus T_\oplus \equiv c_\oplus$, the matrix R^{iJ} is given by

$$R^{iJ} = \begin{pmatrix} c_\chi c_\oplus & c_\chi s_\oplus & -s_\chi \\ -s_\chi & c_\chi & 0 \\ s_\chi c_\oplus & s_\chi s_\oplus & c_\chi \end{pmatrix} \tag{6.10}$$

so that the $\Lambda^i{}_T = -(R\cdot\boldsymbol{\beta})^i$ read

$$\Lambda^x{}_T = -c_\chi c_\oplus \beta^X - c_\chi s_\oplus \beta^Y + s_\chi \beta^Z \tag{6.11}$$

$$\Lambda^y{}_T = s_\oplus \beta^X - c_\oplus \beta^Y \tag{6.12}$$

$$\Lambda^x{}_T = -s_\chi c_\oplus \beta^X - s_\chi s_\oplus \beta^Y - c_\chi \beta^Z, \tag{6.13}$$

where the numerical values of the parameters appearing above are

$$\begin{aligned} \beta_\oplus &\approx 10^{-4}, \quad \text{Earth's orb. vel.} \\ \beta_L &= r_\oplus \omega_\oplus \sin\chi < 10^{-6}, \quad \text{Earth's rot. vel.} \\ \omega_\oplus &= 2\pi/\text{day} \approx 7\times 10^{-5}\, s^{-1}, \quad \text{Earth's rotational ang. vel.} \\ \Omega_\oplus &= 2\pi/\text{year} \approx 2\times 10^{-7}\, s^{-1}, \quad \text{Earth's orbital ang. vel.} \\ \chi &= \text{experiment's co-latitude.} \end{aligned}$$

In the following we discuss some particular LSV scenarios and, for the sake of simplicity, the respective backgrounds are assumed to be constant (time independent), i.e., they are considered in the SCF. In more concrete applications, such as the ones undertaken in Chapters 7 and 8, it is necessary to use the transformations above to translate the background components into the more convenient SCF.

6.5 The Standard Model extension

In 1989 Samuel and Kostelecký started studying scenarios within string theory that could induce LSV via SSB [44]. It soon became clear[13] that LSV could be included in virtually all sectors of the SM – also in general relativity – and a unified framework seemed handy as a means to catalogue all possible coefficients and respective experimental limits.

With this in mind, almost a decade later, Colladay and Kostelecký put forward what would be the soon-to-be called LSV "Standard Model extension" (SME) [287, 288]. It is an attempt to systematically include Lorentz-violating terms to the well-known structure of the SM. The SME is symbolically given by

$$\mathcal{L}_{\rm SME} = \mathcal{L}_{\rm SM} + \mathcal{L}'_{\rm LSV}, \tag{6.14}$$

where $\mathcal{L}'_{\rm LSV}$ is a four-dimensional Lagrangian containing all possible terms involving the fields from the SM, but including background LSV tensors and possibly derivatives. The Lagrangian $\mathcal{L}'_{\rm LSV}$ is to be understood as an effective theory, i.e., the low-energy regime of a more fundamental theory.

According to eq.(6.4), the combinations of fields and derivatives must end up being four dimensional, otherwise suppression factors $\sim 1/M_{\rm Pl}$ should be expected. Dimensionless LSV coefficients – see e.g. $(k_{\rm F})_{\mu\nu\alpha\beta}$ below – must also be suppressed by some ratio $\sim m/M_{\rm Pl}$, where m is a typical mass scale of the low-energy effective theory (e.g., the electron mass). In general, from eq.(6.4), we expect the terms with $k \leq 1$ to be renormalizable, so we shall focus on these when discussing LSV modifications to the free-field Lagrangians.

Furthermore, as mentioned in the end of Section 6.3, $\mathcal{L}_{\rm SME}$ is a (observer) Lorentz invariant, so that all Lorentz indices must match accordingly – this guarantees that physics is independent of the observer's choice of coordinate system. Also, gauge and eventual internal (e.g., $SU(3) \otimes SU(2) \otimes U(1)$) symmetries must be respected.

Since in the next two chapters we are going to deal exclusively with the QED sector of the SME, we shall not delve into its other sectors (electroweak[14], Higgs, QCD, gravity, etc). For these, the interested reader is directed to Refs. [58, 287, 288] and references therein. With this, let us focus on LSV one-lepton QED.

[13] For excellent reviews, see, e.g., Refs.[263, 264], as well as Ref. [58].

[14] As mentioned in Section 6.1, neutrinos have been in the center of some controversy and LSV has indeed been evoked to solve the issue – see, e.g., Ref. [289].

6.5.1 Extended QED

As in standard QED, here we take only electrons (and positrons) and photons as basic fields of the theory, which must keep gauge and observer-Lorentz invariance. Also similar to the usual QED, there are essentially three sectors: only electron, only photon and electron-photon interactions. For this discussion we follow mostly Refs. [288, 290]. We start by the first secor, where the electron is considered alone[15].

Electron sector

The usual purely electronic sector is given simply by the Dirac Lagrangian $\mathcal{L}_{ee} = \bar{\psi}\left(i\gamma^\mu\partial_\mu - m\right)\psi$, where ψ represents the electron and m is its mass. In the spirit of eq.(6.4), the general LSV Lagrangian for a single lepton is

$$\mathcal{L}'_{ee} = \bar{\psi}\left(i\Gamma^\mu\partial_\mu - M\right)\psi \tag{6.15}$$

with ψ representing the electron 4-spinor and

$$\Gamma^\mu = c^{\nu\mu}\gamma_\nu + d^{\nu\mu}\gamma_5\gamma_\nu + e^\mu + if^\mu\gamma_5 + \frac{1}{2}g^{\lambda\nu\mu}\sigma_{\lambda\nu} \tag{6.16}$$

$$M = a_\nu\gamma^\nu + b_\nu\gamma_5\gamma^\nu + \frac{1}{2}H_{\nu\kappa}\sigma^{\nu\kappa}, \tag{6.17}$$

where all coefficients are real. From eq.(6.4) we see that only terms with $k = 0, 1$ are indicated – this is to ensure naïve power-counting renormalizability – but, in general, other terms with different k may also be added.

It is clear that these LSV contributions will modify the equations of motion and, consequently, the dispersion relations. Before we go into these matters, it is important to mention that some LSV coefficients may be eliminated through suitable field redefinitions. For instance, if we define $\xi = e^{ia\cdot x}\psi$ and re-write $\mathcal{L}_{ee} + \mathcal{L}'_{ee}$ in terms of ξ, we find (keeping only a_μ and omitting other coefficients)

$$\begin{aligned}\mathcal{L}_{ee}[\xi] + \mathcal{L}'_{ee}[\xi] &= e^{ia\cdot x}\bar{\xi}\gamma^\mu\left[i\left(-ia_\mu\xi\right) + e^{-ia\cdot x}\partial_\mu\xi\right] - a_\mu\bar{\xi}\gamma^\mu\xi - m\bar{\xi}\xi \\ &= \bar{\xi}\left(i\gamma^\mu\partial_\mu - m\right)\xi \end{aligned} \tag{6.18}$$

where we see that a_μ was completely eliminated. Therefore, in the absence of other LSV coefficients, the theory with or without a_μ is equivalent to the standard Lorentz-preserving free Dirac Lagrangian and no observable effects from this term are expected (this can also be seen in the associated Schrödinger-Pauli equations [291]).

[15] A generalization to include other flavors is straightforward and would require the introduction of flavor-dependent LSV coefficients.

Other field redefinitions are possible in general[16], e.g., the b_μ coefficient could be eliminated via the field transformation $\xi = \exp(-ib\cdot x\gamma_5)\,\psi$, but only if $m = 0$. As this example shows, the field redefinitions become harder to implement if usual (and also LSV) terms are present. This is due to the gamma-matrix algebra and the spacetime dependence (accounted by the derivatives); these factors, together, make it more difficult to eliminate complete LSV terms, as in the simple case of a_μ.

Let us now move on to more interesting issues. The discussion around the general dispersion relations arising from eq.(6.15) with *all* LSV coefficients is quite cumbersome: the Dirac operator $p_\mu\Gamma^\mu - M$ is a (complex) 4×4 matrix in spinor space and the solution to the associated dispersion relations is very involved; the reader is referred to Ref. [290] for further details on the general treatment.

Since, as we saw above, the a_μ may be eliminated through a field redefinition, let us focus on the extended (free) Dirac equation when all LSV coefficients are zero, except b_μ. In this case we have $\left(i\partial\!\!\!/ - \gamma_5 b\!\!\!/ - m\right)\psi = 0$ and the modified dispersion relations (MDR) are obtained by "squaring" twice the wave operator[17]:

$$\left(p^2 + b^2 - m^2\right)^2 + 4m^2b^2 - 4\,(p\cdot b)^2 = 0, \tag{6.19}$$

which has four real roots. Furthermore, we notice that the standard dispersion relation for a massive particle, $p^2 = m^2$, is not fulfiled unless we make $b_\mu \to 0$, as it should.

Again, to avoid cumbersome expressions, let us consider the special case of $\mathbf{b}\equiv 0$, i.e., a pure time-like background $b_\mu = (b_0, 0)$. In this case it is simple to read the MDR from eq.(6.19) [293]

$$(p^0)^2 \equiv \omega_\pm^2 = \mathbf{p}^2 + m^2 + b_0^2 \pm 2|b_0||\mathbf{p}| \tag{6.20}$$

and we highlight that an interesting impact that such LSV MDR may have is to modify (raise or lower) the threshold for well-known processes by correcting decay rates, for example [294].

From eq.(6.20) we are able to extract a few interesting informations about this simple one-fermion LSV model. The first concerns causality, which may be checked (at the classical level[18]) by the group velocity $v_g^\pm = \frac{\partial\omega_\pm}{\partial|\mathbf{p}|}$, which reads

[16] Also some redefinitions which are applicable to first order in the LSV coefficients [287]. See also Table 1 from Ref. [292].

[17] Here we assume the usual plane-wave expansion: $\psi(x)\sim e^{-ip\cdot x}$, with $p^2 = (p^0)^2 - \mathbf{p}^2$.

[18] At the quantum level, i.e., taking the quantized theory in consideration, the appropriate verification should go around the microcausality: the anti-commutator of the fermion fields should be zero for space-like separations. This has been done in Ref. [271] and, for the case where $\mathbf{b} = 0$, the conclusion from the classical analysis is found to hold.

$$v_g^{\pm} = \frac{|\mathbf{p}| \pm b_0}{\sqrt{(|\mathbf{p}| \pm b_0)^2 + m^2}} \leq 1, \tag{6.21}$$

where we see that no signal is propagating with speed greater than that of light ($c = 1$, in our units). Another very interesting – and quite exotic – feature of eq.(7.14) is that, if we keep a space-like $\mathbf{a}$, we find

$$\mathbf{v}_g^{\pm} = \frac{(|\mathbf{p} - \mathbf{a}| - b_0)}{E} \frac{\mathbf{p} - \mathbf{a}}{|\mathbf{p} - \mathbf{a}|}, \tag{6.22}$$

which shows that the velocity may not be parallel to the momentum [271].

Secondly, we must check the stability, what may be done by analysing whether $\omega_{\pm}^2 \geq 0$ or not: if yes, the mode is said to be stable, otherwise it is said to be unstable. The latter would imply that the energy has an imaginary part and may lead to spontaneous decays into ever lower energy states. Looking at eq.(6.20), in principle, there could be values of $b_0 > 0$ that jeopardize the reality of the energy squared. It can be shown, however, that under reasonable circumstances, the risk is not that serious: the instabilities arise only for momentum scales $|\mathbf{p}| \gtrsim \mathcal{O}(M_{\rm Pl})$, thus staying safely away from the present and future experimental reach [295]. At last, but not least, we indicate that the Hamiltonian following from the inclusion of the b_μ term is Hermitian [287, 296], thus guaranteeing that its eigenvalues are real and positive. The usual probabilistic interpretation of the associated quantum mechanics is safe-guarded and we may say that the model is unitary.

Needless to say that these analyses have to be conducted also for other kinds of interval assignments for b_μ (space- or light-like), as well as for *all* other LSV coefficients. As already mentioned, the general treatment with all terms included is quite involved and the interested reader is directed to Refs. [271, 290] and references therein for more details.

As we have seen, the LSV terms that modify exclusively the lepton sector give rise to non-standard dispersion relations and associated energy eigenvalues. These will also induce modifications in the eigenvectors, or better, in the eigenspinors – the solutions to the LSV Dirac equation. This is an important point, as these eigenspinors are used to build the asymptotic states (e.g., in scattering phenomena) and to compute physical observables, such as decay rates and cross sections. Therefore, in principle, the whole paraphernalia[19] attached to these calculations will receive small, but highly non-trivial, LSV-dependent corrections [287, 297].

[19] As examples we can mention the external states, completeness relations, energy-dependent normalization factors for the particle flux, etc. In any case, it is expected that these corrections do not play a role in practical applications, as they are strongly suppressed [287].

These corrections should be specially important when the relevant LSV-modified sector (leptons, photons, etc) is in the final states of any process, as these will require the use of the modified solutions to the free equations of motion (cf. eq.(6.15)). Luckily, in this thesis we do not find situations where this is of practical importance: in Chapter 7 we only apply the LSV term through a vertex insertion, so that we would get only higher-order corrections (in the LSV parameters) by considering the modified external states. Similarly, in Chapter 8 we deal with a non-minimal coupling, i.e., a modification to the electromagnetic interaction vertex, which, at tree level, is unable to lead to MDR such as the ones described above.

Photon sector

The (minimal) photon sector of the SME is composed by the terms with mass dimension $d = 3$ and $d = 4$ with two factors of the photon field [286]. Gauge invariance must be kept and the easiest way of doing this is by employing the field-strength tensor, $F_{\mu\nu} = \partial_\mu A_\nu - \partial_\nu A_\mu$, and its dual, $\tilde{F}_{\mu\nu} = \frac{1}{2}\epsilon_{\mu\nu\kappa\gamma}F^{\kappa\gamma}$, which are themselves gauge invariant. With these criteria in mind, we have

$$\mathcal{L}'_{\gamma\gamma} = \frac{1}{2}\left(k_{\mathrm{AF}}\right)^{\mu}\epsilon_{\mu\nu\alpha\beta}A^{\nu}F^{\alpha\beta} - \frac{1}{4}\left(k_{\mathrm{F}}\right)_{\mu\nu\alpha\beta}F^{\mu\nu}F^{\alpha\beta}\,, \tag{6.23}$$

where $(k_{\mathrm{AF}})^{\mu}$ and $(k_{\mathrm{F}})_{\mu\nu\alpha\beta}$, the LSV coefficients, are dimensionful (dimension of mass) and dimensionless, respectively. The former, a Chern-Simons-like contribution, will be discussed in further detail in Chapter 7, so we will not touch it now. Let us then talk a bit about the latter.

Setting $(k_{\mathrm{AF}})^{\mu} = 0$ for now and applying Noether's variational procedure to eq.(6.23), the equations of motion are found to be

$$\partial_\alpha F_{\mu}{}^{\alpha} + \left(k_{\mathrm{F}}\right)_{\mu\alpha\beta\gamma}\partial^{\alpha}F^{\beta\gamma} = 0, \tag{6.24}$$

where we added the usual Maxwell kinetic term, $-\frac{1}{4}F_{\mu\nu}^2$. The Bianch identities guarantee that $\partial_\mu\tilde{F}^{\mu\nu} = 0$ is left unaltered, so that only the "inhomogeneous" Maxwell equations – if we had included a matter source[20] – are modified. If we work out the wave equations for the electric field in momentum space we obtain

$$\left[\delta^{ij}p^2 + p^i p^j + 2\left(k_{\mathrm{F}}\right)^{i\alpha\beta j}p_\alpha p_\beta\right]\mathbf{E}_j = 0, \tag{6.25}$$

with $p^2 = \omega^2 - \mathbf{p}^2$.

[20] In any case, due to the anti-symmetry of both the field-strength tensor and LSV coefficient, we still have current conservation.

The equation above has some interesting consequences. First of all, from it we may extract the MDR for the photon, which, again, present new propagation modes, namely

$$\omega_{\pm} = (1 + \rho \pm \sigma)\,|\mathbf{p}|, \tag{6.26}$$

where ρ and σ are scalars under observer-Lorentz transformations and linear in combinations of the LSV parameters [286]. Note that when the $(k_{\rm F})_{\mu\alpha\beta\gamma} \to 0$, we recover the usual dispersion relation where the two modes propagate with the same frequency. From eq.(6.26) we may obtain the group velocity as $v_g^{\pm} = \partial\omega_{\pm}/\partial|\mathbf{p}| = 1 + \rho \pm \sigma$, which can indeed be larger than 1. Different from the Lorentz-preserving case, where $\omega = |\mathbf{p}|$, here we have two solutions (modes) for the electric field, $\mathbf{E}_{\pm}$, which means that the two modes propagate with different velocities. This may lead to birefringence in vacuum, which can be used to experimentally test the model by using radiation bursts from far-away (astrophysical) sources; cf. Refs. [58, 286].

In general, the LSV tensor $k_{\rm F}$ possesses the same symmetries as the Riemann tensor, e.g., it is separately anti-symmetric in the $(\mu\nu)$ and $(\alpha\beta)$ pairs and symmetric under $(\mu\nu) \leftrightarrow (\alpha\beta)$ and, for convenience, the components $k_{\rm F}^{\mu\nu\alpha\beta}$ are usually presented in certain defined combinations – see Ref. [286]. The 19 independent components may be separated in two groups, one with ten parameters (sensitive to birefringence) and another with nine parameters (insensitive to it). In Refs. [298–300] the issues of causality, stability and unitarity for the different sub-sectors (divided in parity even or odd, isotropic and anisotropic) were addressed and, due to the length of their analyses, the reader is encouraged to check the aforementioned references for further details. We note, however, that these consistency requirements (causality, stability and unitarity) are not generally fulfiled and difficulties may arise in specific configurations of the LSV coefficients[21].

As a final remark, we note that the operators discussed above are dimension-d operators, namely, $d = 3$ ($(k_{\rm AF})^{\mu}$) and $d = 4$ ($(k_{\rm F})^{\mu\nu\alpha\beta}$); these are called *minimal* terms of the gauge sector of extended QED. It is possible, nevertheless, to write down many other effective operators with higher mass dimension – these are called *non-minimal*. If we keep only two photon fields and increase the number of derivatives, there are 36 operators for $d = 5$ and 126 for $d = 6$, and the number grows very quickly – this is only considering LSV terms that respect explicit gauge invariance [301, 302].

[21] For example, in Ref. [298] the authors find that the so-called anisotropic parity-even sector is non-causal for some specific spatial orientations, even if the LSV background is assumed very small.

Electron-photon interaction sector

Finally, let us discuss the interaction sector of the extended QED. As before, a general requirement[22] is to keep gauge invariance, which is most easily implemented if we work only with the electromagnetic field-strength tensor and its dual. For this reason, and to contrast with the usual minimal coupling of Lorentz-preserving QED, such terms are called *non-minimal*.

A generic non-minimal interaction term which is compatible with the above mentioned requirements is of the form (restricting ourselves to Lagrangians bilinear in the fermion field, ψ)

$$\mathcal{L}'_{e\gamma} \sim g_{\mathrm{LV}} \bar{\psi} \Gamma^{\alpha\beta} \psi F_{\alpha\beta}, \tag{6.27}$$

where g is a dimensionful coupling constant and $\Gamma^{\alpha\beta}$ is some tensor composed by a gamma-matrix structure coupled to LSV tensors. Given that in four dimensions $[\psi] = 3/2$ and $[F_{\mu\nu}] = 2$, we must have $[g_{\mathrm{LV}}] = -1$ to keep the correct dimensionality.

The fact that $[g_{\mathrm{LV}}] = -1 < 0$ means that the coupling constant has dimension of inverse mass, which forcibly introduces a mass scale in our problem – usually assumed to be around the Planck mass [287]. This implies that the contributions from terms such as (6.27) is dominant only at higher energies, being usually suppressed by factors of the Planck mass in low energies (cf. Section 6.2). Such terms are therefore, in principle, not relevant in low-energy applications when compared to the minimal sectors of the SME.

Through naïve power counting we see that this non-minimal coupling is non-renormalizable, and its inclusion in diagrams with increasing numbers of loops could potentially not lead to a converging perturbative series. To blame is the extra derivative in the field-strength tensor, which means that at higher energies the inclusion of more vertices leads to increasing contributions, even if suppressed by a large mass scale. This is to be compared with the situation in standard QED, where the higher-order contributions are correspondingly smaller than the previous ones – this is due to a small (dimensionless) coupling constant and the absence of higher derivatives. In any case, despite its non-renormalizability, non-minimal terms such as (6.27) are still useful if we do not go close to the expected energy scale of the underlying theory[23], i.e., if we work with energies $\mathcal{E} \lesssim g^{-1}$.

[22] Another would be invariance under Lorentz transformations of the observer frame, which may be achieved by correctly matching the Lorentz indices.

[23] This situation is similar to that of the old Fermi four-fermion contact interaction, $\mathcal{L}_{\mathrm{Fermi}} \sim G_{\mathrm{F}} \bar{\psi}_p \psi_n \bar{\psi}_e \psi_\nu$, which gives a good phenomenological description in energy scales $\lesssim 1/\sqrt{G_{\mathrm{F}}} \sim 10^2$ GeV, which is about the typical electroweak scale, where new physics is expected. Here the Fermi interaction works as an effective (non-renormalizable) interaction relative to the high-energy (with Higgs, renormalizable) electroweak theory.

Non-minimal couplings of the kind considered here are LSV corrections to the usual (minimal) QED electron-photon interaction term $\mathcal{L}_{e\gamma} = e\bar{\psi}\gamma_\mu\psi A^\mu$. As discussed in Chapter 3, in the context of spin-1 particles a non-minimal term $\sim ieW^*_\mu W_\nu F^{\mu\nu}$ must be introduced to correct the g-factor from $g = 1$ to $g = 2$, the theoretically predicted tree-level value [159]. Even though the denomination of "non-minimal" in the spin-1 case was somewhat different – it had to do with its non-Abelian origins (cf. Section 3.2.2) – we recognize that in both cases, spin-1 and spin-1/2 coupled to LSV backgrounds, the matter fields are coupled directly to the field-strength tensor of the gauge mediator and not to the gauge potential itself, as in QED. This is the main reason for calling terms like (6.27) non-minimal.

As the observations above indicate, it is possible that LSV non-minimal couplings produce corrections to magnetic and or electric dipole moments for fermions already at tree level; see e.g., Ref. [303] and references therein. In this work a broad variety of possible LSV non-minimal couplings involving tensor backgrounds is discussed and a rather long list of possibilities is presented, including $\mathcal{L}'_{e\gamma} \sim i\lambda_1 T_{\mu\nu}\bar{\psi}\sigma^{\mu\beta}\gamma_5\psi F^{\nu}{}_{\beta}$, $\lambda_2 T_{\mu\nu}\bar{\psi}\sigma^{\mu\beta}\psi F^{\nu}{}_{\beta}$, $\lambda_3\bar{\psi}\left(T_{\alpha\nu}F_{\mu\beta} + T_{\mu\beta}F_{\alpha\nu}\right)\sigma^{\mu\beta}\sigma^{\alpha\nu}\psi$, among others ($\lambda_{1,2,3}$ are coupling constants).

To show how such LSV contributions may produce LSV-induced e.g. magnetic dipole moments, let us examine an application to the electrodynamics of *neutral* particles [304]. For this, let us assume Majorana particles which are governed by a LSV-modified Dirac equation, namely,

$$\left(i\gamma^\mu\partial_\mu - g_{\rm LV}v^\alpha\gamma^\mu\gamma_5\tilde{F}_{\mu\alpha}\right)\Psi = 0, \tag{6.28}$$

where $g_{\rm LV}$ is a coupling constant (dimension of mass^{-1}) and v_μ is a (dimensionless) LSV background 4-vector. We note that the neutral particle would not be able to feel any electromagnetic interaction in usual QED at tree level, but the charge-independent non-minimal coupling present in eq.(6.28) will change that via a direct LSV background-EM field interaction.

To evaluate the possible LSV contribution to the magnetic interaction, it is necessary to find the non-relativistic (NR) Hamiltonian. For this, let us suppose that, in a given frame, the external EM is purely magnetic, so that the equation of motion reads

$$\left[E\gamma^0 - \gamma\cdot\mathbf{p} + g_{\rm LV}v^0(\gamma\cdot\mathbf{B})\gamma_5 - g(\mathbf{v}\cdot\mathbf{B})\gamma^0\gamma_5 - m\right]\Psi = 0, \tag{6.29}$$

where we used that $\tilde{F}_{0i} = \mathbf{B}_i$ e $\tilde{F}_{ij} = \epsilon_{ijk}\mathbf{E}_k = 0$. Now we express the spinor Ψ in its two-component form as $\Psi = (\xi\ \chi)^T$ and, using the standard Dirac representation

for the gamma matrices (cf. Section 2.2), we find the following coupled equations:

$$\left[E_{\rm NR} + g_{\rm LV} v^0 (\sigma \cdot \mathbf{B})\right] \xi - \left[\sigma \cdot \mathbf{p} + g_{\rm LV} (\mathbf{v} \cdot \mathbf{B})\right] \chi = 0 \tag{6.30}$$

$$-\left[2m + g_{\rm LV} v^0 (\sigma \cdot \mathbf{B})\right] \chi + \left[\sigma \cdot \mathbf{p} + g_{\rm LV} (\mathbf{v} \cdot \mathbf{B})\right] \xi = 0, \tag{6.31}$$

where we used the NR approximations: $E_{\rm NR} = E - m$ and $E + m \approx 2m$.

We now use eq.(6.31) to write the "small component" in terms of the large one as $\chi \approx \frac{1}{2m} \left[\sigma \cdot \mathbf{p} + g_{\rm LV} (\mathbf{v} \cdot \mathbf{B})\right] \xi$, where a $g_{\rm LV}$-dependent term in the denominator has been ignored (we assume $m \gg g_{\rm LV} |\mathbf{B}|$). Inserting this into eq.(6.30) we find

$$\left[E_{\rm NR} + g_{\rm LV} v^0 (\sigma \cdot \mathbf{B})\right] \xi - \frac{1}{2m} \left[\sigma \cdot \mathbf{p} + g_{\rm LV} (\mathbf{v} \cdot \mathbf{B})\right]^2 \xi = 0, \tag{6.32}$$

but we may still expand the last piece as $\mathbf{p}^2 + g_{\rm LV}^2 (\mathbf{v} \cdot \mathbf{B})^2 + 2 g_{\rm LV} (\mathbf{v} \cdot \mathbf{B})(\sigma \cdot \mathbf{p})$, so that, identifying $E_{\rm NR} \xi = i \frac{\partial \xi}{\partial t} = H_{\rm NR} \xi$, we see that the NR Hamiltonian is

$$H_{\rm NR} = \frac{\mathbf{p}^2}{2m} - g_{\rm LV} v^0 (\sigma \cdot \mathbf{B}) + \frac{g_{\rm LV}}{m} (\mathbf{v} \cdot \mathbf{B})(\sigma \cdot \mathbf{p}) + \mathcal{O}(g_{\rm LV}^2), \tag{6.33}$$

and the neutral particle is now endowed with a magnetic dipole moment [304].

The strategy outlined above is quite general and has been widely applied to examine the consequences of various LSV couplings in search of possible LSV-induced magnetic or electric dipole moments. In the case above, the LSV contribution is actually the leading-order one – after all the particle is neutral – but for charged leptons these LSV terms constitute corrections to the standard tree-level value ($g = 2$), thus providing anomalous magnetic contributions. Similar considerations apply to electric dipole moments: in e.g. Ref. [303] it is shown how a LSV-modified covariant derivative $D_\mu = \partial_\mu + ieA_\mu + \frac{i\lambda'}{2} \left(k_{\rm F}\right)_{\mu\nu\alpha\beta} \gamma_5 \gamma^\nu F^{\alpha\beta}$ – here $\left(k_{\rm F}\right)_{\mu\nu\alpha\beta}$ is the same as in Section 6.5.1 – results in a NR Hamiltonian $H_{\rm NR} \sim -\tilde{\lambda}'(k_{\rm F}) \left(\boldsymbol{\sigma} \cdot \mathbf{E}\right)$.

Non-minimal couplings of the form (6.27) can also produce other interesting effects. In the case of neutral particles discussed above we have a covariant derivative $D_\mu = \partial_\mu + i g_{\rm LV} v^\nu \gamma_5 \tilde{F}_{\mu\nu}$, but other similar couplings are possible, specially in connection with charged particles, e.g. $D_\mu = \partial_\mu + eA_\mu + i g'_{\rm LV} u^\nu \tilde{F}_{\mu\nu}$. With this LSV coupling, if we take the NR limit, we find that the generalized momentum is given by $\mathbf{\Pi} = \mathbf{p} - e\mathbf{A} + g'_{\rm LV} u^0 \mathbf{B} - g'_{\rm LV} \mathbf{u} \times \mathbf{E}$, which shows that topological phases connected to the LSV background appear and may add to the well-known Aharonov-Bohm and Aharonov-Casher effects [305, 306]. Other possible applications will be discussed in Chapter 8, where we use a LSV non-minimal coupling in the context of some standard QED scatterings [71].

6.6 Partial conclusions

In this chapter we have introduced the concept of Lorentz violation and discussed how it may come about in field theories. In many scenarios beyond the SM it is possible that LSV develops through SSB of local Lorentz symmetry[24] and this leaves a trace in the interactions in the low-energy limit, which is hopefully accessible today. Despite of its name, Lorentz violation is implemented at the particle level, i.e., the violation is associated to Lorentz transformations (rotations and boosts) applied to the particle or to localized field configurations in a given observer inertial frame. In this sense, the LSV Lagrangians are scalar densities under Lorentz transformations of the observer's inertial frame [286]. Also CPT-breaking terms may be included and for terms with mass dimension less than four, the SME (then said to be minimal) is renormalizable.

The SME presents a coherent and systematic framework where the different possibilities of LSV in the various sectors of the SM are implemented. These cover not only the usual SM content, but also the gravitational sector[25]. Here we did not aim at presenting a thorough discussion of the various sectors, but rather at presenting a brief and target-oriented discussion of the most important features of the SME, specially extended QED. For this reason we used well-known examples (indicated by the references) extracted from the literature and adapted by myself.

In Section 6.4 we introduced the Sun-centered frame, which is a quasi-inertial system to which we can conveniently translate the LSV coefficients. The SCF is an example of a *concordant* frame [295], i.e., it is a member of a class of frames in which the LSV coefficients are small (relative to 1 or to an appropriate mass scale) due to the suppression by a heavy mass scale. This is sensible due to the experimental fact that no Lorentz violation has been observed to date and any LSV effects must be tiny. Furthermore, since the Earth moves nonrelativistically relative to the SCF, the notions of *high*/*low*-energy physics on Earth-bound laboratories may be safely assumed to hold also in the SCF.

As a final remark, we note that, since no definitive signal of Lorentz violation has ever been found, it is only possible to obtain upper limits on the different coefficients. For instance, the CPT-odd b_μ (cf. Section 6.5.1) may lead to parity-violating effects in atoms, thus inducing parity-non-conserving transitions and atomic electric

[24] In principle, it would also be possible to have *explicit*, rather than spontaneous, LSV. This is however not possible when gravitation is included [274, 307]. For this reason we have focused on LSV via SSB.

[25] In this introduction we have not touched this sector, as this is out of our scope here. The connection between gravitation and LSV can be further explored in Refs. [263, 264]. See also [274, 307].

dipole moments. With Cs atoms it was found that $|b_0| < 2 \times 10^{-14}$ GeV [308]. As for (combinations of) the spatial components, it is possible that LSV terms of the form (6.15) produce spin-dependent torques measurable by precision torsion pendula. Using this, Heckel *et al* have found $b_{X,Y,Z} < 10^{-31} - 10^{-30}$ GeV [309]. Less stringent limits have been obtained with experiments using e.g. Penning traps (trapped ions) [292]. Further limits are listed in Table D6 from Ref. [58].

The pure gauge sector discussed in Section 6.5.1 also offers opportunities for experimental tests of some of its components – or at least combinations thereof. For example, some of the non-birefringent components $(\tilde{\kappa}_{\mathrm{e}-})^{XY,XZ,YZ,\cdots}$, $(\tilde{\kappa}_{\mathrm{o}+})^{XY,XZ,YZ}$ and $\tilde{\kappa}_{\mathrm{tr}}$[26] can be bound to $< 10^{-18}$ via Michelson-Morley-like experiments looking for deviations in the speed of light (cf. eq.(6.26)) [310]. Further limits are listed in Table D13 from Ref. [58].

Finally, as mentioned in Section 6.5.1, non-minimal electron-photon couplings modify the usual QED basic interaction vertex, so that pretty much all processes in QED are open to receiving corrections from it. As was hopefully clear from Section 6.5.1, there is a broad variety of possible couplings with many different combinations of gamma-matrix structures and LSV background tensors (or vectors). To quote a few possibilities, the LSV coupling involving neutral particles may be constrained by measurements of the magnetic dipole moment of neutrinos to be $g_{\mathrm{LV}} v^0 < 0.9 \times 10^{-10}\, \mu_B$ [304]; for the non-minimal coupling involving $(k_{\mathrm{F}})_{\mu\nu\alpha\beta}$, using the experimental value (and uncertainty) of the magnetic dipole moment of the electron it is found that $|\lambda' (\kappa_{\mathrm{DB}})_{33}| < 2.3 \times 10^{-20}\, \mathrm{eV}^{-1}$, whereas by using data from the electric dipole moment, it is found that $|\lambda' (\kappa_{\mathrm{DB}})_{ii}| < 1.1 \times 10^{-24}\, \mathrm{eV}^{-1}$ [303].

The next two chapters are basically extracted from two of my published works, Refs. [70, 71], which have been expanded by myself to be presented in this thesis. On the first we discuss some laboratory tests of the k_{AF} sector of the pure gauge extended QED, while in the second we work out the scattering cross sections for some QED processes in the presence of a LSV non-minimal coupling.

[26] These are composed by $(\tilde{\kappa}_{\mathrm{e}-})^{jk} = \frac{1}{2}(\kappa_{\mathrm{DE}} - \kappa_{\mathrm{HB}})^{jk} - \frac{1}{3}\delta^{jk}(\kappa_{\mathrm{DE}})^{ii}$, $(\tilde{\kappa}_{\mathrm{o}+})^{jk} = \frac{1}{2}(\kappa_{\mathrm{DB}} + \kappa_{\mathrm{HE}})^{jk}$ and $\tilde{\kappa}_{\mathrm{tr}} = \frac{1}{3}(\kappa_{\mathrm{DE}})^{ii}$, where $(\kappa_{\mathrm{DE}})^{jk} = -2(k_{\mathrm{F}})^{0j0k}$, $(\kappa_{\mathrm{HB}})^{jk} = \frac{1}{2}\epsilon^{jab}\epsilon^{kcd}(k_{\mathrm{F}})^{abcd}$ and $(\kappa_{\mathrm{DB}})^{jk} = -(\kappa_{\mathrm{HE}})^{kj} = (k_{\mathrm{F}})^{0jab}\epsilon^{kab}$. For the limit quoted in the main text these coefficients had to be transformed to the SCF (cf. Section 6.4).

Chapter 7

Constraining the Carroll-Field-Jackiw electrodynamics

This chapter is based upon the published work "Laboratory-based limits on the Carroll-Field-Jackiw Lorentz-violating electrodynamics" [70] whose content has been significantly expanded to help clarify the discussion. This work was done in collaboration with Y.M.P. Gomes and I have done most of the writing and calculational work (I am the first author).

7.1 Introduction

In Chapter 6 we presented the idea and some realizations of Lorentz-symmetry violation (LSV) and here we shall extend the developments presented in Ref. [70], where we investigate the case of a LSV background 4-vector coupled exclusively to the photon sector.

An interesting prospect to implement LSV in the (1 + 3) Maxwell sector was proposed by Carroll, Field and Jackiw [311] through a Chern-Simons-like topological interaction [312] resulting in the following CPT-odd Lagrangian

$$\mathcal{L}_{\rm CFJ} = \frac{1}{2}\epsilon_{\mu\nu\alpha\beta}\,(k_{\rm AF})^{\mu}\,A^{\nu}F^{\alpha\beta}, \tag{7.1}$$

where $A^{\mu} = (\phi,\, \mathbf{A})$ is the usual gauge 4-potential and $\tilde{F}^{\mu\nu} = \frac{1}{2!}\epsilon^{\mu\nu\alpha\beta}F_{\alpha\beta}$ is the dual of the electromagnetic field-strength tensor[1]. As mentioned in Section 6.5.1, this is

[1] We adopt $\epsilon^{0123} = +1$ throughout.

the $d = 3$ part of the gauge sector of extended QED, so the background coefficients $(k_{\rm AF})^\mu$ have canonical dimension of mass[2].

Despite of explicitly containing the gauge potential, the action $\int d^4x \mathcal{L}_{\rm CFJ}$ is actually gauge invariant, but under a rather unusual condition. To see it, consider a gauge transformation $\delta A^\mu = \partial^\mu \Lambda$ with Λ a spacetime-dependent scalar function. Assuming that the $(k_{\rm AF})^\mu$ do not feel gauge transformations, we find

$$\begin{aligned} \delta\mathcal{L}_{\rm CFJ} &= (k_{\rm AF})^\mu \left[(\delta A^\nu)\, \tilde{F}_{\mu\nu} + A^\nu \left(\delta \tilde{F}_{\mu\nu} \right) \right] \\ &= (k_{\rm AF})^\mu \, (\partial^\nu \Lambda)\, \tilde{F}_{\mu\nu} \\ &= -\left[\partial^\nu \, (k_{\rm AF})^\mu \right] \Lambda \tilde{F}_{\mu\nu}, \end{aligned} \tag{7.2}$$

where an integration by parts (allowed inside an integral) with $\delta \tilde{F}_{\mu\nu} = 0$ and $\partial^\nu \tilde{F}_{\mu\nu} = 0$ were used. Therefore, in order to keep the action gauge invariant, it is necessary that $\partial^\nu \, (k_{\rm AF})^\mu = 0$. The simplest solution[3] is to make $k_{\rm AF}$ a fixed, spacetime-independent 4-vector. For this reason, $k_{\rm AF}$ is treated as fixed, thus providing a preferred direction in spacetime (i.e., a background) which breaks Lorentz invariance and isotropy of empty space.

Looking at the symmetries of the terms in the pure lepton part of the SME one may wonder if the b_μ coefficients are not possibly related to the $(k_{\rm AF})^\mu$. This connection would arise if we started with a LSV Lagrangian containing the usual QED terms with the addition of the CPT-odd axial-vector LSV b-term and assumed that the fermions are "heavy" in such a way that they can be integrated out. Given that the CFJ term is quadratic in the photon field, the relevant contribution would come from vacuum polarization and it would lead to $(k_{\rm AF})^\mu = \zeta \, b^\mu$, with ζ independent of whether b is time- or space-like [293]. It is interesting to note that, in case a correspondence is found, it could be used to apply constraints from the photon to the electron sector of the SME.

The exact numerical relation between $(k_{\rm AF})^\mu$ and b^μ, i.e., the value of ζ, has been long debated and a non-exhausting summary is presented in Table 7.1. All in all, despite of the somewhat confusing situation, it seems that the conclusion is that the question of whether the b-sector may induce a $k_{\rm AF}$-sector is regularization-scheme dependent and both nonperturbative and perturbative (in b) approaches may suffer from ambiguities depending on the regularization procedure [315].

---

[2] In the published work [70] we adopted $(k_{\rm AF})^\mu \equiv k_{\rm AF} \, n^\mu$, where $k_{\rm AF}$ concentrates the numerical (dimensionful) factors, while n is simply directional and dimensionless. Here we go with the standard notation.

[3] It is possible, nevertheless, to give it a dynamic nature, where it may be interpreted as a pseudo-scalar field – see e.g. Refs. [308, 313, 314].

Authors	Method	ζ	Perturb. in b?
Klinkhamer [293]	consistency	0	×
Jackiw & Kostelecký [315]	usual	$3/16\pi^2$	×
Chaichian *et al* [316]	proper time	$C/2\pi^2$	✓
Chung & Chung [317]	proper time	$C/2\pi^2$	×
Chan [318]	cov. derivative exp.	$1/8\pi^2$	×
Chung & Oh [319]	cov. derivative exp.	$3/16\pi^2$	✓
Pérez-Victoria [320]	usual	$3/16\pi^2$	×
Ferrari & Raciti [321]	γ_5 regular.	0	×

Table 7.1: Summary of the situation regarding the correspondence between b_μ and $(k_{\rm AF})^\mu$. The constant C is *arbitrarily* set to 1/4 in Refs. [316, 317], but in all cases the choice of regularization is indicated as a source of further ambiguities. For an interesting discussion on the situation, see Ref. [322].

In the words from Chaichian *et al*, "Nevertheless, if the radiatively induced Chern-Simons term has any physical observable effect, it is the comparison with experiment which will fix such ambiguities and ultimately resolve the discrepancies among various results" [316].

In view of the unsolved dispute in the literature, we adopt the following point of view for this work: the electron is insensitive to Lorentz violation and does not couple to any background, only the photons do so. Therefore, in Ref. [70] and in the remaining of this chapter, we assume that the only source of LSV effects is described by the CFJ term, eq.(7.1), and neglect the possibility of it being radiatively induced by other sectors of the SME.

Let us now return to the the LSV-modified CFJ electrodynamics and write down the equations of motion in the presence of an external source $J^\mu = (\rho, \mathbf{J})$,

$$\partial_\mu F^{\mu\nu} = J^\nu - 2\left(k_{\rm AF}\right)_\mu \tilde{F}^{\mu\nu} \quad \text{and} \quad \partial_\mu \tilde{F}^{\mu\nu} = 0, \tag{7.3}$$

which may be expressed in vector form as

$$\begin{aligned}
\boldsymbol{\nabla}\cdot\mathbf{E} &= \rho + 2\mathbf{k}_{\rm AF}\cdot\mathbf{B} && (7.4)\\
\boldsymbol{\nabla}\cdot\mathbf{B} &= 0 && (7.5)\\
\partial_0\mathbf{B} + \boldsymbol{\nabla}\times\mathbf{E} &= 0 && (7.6)\\
-\partial_0\mathbf{E} + \boldsymbol{\nabla}\times\mathbf{B} &= \mathbf{J} + 2k^0_{\rm AF}\mathbf{B} - 2\mathbf{k}_{\rm AF}\times\mathbf{E}, && (7.7)
\end{aligned}$$

where we used that $F^{0i} = -\mathbf{E}_i$ and $F^{ij} = -\epsilon_{ijk}\mathbf{B}_k$. We also note that the background works as a source attached to the EM fields.

It is also interesting to write the modified Maxwell equations in momentum space and in a source-free configuration. Assuming plane-wave solutions[4], we have

$$\begin{aligned} \mathbf{p}\cdot\mathbf{E} &= 2i\mathbf{k}_{\rm AF}\cdot\mathbf{B} && (7.8)\\ \mathbf{p}\cdot\mathbf{B} &= 0 && (7.9)\\ \omega\mathbf{B}-\mathbf{p}\times\mathbf{E} &= 0 && (7.10)\\ \omega\mathbf{E}+\mathbf{p}\times\mathbf{B} &= 2ik^0_{\rm AF}\mathbf{B}-2i\mathbf{k}_{\rm AF}\times\mathbf{E}, && (7.11) \end{aligned}$$

and, from eqs.(7.9) and (7.10), we see that the magnetic field is still transverse and perpendicular to the plane defined by $\mathbf{p}$ and $\mathbf{E}$.

However, from eq.(7.8) we find that the electric field is not transverse any more, but rather displays a longitudinal component proportional to the component of the magnetic field along the LSV background. By (scalar) multiplying the spatial part of the background with eq.(7.10) and applying it to eq.(7.8), we find that the electric field satisfies

$$\left(\mathbf{p}+\frac{2i}{\omega}\mathbf{p}\times\mathbf{k}_{\rm AF}\right)\cdot\mathbf{E}=0, \tag{7.12}$$

so, indeed, there is a $\mathcal{O}(k_{\rm AF})$ projection along the direction of motion. Multiplying the 3-momentum with eq.(7.11) gives the same result in view of eq.(7.9).

Given that $\mathbf{B}\perp\mathbf{p}$, but $\mathbf{E}\not\perp\mathbf{p}$, we see that the Poynting vector $\sim\mathbf{E}\times\mathbf{B}$ is not entirely parallel to the wave vector $\mathbf{p}/\omega$. Indeed, vector multiplying eq.(7.10) by $\mathbf{E}$ we find that $\omega\mathbf{S}\sim\omega\mathbf{E}\times\mathbf{B}=(\mathbf{E})^2\,\mathbf{p}-(\mathbf{p}\cdot\mathbf{E})\,\mathbf{E}$. An analogous situation is encountered in e.g. electro-anisotropic uniaxial media [287, 323].

As mentioned in Section 6.5.1, some components of the background may be problematic when it comes to consistency tests, such as causality and stability. The CFJ term is not free from these either and this may be seen in different levels. Take e.g. the electromagnetic stress-energy tensor, which reads $\Theta^{\mu\nu}=-F^{\mu\alpha}F^{\nu}{}_{\alpha}+\frac{1}{4}\eta^{\mu\nu}F^2_{\alpha\beta}-(k_{\rm AF})^{\nu}\,\tilde{F}^{\mu\alpha}A_{\alpha}$ and satisfies $\partial_\mu\Theta^{\mu\nu}=0$. The Θ^{00} component, which is the energy density, is [287, 311]

$$\Theta^{00}=\frac{\mathbf{E}^2+\left[\mathbf{B}-(k_{\rm AF})^0\,\mathbf{A}\right]^2}{2}-\frac{\left[(k_{\rm AF})^0\right]^2}{2}\mathbf{A}^2. \tag{7.13}$$

and is gauge dependent and not positive-definite, thus signalling possible instabilities. Nonetheless, upon a gauge transformation $\mathbf{A}\to\mathbf{A}-\boldsymbol{\nabla}\xi$ the volume integral which defines the energy of the field is actually left intact, as the extra terms produce only a total derivative. Note that only the time component of $k_{\rm AF}$ is present.

[4]Here we keep the same notation for the momentum-space fields, as no confusion arises.

Let us continue and analyse the dispersion relations by using eq.(7.11) with $\mathbf{B}$ defined via eq.(7.10). We find that the electric field obeys $M_{ij}\mathbf{E}_j = 0$ with $M_{ij} = (\omega^2 - \mathbf{p}^2)\,\delta_{ij} + \mathbf{p}_i\mathbf{p}_j + 2i\left[(k_{\rm AF})_0\,\mathbf{p}_k - \omega\,(\mathbf{k}_{\rm AF})_k\right]\epsilon_{kij}$, whose determinant is required to be zero. In this way we obtain

$$p^4 - 4\,(k_{\rm AF}\cdot p)^2 + 4k_{\rm AF}^2 p^2 = 0, \tag{7.14}$$

which gives the modified dispersion relations. This is a fourth-order polynomial in $p^0 \equiv \omega(\mathbf{p})$, and it will end up generating two propagation modes. To proceed, we need to specify the nature of the background 4-vector and we shall discuss two cases: pure time- and pure space-like backgrounds.

Solving eq.(7.14) for ω^2 in the case where $\mathbf{k}_{\rm AF} = 0$ gives us

$$\omega_\pm^2 = \mathbf{p}^2 \pm 2|\,(k_{\rm AF})^0\,||\mathbf{p}| \tag{7.15}$$

and it is possible that, for low enough momentum, $|\mathbf{p}| < 2|\,(k_{\rm AF})^0\,|$, we find a negative ω_-^2, thus producing an imaginary energy which would cause the associated mode to evolve exponentially. Kostelecký suggested [287] that this could be cured if a small, non-zero mass for the photon is included[5]. This hypothesis has been tested and the result is that no, the unstable behavior associated with a time-like $k_{\rm AF}$ still survives and one cannot guarantee stability in general [324].

Let us now look into the group velocity associated with these modes. From eq.(7.14) we have

$$v_g^\pm = \frac{\partial\omega_\pm}{\partial|\mathbf{p}|} = \frac{|\mathbf{p}| \pm |\,(k_{\rm AF})^0\,|}{\sqrt{\mathbf{p}^2 \pm 2|\,(k_{\rm AF})^0\,||\mathbf{p}|}}, \tag{7.16}$$

which is again problematic for low momenta (it is also singular). The front velocity $v_{\rm f}^\pm = \lim\limits_{|\mathbf{p}|\to\infty}\dfrac{\omega_\pm}{|\mathbf{p}|}$ can be computed and gives one, as it should, but the discussion above shows that, in general, a time-like background is not a consistent choice[6]. Though not explicitly discussed, this case is also non-unitary [325], even in the presence of a small photon mass [324].

Since a time-like background presents problems, let us now study the case of a space-like background. Defining $\cos\psi = \frac{\mathbf{p}\cdot\mathbf{k}_{\rm AF}}{|\mathbf{p}||\mathbf{k}_{\rm AF}|}$, the energy solutions satisfy

$$\omega_\pm^2 = \mathbf{p}^2 + 2\mathbf{k}_{\rm AF}^2 \pm 2|\mathbf{k}_{\rm AF}|\sqrt{\mathbf{k}_{\rm AF}^2 + \mathbf{p}^2\cos^2\psi}, \tag{7.17}$$

[5]He went no further, since this would probably be "too much new physics at the same time".

[6]The quantum field theoretical analysis confirms the classical arguments showed here. For a complete discussion, see Ref. [325] and references therein.

and, again, it is not clear whether $\omega_-^2 \geq 0$. To see that this is indeed the case, it suffices to notice that, for $x = |\mathbf{k}_{\rm AF}|/|\mathbf{p}| \ll 1$, the inequality $1+2x^2 \geq 2\sqrt{x^4 + x^2\cos^2\psi}$ always holds. Since $\omega_\pm^2 \geq 0$, stability is guaranteed.

Regarding the causality of the theory, one needs to check whether the front velocity (defined above) is equal to one. Using eq.(7.17) and the variable x previously defined, we find that the phase velocity – which in general does not need to be bound to ≤ 1 – is given by

$$v_{\rm p}^{\pm} = \frac{\omega_\pm}{|\mathbf{p}|} = \sqrt{1 + 2x^2 \pm 2\sqrt{x^4 + x^2\cos^2\psi}}, \tag{7.18}$$

so that, when $x \to 0$, we have $v_{\rm f}^{\pm} = 1$. It can also be verified that the group velocity satisfies $v_{\rm g}^{\pm} \leq 1$. This shows that the space-like CFJ model is safe from non-causal behavior (it is also unitary [325]).

In summary, the usual Maxwell electrodynamics incremented by the CFJ interaction defined by eq.(7.1) is stable, causal and unitary from both classical and quantum points of view provided we are working with a pure space-like $k_{\rm AF}$ [325]. This is also true if a non-zero Proca-like mass term for the photon is included [324]. On the other hand, time- and light-like backgrounds are potentially problematic [293, 311, 324, 326]. A space-like background is therefore the only healthy scenario available, but we shall keep the calculations generic as far as possible, specializing to space-like components only at the very end.

An important remark is in order at this point: the considerations above apply to a truly fixed, time-independent background. These requirements are only explicitly met in an inertial reference frame. This is not the case of the Earth due to its sidereal and orbital motions: in the laboratory the background would seem to rotate. As discussed in Section 6.4, a convenient and approximately inertial frame is, for example, the one attached to the Sun – the so-called Sun-centered frame (SCF) – which is broadly used in the literature [58, 286].

In order to translate the accessible, but time-dependent, background as observed on Earth, $(k_{\rm AF})_{\rm lab}$, in terms of combinations of the constant $(k_{\rm AF})_{\rm SCF}$, we employ a general Lorentz transformation, i.e., $(k_{\rm AF})^\mu_{\rm lab} = \Lambda^\mu{}_\nu \, (k_{\rm AF})^\nu_{\rm SCF}$, where $\Lambda^\mu{}_\nu$ is given in Section 6.4. From eqs.(6.6) we have $\Lambda^i{}_T \sim \beta \lesssim 10^{-4}$, so that, ignoring subdominant boost effects, we may write $(k_{\rm AF})^0_{\rm lab} \simeq (k_{\rm AF})^T_{\rm SCF} \equiv 0$ and $(k_{\rm AF})^i_{\rm lab} \simeq R^{iJ}(\chi, T_\oplus) \, (k_{\rm AF})^J_{\rm SCF}$, where the rotation matrix is explicitly time dependent.

Since experiments are usually conducted over long time scales, the LSV signatures observed in Earth-bound experiments would be effectively time averaged. The only non-vanishing (time-averaged) spatial components are $(k_{\rm AF})^x_{\rm lab} = -\sin\chi \, (k_{\rm AF})^Z_{\rm SCF}$

and $(k_{\rm AF})^z_{\rm lab} = \cos\chi\ (k_{\rm AF})^Z_{\rm SCF}$, with χ the geographic co-latitude. The effects we consider are linear in $k_{\rm AF}$, so only $(k_{\rm AF})^{x,z}_{\rm lab}$ will be relevant and both may be expressed in terms of $(k_{\rm AF})^Z_{\rm SCF}$. Our goal is to constrain it.

The CFJ Lagrangian would induce optical effects during the propagation of radiation through vacuum (see Section 7.4), and Carroll, Field and Jackiw used data on the rotation of the plane of polarization from distant galaxies in order to impose strong limits on $k_{\rm AF}$. Given that no significant evidence of such effects was found, only an upper bound was obtained, namely, $k_{\rm AF} < 10^{-42}\,{\rm GeV}$ [311, 314, 327]. Other limits have been searched for in many contexts, mainly astrophysical, e.g. CMB polarization [328, 329], and are currently as strict as $k_{\rm AF} \lesssim 10^{-43}\,{\rm GeV}$ (see Table D12 in Ref. [58] and references therein).

Our objective here is to extract consequences from eq.(7.1) in the context of systems available at much shorter distance scales, where Earth-bound laboratory experiments may be used to constrain the predicted LSV effects. This is a valid effort, given that the apparatus is under the experimenter's control, as opposed to cosmological or astrophysical tests, where sizeable uncertainties may arise due to complicated models describing the interstellar medium and light propagation therein. We discuss LSV effects in the context of the CFJ modification of QED in two main fronts: energy shifts in the spectrum of the hydrogen atom and the generation of an electric dipole moment for charged leptons. We also briefly address measurements of rotation in the polarization of light in cavities.

As we shall see, the LSV-induced corrections to the Coulomb potential appear already at tree level via spin-dependent interaction potentials. For the leptonic electric dipole moment (ℓEDM), on the other hand, it is necessary to compute the one-loop correction to the corresponding form factor, which is found to be explicitly momentum dependent, thus theoretically allowing for an enhancement at high energies. Despite of this interesting feature, we expect it to remain inaccessible to experiment in the foreseeable future. Resonant cavities would present, nonetheless, a good prospect to perform local tests of LSV and to potentially constrain $(k_{\rm AF})^Z_{\rm SCF}$ even further.

The rest of this chapter was extracted from my published work [70] with eventual expansions to help clarify a few points. The next sections are organised as follows: in Section 7.2 I discuss the interparticle potential between leptons and apply it to the hydrogen atom and, in Section 7.3, I calculate the CFJ contribution to the ℓEDM. In Section 7.4 I address some classical features of the model and connect it to polarization measurements in a cavity. Section 7.5 is devoted to our concluding remarks. Natural units ($c = \hbar = 1$) are used throughout.

7.2 Interparticle potential

The CFJ Lagrangian, eq.(7.1), modifies the quadratic piece of the usual Maxwell sector, therefore altering the propagator of light. This modification entails that photon-mediated interactions will necessarily include a (small) LSV signature, possibly giving rise to anisotropies involving the fixed background.

The relatively high precision attained in spectroscopy experiments is a motivation to consider the effect of the CFJ corrections to the Coulomb potential in the study of atomic systems, the simplest of which is the hydrogen atom. To do so, one needs to compute the interaction energy between the proton – here treated as a point-like, structureless fermion – and the electron. The interaction of two spin-1/2 fermions can be treated in the non-relativistic (NR) regime through the concept of interparticle potential, which is given by the first Born approximation [113] as $V(r) = -\int \frac{d^3\mathbf{q}}{(2\pi)^3}\mathcal{M}(\mathbf{q})e^{i\mathbf{q}\cdot\mathbf{r}}$, where $\mathcal{M}$ is the NR amplitude, $\mathbf{q}$ is the momentum transfer and $\mathbf{r}$ is the relative position vector (cf. Chapter 2).

The one-photon exchange amplitude may be schematically written as $\mathcal{M} \sim J_1^\mu \langle A_\mu A_\nu \rangle J_2^\nu$, where $J_{1,2}^\mu$ are the fermion currents[7]. Here $\langle A_\mu A_\nu \rangle$ is the effective photon propagator. Given that LSV effects are expected to be tiny, we do not use the full photon propagator [324, 325], but merely consider the CFJ term (7.1) as a true bilinear interaction in the photon sector, i.e., an effective vertex to be inserted into the usual QED propagator, $\langle A_\mu A_\nu \rangle_0 = \frac{-i\eta_{\mu\nu}}{p^2+i\varepsilon}$. Under these assumptions one may write the CFJ vertex as [330, 331]

$$V_{\gamma\gamma}^{\mu\nu} = 2\left(k_{\mathrm{AF}}\right)_\alpha \epsilon^{\mu\alpha\beta\nu} p_\beta, \tag{7.19}$$

while the QED tree-level vertex remains unaltered and reads $V_{\ell\ell\gamma}^\mu = ie\gamma^\mu$.

We consider the interaction in the center of mass (CM) frame, in which fermion "1" has incoming and outgoing momenta denoted by $P = p + q/2$ and $P' = p - q/2$, respectively. Here, p is the average momentum and q is the momentum carried by the virtual photon. Similar definitions hold for fermion "2" (with $P \to -P$ and $P' \to -P'$). Applying the Feynman rules and noting that $q_\mu \left[\bar{u}\gamma^\mu u\right]_{1,2} = 0$ for the conserved external currents, we obtain

$$i\mathcal{M} = \frac{2e_1e_2}{(q^2)^2}\left[\bar{u}\gamma^\sigma u\right]_1 \epsilon_{\sigma\alpha\beta\rho}\left(k_{\mathrm{AF}}\right)^\alpha q^\beta \left[\bar{u}\gamma^\rho u\right]_2, \tag{7.20}$$

where we assume an elastic interaction, i.e., $q^\mu = (0, \mathbf{q}) \to q^2 = -\mathbf{q}^2$.

[7] The currents are built from on-shell (external) spinors. Here we do not include any LSV effects in the matter sector, so the currents will be constructed with the standard (Lorentz-preserving) free solutions of the Dirac equation.

As discussed in Section 7.1, the background above is the one measured in the lab and, for the sake of simplicity, we will only transform to the SCF variables in the very end.

Following eqs.(2.8) and (2.9), in the NR limit, the current for fermion 1 has components $[\bar{u}\gamma^0 u]_1 \sim 1$ and $[\bar{u}\gamma^i u]_1 = \frac{\mathbf{p}_i}{m_1} - \frac{i}{2m_1}\epsilon_{ijk}\,\mathbf{q}_j\langle\sigma_k\rangle_1$, with similar results for current 2, provided one makes the appropriate changes in momenta ($\mathbf{p} \to -\mathbf{p}$ and $\mathbf{q} \to -\mathbf{q}$). In our notation $\langle\sigma\rangle_{1,2} = \chi^\dagger\sigma_{1,2}\chi$, with χ being the basic spin-up or -down spinor satisfying $\chi_a^\dagger\chi_b = \delta_{ab}$, and $\sigma_{1,2}$ the usual Pauli spin matrices acting on particles 1 and 2, respectively.

We now plug eq.(7.20) with a pure space-like background into the definition of $V(r)$ in order to obtain the following potentials[8]

$$V_{\mathbf{p}}(r) = \frac{\alpha}{\mu r}\,(\mathbf{k}_{\rm AF}\cdot\mathbf{L}) \tag{7.21}$$

$$V_{\boldsymbol{\sigma}}(r) = \frac{\alpha}{2m_1m_2r}\left[m_1\mathbf{k}_{\rm AF}\cdot\langle\boldsymbol{\sigma}\rangle_2 + m_1(\mathbf{k}_{\rm AF}\cdot\hat{\mathbf{r}})\,(\hat{\mathbf{r}}\cdot\langle\boldsymbol{\sigma}\rangle_2) + 1\leftrightarrow 2\right], \tag{7.22}$$

where μ is the reduced mass of the system and $\mathbf{L} = \mathbf{r}\times\mathbf{p}$ is the orbital angular momentum. The electric charges were set as $e_1 = -e_2 = \sqrt{4\pi\alpha}$, with $\alpha \simeq 1/137$ being the electromagnetic fine structure constant. The final result is $\delta V_{\rm C}(r) = V_{\mathbf{p}}(r) + V_{\boldsymbol{\sigma}}(r)$, and it represents an additional LSV contribution to the well-known Coulomb interaction between two charges. We note, furthermore, the pseudo-scalar character of these potentials – a sign of their parity-odd origins.

The potentials above could induce deviations in the dominant Coulomb force in the form of possible angle-dependent corrections e.g. to the inverse-square law. These could be observable in experiments involving e.g. spin-polarized macroscopic objects [105]. If, for simplicity, we consider instead the interaction energy between two charged – but unpolarized – bodies as given by $\delta V_{\rm C}(r) = V_{\mathbf{p}}(r)$, we may extract the force per interacting pair of particles as

$$\mathbf{f}_{\rm LSV} = \frac{\alpha}{m_1 r}\left[(\mathbf{k}_{\rm AF}\times\mathbf{p}) + \frac{1}{r}\,(\mathbf{k}_{\rm AF}\cdot\mathbf{L})\,\hat{\mathbf{r}}\right], \tag{7.23}$$

where we assumed that r is much larger than the typical dimensions of bodies "1" and "2" (with $m_2 \gg m_1$ and fixed at the origin). The total force would be $\mathcal{N}_{\rm eff}\mathbf{f}_{\rm LSV}$, where $\mathcal{N}_{\rm eff}$ describes the effective number of interacting particles. This force would act as a small velocity-dependent perturbation to the dominating Coulomb (and gravitational) interaction between the two electrically charged objects.

[8]Notice that the denominator of eq.(7.20) presents a $\mathbf{q}^4$ dependence [113]. Furthermore, please note that here we depart from the conventions used in Chapters 2 and 3 and do not explicitly keep the $\delta_{1,2}$ factors in the expressions of the potentials.

The first term in eq.(7.23) represents a precession of the 3-momentum $\mathbf{p}$ around the axis defined by $\mathbf{k}_{\rm AF}$. To see this it suffices to consider that $\mathbf{p}\cdot\frac{d\mathbf{p}}{dt}=0$, so that $|\mathbf{p}|$ is constant (time-independent). Similarly, the angle given by $\cos\vartheta=\frac{\mathbf{k}_{\rm AF}\cdot\mathbf{p}}{|\mathbf{k}_{\rm AF}||\mathbf{P}|}$ is also fixed in time[9], so that the 3-momentum circles around the direction of $\mathbf{k}_{\rm AF}$. The second term shares more similarities with the typical Coulomb force $\sim\hat{\mathbf{r}}/r^2$, but it contains an unusual dependence on angular momentum, which also controls whether this term is attractive or repulsive. Besides, the interaction from eq.(7.24) may also induce a spontaneous torque on a pair of charges [332].

We now turn to our main interest: the application of our results, eqs.(7.21) and (7.22), to the hydrogen atom. Given that the proton is a thousand times heavier than the electron, $\delta V_{\rm C}(r)$ reads

$$\delta V_{\rm C}^{\rm H}(r)=\frac{\alpha}{m_e r}\left[\mathbf{k}_{\rm AF}\cdot\left(\mathbf{L}+\frac{1}{2}\langle\boldsymbol{\sigma}\rangle\right)+\frac{1}{2}\left(\hat{\mathbf{r}}\cdot\mathbf{k}_{\rm AF}\right)\left(\hat{\mathbf{r}}\cdot\langle\boldsymbol{\sigma}\rangle\right)\right], \tag{7.24}$$

which represents a Lorentz violating CPT-odd correction to the electron-proton electromagnetic interaction. According to usual quantum-mechanical perturbation theory, in order to evaluate the first-order energy shift associated with this perturbation, we need to calculate $\Delta E_{\rm LSV}^{\rm H}=\langle\psi^0|\delta V_{\rm C}^{\rm H}|\psi^0\rangle$, with $|\psi^0\rangle$ being eigenstates of the free hydrogen atom.

Since the problem involves not only the orbital angular momentum, but also the spin degrees of freedom, we build the angular wave functions for the total angular momentum $\mathbf{J}=\mathbf{L}+\mathbf{S}$, which are given below for the case of a generic orbital angular momentum $\mathbf{L}$ coupled to a spin-1/2:

$$\begin{aligned}\Theta_{j=\ell+\frac{1}{2}}(\theta,\phi) &= \sqrt{\frac{\ell+m_\ell+1}{2\ell+1}}Y_{\ell,m_\ell}(\theta,\phi)\,\chi_+ + \\ &+ \sqrt{\frac{\ell-m_\ell}{2\ell+1}}Y_{\ell,m_\ell+1}(\theta,\phi)\,\chi_- \qquad (7.25)\\ \Theta_{j=\ell-\frac{1}{2}}(\theta,\phi) &= \sqrt{\frac{\ell-m_\ell}{2\ell+1}}Y_{\ell,m_\ell}(\theta,\phi)\,\chi_+ + \\ &- \sqrt{\frac{\ell+m_\ell+1}{2\ell+1}}Y_{\ell,m_\ell+1}(\theta,\phi)\,\chi_- \qquad (7.26)\end{aligned}$$

both with $m_j=m_\ell+1/2$. The final normalized wave functions are $\psi^0(r,\theta,\phi)=R_{n,\ell}(r)\Theta_j(\theta,\phi)$, where $Y_{\ell,m_\ell}(\theta,\phi)$ and $R_{n,\ell}(r)$ are the usual spherical harmonics and radial function for the hydrogen atom, and $\chi_\pm$ are the spin eigenfunctions. Here n, ℓ and m_ℓ are the principal, angular and azimuthal quantum numbers, respectively.

[9]For small enough periods where the time-dependence of $\mathbf{k}_{\rm AF}$ itself is negligeable.

As discussed in Section 7.1, after averaging, the background as seen in the lab is given by $\mathbf{k}_{\rm AF} \equiv (\mathbf{k}_{\rm AF})_{\rm lab} = (k^x, 0, k^z)$, where we omit the sub-scripts for convenience. With this, the total energy shift is given by $\Delta E^{\rm H}_{\rm LSV} = \Delta E_1 + \Delta E_2 + \Delta E_3$, where

$$\Delta E_1 = \mathcal{G}\left[k^x\langle L_x + \frac{1}{2}\sigma_x\rangle + k^z\langle L_z + \frac{1}{2}\sigma_z\rangle\right] \tag{7.27}$$

$$\Delta E_2 = \frac{\mathcal{G}k^x}{2}\langle \sin\theta\cos\phi\,(\hat{\mathbf{r}}\cdot\sigma)\rangle \tag{7.28}$$

$$\Delta E_3 = \frac{\mathcal{G}k^z}{2}\langle \cos\theta\,(\hat{\mathbf{r}}\cdot\sigma)\rangle \tag{7.29}$$

with $\mathcal{G} = \frac{\alpha}{m_e}\overline{\langle r^{-1}\rangle} = \frac{\alpha}{m_e a_0 n^2}$, where $a_0 = 2.68\times10^{-4}\,\mathrm{eV}^{-1}$ is the Bohr radius. It is easy to check that, for $j = \ell + 1/2$, we have $\langle\psi^0|L_z|\psi^0\rangle = m_\ell + \frac{\ell - m_\ell}{2\ell+1}$ and $\langle\psi^0|\sigma_z/2|\psi^0\rangle = \frac{m_\ell+1/2}{2\ell+1}$, so that

$$\Delta E_1 = \frac{\alpha k^z_{\rm lab}}{m_e a_0 n^2}\,(m_\ell + 1/2)\,, \tag{7.30}$$

where we used that the contribution proportional to k^x vanishes due to the orthogonality of the functions involved. Similar arguments lead to $\Delta E_2 = 0$.

Finally, ΔE_3 may be written as $\Delta E_3 = \frac{\alpha k^z_{\rm lab}}{2m_e a_0 n^2}\delta\mathcal{E}_3$ and, after employing the algebra of angular momentum [333], we find $\delta\mathcal{E}_3 = \frac{2(m_\ell+1/2)}{(2\ell+1)(2\ell+3)}$, so that our final result reads[10]

$$\Delta E^{\rm H}_{\rm LSV} = \frac{4\alpha\,(k_{\rm AF})^z_{\rm lab}}{m_e a_0}\frac{m_\ell + 1/2}{n^2}\frac{(\ell+1)^2}{(2\ell+1)(2\ell+3)}, \tag{7.31}$$

where we returned all sub-scripts for notational completeness.

The quantity obtained above represents the energy shift to the spectral lines of hydrogen due to Lorentz violating effects. The aforementioned spectrum is known to a high level of accuracy and the fact that no deviations have been found allows us to place an upper bound on $\Delta E^{\rm H}_{\rm LSV}$. Optimistically, we may use the currently best precision in spectroscopic measurements, $\epsilon^{\Delta E^{\rm H}}_{\rm exp} = 4\times10^{-15}\,\mathrm{eV}$ [59], and demand that $\Delta E^{\rm H}_{\rm LSV} < \epsilon^{\Delta E^{\rm H}}_{\rm exp}$, i.e., we demand that the LSV effect lies below experimental uncertainty. From this requirement we obtain the upper bound

$$(k_{\rm AF})^Z_{\rm SCF} \lesssim 2\times10^{-19}\,\mathrm{GeV} \tag{7.32}$$

at the $1\,\sigma$ level. Above we have assumed $\frac{m_\ell+1/2}{n^2}\frac{(\ell+1)^2}{(2\ell+1)(2\ell+3)} \sim \mathcal{O}(10^{-1})$, also including the co-latitude factors (with $\sin\chi \approx \cos\chi$).

[10] A similar expression is valid for the $j = \ell - 1/2$ case.

7.3 Electric dipole moment

If an elementary particle possesses a non-zero electric dipole moment $\mathbf{d}$, it has to point in the direction of its spin, since this is the only vector available in the rest frame of the particle. When placed in an external electric field the particle will be subject to an interaction of the form $-\mathbf{d}\cdot\mathbf{E}$, which can be recast as $-d(\mathbf{S}\cdot\mathbf{E})$. This interaction violates P- and T-symmetries [334]. Standard QED, on the other hand, is parity-invariant, so that such an electric dipole interaction cannot be described by pure QED processes, that is, $d^{\mathrm{QED}} \equiv 0$.

Within the SM it is possible to generate a small leptonic EDM when strong and electroweak interactions are taken into account [334–336]. For the electron, its theoretical magnitude is bounded by $|d_e^{\mathrm{SM}}| < 10^{-38}\,\mathrm{e}\cdot\mathrm{cm}$, while the best experimental limit is $|d_e^{\mathrm{exp}}| < 8.7\times10^{-29}\,\mathrm{e}\cdot\mathrm{cm}$, at 90% C.L. [60]. The relatively strong experimental bounds on d_e can be used as a means to extract limits on the properties of new particles, such as mirror particles [336], axions [128, 337], supersymmetric particles [334, 338] and Majorana neutrinos[11] [339].

We now turn to the calculation of the LSV contribution to d_ℓ. It is clear that the tree-level contribution to the ℓEDM is zero in the CFJ scenario: the tree-level QED $\ell\ell\gamma$ vertex remains unaltered as the CFJ term only changes the Maxwell sector, so we must look at higher orders.

The first non-zero contribution comes from the one-loop vertex correction diagram, as shown in Fig. (7.1). Following the momentum assignments we have

$$\Lambda_\mu(p,p') = -2e^2\epsilon^{\nu\alpha\beta\rho}\left(k_{\mathrm{AF}}\right)_\alpha \times I_{\beta\nu\mu\rho}(p,p'), \tag{7.33}$$

where

$$I_{\beta\nu\mu\rho}(p,p') = \int \frac{d^4k}{(2\pi)^4}\frac{\gamma_\nu\left(\not{p}'-\not{k}+m_\ell\right)\gamma_\mu\left(\not{p}-\not{k}+m_\ell\right)\gamma_\rho k_\beta}{\left(k^2\right)^2\left[(p'-k)^2-m_\ell^2\right]\left[(p-k)^2-m_\ell^2\right]}, \tag{7.34}$$

and we observe that the superficial degree of divergence of this diagram is -1, that is, it behaves as $\sim 1/k$ in the high-energy (UV) limit. This is confirmed by the expression $D = 4-\frac{3}{2}E_\psi - E_\gamma - V_{\mathrm{AF}}$, with the respective variables being the number of external fermion and photon legs, and the number of vertex insertions [331]. Remembering that the corresponding diagram in usual QED describing the anomalous g-factor displays a superficial logarithmic divergence, we conclude that the role of the vertex insertion is to reduce the degree of divergence and render the diagram UV finite.

[11] As discussed in Section 6.5.1, Lorentz violation may also contribute via non-minimal couplings.

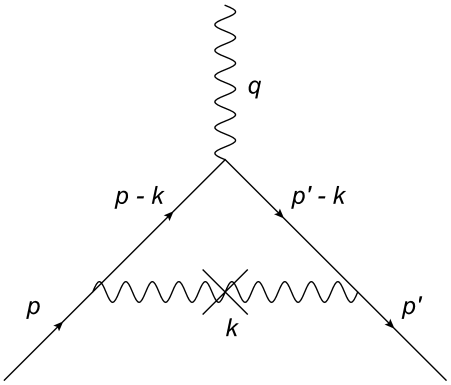

Figure 7.1: Vertex structure and momenta attributions; the cross indicates the vertex insertion.

Since the integral in eq.(7.34) is finite in $3+1$ dimensions, there is no need to regularize it and we directly evaluate the vertex correction as

$$\Lambda_\mu(p,p') = -\frac{ie^2}{64\pi^2 m_\ell^2}\epsilon^{\nu\alpha\beta\rho}\left(k_{\rm AF}\right)_\alpha T_{\beta\nu\mu\rho}(p,p') \tag{7.35}$$

with $T_{\beta\nu\mu\rho}$ involving products of up to five gamma matrices. We do not give its expressions here, as it is not much enlightening. The vertex $\Lambda_\mu(p,p')$ is the LSV contribution to d_ℓ we look for, but, in order to extract it, we need to obtain the corresponding form factor.

The electromagnetic current can be decomposed as $\langle p'|J^\mu_{\rm em}|p\rangle = i\frac{\sigma^{\mu\nu}\gamma_5}{2m_\ell}q_\nu F_{\rm edm}(q^2)+\cdots$, where $F_{\rm edm}(q^2)$ is the desired form factor and the ellipsis denotes the other Lorentz structures and their respective form factors, which are not of interest here [340]. Above $q = p - p'$ is the momentum transfer. As stated in Section 7.1, in this chapter (and in [70]) we consider only the LSV effects in the photon sector, so no other form factor other than $F_{\rm edm}(q^2)$ is relevant, as the free Dirac equation remains unaltered. The vertex function $\Lambda_\mu(p,p')$ plays the role of a LSV correction to the usual electromagnetic current and our task is to extract $F_{\rm edm}(q^2)$ and read the ℓEDM, which is then given by $d_\ell = -F_{\rm edm}(q^2=0)/2m_\ell$.

Obtaining $F_{\rm edm}(q^2)$ is cumbersome due to the complicated form of $\Lambda_\mu(p,p')$, or rather, of $T_{\beta\nu\mu\rho}(p,p')$. It is nevertheless possible to simplify matters by applying an appropriate projector [341]

$$\mathcal{P}^\mu_{\rm edm} = \frac{m_\ell\,(p+p')^\mu}{q^4 - 4m_\ell^2 q^2}\left[\left(\not{p}+m_\ell\right)\gamma_5\left(\not{p}'+m_\ell\right)\right], \tag{7.36}$$

which automatically selects the form factor we want. The projector above acts on $\Lambda_\mu(p,p')$ and we obtain $F_{\rm edm}(q^2) = {\rm Tr}\left[\Lambda_\mu\mathcal{P}^\mu_{\rm edm}\right]$, with the trace evaluated for external

(on-shell) leptons, i.e., $p^2 = p'^2 = m_\ell^2$ and $p \cdot p' = m_\ell^2 - q^2/2$. It is convenient to leave $q^2 \neq 0$ in order to extract the finite contributions from the trace above in the limit of massless photons. This task may be performed in an automated fashion with the Package-X [342], and the form factor is found to be:

$$F_{\rm edm}(q^2 = 0) = -\frac{e^2}{12\pi^2 m_\ell^2} q \cdot k_{\rm AF} + \text{IR}, \tag{7.37}$$

where IR indicates infra-red terms and $q = p - p'$.

Such divergences appear as $1/x$ factors in the Feynman integrals ($x \to 0$) due to $m_\gamma = 0$ and as $1/q^2$ factors in the traces. The appearance of the latter may be interpreted as follows. We are considering the CFJ correction as a true vertex [330, 331] and not using the complete photon propagator – this is essentially equivalent to taking only the lowest-order term in $|\mathbf{k}_{\rm AF}|/|\mathbf{q}|$ in the expansion of the complete propagator. However, the loop integration does not contemplate only high momenta, but also regions where $|\mathbf{k}_{\rm AF}|/|\mathbf{q}| \ll 1$ may not be fulfilled. We therefore expect these divergences to vanish upon using the complete LSV-modified propagator.

Finally, by using the definition of the EDM in terms of the associated form factor, $d_\ell = -F_{\rm edm}(q^2 = 0)/2m_\ell$, we find

$$d_\ell = \frac{\alpha}{6\pi m_\ell^3} \left(q \cdot k_{\rm AF}\right), \tag{7.38}$$

which shows that the LSV-induced ℓEDM is momentum dependent. A similar effect was found in Ref. [343] for a different sector of the SME, but with a quadratic momentum dependence[12].

It is interesting to note, though not surprising, that, in a spacetime with a non-dynamic background, the spin is not the only vector available to support the electric (or magnetic) moment of an elementary particle. Furthermore, in order to build the scalar d_ℓ we need another vector, and the only possibilities are p and p' or, in our case, the special combination given by $q = p - p'$. This may be interpreted in terms of an interplay between the background and the external electromagnetic field, which carries the momentum transfer q, so that, together, they produce a non-zero ℓEDM, i.e., induce an asymmetry in the charge distribution of the lepton.

We note, however, that the form of the ℓEDM as given by eq.(7.38) is not helpful from the experimental point of view: for an elastic interaction ($q^0 \approx 0$) with $|\mathbf{q}|^2 \ll m_\ell^2$ we have $d_\ell \sim 0$. Besides this, two aspects are relevant here: the nature of the measurements (e.g. as performed by ACME [60]) and its time scale.

[12]Incidentally, in their case, this quadratic dependence means that their result can be applied also in circular geometries without the problems reported below.

Let us first decompose the (say) initial momentum of the electron as $\mathbf{p} = \mathbf{p}_{\rm m} + \mathbf{p}_{\rm s}$, where $\mathbf{p}_{\rm m,s}$ denote the components of the momentum relative to the molecule and the SCF, respectively. The first aspect is connected with the form of $d_\ell \sim \mathbf{p}\cdot\mathbf{k}_{\rm AF}$ and the fact that ACME's measurements were performed with (ThO) molecules, around which the electrons quickly revolve. Being bound to it, their momenta are also limited and, over time, average to zero, i.e., $\langle \mathbf{p}_m \rangle = 0$. Similar arguments would apply for "free" relativistic leptons in storage rings [344, 345]. This brings us to the second point.

Since $\mathbf{p}_{\rm m}$ does not contribute, one should consider the general motion of Earth and the experiment attached to it relative to the SCF (cf. Section 6.4). The data from ACME's latest result was taken during $\sim$ 10 days, but these were spread over months, and their analysis was not sensitive to such possible long-term time modulations. The momentum of the laboratory relative to the SCF is $\mathbf{p}_{\rm s} \sim \boldsymbol{\beta}$, with the boost factor $\boldsymbol{\beta}$ given in Section 6.4, where it becomes clear that all components of $\mathbf{p}_{\rm s}$ are periodic functions of time. Therefore, the time-averaged LSV effects $\sim \langle\boldsymbol{\beta}\rangle$ also vanish and the application of the upper limit on the eEDM as a means to constrain the space-like LSV parameters is not possible[13].

In any case, in a speculative note, if we *could* use the bound on the LSV parameter given in Ref. [58], $k_{\rm AF} \sim 10^{-43}\,$GeV, the energy (or momentum) necessary to reach the upper limit of $|d_e^{\rm exp}|$ would be $\sim 10^{21}\,$GeV. This indicates that the CFJ contribution to the eEDM would only be sensible for extreme energies, around the Planck scale, $E_{\rm Pl} \simeq 10^{19}\,$GeV, therefore remaining out of experimental reach for the foreseeable future. This suggests that the CFJ model induces only very small effects – too small perhaps – and is, therefore, not responsible for a finite eEDM, should one be eventually found.

7.4 Resonant cavities

As we have seen in Section 7.1, adding eq.(7.1) to the usual Maxwell kinetic term, $-\frac{1}{4}F_{\mu\nu}F^{\mu\nu}$, gives us a LSV-modified electrodynamics where a constant vector selects a preferred direction in spacetime. Also in Section 7.1 we discussed the ensuing Maxwell equations and, by analysing the equations of motion for the electric field we could read off the modified dispersion relations, cf. eqs.(7.15) and (7.17). We also discussed the fact that time-like backgrounds are not satisfactory, so we keep working with the pure space-like case.

[13] I am very thankful to V.A. Kostelecký, E. West and B. O'Leary, the last two are members of the ACME experiment, for bringing these arguments to my attention.

Due to the degree of the polynomial (7.14) we find that there is not only one, but two propagation modes[14], which depend on the form of $k_{\rm AF}$ (if this goes to zero we recover the usual results). This can be seen if we remember that the CFJ electrodynamics is linear, i.e., no factors of $\mathbf{E}^2$ or higher appear in the equations of motion, thus implying that the superposition principle still holds for the solutions of the wave equation.

A general solution can be written in terms of a linear combination of plane waves, each with a different energy, ω_+ or ω_-:

$$\mathbf{E}(x,t) = \left[\mathcal{E}_+\hat{\mathbf{e}}_+ e^{-i\omega_+ t} + \mathcal{E}_-\hat{\mathbf{e}}_- e^{-i\omega_- t}\right] e^{ipx}, \tag{7.39}$$

where $\mathcal{E}_\pm$ are complex amplitudes and $\hat{\mathbf{e}}_\pm$ are unit vectors. The energies are approximately given by (cf. eq.(7.17))

$$\omega_\pm = |\mathbf{p}| \pm |\mathbf{k}_{\rm AF}|\cos\psi + \mathcal{O}(|\mathbf{k}_{\rm AF}|^2/|\mathbf{p}|^2) \tag{7.40}$$

with $\cos\psi = \mathbf{p}\cdot\mathbf{k}_{\rm AF}/|\mathbf{p}||\mathbf{k}_{\rm AF}|$. This means that, due to the $\pm$ signs, the two modes propagate with different phase velocities and, more interestingly, that the polarization plane is rotated by an amount $\Delta \simeq (\mathbf{k}_{\rm AF})^x_{\rm lab} L\cos\psi$ after travelling a length L [311] (assuming that the experiment lies in the xy plane in the reference frame of the lab and remembering that the y-component vanishes).

A similar effect, Faraday rotation, is observed whenever a linearly polarized wave passes through a dielectric exposed to an external magnetic field (aligned with the wave vector). Incidentally, if we express $\mathbf{E}$ and $\mathbf{B}$ in terms of the scalar and vector potentials, ϕ and $\mathbf{A}$, in the RHS of eqs.(7.8) and (7.11), we arrive at LSV-modified Maxwell equations which are formally identical to its Lorentz-preserving counterpart in a dielectric medium, but here $\mathbf{P}\sim\mathbf{k}_{\rm AF}\times\mathbf{A}$ and $\mathbf{M}\sim\phi\,\mathbf{k}_{\rm AF}$ play the role of the polarization and magnetization, respectively [287, 311].

Experiments such as PVLAS [61] use low-loss resonant cavities to search for the electromagnetic properties of the vacuum – be it from non-linear QED effects [346, 347] or new physics (ALPs, hidden photons, etc) – with intense lasers, and are very sensitive to rotations in polarization. Inside the cavity the laser swings back and forth and, at every reflection its propagation is reversed. The space-like LSV background, however, remains fixed, so that $\cos\psi\to-\cos\psi$, i.e., the net rotation before and after reflection cancels on average. Therefore, we use just one pass.

[14]Here we mean that a propagation mode is defined by the dispersion relations. In the simpler pure Maxwell case, we have $\omega^2=\mathbf{p}^2$, so that the propagation mode has energy $\omega(\mathbf{p})=|\mathbf{p}|$ and the plane-wave solutions are built from $\mathbf{E}\sim\hat{\mathbf{e}}_{\perp\,\mathbf{p}}\exp\left[i\left(\omega(\mathbf{p})t-\mathbf{p}\cdot\mathbf{r}\right)\right]$. Here we imagine a complex vector and, for practical calculation, we take its real part.

Resonant cavities are usually designed to allow for the largest number possible of reflections (passes), therefore amplifying the effective length covered by the laser. These induce rotations in the polarization that may overshadow our LSV signal given by $\Delta \simeq (\mathbf{k}_{\rm AF})^x_{\rm lab}\, L \cos\psi$. In fact, since no BSM signal has been claimed from the latest results from PVLAS [61], we may assume that the LSV signal (rotation) lies below the expected background[15] $b_{\rm exp} \sim 5 \times 10^{-7}$.

With this assumption we may estimate that the LSV parameters in terms of the time-averaged SCF variable $(k_{\rm AF})^Z_{\rm SCF}$, cf. Section 7.1, fulfill $\Delta < b_{\rm exp}$, which can be turned into the upper bound $(k_{\rm AF})^Z_{\rm SCF} \lesssim \frac{b_{\rm exp}}{L_1 \cos\psi}$. Here we must use just one pass[16], so $L = L_1 = 1.6$ m, and we assume $\cos\psi \sim 0.1$. With this we find

$$(k_{\rm AF})^Z_{\rm SCF} \lesssim 6 \times 10^{-22}\,{\rm GeV}. \tag{7.41}$$

We note that more precise measurements and larger L_1 from e.g. the BMV experiment [349] could potentially improve this upper limit and, hopefully, eventually supersede the astrophysical bounds [58, 311].

As discussed in Section 7.1, a time-like background brings theoretical difficulties; this is the reason why we assumed $(k_{\rm AF})^T_{\rm SCF} \equiv 0$ so far. However, if we insist on considering this possibility, we might be able to find a stringent bound on it. We work in the same approximation level as with the space-like components, i.e., we neglect effects of order $\beta \lesssim 10^{-4}$, so that $(k_{\rm AF})^0_{\rm lab} = (k_{\rm AF})^T_{\rm SCF} + \mathcal{O}(\beta)$ – here the $\mathcal{O}(\beta)$ contributions are all time-dependent and are effectively washed away after time averaging.

Working out the dispersion relation, eq.(7.14), for this specific case, we find that the two frequency modes induce a rotation in the polarization given by $\Delta \simeq (k_{\rm AF})^0_{\rm lab}\, L$. This rotation does not depend on the projection of the linear momentum onto the (space-like) background, so there is no cancellation upon reflection and we may use $L = N \times L_1$, with $N \approx 4.4 \times 10^5$ passes. We may then estimate that $(k_{\rm AF})^T_{\rm SCF} \lesssim \frac{b_{\rm exp}}{N \times L_1}$, which leads to the following upper limit on a pure time-like LSV background:

$$(k_{\rm AF})^T_{\rm SCF} \lesssim 1 \times 10^{-27}\,{\rm GeV}, \tag{7.42}$$

which supports the theoretical indications that $(k_{\rm AF})^T$ should be either exactly zero or extremely small [293, 311, 324, 326].

[15] This is roughly read off from Fig. 7 in Ref. [61] at zero frequency (this is a "naked-eye" estimate, since it might be that this particular point is not so accurately depicted as in older versions of the experiment [348]). The zero-frequency requirement is sensible, since Earth's typical rotational and/or orbital frequencies are $\lesssim 10^{-4}$.

[16] $L_1 = 1.6\,{\rm m} = 8.1 \times 10^{15}\,{\rm GeV}^{-1}$.

7.5 Partial conclusions

In this chapter we have studied a modification of standard QED proposed by Carroll, Field and Jackiw, eq.(7.1), in a few contexts: the interaction potential between spin-1/2 fermions and the associated quantum-mechanical corrections to the spectrum of the hydrogen atom, the electric dipole moment of charged leptons, as well as an application to resonant cavities, which incidentally provided the best upper bound on the LSV parameters. The bounds obtained are far less strict than those of Ref. [311] and those listed in Ref. [58], but contrary to them, ours were extracted from local phenomena and experiments, therefore not depending upon astrophysical observations over cosmological distance scales.

Our study of the interparticle potential mediated by the LSV-modified propagator led us to spin-dependent interactions which could interfere with the dominant Coulomb and gravitational forces between (un)polarized charged macroscopic objects. Next, we applied $\delta V_{\rm C}(r)$ as a time-independent quantum-mechanical perturbation to the hydrogen atom, obtaining $\Delta E^{\rm H}_{\rm LSV}$, eq.(7.31), as a correction to the fine structure of the energy spectrum. No deviation of the expected spectrum is seen, so we may impose that the CFJ corrections be smaller than the associated experimental uncertainties, thus leading to the upper bound $(k_{\rm AF})^{Z}_{\rm SCF} \lesssim 2 \times 10^{-19}\,{\rm GeV}$ [70].

The background-dependent correction $\delta V^{\rm H}_{\rm C}(r)$, eq.(7.24), produces not only energy shifts in the spectrum, but may also induce changes in the (free) wave functions themselves. Such perturbed states ($|\psi^1\rangle$) could give rise to other interesting effects, such as the generation of atomic electric dipole moments, $\langle\psi^1|e\mathbf{R}|\psi^1\rangle$, as well as induce non-zero quadrupole moments in the otherwise spherically symmetric ground state of the hydrogen atom [350, 351].

In Section 7.3 we found that the background 4-vector may serve as support for a non-zero ℓEDM, which is also explicitly momentum-dependent, see eq.(7.38). However, due to the dependence of d_ℓ on $q = p - p'$ and the experimental techniques used to measure it, we have seen that the CFJ-induced EDM cannot be easily constrained. For this reason we were unable to set upper bounds.

Finally, from the non-observation of an LSV-induced polarization rotation in vacuum analogous to Faraday rotations we found $(k_{\rm AF})^{Z}_{\rm SCF} \lesssim 6 \times 10^{-22}\,{\rm GeV}$ [70]. We have not gone in the details of the cavity design, but rather outlined a general estimate. A closer analysis of the cavity operation and geometry would be able to refine it further and our discussion indicates that this is a promising way to study not only non-linear properties of the QED vacuum or new beyond the Standard Model particles, but also Lorentz violation and its induced effects on the electromagnetic vacuum [353].

Furthermore, we would like to note that the extrapolation made at the end of Section 7.4 to obtain eq.(7.42) could also be applied to the results in Section 7.2, but the limits on the time-component of the background would be essentially of the same order of magnitude as the one for the spatial components (cf. eq.(7.32)). For this reason we refrain from re-doing the calculation explicitly for this case[17]. As a final remark we would like to indicate that the results obtained in this chapter (following Ref. [70]) have been added to the Data Tables, Table D13, edited by Kostelecký and Russel [58] in its 2017 update (v10 on arXiv).

The content and results of this chapter stem from the cited references, parts of my own published work [70] – in collaboration with Yuri Gomes – and original independent modifications thereof. I have done most of the writing and calculational work (I am the first author) in Ref. [70]. I am thankful to Gustavo Pazzini de Brito for the discussion around Section 7.1.

[17] Also, the conclusions in Section 7.3 would not change by assuming a non-zero time-like component as we are in a regime where $q^0 \approx 0$, so we would still be unable to apply the experimental limits.

Chapter 8

Lorentz violation in simple QED processes

This chapter is based upon the published work "Lorentz violation in simple QED processes" [71] whose content has been significantly expanded to help clarify the discussion. This work was done in collaboration with G.P. de Brito, C. Marques, D. Kroff and J.T Guaitolini Jr, and I have done most of the writing, while the calculational work was equally shared (I am the first author).

8.1 Introduction

In Chapter 6 we have discussed the Standard Model extension (SME) and, in particular, the LSV extension of one-lepton QED. We saw that such an extension is made out of basically three sectors dealing with only leptons, only photons and lepton-photon interactions. The last one is the focus of this chapter, which is based upon my own published work [71] with some parts expanded for the sake of clarity and completeness.

An interesting way to introduce Lorentz violation in the otherwise Lorentz-preserving QED is to modify the electron-photon vertex directly. This can be done in a gauge-invariant way by coupling a constant, i.e., spacetime-independent, 4-vector background ξ^μ with the usual field-strength tensor $F_{\mu\nu}$. This derivative coupling would therefore modify the standard QED Lagrangian, which now reads

$$\mathcal{L} = -\frac{1}{4}F_{\mu\nu}^2 + \bar{\psi}(i\gamma^\mu\partial_\mu - eA_\mu\gamma^\mu - m)\psi + \xi^\mu\bar{\psi}\gamma^\nu\psi F_{\mu\nu}, \tag{8.1}$$

where m and e are the electron's mass and electric charge, respectively. We omit the gauge-fixing term here, since we are dealing with conserved external currents.

The LSV background ξ is a non-minimal coupling (in the sense discussed in Section 6.5.1) with canonical dimensions of inverse mass. This LSV scenario has been proposed in Ref. [305] in the context of topological phases[1] and represents a very simple gauge-invariant non-minimal coupling possibility. Given that ξ is fixed, it plays the role of a non-dynamical background and Lorentz symmetry is broken, as it selects a preferred direction in spacetime.

It is easy to see that this LSV interaction acts as a non-minimal coupling changing the usual covariant derivative to $D_\mu = \partial_\mu + ieA_\mu + i\xi^\nu F_{\mu\nu}$. Due to $F_{\mu\nu}$, the extra term is clearly gauge invariant. This CPT-even modification affects all electron-photon interactions already at tree level and similar derivative non-minimal couplings have also been proposed in several instances: quantum mechanics and the hydrogen atom [354], magnetic and electric dipole moments of various systems [334, 355] and scattering processes [356].

Here we will focus on the latter and discuss the impact of the last term in eq.(8.1) in a few simple QED reactions, namely: Compton and Bhabha scatterings, electron-positron annihilation and the life time of para-positronium. For simplicity, in the following we will only keep terms in the squared amplitudes – and consequently also in the differential cross sections and decay rates – up to leading order in the LSV parameter, which is taken as small (relative to the mass of the electron). This is a good level of approximation, once LSV effects have not been conclusively observed, so it is expected that the associated parameters are very small. Also, as can be seen from the mass dimension of the LSV 4-vector, $[\xi] = \text{mass}^{-1}$, we are considering a dimension-5 operator, and we shall restrict our analysis to tree-level processes, where we can ignore renormalizability-related issues; see Section 6.5.1.

Scattering processes have also been considered in detail in Ref. [297], where the authors find that, due to modifications in the propagators (already at tree level), linear momentum and velocity may be misaligned (cf. Section 6.5.1), therefore making the task of computing cross sections trickier. In this chapter (and in Ref. [71]) we evade this issue, as eq.(8.1) only affects the electron-photon interaction, whereas the bare propagators are left intact[2]. Possible modifications may nevertheless arise at the quantum level, though. This issue is very interesting, but lies outside of our scope, so for the rest of this chapter we consider eq.(8.1) as the one and only source of LSV.

[1] Looking at the Dirac equation following from eq.(8.1) we see that this term would modify the canonical momentum, thus introducing a LSV contribution to the Aharonov-Bohm and Aharonov-Casher effects involving charged particles. Most interesting is the possibility that a neutral particle subject to a similar coupling displays such topological phase effects, as mentioned in Section 6.5 (see also e.g. Ref. [305]).

[2] I am thankful to V.A. Kostelecký for pointing this out in a private communication.

The 4-vector ξ plays the role of a fixed background and it can be conveniently decomposed in spherical coordinates, with the axes adequately chosen according to the process of interest. The polar (θ_ξ) and azimuthal (ϕ_ξ) angles are fixed relative to the experimental set-up at a given time[3] and, as will become clear in the following, the extra momentum factor introduced by the LSV non-minimal coupling will produce terms proportional to $\xi \cdot p_i$, where p_i are the momenta of the in-coming and/or outgoing particles.

These momentum-dependent terms will be responsible for new angle and energy profiles for the cross sections of the reactions considered here. An interesting point is that the experiments cannot be built so that they are particularly symmetric relative to the LSV background, meaning that the latter will induce the breaking of rotational symmetry. This will manifest itself most visibly through the dependence of some cross sections on the azimuthal angle – something that is not quite expected when the target is point like[4]. This non-standard feature acts as a LSV signature to be searched for experimentally.

The LSV-modified Lagrangian, eq.(8.1), translates into an extension of the usual QED $ee\gamma$ vertex, namely

$$i\Gamma^\mu = ie\gamma^\mu + \not{q}\,\xi^\mu - (\xi \cdot q)\gamma^\mu, \tag{8.2}$$

with q representing the 4-momentum carried by the photon line, conventioned as being positive (negative) for in-coming (outgoing) photons. In Fig. 8.1 below we present the generic s-, t- and u-channel tree-level Feynman diagrams that contribute to the processes we consider. The blob indicates the modified vertex, eq.(8.2). For Bhabha and Compton scatterings only the s- and t-channels play a role, whereas for electron-positron annihilation only the t- and u-channels contribute.

Our goal is to obtain the modifications brought up by the LSV piece of the new vertex and, through experimental limits on deviations from the Lorentz-preserving QED, establish upper bounds on the components of ξ. The LSV parameters associated with other similar derivative non-minimal couplings (e.g. involving the dual field-strength tensor) have been constrained to be $\lesssim 10^{-3}\,\mathrm{GeV}^{-1}$ [356], and we shall extract limits of similar magnitude from Bhabha scattering and unpolarized electron-positron annihilation, while the bounds from para-positronium are somewhat looser.

[3] See discussion in Section 6.4 and below.

[4] In the sense that, if the target has some spatial structure, it might be that the scattering depends on the azimuthal angle. In our case there is no internal structure asigned to the targets, but the interaction itself is angle-dependent and this will be transferred to the cross sections.

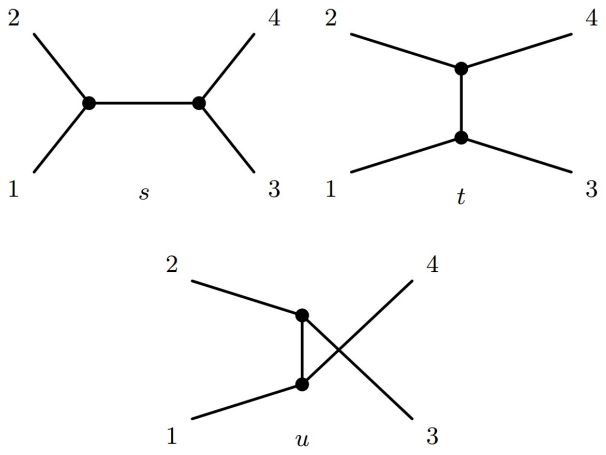

Figure 8.1: Feynman diagrams contributing to the processes considered and associated Mandelstam variables. The blob represents the effective vertex, eq.(8.2).

A practical comment is important here: the background ξ is assumed to be fixed in spacetime. This is explicit only in an approximately inertial reference frame, e.g. the SCF [286]; in comparison, Earth is not "inertial enough" due to its sidereal and orbital motions. Consequently, in Earth-bound experiments the LSV observables should display time modulations. Since experiments are not performed entirely during small fractions of a single day, but over periods of days spread over months or years, the experimental signals would effectively give information on the time-averaged LSV parameters.

To discuss the time dependence it is necessary to express the laboratory-frame components $\xi^\mu = \xi^\mu_{\rm lab}$ in terms of the components $\xi^\mu_{\rm SCF}$, which are static in the SCF. Following Refs. [58, 286] and Section 6.4, we find that, up to $\mathcal{O}(\beta)$, Earth's orbital velocity $\sim 10^{-4}$,

$$\xi^0_{\rm lab} = \xi^T_{\rm SCF} + \mathcal{O}(\beta) \tag{8.3}$$

$$\xi^i_{\rm lab} = R^{iJ}(\chi, T)\xi^J_{\rm SCF} + \mathcal{O}(\beta), \tag{8.4}$$

where $R^{iJ}(\chi, T)$ is the rotation matrix given in eq.(6.10). These expressions clearly display the time-dependent nature of the background 4-vector – specially its spatial part – in the Earth-bound reference frame.

In the context of the approximations above, the time components are easily factored out from the squared amplitudes. This is not so simple for the spatial components, which involve a time-dependent rotation matrix. As one of our goals is to place bounds on the LSV parameters, we need to compare our results with the experimental ones (or rather, their uncertainties). Also, due to the periodic motions

of the Earth, we must include the time-averaging procedure in our computations. This is a trivial task for the time components, as – within our approximations – they are identical in both frames.

On the other hand, the space components in the laboratory frame always come together with the time average of some rotation (actually, of this squared). This yields a cumbersome expression which is not easily readable or even converted into a practical (or useful) bound. Therefore we only explicitly present the limits on the time components of the background. The corresponding limits on combinations of the space components should be about the same order of magnitude as the ones for the time components, as we do not expect the time averaging to be strongly suppressive. In what follows we state the results with coefficients expressed in the Earth frame and in Section 8.5 we translate them to the SCF variables.

This chapter is organized as follows: in Section 8.2 and 8.3 we present and discuss the LSV-modified Compton and Bhabha scatterings, respectively, while in Section 8.4 we analyse the unpolarized electron-positron annihilation in two photons. We also used the life time of para-positronium to find an upper limit on the LSV parameters. In Section 8.5 we present our concluding remarks. In our calculations we have used the Package-X [342] to automatically evaluate the traces and contractions from the averaging procedure. We use natural units ($c = \hbar = 1$) throughout and the fine structure constant is $\alpha = e^2/4\pi \simeq 1/137$.

8.2 Compton scattering

As a preliminary examination of the effect of the modified vertex we consider Compton scattering, i.e., the process by which radiation of energy ω is scattered by a free electron (assumed to be at rest). The final outgoing photons are emitted with a different energy $\omega' \leq \omega$ at an angle θ and, due to 4-momentum conservation, we find that the initial and final photon energies are related via

$$\frac{\omega'}{\omega} = \left[1 + \frac{\omega}{m}(1 - \cos\theta)\right]^{-1}, \tag{8.5}$$

which is the well-known Compton frequency shift. In this section we will focus on two opposite energy regimes: $\omega \ll m$ and $\omega \gg m$. In the former, the process is elastic, i.e., $\omega' \simeq \omega$, while in the latter the Compton formula gives $\omega' \simeq m(1 - \cos\theta)^{-1}$.

It is interesting to notice that this result is not modified by the kind of LSV scenario we are considering here and it only depends on the polar angle θ. Modifications of this formula do arise when LSV in the pure lepton part is introduced, as this

forces a correction to the dispersion relations (cf. Section 6.5.1). The consequence is that the on-shell condition $p^2 = m^2$, which is central to the calculation leading to eq.(8.5), is modified and the energy of the outgoing photon is not the same as above [297].

In QED, the electron-photon scattering, $e^-(p_1) + \gamma(p_2) \to \gamma(p_3) + e^-(p_4)$, is represented by the s- and t-channel diagrams in Fig. 8.1. This process was first studied by Klein and Nishima [357] and was one of the first applications of the then new Dirac quantum mechanics. The unpolarized differential cross section is

$$\frac{d\sigma^{e\gamma}_{\rm QED}}{d\Omega} = \frac{\alpha^2}{2m^2}\left(\frac{\omega'}{\omega}\right)^2\left[\frac{\omega'}{\omega} + \frac{\omega}{\omega'} - \sin^2\theta\right], \tag{8.6}$$

whose low-energy limit reproduces the classical Thomson scattering differential cross section $\sim (1 + \cos^2\theta)$, which is energy independent. One must note that, as mentioned above, both Compton and Thomson results are dependent on the polar angle θ, but not on the azimuthal angle ϕ. This reflects, to some extent, the fact that the scattering center is symmetrical and that the interaction *per se* does not introduce extra anisotropies.

We wish to determine the effect of $i\Gamma^\mu$ to the scattering of radiation off static free electrons. The total amplitude for this process may be decomposed in two pieces, a pure QED piece and a LSV one, $\mathcal{M}_{\rm tot} = \mathcal{M}_{\rm QED} + \mathcal{M}_\xi$. Here we will work with unpolarized electrons and photons in the laboratory reference frame, with the electron initially at rest. In this particular frame, the initial momenta of the electron and photon are $p_1 = m(1,0,0,0)$ and $p_2 = \omega(1,0,0,1)$, whereas their final momenta are $p_3 = \omega'(1, \sin\theta\cos\phi, \sin\theta\sin\phi, \cos\theta)$ and $p_4 = p_1 + p_2 - p_3$.

The deviation from the Klein-Nishima result is determined by $\langle|\mathcal{M}_{\rm LSV}|^2\rangle = \langle\mathcal{M}_{\rm QED}\mathcal{M}^*_\xi\rangle + \langle\mathcal{M}^*_{\rm QED}\mathcal{M}_\xi\rangle + \langle|\mathcal{M}_\xi|^2\rangle$, where, henceforth $\langle\cdots\rangle$ indicates average over spins and polarizations[5]. Here $\mathcal{M}_\xi$ contains, in principle, terms of first and second order in the background coming from the insertion of $i\Gamma^\mu$ in one or two of the vertices in the s- and t-diagrams in Fig. 8.1 – there are six such diagrams with LSV vertices and two without (these compose $\mathcal{M}_{\rm QED}$). Given that the background is expected to be small (relative to m), we shall only keep terms in $\langle|\mathcal{M}_{\rm LSV}|^2\rangle$ up to $\mathcal{O}(\xi^2)$, which turns out to be the leading order, as part of the QED-LSV interference terms – the ones of $\mathcal{O}(\xi)$ – are purely imaginary, thus cancelling automatically.

[5]Again, the LSV scenario we are working with creates no new complication in the averaging process, as the completeness relations for spinors and polarization vectors are not affected.

The unpolarized LSV-modified Klein-Nishima formula is then given by

$$\frac{d\sigma^{e\gamma}_{\text{LSV}}}{d\Omega} = \frac{\alpha}{8\pi m^2}[(\xi\cdot p_2)^2 + (\xi\cdot p_3)^2]\left(\frac{\omega'}{\omega}\right)^2\left[\frac{\omega'}{\omega} + \frac{\omega}{\omega'} - \sin^2\theta\right] \tag{8.7}$$

and we notice that, incidentally, this result shares great similarity with its Lorentz-preserving counterpart, eq.(8.6). Since $(\xi\cdot p_2)^2 \simeq \omega^2$ and $(\xi\cdot p_3)^2 \simeq \omega'^2$, the LSV Klein-Nishima formula, eq.(8.7), can be distinguished from the standard one, eq.(8.6), not only by its angular dependence, but also through the energy dependence of its profile.

The general energy behavior of eq.(8.7) is interesting: if we define $x = \omega/m$ and $\mathcal{P}(x,\theta) = 1 + x(1-\cos\theta)$, we may rewrite the LSV-modified Klein-Nishima formula as (cf. eq.(8.5))

$$\frac{d\sigma^{e\gamma}_{\text{LSV}}}{d\Omega} = \frac{\alpha\tilde{\xi}^2}{8\pi}\frac{x^2}{\mathcal{P}(x,\theta)^2}\left[1+\mathcal{P}(x,\theta)^{-2}\right]\left[\mathcal{P}(x,\theta) + \frac{1}{\mathcal{P}(x,\theta)} - \sin^2\theta\right], \tag{8.8}$$

with $\tilde{\xi}^2$ containing the dimensionless angular factors from $(\xi\cdot p_2)^2 + (\xi\cdot p_3)^2$. The extra x^2 energy factor in the numerator owes its presence to the electromagnetic field-strength tensor in the LSV non-minimal coupling.

For low-frequency incident radiation ($x \ll 1$) we notice that $\mathcal{P}(x,\theta) \to 1$, so that, apart from trigonometric functions, $\frac{d\sigma^{e\gamma}_{\text{LSV}}}{d\Omega} \sim x^2$. This means that, relative to the standard Thomson result, the low-energy limit of the LSV differential cross section is generally strongly suppressed, thus compromising any hope of experimental verification in this energy regime.

On the other extreme of the spectrum, for high frequencies ($x \gg 1$), we have $\mathcal{P}(x,\theta) \to x$, modulo angular factors, so that $\mathcal{P}(x,\theta)^{-1} \sim 0$ while $x\mathcal{P}(x,\theta)^{-1} \sim 1$. With this we find a linear energy dependence, $\frac{d\sigma^{e\gamma}_{\text{LSV}}}{d\Omega} \sim x$, and we conclude that the LSV-induced modifications are actually amplified in the high-energy regime. It is worthwhile mentioning that the corresponding limit of the usual Klein-Nishima formula (for not too small scattering angles) is found to be $\frac{d\sigma^{e\gamma}_{\text{QED}}}{d\Omega} \sim x^{-1}$, i.e., classically the electron is not a good scattering target for highly energetic incident photons. This is clearly contrasting with our LSV results, whose signal may be optimally distinguished from those of standard QED at increasing energies.

As stated above, we are interested in determining the angular profiles emerging in the low- and high-energy limits. Let us then start with the first, where we may assume that the electron is a fixed target and the photon bounces off elastically, i.e., $\omega' \simeq \omega$. To proceed we need to specify the nature of the background and evaluate eq.(8.7) accordingly, so we choose to start with $\xi^\mu = (\xi^0, 0)$. In this scenario all

angular information contained in $\xi\cdot p_2$ and $\xi\cdot p_3$ is lost and $(\xi\cdot p_2)^2+(\xi\cdot p_3)^2 \to 2\xi_0^2\omega^2$. The LSV differential cross section becomes

$$\frac{d\sigma^{e\gamma,\,\xi_0}_{\text{LSV}}}{d\Omega} = \frac{\alpha\xi_0^2}{4\pi}\left(\frac{\omega}{m}\right)^2\left[1+\cos^2\theta\right], \tag{8.9}$$

whose angular profile is the same as in the classical Thomson result. Numerically, however, this differential cross section is heavily suppressed relative to the QED one not only via the small background, but also through the extra $(\omega/m)^2$ factor.

We consider next the case of a space-like background $\xi^\mu = (0, \boldsymbol{\xi})$, for which we expect stronger angular dependence relative to the QED case. For simplicity, we consider two physically interesting scenarios, namely, $\boldsymbol{\xi} \parallel \hat{\mathbf{z}}$ and $\boldsymbol{\xi} \perp \hat{\mathbf{z}}$. The first case corresponds to a background aligned with the direction of propagation of the incident photon, while the second is lying in the plane transverse to it. For $\boldsymbol{\xi} \parallel \hat{\mathbf{z}}$, i.e., $\theta_\xi = 0$, there is no azimuthal dependence, but an additional $(1+\cos^2\theta)$ factor is found:

$$\frac{d\sigma^{e\gamma,\,\parallel}_{\text{LSV}}}{d\Omega} = \frac{\alpha|\boldsymbol{\xi}|^2}{8\pi}\left(\frac{\omega}{m}\right)^2\left[1+\cos^2\theta\right]^2. \tag{8.10}$$

More interesting is the second scenario: a transverse background with $(\xi\cdot p_2)^2 = 0$ and $(\xi\cdot p_3)^2 = |\boldsymbol{\xi}|^2\omega^2\sin^2\theta\cos^2(\phi-\phi_\xi)$, showing that, in these circumstances, a distinctive azimuthal signature appears. The differential cross section is

$$\frac{d\sigma^{e\gamma,\,\perp}_{\text{LSV}}}{d\Omega} = \frac{\alpha|\boldsymbol{\xi}|^2}{8\pi}\left(\frac{\omega}{m}\right)^2\sin^2\theta\cos^2(\phi-\phi_\xi)\left[1+\cos^2\theta\right], \tag{8.11}$$

whose instantaneous angular profile is plotted in Fig. 8.2 for different relative orientations of the background in the transverse xy-plane. It becomes clear that, given the time-dependent character of the background (i.e., $\phi_\xi = \phi_\xi(T)$), the shape of the differential cross section seems to "walk" as time goes by, thus revealing the instantaneous effects of sidereal and orbital motions on the physical observable (here the differential cross section).

Now we turn to the high-energy regime, $\omega \gg m$. As pointed out in the beginning of this section, the Compton formula indicates that ω' is approximately ω-independent and $\left(\frac{\omega'}{\omega}\right)^2\left[\frac{\omega'}{\omega}+\frac{\omega}{\omega'}-\sin^2\theta\right] \simeq \frac{m}{\omega(1-\cos\theta)}$ in such a way that the differential cross section becomes

$$\frac{d\sigma^{e\gamma}_{\text{QED}}}{d\Omega} = \frac{\alpha^2}{2m\omega}\left(1-\cos\theta\right)^{-1}. \tag{8.12}$$

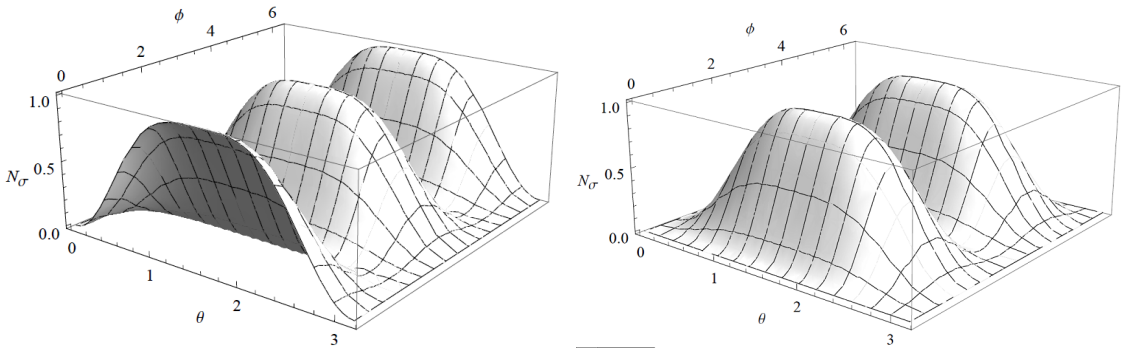

Figure 8.2: Instantaneous angular profile (low-energy regime) of eq.(8.11) for $\phi_\xi = 0$ (left) and $\phi_\xi = \pi/2$ (right), with $N_\sigma = \left[\frac{\alpha|\boldsymbol{\xi}|^2}{8\pi}\left(\frac{\omega}{m}\right)^2\right]^{-1} d\sigma^{e\gamma,\perp}_{\rm LSV}/d\Omega$.

As before, let us first consider $\xi^\mu = (\xi^0, 0)$, where $(\xi \cdot p_2)^2 \to \xi_0^2\omega^2$, but now, different from the $\omega \ll m$ case, the contribution from $(\xi \cdot p_3)^2$ is negligeable to $\mathcal{O}(m^2/\omega^2)$. The LSV differential cross section for a time-like background is then

$$\frac{d\sigma^{e\gamma,\,\xi_0}_{\rm LSV}}{d\Omega} = \frac{\alpha\xi_0^2}{8\pi}\frac{\omega}{m(1-\cos\theta)}, \tag{8.13}$$

whose angular dependence is the same as in eq.(8.12). A time-like background is not able to modify the angular profile of the differential cross sections, what is reasonable if one considers that this component does not select any direction in space.

We move next to the case of a pure space-like background and we again focus on the particular scenarios where we have instantaneously $\boldsymbol{\xi} \parallel \hat{\mathbf{z}}$ and $\boldsymbol{\xi} \perp \hat{\mathbf{z}}$. Proceeding as in the low-energy case, we find that the respective LSV differential cross sections are

$$\frac{d\sigma^{e\gamma,\,\parallel}_{\rm LSV}}{d\Omega} = \frac{\alpha|\boldsymbol{\xi}|^2}{8\pi}\frac{\omega}{m(1-\cos\theta)} + \mathcal{O}(m^2/\omega^2), \quad \text{for } \theta_\xi = 0 \tag{8.14}$$

$$\frac{d\sigma^{e\gamma,\,\perp}_{\rm LSV}}{d\Omega} \sim \mathcal{O}(m/\omega), \quad \text{for } \theta_\xi = \pi/2. \tag{8.15}$$

Equation (8.15) owes its seemingly odd energy behavior to the fact that, for $\theta_\xi = \pi/2$, $\xi\cdot p_2 = 0$ while $\xi\cdot p_3 \sim \omega' \sim m$, and no extra ω^2 factor from $(\xi\cdot p_2)^2 + (\xi\cdot p_3)^2$ is available to cancel the remaining ω^{-1} from phase space. The unexpected absence of azimuthal dependence in eq.(8.15) – as opposed to eq.(8.11) – is not a general feature, though. For $\theta_\xi \neq \pi/2$ the distinctive ϕ-dependent contribution is recovered, albeit being strongly suppressed, since $\xi \cdot p_2 \sim \omega\cos\theta_\xi \neq 0$ dominates over $\xi \cdot p_3 \sim m\cos(\phi - \phi_\xi)$. In this more general situation, the aforementioned linear energy dependence of $\frac{d\sigma^{e\gamma,\,\perp}_{\rm LSV}}{d\Omega}$ is also expected to be re-obtained.

In Ref. [358] Compton scattering is also considered in a LSV scenario with the $\not{b}\gamma_5$ modification to the Dirac equation [295]. There the differential cross section grows very rapidly for low energies (not the case here), so not recovering the classical Thomson result.

Furthermore, for $\omega \gg m$ the differential cross sections typically grow with $\sim \omega$, as eq.(8.8) anticipated. This is not surprising, since the LSV term is non-renormalizable and its validity is limited to some high, but finite energy scale. We, on the other hand, are working at much lower energies, below the electroweak scale ~ 100 GeV, where QED is also modified, so our results are in order as long as we do not go way beyond this scale.

8.3 Bhabha scattering

Bhabha scattering is the ultra-relativistic scattering of electrons and positrons and is one of the most basic and well-studied processes, serving as a high-luminosity monitor and a tool for the study of both QED and electroweak interactions [359–361]. Due to its relative simplicity, it has been used as a test for different beyond the Standard Model scenarios, such as theories with extra dimensions [362], generalized QEDs [363] and LSV [356].

In this section[6] we investigate the LSV-modified amplitudes for Bhabha scattering in the context of the Lagrangian from eq.(8.1), but, before we proceed with our computations, let us briefly recall the main results from usual QED. The electron-positron scattering, $e^-(p_1) + e^+(p_2) \to e^-(p_3) + e^+(p_4)$, is usually evaluated in the center of mass (CM) frame and can be represented by the s- and t-channel Feynman diagrams depicted in Fig. 8.1.

For our purposes, we will restrict ourselves to unpolarized cross sections, hence, we have to average the squared amplitude over spins. In the CM frame the 4-momenta of the incoming (ultra-relativistic) particles are $p_1 = (E, \mathbf{p})$ and $p_2 = (E, -\mathbf{p})$, while, for the outgoing particles, $p_3 = (E, \mathbf{p}')$ and $p_4 = (E, -\mathbf{p}')$, with $E = E_{\text{CM}}/2$. For definitiveness, let us consider the initial momenta oriented along the z-axis, i.e., $\mathbf{p} = E\,\hat{\mathbf{z}}$, while the final momentum is $\mathbf{p}' = E\,(\sin\theta\cos\phi, \sin\theta\sin\phi, \cos\theta)$. With these definitions, the unpolarized differential cross section is

$$\frac{d\sigma^{ee}_{\text{QED}}}{d\Omega} = \frac{\alpha^2(7+\cos 2\theta)}{16E^2_{\text{CM}}(\cos\theta - 1)^2}. \tag{8.16}$$

[6] The calculations from this section were performed by Gustavo Pazzini de Brito, Judismar Guaitolini Jr and Célio Marques, all co-authors in the published work [71]. With their approval, I present the results for the sake of completeness.

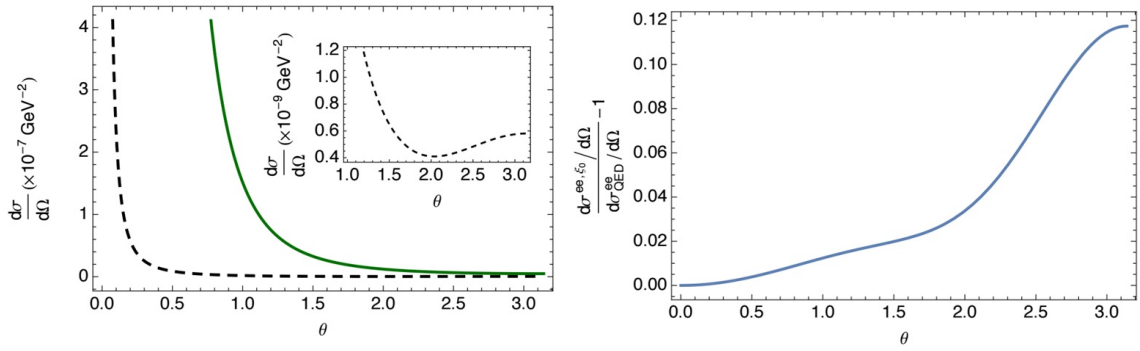

Figure 8.3: Left panel: differential cross sections for the usual QED (solid line) and the time-like LSV contribution (dashed line) assuming $\xi_0 = 10^{-3}\,\text{GeV}^{-1}$; the inset shows the non-monotonic angular dependence of the LSV sector. Right panel: deviation (LHS of eq.(8.18)) as a function of the scattering angle.

Using eq.(8.2) one can compute the spin-averaged Feynman amplitude, $\langle|\mathcal{M}_{\text{tot}}|^2\rangle$, whose complete expression contains the usual QED contribution leading to eq.(8.16) and an additional LSV term, $\langle|\mathcal{M}_{\text{LSV}}|^2\rangle \sim \mathcal{O}(\xi^2)$. To present the differential cross section, let us divide our analysis in the physically meaningful cases of pure time- and space-like backgrounds. The total differential cross section is composed of the QED contribution, eq.(8.16), with an additional term coming from $\langle|\mathcal{M}_{\text{LSV}}|^2\rangle$. For a pure time-like background, we find (left panel of Fig. 8.3)

$$\frac{d\sigma^{ee,\,\xi_0}}{d\Omega} = \frac{\alpha^2(7+\cos 2\theta)}{16E_{\text{CM}}^2(\cos\theta-1)^2} + \frac{\alpha\,\xi_0^2\,(\cos\theta + 2\cos^2\theta - \cos^3\theta + 2)\sin^2\frac{\theta}{2}}{4\pi(\cos\theta-1)^2}. \tag{8.17}$$

Small deviations from the usual tree-level results from QED for Bhabha scattering have been experimentally bounded at $\sqrt{s} = 29\,\text{GeV}$ and $|\cos\theta| < 0.55$ at the PEP storage ring (Stanford) as (at 95% CL) [364]

$$\left|\frac{d\sigma^{ee,\,\xi_0}/d\Omega}{d\sigma^{ee}_{\text{QED}}/d\Omega} - 1\right| \lesssim \frac{3E_{\text{CM}}^2}{\Lambda^2}, \tag{8.18}$$

where Λ parametrizes deviations from the theoretical results.

From eq.(8.17) we see that, discounting the angular dependence from both QED and LSV contributions, the leading order contribution for the LHS of eq.(8.18) is of order $\sim \xi_0^2 E_{\text{CM}}^2/\alpha^2$. Comparing with the RHS of eq.(8.18) we arrive at $\xi_0 \lesssim \sqrt{\alpha}/\Lambda$ so that, plugging $\Lambda \sim 200\,\text{GeV}$ [364], we obtain

$$\xi_0 \lesssim 10^{-3}\,\text{GeV}^{-1}. \tag{8.19}$$

As one can see from the right panel in Fig. 8.3, where the upper limit obtained above is assumed, the deviation from pure QED grows considerably with the scattering angle. We remark, however, that our estimate is consistent: the experimental limit used is valid for $|\cos\theta| < 0.55$ with the upper bound $3E_{\rm CM}^2/\Lambda^2 \sim 0.06$ [364]. In this angular range we have $\left|\frac{d\sigma^{ee,\,\xi_0}/d\Omega}{d\sigma^{ee}_{\rm QED}/d\Omega} - 1\right| \sim 0.03$, cf. LHS of eq.(8.18) with $\xi_0 = 10^{-3}\,\text{GeV}^{-1}$, showing that our leading-order analysis is valid.

Despite of the apparently similar sizes of the LSV and QED contributions in the left panel of Fig. 8.3 for large θ, we see from the right panel that, for $\theta \simeq \pi$, $\left|\frac{d\sigma^{ee,\,\xi_0}/d\Omega}{d\sigma^{ee}_{\rm QED}/d\Omega} - 1\right|$ attains a maximum. This large-angle region is however hardly accessible in collision experiments and lies beyond the scope of the experimental limit used above [364], i.e., $|\cos\theta| < 0.55$ (i.e., $0.98 \leq \theta \leq 2.1$). For smaller values of ξ_0 this deviation decreases accordingly. The right panel in Fig. 8.3 suggests that measurements in the backward direction would be a promising way – though technically challenging – to look for signals of a purely time-like LSV background.

Now we turn to the case of a purely spatial background 4-vector, $\xi^\mu = (0, \boldsymbol{\xi})$. In this situation, the pure LSV piece of the differential cross section is found to be

$$\begin{aligned}\frac{d\sigma^{ee,\,\boldsymbol{\xi}}_{\rm LSV}}{d\Omega} &= \frac{\alpha\,|\boldsymbol{\xi}|^2\,(17\cos\theta + 2\cos 2\theta - \cos 3\theta + 46)}{128\pi(\cos\theta - 1)^2} \\ &\times \left[\cos(\phi - \phi_\xi)\sin\theta\sin\theta_\xi + (\cos\theta - 1)\cos\theta_\xi\right]^2, \end{aligned} \tag{8.20}$$

and the expression for the complete differential cross section is, as before, the combination of the equation above with the standard QED result, cf. eq.(8.16).

The analysis here is more involved due to the number of angular parameters, hence we focus on two particularizations to better illustrate the effect of the LSV terms. First, let us take a background vector parallel to the z-axis ($\theta_\xi = 0$), for which the total differential cross section (QED + LSV) is given by

$$\begin{aligned}\frac{d\sigma^{ee,\,\parallel}}{d\Omega} &= \frac{\alpha^2(7 + \cos 2\theta)}{16E_{\rm CM}^2(\cos\theta - 1)^2} \\ &+ \frac{\alpha\,|\boldsymbol{\xi}|^2(17\cos\theta + 2\cos 2\theta - \cos 3\theta + 46)\sin^4\frac{\theta}{2}}{32\pi(\cos\theta - 1)^2}. \end{aligned} \tag{8.21}$$

Second, we consider $\boldsymbol{\xi}$ in the transverse xy-plane ($\theta_\xi = \pi/2$, see Fig. 8.4), where

$$\begin{aligned}\frac{d\sigma^{ee,\,\perp}}{d\Omega} &= \frac{\alpha^2(7 + \cos 2\theta)}{16E_{\rm CM}^2(\cos\theta - 1)^2} + \frac{\alpha\,|\boldsymbol{\xi}|^2\cos^2(\phi - \phi_\xi)\sin^2\theta}{32\pi(\cos\theta - 1)^2} \\ &+ \frac{\alpha\,|\boldsymbol{\xi}|^2(17\cos\theta + 2\cos 2\theta - \cos 3\theta + 46)}{32\pi(\cos\theta - 1)^2}. \end{aligned} \tag{8.22}$$

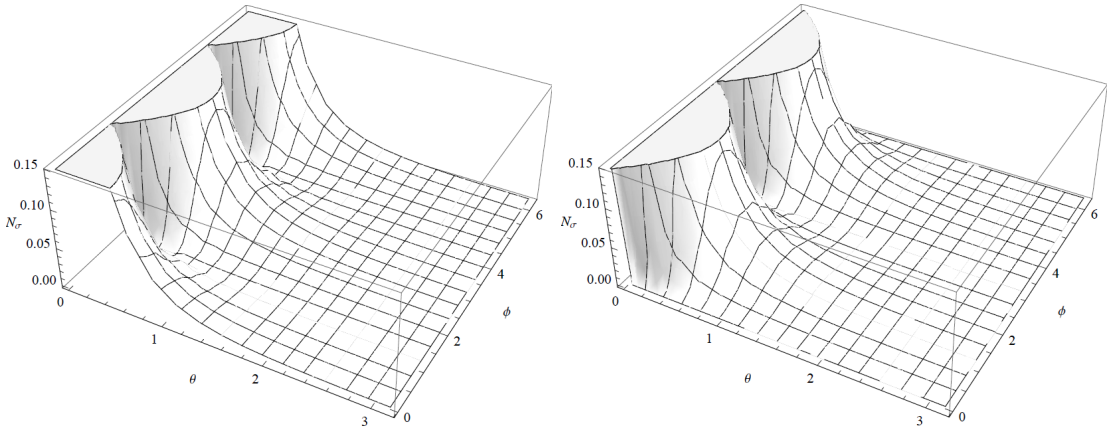

Figure 8.4: Instantaneous LSV differential cross sections for pure space-like background ($\boldsymbol{\xi} \perp \hat{\mathbf{z}}$, i.e,. $\theta_\xi = \pi/2$). The vertical axes are given by $N_\sigma = [\alpha|\boldsymbol{\xi}|^2]^{-1} d\sigma^{ee,\perp}_{\text{LSV}}/d\Omega$ with $\phi_\xi = 0$ (left) and $\phi_\xi = \pi/2$ (right).

From eqs.(8.21) and (8.22) it is clear that the LSV contribution (up to $\mathcal{O}(\xi^2)$) is energy independent – a consequence of the momentum-dependent LSV vertex – while the QED result falls with E_{CM}^{-2}. For this reason, with experiments performed at increasingly higher energies, the total differential cross section should, in principle, display an unexpected *plateau* for fixed and preferably small scattering angles, what may be hard to observe experimentally, though. Also, the energies necessary to make this plateau visible would likely be beyond the validity domain of the effective treatment we adopt, as the LSV coupling originates from a dimension-5 operator.

Furthermore, there is no resulting azimuthal dependence in the case of a background parallel to the beam axis (as expected), whereas the transverse case is clearly ϕ-dependent. This feature is very distinctive in comparison with the QED result and could, in principle, be visible in high-energy collision experiments.

8.4 Pair annihilation

Electron-positron (e^-e^+) annihilation may have several different final states [365, 366], e.g. e^-e^+, $\mu^-\mu^+$, $N\gamma$ ($N > 1$), etc, but here we are interested in the last case with $N = 2$, which is the dominating channel with photons in the final state. The practical importance of this reaction lies in the fact that, in e^-e^+ colliders, it represents a large source of background, as it has no lower energy threshold, unlike $e^- + e^+ \to f^- + f^+$, with $f = e, \mu, \tau, \cdots$. A thorough understanding of its features is therefore fundamental to produce precision measurements and to correctly discriminate possible new physics.

This process has also been used to study the electroweak interactions between leptons and quarks exchanging γ or Z^0 bosons in large experiments, such as PETRA, PEP and LEP. Here, however, we limit ourselves to pure QED + LSV effects, not taking the full electroweak contributions due to Z^0 exchange into account. This is a safe assumption, since we are aiming at CM energies $\sqrt{s} = 29$ GeV $< m_{_{Z^0}}$, where $\gamma - Z^0$ interference may be neglected [364].

Following Ref. [71], below we present two discussions: the calculation of the LSV-modified unpolarized differential cross section for e^-e^+ annihilation in two photons and the LSV correction to the decay rate of para-positronium.

8.4.1 Unpolarized differential cross section

The production of two photons via pair annihilation, $e^-(p_1) + e^+(p_2) \to \gamma(p_3) + \gamma(p_4)$, is represented at tree level by the t- and u-channel Feynman diagrams displayed in Fig. 8.1. Here we are interested in the unpolarized differential cross section in the CM, i.e., we do not keep track of spin orientations and polarizations. In standard QED it is found that [4]

$$\frac{d\sigma^{\gamma\gamma}_{\text{QED}}}{d\Omega} = \frac{\alpha^2}{2E^2_{\text{CM}}} \frac{1+\cos^2\theta}{\sin^2\theta}, \tag{8.23}$$

where the ultra-relativistic limit is assumed: $E = E_{\text{CM}}/2 \simeq |\mathbf{p}| \gg m$. The process is evaluated in the CM frame, where $p_1 = (E, \mathbf{p})$ and $p_2 = (E, -\mathbf{p})$ with $\mathbf{p} = E\hat{\mathbf{z}}$, while $p_3 = (E, \mathbf{k})$ and $p_4 = (E, -\mathbf{k})$, with $|\mathbf{k}| = E$ for the final-state photons. A symmetry factor $S = 1/2$ accounts for the identical particles in the final state.

As in Section 8.3, we are interested in the total differential cross section for this process with the modified vertex, so that a comparison with experimental limits may constrain the LSV parameters. The detailed calculation of the squared amplitude and its subsequent averaging is a lengthy and cumbersome task, but it can be greatly simplified by noting that the amplitude for pair annihilation is connected to that of Compton scattering through crossing symmetry.

Following this procedure we find that, as with Compton scattering, eq.(8.7), the squared amplitude for e^-e^+ annihilation brings the LSV effects as a pre-factor of $(\xi \cdot p_3)^2 + (\xi \cdot p_4)^2$, so that, applying the kinematics mentioned above, we find that this factor becomes

$$(\xi \cdot p_3)^2 + (\xi \cdot p_4)^2 = \frac{E^2_{\text{CM}}}{2}\left[\xi_0^2 + |\boldsymbol{\xi}|^2 f^2(\theta, \phi, \theta_\xi, \phi_\xi)\right], \tag{8.24}$$

where $f(\theta, \phi, \theta_\xi, \phi_\xi) = \sin\theta \sin\theta_\xi \cos(\phi - \phi_\xi) + \cos\theta\cos\theta_\xi$.

The instantaneous total differential cross section in the high-energy limit, up to $\mathcal{O}(\xi^2)$, can then be conveniently expressed as

$$\frac{d\sigma^{\gamma\gamma}}{d\Omega} = \frac{\alpha^2}{2E_{\text{CM}}^2}\frac{1+\cos^2\theta}{\sin^2\theta}\left[1+\frac{E_{\text{CM}}^2}{16\pi\alpha}\left[\xi_0^2+|\boldsymbol{\xi}|^2 f^2(\theta,\phi,\theta_\xi,\phi_\xi)\right]\right], \tag{8.25}$$

and we notice that, as with Bhabha scattering, the LSV contribution is overall energy independent. An analysis of the angular dependence of the LSV piece of eq.(8.25) for a purely space-like background would lead to conclusions similar to those of the previous sections: for $\boldsymbol{\xi}$ aligned with the initial electron-positron motion, there is no ϕ-dependence, only an extra $\sim \cos^2\theta$ factor is added, while, for a transverse background, similar peaks as those depicted in Fig. 8.2 are expected. Furthermore, in this latter configuration, the forward peak ($\theta \to 0$) is absent due to the additional $\sin^2\theta$ factor from eq.(8.24).

We are now ready to compare eq.(8.25) with eq.(8.23) in a more concrete way. The deviation from the standard QED tree-level prediction for the differential cross section for e^-e^+ annihilation is bounded by experiment (PEP) via

$$\left|\frac{d\sigma^{\gamma\gamma,\,\xi_0}/d\Omega}{d\sigma^{\gamma\gamma}_{\text{QED}}/d\Omega}-1\right| \lesssim \frac{E_{\text{CM}}^4}{2\tilde{\Lambda}^4}, \tag{8.26}$$

at 95% CL with $\tilde{\Lambda} = 59\,\text{GeV}$ at $\sqrt{s} = 29\,\text{GeV}$ [364]. Plugging eq.(8.25) for a pure time-like background into eq.(8.26) and discounting the angular dependence from both QED and LSV contributions we find that $\xi_0 \lesssim \sqrt{8\pi\alpha}E_{\text{CM}}/\tilde{\Lambda}^2$, which gives

$$\xi_0 \lesssim 10^{-3}\,\text{GeV}^{-1}. \tag{8.27}$$

8.4.2 Life time of para-positronium

Positronium is the unstable bound state of an electron and a positron. It was predicted in 1934 by Mohorovicic [367] and experimentally observed by Deutsch in 1951 [368]. Its main decay channels are in two or three photons for the singlet (para-positronium, p-Ps) and triplet (ortho-positronium, o-Ps) spin states, respectively [369]. Here we shall focus on the LSV contribution to the life time of p-Ps, given in QED by the inverse of the decay rate[7], $\Gamma_{2\gamma,\,\text{QED}} = \frac{m\alpha^5}{2}$. Its experimental value, which agrees well with theory [370, 371], was measured to be 125 ps, with a relative precision of 215 ppm, that is $\delta_\tau \sim 10^{-4}$ [372].

[7]The decay in two photons is the dominating channel (largest branching ratio). The contributions of decays into four, six, etc photons is small relative to that into two. Moreover, o-Ps decays preferably in three photons, which is a higher-order process than the one considered here.

The decay rate of o-Ps, despite of its longer life time, is not significantly more precise than that of p-Ps and its relative precision reads 150 ppm [373]. The former is, however, a higher-order process in QED, so we go for the simplest one, p-Ps, without significant loss regarding the outcoming bound on the LSV parameters.

Although closely related to the calculation performed above, the decay rate of p-Ps in two photons does not follow as a direct sub-product of the previous results. Indeed, when computing the cross section for pair annihilation we were interested in the unpolarized result in the ultra-relativistic limit, whereas in the present case[8] we consider that the kinetic energies of both the electron and the positron are much smaller than their rest energies. We also take the spin-polarized case of the singlet state[9].

The particulars of this calculation follow closely those of Ref. [21], so we do not repeat them here explicitly. We remark, however, that the most important step is to anti-symmetrize the final amplitude with regard to the initial and final spin and polarizations to form the singlet state, while keeping only the lowest order contribution in the LSV background. The squared amplitude, which displays no interference between the pure QED and the LSV sectors, ends up being only sensitive to the time component of the background vector and reads

$$|\mathcal{M}_{\rm tot}|^2 = |\mathcal{M}_{\rm QED}|^2 + |\mathcal{M}_{\rm LSV}|^2 = 16e^4\left(1 + 4\frac{m^2\xi_0^2}{e^2}\right). \tag{8.28}$$

From eq.(8.28) we see that the result is isotropic and the differential cross section in the CM is given by[10]

$$\frac{d\sigma}{d\Omega} = \frac{|\mathcal{M}_{\rm tot}|^2}{(16\pi m)^2\, v}, \tag{8.29}$$

which can be immediately integrated over the solid angle (the amplitude is isotropic). The decay rate is given by $\Gamma = v\sigma|\psi(0)|^2$, with $|\psi(0)|^2 = \alpha^3 m^3/8\pi$ being the squared wave function of positronium[11] in its ground state [21]. Finally, including eq.(8.28), the decay rate is given by

$$\Gamma_{2\gamma} = \frac{m\alpha^5}{2}\left(1 + \frac{m^2\xi_0^2}{\pi\alpha}\right). \tag{8.30}$$

[8]The calculations from this section were performed by Daniel Kroff, co-author in the published work [71]. With his approval, I present the results for the sake of completeness.

[9]That is, we are considering the case where the two initial particles have their spins anti-parallel with $S = 0$ and projection over the, say, z-axis $M_S = 0$.

[10]The non-relativistic velocity v appears here but will be cancelled in the calculation of the decay rate.

[11]The wave functions for positronium may be read directly from those for usual hydrogen, but with the Bohr radius corrected for the reduced mass of the system, $a_0 = (\alpha\mu)^{-1} \to a_0(\mathrm{Ps}) = 2a_0(\mathrm{H})$.

Assuming the LSV part to be very small ($\xi_0^2 m^2 \ll 1$), we may write the modified life time of p-Ps to leading order as

$$\tau_{_{2\gamma}} \equiv \Gamma_{2\gamma}^{-1} \simeq \frac{2}{m\alpha^5}\left(1 - \frac{m^2\xi_0^2}{\pi\alpha}\right), \tag{8.31}$$

and, once more, given that no deviations from QED have been reported, we may only set upper limits on the LSV coefficient. We do that by requiring that the LSV correction to the life time does not extrapolate the experimental error, i.e.,

$$\left|\frac{\tau_{_{2\gamma}}}{\tau_{_{2\gamma,\,\mathrm{QED}}}} - 1\right| \lesssim \delta_\tau, \tag{8.32}$$

which amounts to a $1\,\sigma$ upper bound, which reads

$$\xi_0 \lesssim 1\,\mathrm{GeV}^{-1}. \tag{8.33}$$

It is important to highlight that other authors have considered the effects of different LSV sectors in positronium (e.g. Refs. [374, 375]). In this context, the results for spectroscopy measurements are specially interesting, for these experiments are extremely precise, what could give more restrictive bounds on the LSV parameters.

8.5 Partial conclusions

In this chapter we have discussed the modifications in simple QED processes due to the inclusion of a new non-minimal coupling between the electron and the photon [305], eq.(8.1). We found that novel energy- and angle-dependent corrections arise already at lowest order in the LSV parameter and, up to this order, we were able to establish upper limits on ξ_0 by demanding that the LSV-modified physics does not exceed the established QED results by more than a few percent – see eqs.(8.18), (8.26) and eq.(8.32). As indicated in Section 8.1, similar limits on $|\boldsymbol{\xi}|$ should be expected.

We have focused on separately purely time- or space-like background configurations, as is customary in the field of LSV, but it is clear that such a division is arbitrary – if such a background exists, it would likely be a non-trivial mixture of such components. However, since we are interested in estimating upper bounds for the background ξ, we refrain from stating a more general result taking a background with time- and space-like components, as this would not improve neither the readability of the results nor the bounds obtained.

We have found that, for a pure space-like background, the instantaneous LSV-modified differential cross sections generally present periodic contours as a function of the azimuthal angle – see e.g. Figs. 8.2 and 8.4. The respective pure QED processes do not discriminate different ϕ-orientations and this is a clear LSV signal that could be searched for in collider experiments. Another interesting feature is the scaling of the LSV contributions with energy, which enhances its effects in high-energy experiments (in contrast to the QED contributions), possibly allowing for future direct tests of LSV.

In the last section we found an upper bound on ξ_0 by calculating the decay rate of p-Ps, which turned out to be a thousand times weaker than the others. The limit from p-Ps owes its relative weakness to the fact that, contrary to the other processes studied, p-Ps is treated as a highly non-relativistic system: the initial e^-e^+ pair is taken as being practically at rest. The LSV non-minimal coupling brings an energy-dependent correction, which, in the low-energy limit ($\mathbf{p} \simeq 0$ and $E \simeq m$), means that the LSV correction to the decay rate becomes $|\mathcal{M}_{\text{LSV}}|^2 \sim \xi_0^2 E^2 \to \xi_0^2 m^2$, which is also expected on purely dimensional grounds. These considerations, combined with the relatively large uncertainty ($\delta_\tau = 215\,\text{ppm}$), are responsible for the looser bound quoted in eq.(8.33). As mentioned in the end of Section 8.4.2, an application of our modified vertex to the spectrum of simple atoms (e.g., hydrogen) may improve the limits quite significantly, as spectroscopic measurements reach uncertainties as low as 10^{-15} [59].

It is worthwhile pointing out that o-Ps, being the triplet spin state of positronium, naturally offers a 3-vector (the initial polarization) that should couple to the external LSV space-like background, should it exist. This means that an analysis of o-Ps could probably bring information on the spatial components of the background, which would likely generate anisotropies. However, as mentioned earlier, this is a higher-order process and goes beyond the scope of the present work. In any case, since the experimental uncertainty is of similar size as for p-Ps [373], we do not expect much better limits[12].

Furthermore, even though p-Ps may be used to extract upper limits on the background, it is probably does not provide a "smoking gun" for LSV, since other scenarios beyond the Standard Model could possibly generate similar effects. In this context, it is possible that o-Ps, being a triplet state, may be directionally more sensitive to a fixed spatial background, thus more sensitive to sidereal variations, which could provide an unambiguous signal of LSV.

[12] Actually, with one more factor of $\alpha \simeq 1/137$, we may expect the limits to be about a hundred times weaker.

In the discussions presented in this chapter we have translated the background from the laboratory frame in terms of the components in the SCF and, on the way, we ignored the boost factors. This is a reasonable approximation and this means that the temporal and spatial components do not mix, cf. Sections 6.4 and8.1. This implies that our independent analysis of pure time- and space-like backgrounds may be extended to the components in the SCF. For the case where $\xi^J_{\rm SCF} \equiv 0$, the upper bounds from eqs.(8.19) and (8.27) immediately translate to

$$\xi^T_{\rm SCF} \lesssim 10^{-3}\,{\rm GeV}^{-1}, \tag{8.34}$$

whereas from eq.(8.33) we get $\xi^T_{\rm SCF} \lesssim 1\,{\rm GeV}^{-1}$.

Contrary to the pure time-like case which is relatively simple, the pure space-like scenario ($\xi^T_{\rm SCF} \equiv 0$) is significantly more complicated. This is due to the contractions with the 3-momenta of the participating particles. For this reason we choose not to display the result in terms of the SCF variables, as no new significant physical information would be conveyed.

Finally, we would like to indicate that other sectors from the SME could also induce effects in scattering processes, e.g. the $k_{\rm AF}$ and $k_{\rm F}$ contributions to the photon sector. Since both enter in the quadratic part of the Maxwell Lagrangian, they would modify the photon propagator, also demanding corrections to the dispersion relations (see e.g. Ref. [300]). These corrections would also be momentum-dependent and would potentially lead to modifications in the (differential) cross sections in QED processes, including the ones treated above. While Schreck [300] has already discussed the $k_{\rm F}$ sector in connection to Compton scattering, a similar analysis of the Carroll-Field-Jackiw $k_{\rm AF}$ term [311] (cf. Chapter 7) would be possible, as it could provide complementary local bounds on this LSV parameter. We do not expect, however, that the upper bounds from such an analysis would be competitive either with the ones obtained in Ref. [70] or in Refs. [58, 311].

Besides the points addressed so far, it is also possible that the class of non-minimal couplings studied here – also with axial couplings containing γ_5 – could produce interesting contributions to the $g-2$ of the electron (or more interestingly, of the muon) already at tree level [303]; see also discussion in Section 6.5.1. The tight experimental constraints on $a_{e,\mu} = (g-2)/2$ together with the expected momentum dependence of the extra LSV vertices could allow for better upper limits on ξ^μ. The task of evaluating this prospect is an open topic for future research.

As a final remark we would like to indicate that the results obtained in this chapter (following Ref. [71]) have been added to the Data Tables, Table D20, edited by Kostelecký and Russel [58] in its 2017 update (v10 on arXiv).

I would like to highlight that the content and results presented in this chapter are derived from my own published work [71] in collaboration with Gustavo Pazzini, Celio Marques, Judismar Guaitolini and Daniel Kroff. Some sections of Ref. [71] were of responsibility and authorship of my co-authors and I have expanded them for this thesis – they are adequately indicated as being adaptations of the work of others. In Ref. [71] I have done most of the writing, while the calculational work was equally shared (I am the first author). The plots in Fig. 8.3 were produced by Daniel Kroff.

Concluding remarks

In this thesis I have discussed the research topics with which I worked during my PhD. These topics are: topological mediators and spin-dependent potentials, axion-like particles, and Lorentz-violating models. Given that these subjects are not directly related, I have dedicated separate parts for each of them hoping to simplify the presentation without an explicit attempt to artificially unify them.

As already mentioned in the Presentation, these subjects are distinct in the sense that they do not directly intersect, but they do share something: they are low-energy features of high-energy, beyond the Standard Model theories. This common aspect justifies our efforts – here pursued in basically three fronts – once it is expected that models trying to solve the aforementioned physical issues resort to postulating new particles, energy scales and symmetry schemes. The aftermath is that, besides (tentatively) solving the original problem, new phenomena are predicted. This thesis deals with some of these novel effects.

After each of the chapters I have included a partial conclusion. The idea behind this construction is to locally summarize the discussions made and the results attained. In this interim, here I will not present a detailed *repetitorium* of the contents already discussed. The objective here is rather to present a brief overview of the themes worked throughout the thesis and indicate some lines of work which could be pursued in the future. For this I will follow the order adopted so far.

Part I: topological mediators and spin-dependent potentials

In the first part we have discussed how microscopic interactions can be used to determine the macroscopic potentials between particles with different spins and mediated by different bosons. In particular, in Chapters 1 and 2, which are largely based upon Ref. [66], we have considered the possibility that spin-1 mediators obtain their mass not through the typical Proca mass term, but rather via a Chern-Simons-like topological term.

This scenario was implemented by taking two fields, a 2-rank tensor and a 4-vector, connected via a topological coupling in a model called CSKR (Cremmer-Scherk-Kalb-Ramond). The presence of possibly more degrees of freedom was felt specially in the presence of a direct coupling between matter and the tensor field[13]. This led us to a large variety of spin- and velocity-dependent potentials that could lead to differences in the interaction of spin-polarized sources, thus allowing a possible identification of the mediator as being topological or not.

In the context of our published work [66] I would like to indicate a possible future direction[14]: modify the CSKR model to include other kinds of new physics. A possibility would involve the so-called hidden photon (a.k.a. paraphoton or dark photon), a hypothetical neutral vector particle predicted in extensions of the Standard Model [41, 42]. This particle is only accessible[15] through its kinetic mixing with photons $\sim F_{\mu\nu}H^{\mu\nu}$, where F and H are the field-strength tensors for the photon and hidden photon, respectively. This mixing leads to photon-hidden photon oscillations – similar to neutrino oscillations – which could be detectable in e.g. "light shining through a wall" experiments [213].

The idea would be to extend the CSKR system to include the hidden photon and have it topologically couple with the 2-rank tensor (cf. Section 1.3). In this way both vector fields obtain their masses. The kinetic mixing between photon and hidden photon would not be modified, but now the hidden photon would not have a gauge-breaking mass term, but rather a topologically gauge-invariant one.

Preliminary calculations have shown that the procedure discussed in Section 1.3 can be applied in this extended configuration, thus leading to the usual Proca-like – but gauge-invariant – formulation of the photon-hidden-photon interaction Lagrangian. As also indicated in Section 1.3, the fulfilment of this program is only possible in the absence of matter described by tensor currents which may be coupled directly to the 2-rank Kalb-Ramond tensor. In this case the "substitution" $\tilde{G} \leftrightarrow B$ involves the inverse of a derivative, thus leading to non-local interactions. In this sense, the presence of such an interaction ($\sim J_{\mu\nu}B^{\mu\nu}$) would not allow us to transition from a topological mass to a Proca-like one.

[13] As discussed in Section 1.3, this was exactly the case for which we could not make the field redefinitions that take the CSKR Lagrangian into a Proca-like one.

[14] Yet another possibility would be to investigate higher-order contributions to the interaction energy between given sources. This has been done in many contexts (see e.g. Refs. [109, 122, 376]). I do not believe this would be a worthwhile contribution, however, as the corrections are expected to be minute. Kim Veiga (co-author in Ref. [67]) is currently looking at tree-level potentials in higher orders in $\mathbf{p}/m$.

[15] This kinetic mixing may be rotated away and the mixing parameter ends up in the interaction sector.

Assuming such a coupling, we would have to consider the three fields together[16], so that we would effectively have a topologically massive hidden photon. This idea is in very early stages and we still have to check if it brings new and interesting phenomenology[17] and, if yes, look for possible applications.

Part II: axion-like particles

In Chapter 4 we introduced the axion in the context of QCD and in Chapter 5 we discussed a generalization – axion-like particles (ALPs) – which couples directly to the electromagentic field. We saw that this coupling also constitutes the best chance of observing its effects, as these pseudo-scalar particles may be produced in the presence of electromagnetic fields via the Primakoff effect.

Most of the literature is focused on very light ALPs, but we concentrated our efforts on rather heavier ALPs with $10\,\mathrm{keV} \lesssim m_a \lesssim 100\,\mathrm{MeV}$. With masses in this range ALP-photon conversion in magnetic fields (e.g. in the galaxy) is not effective [56]. Instead, in this case the most interesting detection channel is through ALP *decay* in two photons, usually in the gamma-ray region.

The central idea is that (heavy) ALPs could be copiously produced during the core collapse leading to supernovae, thus producing a signal of gamma rays. Given that the ALPs are massive, initial propagation and subsequent decay are not collinear, thus leading to an angular smearing and potentially large time delays of the ALP-originated radiation. Unfortunately, however, no such signal was observed. Through this "null result" we were able to extract limits on the mass and coupling of ALPs, also showing the expected sensitivities in case the red supergiant Betelgeuse explodes in a supernova event in the near future ($\sim 10^5$ years).

In Chapter 5 we focused on the concrete case of SN 1987A, which is the best studied supernova in the history of astronomy (it was actually the closest supernova in the modern era). Even with this elevated status, we were barely able to capture its onset: we were actually lucky to have *any* gamma-ray instrument available to record a possible signal. The Gamma-Ray Spectrometer was mounted on the satellite-borne Solar Maximum Mission [57] and was sensitive in the $4.1 - 100$ MeV range (half-sky field of view). Following Fig. 5.2 we see that this energy range – also the one we explicitly used ($25 - 100$ MeV) – is close to optimal, since this allows the capture of the peak of the ALP production, which takes place at $E_a \sim 80$ MeV.

[16] That is, we cannot simply keep one of the vector fields after it dynamically absorbed the other degrees of freedom from the 2-rank tensor (cf. Chapter 1).

[17] For example, how would the topological mass term change the dynamics of photon-hidden-photon oscillations?

In Section 5.4.2 we discussed the case of Betelgeuse, which is ~ 250 times closer than SN 1987A. ALP production would procede in a similar way as with SN 1987A, but the proximity would cause the gamma-ray flux on Earth to increase by a factor of $\sim (250)^2$. Besides this, the gamma-ray detectors have improved since 1987, so the sensitivity itself is much better. Unfortunately, the overall sensitivity obtained by employing the Fermi-LAT [250] detector is reduced by its energy acceptance – $E_\gamma > 100$ MeV up to ~ 300 GeV – which causes the detector to miss the peak of ALP production; this was quantified in $P_{\text{acceptance}} \sim 0.06$, cf. Section 5.2.2. Even with this hindrance, the projected bounds for Betelgeuse show a significant improvement over the one from SN 1987A, cf. Fig. 5.9.

We mentioned new detectors, cf. Section 5.5, such as e-ASTROGAM [251], ComPair [252], or PANGU [253]. These are all planned to improve on the successful heritage from Fermi-LAT and other instruments. All three have broad field of view ($\sim$ full sky) and angular resolution below $\sim 1^\circ$. This last factor, which is important for source identification in other contexts (gamma-ray bursts, extra-galatic sources, etc), can also be useful for indirect ALP detection. In Section 5.3.3 we have shown that the ALP-originated halos are not expected to be $\gtrsim 1^\circ$ within the excluded regions (also for Betelgeuse, cf. Fig. 5.10), but for $g_{a\gamma\gamma} \lesssim 10^{-12}\,\text{GeV}^{-1}$ and $m_a \sim$ MeV it is possible that ALP-originated halos achieve sizeable angular ranges.

Finally, the most interesting feature of these new instruments is the capacity to detect gamma rays (also) in the lower-MeV range with sensitivities up to 10 times better than Fermi-LAT: e-ASTROGAM [251] is sensitive to the $0.3\,\text{MeV} - 3$ GeV range; ComPair [252] to the $0.5 - 100$ MeV range and PANGU [253] to the $10\,\text{MeV} - 1$ GeV range.

Figure 5.2 shows the ALP production for nearly massless ALPs, while Fig. 5.3 shows that the production for massive ALPs is not very different from the one for almost massless ALPs for masses below some tens MeV[18]. This shows that gamma-ray detectors with sensitivities starting in the few MeV region may be also sensitive to ALPs with similarly small masses – possibly smaller than the ones we analyzed. We conclude that these instruments are actually ideal means to detect ALPs with masses up to 100 MeV. With sufficient sensitivity – hopefully enough to overcome the suppression in ALP production that kicks in for large masses (cf. Fig. 5.3) – also larger masses could be probed.

[18]Furthermore, we know that the spectrum needs to be such that $E_a \geq m_a$. For large masses, this pushes the peak of the production towards higher energies.

Part III: Lorentz-violating models

The third part was dedicated to a possible signal of the breaking of Lorentz symmetry. The essential process by which Lorentz-symmetry violation (LSV) would be implemented is via the spontaneous breaking of a symmetry involving not a (Lorentz) scalar, like the Higgs, but a general tensor field. The vacuum expectation value of this field would provide a spacetime fixed object that induces fundamental anisotropies that could produce observable effects, cf. Chapter 6.

Despite of intense experimental research, there has been no definitive signal of any LSV effects. Since LSV may appear in all sectors of the Standard Model, a general framework – the so-called Standard Model Extension (SME) – has been developed by Kostelecký *et al.* to allow for a systematic account of experimental limits on the various LSV coefficients. In this thesis I have reported results solely from the QED sector of the SME: in Chapter 7 we discussed a Chern-Simons-like modification to the photon sector of extended QED [70, 311], whereas in Chapter 8 we studied a modification of the electron-photon vertex via a non-minimal coupling [71]. The main results from both chapters have been added to the Data Tables from Kostelecký and Russel [58].

So far there is no phenomenon undoubtedly pointing to LSV, but this does not mean that it is not out there. In a quite similar way as with ALPs, LSV is a feature of (some) string theories, so it is valid to look for possible phenomenological signatures that could at least place upper limits on some coefficients.

A possible road for future tests of LSV couplings could be related to the proton radius. Since 2010 there is evidence that the different measurements – via electron-proton scattering and spectroscopy of usual and muonic hydrogen – do not quite agree on the value of the proton radius [377–379], what could be explained by new physics. In fact, the latest disagreeing measurements involve the energy levels in muonic hydrogen, which can be converted in information on the proton radius. Muonic hydrogen is especially interesting in the study of proton structure: since $m_\mu \sim 200\, m_e$, the associated Bohr radius is smaller than in electronic hydrogen, so the muon can probe deeper. It seems therefore plausible that some sort of *muonphilic* electromagnetic effect is at play.

In this regard, it would be interesting to test LSV-modified muon-photon non-minimal couplings in the spirit of eq.(8.1). Such couplings would modify the interaction between protons and muons, and consequently the energy levels of their bound state. The observed difference in the proton radius, which is extracted from the spectrum, could be attributed to a LSV background that specifically discriminates the muon (i.e., it does not interfere with the electron-photon interaction).

Naïvely supposing that we are talking about a spherical (charge) distribution, then, if LSV is at play, it would be reasonable to guess that the "most relevant" component would be the zeroth one, which is naturally isotropic (perhaps in the SCF). Some of the results from Chapter 8 also seem to point in this direction, since some of the LSV-modified differential cross sections did not introduce new angular dependences when the background 4-vector had only the time component. Moreover, in the discussion around p-Ps, cf. Section 8.4.2, we saw that only ξ_0 played a role. Whether this will be the case with other forms of non-minimal couplings in the context of the energy spectrum of muonic hydrogen is still an open question.

Similarly, there is a discrepancy between the values for the muon magnetic dipole moment from the prediction of the Standard Model and experiment [2, 380–382], which could also be addressed by a muonphilic LSV non-minimal coupling. Incidentally, this application would closely follow the systematics of the calculation leading to eq.(6.33), which is basically obtaining the non-relativistic limit of the Dirac equation (Schrödinger-Pauli equation) with the LSV coupling.

Exploring different couplings of the muon with the electromagnetic field, the non-relativistic Dirac equation will provide a Hamiltonian with a number of terms, some hopefully proportional to $\boldsymbol{\sigma} \cdot \mathbf{B}$ – an indication of a contribution to the magnetic dipole moment. We expect to retrieve the standard $g_0 = 2$ from the Lorentz-preserving part of the Hamiltonian, but there will be other terms dependent on the background 4-vector which may be used to explain the aforementioned discrepancy between theoretical calculations and experiment. By comparing the measured discrepancy with the predicted LSV contribution to the g-value, we should be able to find a range of values for the LSV coefficients that accounts for the observed disparity between theory and experiment.

This thesis focused on testing phenomenological consequences of BSM scenarios in low-energy settings. While the specifics of the underlying high-energy theories may vary, e.g. number of predicted particles, their masses and possible symmetry-breaking scales, the low-energy patterns examined are quite general: 2-rank tensors, spin-1 intermediate bosons, axion-like particles and Lorentz-violating backgrounds, all generically featured in many SM extensions. In this sense, the investigations pursued here have reached their purported objective of setting new upper bounds[19] on BSM effective theories. The overall conclusion is that, despite living naturally in the high-energy domain, BSM scenarios may be efficiently probed via low-energy tests, which have once more proved to be powerful tools to constrain new physics.

[19] In Part I we do not obtain upper limits: we identify instances where BSM signals might be testable.

Bibliography

[1] S.F. Novaes, *Standard Model: an introduction*, published in "Particle and Fields", Proceedings of the X J.A. Swieca Summer School (World Scientific, Singapore, 2000). ArXiv:hep-ph/0001283.

[2] C. Patrignani *et al.* (Particle Data Group), *Review of particle physics*, Chin. Phys. C **40**, 100001 (2016).

[3] A. Salam, J.C. Ward, *On a gauge theory of elementary interactions*, Nuovo Cim. **19**, 165 (1961).

[4] F. Mandl, G. Shaw, *Quantum field theory*, 2^{nd} Edition, John Wiley & Sons Ltd (2010).

[5] A. Salam, *On parity conservation and neutrino mass*, Nuovo Cim. **5**, 299 (1957).

[6] C.S. Wu, E. Ambler, R.W. Hayward, D.D. Hoppes, R.P. Hudson, *Experimental test of parity conservation in beta decay*, Phys. Rev. **105**, 1413 (1957).

[7] T.D. Lee, C.N. Yang, *Parity nonconservation and a two-component theory of the neutrino*, Phys. Rev. **105**, 1671 (1957).

[8] S. Weinberg, *A model of leptons*, Phys. Rev. Lett. **19**, 1264 (1967).

[9] A. Salam, J.C. Ward, *Electromagnetic and weak interactions*, Phys. Lett. **13**, 168 (1964).

[10] A. Salam. Proc. 8^{th} Nobel Symposium, edited by N. Svartholm (Almqivst and Wiksells, Stockholm) (1969).

[11] S. Glashow, *Partial symmetries of weak interactions*, Nucl. Phys. **22**, 579 (1961).

[12] F.J. Hasert *et al.*, *Search for elastic muon-neutrino electron scattering*, Phys. Lett. B **46** 138 (1973).

[13] G. Arnison, *et al.* (UA1 collaboration), *Experimental observation of isolated large transverse energy electrons with associated missing energy at* $\sqrt{s} = 540$ *GeV*, Phys. Lett. B **122** B, 103 (1983).

[14] G. Arnison, *et al.* (UA1 collaboration), *Experimental observation of lepton pairs of invariant mass around* $95\,\mathrm{GeV/c^2}$ *at the CERN SPS collider*, Phys. Lett. B **126** B, 398 (1983).

[15] The ATLAS collaboration, *Observation of a new particle in the search for the Standard Model Higgs boson with the ATLAS detector at the LHC*, Phys. Lett. B **716**, 1 (2012).

[16] The CMS ollaboration, *Observation of a new boson at a mass of 125 GeV with the CMS experiment at the LHC*, Phys. Lett. B **716**, 30 (2012).

[17] M. Herrero, *The Standard Model*, lectures presented at the NATO ASI 98 School, Techniques and Concepts of High Energy Physics; St. Croix, Virgin Islands, USA, June 18-29 1998. ArXiv:hep-ph/9812242.

[18] J. Butterworth, *The Standard Model: how far can it go and how can we tell*, arXiv:hep-ex/1601.02759v2.

[19] J. Elis, *Outstanding questions: physics beyond the Standard Model*, Phil. Trans. Roy. Soc. Lond. A **370**, 818 (2012).

[20] V. Gribov, B. Pontecorvo, *Neutrino astronomy and lepton charge*, Phys. Lett. B **28**, 493 (1969).

[21] D. Griffiths, *Introduction to elementary particles*, 2^{nd} ed., Wiley VCH-Verlag (2009).

[22] N. Arkani-Hamed, S. Dimopoulos, G.R. Dvali, *Phenomenology, astrophysics and cosmology of theories with submillimeter dimensions and TeV scale quantum gravity*, Phys. Rev., D **59**, 086004 (1999).

[23] J.G. Taylor, *A Review of supersymmetry and supergravity*, Prog. Part. Nucl. Phys. **12**, 1 (1984).

[24] J. Pati, A. Salam, *Unified lepton-hadron symmetry and a gauge theory of the basic interactions*, Phys. Rev. D **8**, 1240 (1973).

[25] S.P. Martin, *A supersymmetry primer*, arXiv:hep-ph/9709356v7.

[26] S. Raby, *Grand unified theories*, arXiv:hep-ph/0608183.

[27] P. Langacker, *Grand unified theories and proton decay*, Phys. Rept. **72**, 185 (1981).

[28] L.E. Ibanez, *Recent developments in physics far beyond the Standard Model*, arXiv:hep-ph/9901292.

[29] T. Weigand, *Introduction to string theory*, Skript Wintersemester 2011/12, Institut für theoretische Physik, Universität Heidelberg.

[30] G. Aldazabal, L.E. Ibanez, F. Quevedo, A.M. Uranga, *D-branes at singularities: a bottom-up approach to the string embedding of the Standard Model*, JHEP **0008**, 002 (2000).

[31] D. Lüst, *Intersecting brane worlds – a path to the Standard Model?*, Class. Quant. Grav. **21**, 1399 (2004).

[32] R. Essig, J.A. Jaros, W. Wester *et al.*, *Dark sectors and new, light, weakly-coupled particles*, arXiv:hep-ph/1311.0029.

[33] K. Benakli, *Phenomenology of low quantum gravity scale models*, Phys. Rev. D **60**, 104002 (1999).

[34] C.P. Burgess, L.E. Ibanez, F. Quevedo, *Strings at the intermediate scale, or is the Fermi scale dual to the Planck scale?*, Phys. Lett. B **447**, 257 (1999).

[35] T. Banks, M. Dine, *Couplings and scales in strongly coupled heterotic string theory*, Nucl. Phys. B **479**, 173 (1996).

[36] K. Choi, *Axions and the strong CP problem in M-theory*, Phys. Rev. D **56**, 6588 (1997).

[37] E. Witten, *Some properties of $O(32)$ superstrings*, Phys. Lett. B **149**, 351 (1984).

[38] N. Arkani-Hamed, S. Dimopoulos, G. Dvali, *Phenomenology, astrophysics and cosmology of theories with sub-millimeter dimensions and TeV scale quantum gravity*, Phys. Rev. D **59**, 086004 (1999).

[39] P.W. Graham, I.G. Irastorza, S.K. Lamoreaux, A. Lindner, K.A. van Bibber, *Experimental searches for the axion and axion-like particles*, Annual Review of Nuclear and Particle Science **65**, 485 (2015). ArXiv:hep-ex/1602.00039.

[40] M. Cicoli, M. Goodsell, A. Ringwald, *The type IIB string axiverse and its low-energy phenomenology*, JHEP **1210**, 146 (2012).

[41] B. Holdom, *Two $U(1)$'s and ϵ charge shifts*, Phys. Lett. B **166**, 196 (1986).

[42] L.B. Okun, *Limits on electrodynamics: paraphotons?*, Sov. Phys. JETP **56**, 502 (1982).

[43] S.A. Abel, J. Santiago, *Constraining the string scale: from Planck to Weak and back again*, J. Phys. G **30**, 83 (2004).

[44] V.A. Kostelecký, S. Samuel, *Spontaneous breaking of Lorentz symmetry in string theory*, Phys. Rev. D **39**, 683685 (1989).

[45] V.A. Kostelecký, R. Potting, *Expectation values, Lorentz invariance, and CPT in the open bosonic string*, Phys. Lett. B **381**, 89 (1996).

[46] Y. Tang, *Vacuum stability in the Standard Model*, Mod. Phys. Lett. A **28**, 1330002 (2013).

[47] K. Choi, J.E. Kim, *Harmful axions in superstring models*, Phys. Lett. B **154**, 393 (1985).

[48] C. Autermann, *Experimental status of supersymmetry after the LHC run-I*, Prog. Part. Nucl. Phys. **90**, 125 (2016).

[49] D.J.H. Chung, L.L. Everett, G.L. Kane, S.F. King, J. Lykken, L.-T. Wang, *The soft supersymmetry-breaking Lagrangian: theory and applications*, Phys. Rept. **407**, 1 (2005).

[50] M.J. Ramsey-Musolf, S. Su, *Low energy precision test of supersymmetry*, Phys. Rept. **456**, 1 (2008).

[51] V. Dzhunushaliev, D. Singleton, *Experimental test for extra dimensions in Kaluza-Klein gravity*, Gen. Rel. Grav. **32**, 271 (2000).

[52] J.A. Casas1, C.P. Martin, A.H. Vozmediano, *Experimental tests of extra dimensions*, Phys. Lett. B **186**, 29 (1987).

[53] D. Choudhury, K. Ghosh, *Bounds on universal extra dimension from LHC Run I and II data*, Phys. Lett. B **763**, 155 (2016).

[54] K. Mimasu, V. Sanz, *ALPs at colliders*, JHEP **1506**, 173 (2015).

[55] J. Jaeckel, M. Jankowiak, M. Spannowsky, *LHC probes the hidden sector*, Phys. Dark Univ. **2**, 111 (2013).

[56] A. Payez, C. Evoli, T. Fischer, M. Giannotti, A. Mirizzi, A. Ringwald, *Reviewing the SN 1987A gamma-ray limit on ultra-light axion-like particles*, JCAP 1502, 006 (2015).

[57] E. Chupp, T. Verstrand, C. Reppin, *Experimental limits on the radiative decay of SN 1987A neutrinos*, Phys. Rev. Lett. **62**, 505 (1989).

[58] V.A. Kostelecký, N. Russel, *Data tables for Lorentz and CPT violation*, Rev. Mod. Phys. **83**, 11 (2011). ArXiv:hep-ph/0801.0287v10.

[59] C.G. Parthey *et al.*, *Improved measurement of the hydrogen 1S-2S transition frequency*, Phys. Rev. Lett. **107**, 203001 (2011). ArXiv:physics/1107.3101.

[60] The ACME Collaboration, *Order of magnitude smaller limit on the electric dipole moment of the electron*, Science **343**, 269 (2014).

[61] F. Della Valle, E. Milotti, A. Ejlli, U. Gastaldi, G. Messineo, G. Zavattini, R. Pengo, G. Ruoso, *The PVLAS experiment: measuring vacuum magnetic birefringence and dichroism with a birefringent Fabry–Perot cavity*, Eur. Phys. J. C **76**, 24 (2016).

[62] E.G. Adelberger, *Torsion-balance probes of fundamental physics*, arXiv:hep-ex/1308.3213.

[63] W.A. Terrano, E.G. Adelberger, J.G. Lee, B.R. Heckel, *Short-range spin-dependent interactions of electrons: a probe for exotic pseudo-Goldstone bosons*, Phys. Rev. Lett **115**, 201801 (2015).

[64] D.J. Kapner, T.S. Cook, E.G. Adelberger, J.H. Gundlach, B.R. Heckel, C.D. Hoyle, H.E. Swanson, *Tests of the gravitational inverse-square law below the dark-energy length scale*, Phys. Rev. Lett. **98**, 021101 (2007).

[65] J. Jaeckel, A. Ringwald, *The low-energy frontier of particle physics*, Ann. Rev. Nucl. Part. Sci. **60**, 405 (2010).

[66] F.A. Gomes Ferreira, P.C. Malta, L.P.R. Ospedal, J.A. Helayël-Neto, *Topologically massive spin-1 particles and spin-dependent potentials*, Eur. Phys. J. C **75**, 232 (2015). ArXiv:hep-th/1411.3991v2.

[67] P.C. Malta, L.P.R. Ospedal, K. Veiga, J.A. Helayël-Neto, *Comparative aspects of spin-dependent interaction potentials for spin-1/2 and spin-1 matter fields*, Adv. High Energy Phys. **2016**, 2531436 (2016). ArXiv:hep-th/1510.03291v6.

[68] P.C. Malta, L.P.R. Ospedal, K. Veiga, J.A. Helayël-Neto, *Corrigendum for "Comparative aspects of spin-dependent interaction potentials for spin-1/2 and spin-1 matter fields"*, Adv. High Energy Phys. **2017**, 9152437 (2017). ArXiv:hep-th/1510.03291v6.

[69] J. Jaeckel, P.C. Malta, J. Redondo, *Decay photons from the ALP burst of type-II supernovae*. ArXiv:hep-ph/1702.02964.

[70] Y.M.P. Gomes, P.C. Malta, *Laboratory-based limits on the Carroll-Field-Jackiw Lorentz-violating electrodynamics*, Phys. Rev. D **94**, 025031 (2016). ArXiv:hep-ph/1604.01102v4.

[71] G.P. de Brito, J.T. Guaitolini Junior, D. Kroff, P.C. Malta, C. Marques, *Lorentz violation in simple QED processes*, Phys. Rev. D **94**, 056005 (2016). ArXiv:hep-ph/1605.08059v3.

[72] G.P. de Brito, P.C. Malta, L.P.R. Ospedal, *Spin- and velocity-dependent non-relativistic potentials in modified electrodynamics*, Phys. Rev. D **95**, 016006 (2017). ArXiv:hep-th/1612.01181v2.

[73] L.H. Ryder, *Quantum Field Theory*, Cambridge University Press, 2^{nd} edition (1996).

[74] S. Weinberg, *The quantum theory of fields, vol. 1*, Cambridge University Press (1995).

[75] O. Klein, *proceedings of the Symposium on "Les nouvelles theories de la physique"*, Warsaw (1938).

[76] F. Englert, R. Brout, *Broken symmetry and the mass of gauge vector mesons*, Phys. Rev. Lett. **13**, 321 (1964).

[77] G.S. Guralnik, C.R. Hagen, T.W.B. Kibble, *Global conservation laws and massless particles*, Phys. Rev. Lett. **13**, 585 (1964).

[78] P.W. Higgs, *Broken symmetry and the masses of gauge bosons*, Phys. Rev. Lett. **13**, 508 (1964).

[79] L. Susskind, *Dynamics of spontaneous symmetry breaking in the Weinberg-Salam theory*, Phys. Rev. D **20**, 2619 (1979).

[80] W.A. Bardeen, C.T. Hill, M. Lindner, *Minimal dynamical symmetry breaking of the standard model*, Phys. Rev. D **41**, 1647 (1990).

[81] Y. Nambu and G. Jona-Lasinio, *Dynamical model of elementary particles based on an analogy with superconductivity. I*, Phys. Rev. **122**, 345 (1961).

[82] Y. Nambu and G. Jona-Lasinio, *Dynamical model of elementary particles based on an analogy with superconductivity. II*, Phys. Rev. **124**, 246 (1961).

[83] T. Alanne, D.B. Franzosi, M.T. Frandsen, *Testing a dynamical origin of Standard Model fermion masses*. ArXiv:hep-ph/1607.01440.

[84] H. Gies, J. Jaeckel, C. Wetterich, *Towards a renormalizable standard model without fundamental Higgs scalar*, Phys. Rev. D **69**, 105008 (2004).

[85] E. Cremmer, J. Scherk, *Spontaneous dynamical breaking of gauge symmetry in dual systems*, Nucl. Phys. B **72**, 117 (1974).

[86] M. Kalb, P. Ramond, *Classical direct interstring action*, Phys. Rev. D **9**, 2273 (1974).

[87] C. Teitelboim, *Gauge invariance for extended objects*, Phys. Lett. B **167**, 63 (1986).

[88] C. Teitelboim, *Monopoles of higher rank*, Phys. Lett. B **167**, 69 (1986).

[89] S.J. Gates Jr., *Super p-form gauge superfields*, Nucl. Phys. B **184**, 381 (1981).

[90] P. Binétruy, G. Girardi, R. Grimm, *Supergravity couplings: a geometric formulation*, Phys. Rept. **343**, 255 (2001).

[91] B. de Wit, *Supergravity*, based on lectures presented at the 2001 Les Houches Summer School. ArXiv:hep-th/0212245v1.

[92] Winder Alexander de Moura Melo, *Abelian magnetic monopoles and quantization of the topological mass in (3 + 1) dimensions*, M.Sc. dissertation (in Portuguese), CBPF (1997).

[93] W.A. Moura-Melo, N. Panza, J.A. Helayël-Neto, *On massive vector bosons and Abelian magnetic monopoles in D = (3+1): a possible way to quantise the topological mass parameter*, Int. J. Mod. Phys. A **14**, 3949 (1999).

[94] T.J. Allen, M.J. Bowick, A. Lahiri, *Topological mass generation in 3+1 dimensions*, Mod. Phys. Lett. A **6**, 559 (1991).

[95] S. Kamefuchi, L. O' Raifeartaigh, A. Salam, *Change of variables and equivalence theorems in Quantum Field Theory*, Nuc. Phys. **28**, 529 (1961).

[96] C.N. Ferreira, J.A. Helayël-Neto, M.B.D.S.M. Porto, *Cosmic string configuration in the supersymmetric CSKR theory*, Nucl. Phys. B **620**, 181 (2002). ArXiv:hep-th/0101008v2.

[97] R.J. Rivers, *Lagrangean theory for neutral massive spin-2 fields*, Nuovo Cimento **34**, 387 (1964).

[98] R. Kuhfuss, J. Nitsch, *Propagating modes in gauge field theories of gravity*, Gen. Rel. Grav. **18**, 1207 (1986).

[99] D. Birmingham, M. Blau, M. Rakowski, G. Thompson, *Topological field theory*, Phys. Rept. **209**, 129 (1991).

[100] M. Leblanc, R. Manckenzie, P.K. Panigrahi, R. Ray, *Induced BF term and photon mass generation in $3+1$ dimensions*, Int. J. of Mod. Phys. A **9**, 4717 (1994).

[101] M.C. Diamantini, G. Guarnaccia, C.A. Trugenberger, *Gauge invariant photon mass induced by vortex gauge interactions*, J. Phys. A: Math. Theor. **47**, 092001 (2014).

[102] M.B. Cantcheff, *Doublet groups, extended Lie algebras, and well defined gauge theories for the two form field*, Int. J. Mod. Phys. A **20**, 2673 (2005).

[103] M.B. Cantcheff, *Two form gauge field theories and 'no go' for Yang-Mills relativistic actions*, Phys. Lett. B **581**, 119 (2004).

[104] E.G. Adelberger, B.R. Heckel, C.W. Stubbs, W.F. Rogers, *Searches for new macroscopic forces*, Ann. Rev. Nucl. Part. Sci. **41**, 269 (1991).

[105] E.G. Adelberger, B.R. Heckel, A.E. Nelson, *Tests of the gravitational inverse-square law*, Ann. Rev. Nucl. Part. Sci. **53**, 77 (2003).

[106] M.G. Tarallo, T. Mazzoni, N. Poli, D.V. Sutyrin, X. Zhang, G.M. Tino, *Test of Einstein equivalence principle for 0-spin and half-integer-spin atoms: search for spin-gravity coupling effects*, Phys. Rev. Lett. **113**, 023005 (2014). ArXiv:physics/1403.1161v2.

[107] J.E. Moody, Frank Wilczek, *New macroscopic forces?*, Phys. Rev. D **30**, 130 (1984).

[108] P. Fayet, *A new long-range force?*, Phys. Lett. B **171**, 261 (1986).

[109] B.R. Holstein, *Long range electromagnetic effects involving neutral systems and effective field theory*, Phys. Rev. D **78**, 013001 (2008).

[110] J.L. Hewett, T.G. Rizzo, *Low-energy phenomenology of Superstring-inspired E_6 models*, Phys. Rep. **183**, 193 (1989).

[111] A. Leike, *The phenomenology of extra neutral gauge bosons*, Phys. Rept. **317**, 143 (1999).

[112] P. Langacker, *The physics of heavy Z' gauge bosons*, Rev. Mod. Phys. **81**, 1199 (2009).

[113] B.A. Dobrescu, I. Mocioiu, *Spin-dependent macroscopic forces from new particle exchange*, J. High Energy Phys. **11**, 005 (2006).

[114] L. Hunter, J. Gordon, S. Peck, D. Ang, J.-F. Lin, *Using the Earth as a polarized electron source to search for long-range spin-spin interactions*, Science **339**, 928 (2013).

[115] M.P. Ledbetter, M.V. Romalis, D.F. Jackson Kimball, *Constraints on short-range spin-dependent interactions from scalar spin-spin coupling in deuterated molecular hydrogen*, Phys. Rev. Lett. **110**, 040402 (2013).

[116] B.R. Heckel, W.A. Terrano, E.G. Adelberger, *Limits on exotic long-range spin-spin interactions of electrons*, Phys. Rev. Lett. **111**, 151802 (2013).

[117] S. Kotler *et al.*, *Measurement of the magnetic interaction between two bound electrons of two separate ions*, Nature **510**, 376 (2014).

[118] Michele Maggiore, *A modern introduction to quantum field theory*, Oxford University Press (2005).

[119] B.R. Holstein, A. Ross, *Spin effects in long-range electromagnetic scattering.* ArXiv:hep-ph/0802.0715v1.

[120] B.R. Holstein, *Analytical on-shell calculation of low energy higher order scattering.* ArXiv:hep-ph/1609.00714.

[121] B.R. Holstein, A. Ross, *Spin effects in long-range gravitational scattering.* ArXiv:hep-th/0802.0716.

[122] G. Feinberg, J. Sucher, C.-K. Au, *The dispersion theory of dispersive forces*, Phys. Rep. **180**, 83 (1989).

[123] D. Cocuroci, M.J. Neves, L.P.R. Ospedal, J.A. Helayël-Neto, *A 3-form Gauge Potential in 5D in connection with a Possible Dark Sector of 4D-Electrodynamics*, Eur. Phys. J. C **75**, 322 (2015). ArXiv:hep-th/1311.6735v4.

[124] T.M. Leslie, J.C. Long, *Prospects for electron spin-dependent short-range force experiments with rare earth iron garnet test masses*, Phys. Rev. D **89**, 114022 (2014).

[125] J.L. Feng, B. Fornal, I. Galon, S. Gardner, J. Smolinsky, T.M.P. Tait, P. Tanedo, *Particle physics models for the 17 MeV anomaly in beryllium nuclear decays*, arXiv:hep-ph/1608.03591v1.

[126] A. Krasznahorkay *et al.*, *Observation of anomalous internal pair creation in Be8: a possible indication of a light, neutral boson*, Phys. Rev. Lett. **116**, 042501 (2016). ArXiv:nucl-ex/1504.01527.

[127] G. Vasilakis, J. M. Brown, T.W. Kornack, M.V. Romalis, *Limits on new long range nuclear spin-dependent forces set with a $K-^3He$ comagnetometer*, Phys. Rev. Lett. **103**, 261801 (2009).

[128] S. Mantry, M. Pitschmann, M.J. Ramsey-Musolf, *Distinguishing axions from generic light scalars using EDM and fifth-force experiments*, Phys. Rev. D **90**, 054016 (2014). ArXiv:hep-ph/1401.7339.

[129] A. Salam, P.T. Matthews, *The renormalization of meson theories*, Rev. Mod. Phys. **23**, 311 (1951).

[130] A. Salam, *Renormalized S-matrix for scalar electrodynamics*, Phys. Rev. **86**, 731 (1952).

[131] A. Salam, *Renormalization of scalar electrodynamics using β-formalism*, Proc. Royal Soc. London A **211**, 276 (1952).

[132] A. Salam, A. Komar, *Renormalization problem for vector meson theories*, Nucl. Phys. **21**, 624 (1960).

[133] A. Salam, *Renormalizability of gauge theories*, Phys. Rev. **127**, 331 (1962).

[134] A. Salam, *Renormalizable electrodynamics of vector mesons*, Phys. Rev. **130**, 1287 (1963).

[135] T.D. Lee, C.N. Yang, *Theory of charged and vector mesons interacting with the electromagnetic field*, Phys. Rev. **128**, 885 (1962).

[136] A. Salam, R. Delbourgo, *Renormalizable electrodynamics of scalar and vector mesons. II*, Phys. Rev. B **135**, 1398 (1964).

[137] K.H. Tzou, *Covariant electrodynamics of charged mesons of spin one with arbitrary anomalous magnetic moment*, Il Nuovo Cim. **33**, 286 (1964).

[138] H. Aronson, *Spin-1 electrodynamics with an electric quadrupole moment*, Phys. Rev. **186**, 1434 (1969).

[139] G. Velo, D. Zwanziger, Noncausality and other defects of interaction Lagrangeans for partciles with spin one and higher, Phys. Rev. **188**, 2218 (1969).

[140] M. Gomez-Bock *et al.*, *Concepts of electroweak symmetry breaking and Higgs physics*, arXiv:hep-ph/0712.2419.

[141] J.F. Nieves, P.B. Pal, *Electromagnetic properties of neutral and charged spin-1 particles*, Phys. Rev. D **55**, 3118 (1997).

[142] A.J. Silenko, *Analysis of wave equations for spin-1 particles interacting with an electromagnetic field*, arXiv:hep-th/0404074.

[143] A.J. Silenko, *The motion of particle spin in a nonuniform electromagnetic field*, J. Exp. Theor. Phys. **96**, 775 (2003).

[144] A.J. Silenko, *Polarization of spin-1 particles in a uniform magnetic field*, Eur. Phys. J. C **57**, 595 (2008).

[145] A.J. Silenko, *Quantum mechanical description of spin-1 particles with electric dipole moments*, Phys. Rev. D **87**, 073015 (2013).

[146] A. Ross, B.R. Holstein, *Spin effects in the effective quantum field theory of general relativity*, J. Phys. A: Math. Theor. **40**, 6973 (2007).

[147] E.G. Delgado-Acosta *et al.*, *Electromagnetic multipole moments of elementary spin-1/2 and -3/2 particles*, Phys. Rev. D **85**, 116006 (2012).

[148] E.G. Delgado-Acosta *et al.*, *Compton scattering off massive fundamental bosons of pure spin-1*, Phys. Rev. D **87**, 096010 (2013).

[149] M. Napsuciale, S. Goméz-Ávila, *Parity-based formalism for high spin matter fields*, arXiv:hep-ph/1309.0968.

[150] N.E.J. Bjerrum-Bohr, B.R. Holstein, L. Planté, P. Vanhove, *Graviton-photon scattering*, Phys. Rev. D **91**, 064008 (2015).

[151] L.R. Hunter, D.G. Ang, *Using geoelectrons to search for velocity-dependent spin-spin interactions*, Phys. Rev. Lett. **112**, 091803 (2009).

[152] M. Agnello *et al.*, *Evidence for heavy hyperhydrogen HΛ6*, Phys. Rev. Lett. **108**, 042501 (2012).

[153] T.O. Yamamoto *et al.*, *Observation of spin-dependent charge symmetry breaking in ΛN interaction: γ-ray spectroscopy of HeΛ4*, Phys. Rev. Lett. **115**, 222501 (2015).

[154] F. London, H. London, *The elecromagnetic equations of the superconductor*, Proc. R. Soc. London A **149**, 71 (1935).

[155] M. Napsuciale, S. Rodríguez, R. Ferro-Hernández, S. Gómez-Ávila, *Spin one matter fields*, arXiv:hep-ph/1509.07938.

[156] W. Gordon, *Der Strom der Diracschen Elektronentheorie*, Z. Phys. **50**, 630 (1928).

[157] D.G. Boulware, *Renormalizability of massive non-Abelian gauge fields: a functional integral approach*, Ann. of Phys. **56**, 140 (1970).

[158] C. Itzykson, J.B. Zuber, *Quantum field theory*, McGraw-Hill, New York (1980).

[159] S. Ferrara, M. Porrati, V. Teledgi, *$g = 2$ as a natural value of the tree-level gyromagnetic ratio of elementary particles*, Phys. Rev. D **46**, 3529 (1992).

[160] R. Jackiw, *$g = 2$ as a gauge condition*, Phys. Rev. D **57**, 2635 (1998).

[161] S. Fidelman *et al.*, *Review of particle physics*, Phys. Lett. B **592**, 1 (2004).

[162] G.W.F. Drake (ed.), *Springer handbook of atomic, molecular and optical physics*, Springer Ed. (2006).

[163] O. Hashimoto, H. Tamura, *Spectroscopy of Λ hypernuclei*, Prog. Part. Nucl. Phys. **57**, 564 (2006).

[164] P.A.M. Dirac, *An extensible model of the electron*, Proc. R. Soc. London A **268**, 57 (1962).

[165] L. Fabbri, *A classical calculation of the leptonic magnetic moment*, Int. J. Theor. Phys. **55**, 669 (2016).

[166] S. Dain, *Bekenstein bounds and inequalities between size, charge, angular momentum and energy for bodies*, Phys. Rev. D **92**, 044033 (2015).

[167] D. Bernard, *On the potential of light-by-light scattering for invisible axion detection*, Nucl. Phys. Proc. Suppl. **72**, 201 (1999).

[168] M. Cicoli, *Axion-like particles from string compactifications*, arXiv:hep-th/1309.6988.

[169] M.E. Peskin, D.V. Schroeder, *An introduction to quantum field theory*, Westview Press (2005).

[170] T.-P. Cheng, L.-F. Li, *Gauge theory of elementary particle physics*, Oxford University Press (2002).

[171] S. Weinberg, *The U(1) problem*, Phys. Rev. D **11**, 3583 (1975).

[172] M. Creutz, *Anomalies and chiral symmetry in QCD*, Annals Phys. **324**, 1573 (2009). ArXiv:hep-ph/0901.0150.

[173] R.D. Peccei, *The strong CP problem and axions*, Lect. Notes Phys. **741**, 3 (2008). ArXiv:hep-ph/0607268.

[174] G.L. Glashow, R. Jackiw, S.-S. Shei, *Electromagnetic decays of pseudoscalar mesons*, Phys. Rev. **187**, 1916 (1969).

[175] S.L. Adler, *Axial-vector vertex in spinor electrodynamics*, Phys. Rev. **177**, 2426 (1969).

[176] W.A. Bardeen, *Anomalous Ward identities in spinor field theories*, Phys. Rev. **184** 1848 (1969).

[177] W.A. Bardeen, *Anomalous currents in gauge field theories*, Nucl. Phys. B **75**, 246 (1974).

[178] G. 't Hooft, *Symmetry breaking through Bell-Jackiw anomalies*, Phys. Rev. Lett. **37**, 8 (1976).

[179] G. 't Hooft, *Computation of the quantum effects due to a four-dimensional pseudoparticle*, Phys. Rev. D **14**, 3432 (1976).

[180] G. 't Hooft, *How instantons solve the $U(1)$ problem*, Phys. Rep. **142**, 357 (1986).

[181] E. Vicari, H. Panagopoulos, *Theta dependence of SU(N) gauge theories in the presence of a topological term*, Phys. Rep. **470**, 93 (2009).

[182] R.J. Crewhter, P. Di Vecchia, G. Veneziano, E. Witten, *Chiral estimate of the electric dipole moment of the neutron in quantum chromodynamics*, Phys. Lett. B **88**, 123 (1979).

[183] R.D. Peccei, H.R. Quinn, *CP conservation in the presence of instantons*, Phys. Rev. Lett. **38**, 1440 (1977).

[184] S. Weinberg, *A new light boson?*, Phys. Rev. Lett. **40**, 223 (1978).

[185] F. Wilczek, *Problem of strong P and T invariance in the presence of instantons*, Phys. Rev. D **40**, 279 (1978).

[186] C.G. Callan, R.F. Dashen, D.J. Gross, *Toward a theory of the strong interactions*, Phys. Rev. D **17**, 2717 (1978).

[187] C.G. Callan, R.F. Dashen, D.J. Gross, *A theory of hadronic structure*, Phys. Rev. D **19**, 1826 (1979).

[188] W.A. Bardeen, S.H.H. Tye, *Current algebra applied to properties of the light Higgs boson*, Phys. Lett. B **74**, 580 (1978).

[189] W.A. Bardeen, R.D. Peccei, T. Yanagida, *Constraints on variant axion models*, Nucl. Phys. B **279**, 401 (1987).

[190] H.Y. Cheng, *The strong CP problem revisited*, Phys. Rept. *158*, 1 (1988).

[191] G.G. Raffelt, *Astrophysical methods to constrain axions and other novel particle phenomena*, Phys. Rept. **198**, 1 (1990).

[192] J.E. Kim, *Light pseudoscalars, particle physics and cosmology*, Phys. Rept. **150**, 1 (1987).

[193] J.E. Kim, *Weak interaction singlet and strong CP invariance*, Phys. Rev. Lett. **43**, 103 (1979).

[194] M.A. Shifman, A.I. Vainshtein, V.I. Zakharov, *Can confinement ensure natural CP invariance of strong interactions?*, Nucl. Phys. B **166**, 493 (1980).

[195] M. Dine, W. Fischler, M. Srednicki, *A simple solution to the strong CP problem with a harmless axion*, Phys. Lett. B **104**, 199 (1981).

[196] A. R. Zhitnitsky, *On possible suppression of the axion hadron interactions*, Sov. J. Nucl. Phys. **31**, 260 (1980).

[197] F. Zwicky, *On the masses of nebulae and of clusters of nebulae*, Astrophys. J. **86**, 217 (1937).

[198] H.W. Babcock, *The rotation of the Andromeda Nebula*, Lick Observatory Bulletin **19**, 41 (1939).

[199] D. Clowe, M. Bradac, A.H. Gonzalez, M. Markevitch, S.W. Randall, *et al.*, *A direct empirical proof of the existence of dark matter*, Astrophys. J. **648**, L109-113 (2006).

[200] G. Bertone, D. Hooper, J. Silk, *Particle dark matter: evidence, candidates and constraints*, Phys. Rept. **405**, 279 (2005).

[201] J. Einasto, *Dark matter*, Astronomy and Astrophysics 2010, eds. Oddbjorn Engvold, Rolf Stabell, Bozena Czerny, John Lattanzio, in Encyclopedia of Life Support Systems (EOLSS), developed under the Auspices of the UNESCO, Eolss Publishers, Oxford ,UK. ArXiv:astro-ph.CO/0901.0632v2.

[202] G. Bertone, D. Hooper, *A history of dark matter*, arXiv:astro-ph/1605.04909v2.

[203] J.A.R. Cembranos, *Modified gravity and dark matter*, arXiv:hep-ph/1512.08752v1.

[204] T. Clifton, P.G. Ferreira, A. Padilla, C. Skordis, *Modified gravity and cosmology*, Phys. Rep. **513**, 1 (2012).

[205] M. Milgrom, J. Bekenstein, *The modified Newtonian dynamics as an alternative to hidden matter*, in Dark Matter in the Universe (IAU Symposium No. 117), Eds. J. Kormendy and G.R. Knapp, p. 319-330, Dordrecht (1987).

[206] G.W. Angus, H. Shan, H. Zhao, B. Famaey, *On the law of gravity, the mass of neutrinos and the proof of dark matter*, Astrophys. J. **654**, L13-L16 (2007).

[207] L.D. Duffy, K. van Bibber, *Axions as dark matter particles*, New J. Phys. **11**, 105008 (2009). ArXiv:hep-ph/0904.3346.

[208] D.J.E. Marsh, *Axion cosmology*, Phys. Rep. **643**, 1-79 (2016). ArXiv:astro-ph.CO/1510.07633v2.

[209] M. Taoso, G. Bertone, A. Masiero, *Dark matter candidates: a ten-point test*, JCAP **0803**, 022 (2008).

[210] P. Sikvie, *Axion cosmology*, Lect. Notes Phys. **741**, 19 (2008).

[211] H. Primakoff, *Photo-production of neutral mesons in nuclear electric fields and the mean life of the neutral meson*, Phys. Rev. **81**, 899 (1951).

[212] D.A. Dicus, E.W. Kolb, V.L. Teplitz, R.V. Wagoner, *Astrophysical bounds on the masses of axions and Higgs particles*, Phys. Rev. D **18**, 1829 (1978).

[213] J. Redondo, A. Ringwald, *Light shining through walls*, Contemp. Phys. **52**, 211-236 (2011).

[214] R. Ballou *et al.* (OSQAR Collaboration), *New exclusion limits on scalar and pseudoscalar axionlike particles from light shining through a wall*, Phys. Rev. D **92**, 092002 (2015).

[215] G.G. Raffelt, *Stars as laboratories for fundamental physics*, University of Chicago Press (1996).

[216] J. Jaeckel, *Axions, their relatives and prospects for the future*, J. Phys. Conf. Ser. **65**, 012008 (2007). ArXiv:hep-ph/0702060.

[217] A. Ayala, I. Domínguez, M. Giannotti, A. Mirizzi, O. Straniero, *Revisiting the bound on axion-photon coupling from globular clusters*, Phys. Rev. Lett. **113**, 191302 (2014).

[218] N. Viaux, M. Catelan, P. B. Stetson, G. G. Raffelt, J. Redondo, A. A. R. Valcarce, A. Weiss, *Neutrino and axion bounds from the globular cluster M5 (NGC 5904)*, Phys. Rev. Lett. **111**, 231301 (2013).

[219] A. Ringwald, *Exploring the role of axions and other WISPs in the dark universe*, Phys. Dark Univ. **1**, 116 (2012).

[220] C. Coriano, N. Irges, *Windows over a new low-energy axion*, Phys. Lett. B **651**, 298 (2007).

[221] A.G. Dias, A.C.B. Machado, C.C. Nishi, A. Ringwald, P. Vaudrevange, *The quest for an intermediate-scale accidental axion and further ALPs*, JHEP **1406**, 037 (2014).

[222] A. Arvanitaki, S. Dimopoulos, S. Dubovsky, N. Kaloper, J. March-Russell, *String axiverse*, Phys. Rev. D **81**, 123530 (2010).

[223] A. Ringwald, *Axions and axion-like particles*, arXiv:hep-ph/1407.0546v1.

[224] A. Dar, S. Dado, *Constraints on the lifetime of massive neutrinos from SN1987A*, Phys. Rev. Lett. **59**, 2368 (1987).

[225] S. Dutta, A. Goyal, *Constraints on astro-unparticle physics from SN 1987A*, JCAP **0803**, 027 (2008).

[226] J. Ellis, K.A. Olive, S. Sarkar, D.W. Sciama, *Low mass photinos and supernova SN 1987A*, Phys. Lett. B **215**, 404 (1988).

[227] G.G. Raffelt, *Astrophysical axion bounds*, Lect. Notes Phys. **741**, 51-71 (2008).

[228] G.G. Raffelt, L. Stodolsky, *Mixing of the photon with low mass particles*, Phys. Rev. D **37**, 1237 (1988).

[229] P. Sikvie, *Experimental tests of the invisible axion*, Phys. Rev. Lett. **51**, 1415 (1983). Erratum-*ibid* **52**, 695 (1984).

[230] J.W. Brockway, E.D. Carlson, G.G. Raffelt, *SN 1987A gamma-ray limits on the conversion of pseudoscalars*, Phys. Lett. B **383**, 439 (1996).

[231] J. A. Grifols, E. Masso, R. Toldra, *Gamma rays from SN 1987A due to pseudoscalar conversion*, Phys. Rev. Lett. **77**, 2372 (1996).

[232] A. De Angelis, M. Roncadelli, O. Mansutti, *Evidence for a new light spin-zero boson from cosmological gamma-ray propagation?*, Phys. Rev. D **76**, 121301 (2007).

[233] M. Simet, D. Hooper, P.D. Serpico, *The Milky Way as a kiloparsec-scale axionscope*, Phys. Rev. D **77**, 063001 (2008).

[234] D. Hooper, P.D. Serpico, *Detecting axion-like particles with gamma ray telescopes*, Phys. Rev. Lett. **99**, 231102 (2007).

[235] M. Giannotti, L.D. Duffy, R. Nita, *New constraints for heavy axion-like particles from supernovae*, JCAP 01, 015 (2011).

[236] D. Cadamuro, J. Redondo, *Cosmological bounds on pseudo Nambu-Goldstone bosons*, JCAP 02, 032 (2012).

[237] S.E. Woosley, A. Heger, T.A. Weaver, N. Langer, *SN 1987A - presupernova evolution and the progenitor star*, "SN 1987A: ten years later", eds. M.M. Philips and N.B. Suntzeff, PASPC. Arxiv:astro-ph/9705.146v1.

[238] A. Burrows, *Perspectives on core-collapse supernova theory*, Rev. Mod. Phys. **85**, 245 (2013).

[239] S.E. Woosley, A. Heger, T.A. Weaver, *The evolution and explosion of massive stars*, Rev. Mod. Phys. **74**, 1015 (2002).

[240] A. Dar, *Supernova 1987A - ten years after*. ArXiv:hep-ph/9707501.

[241] D. Kazanas, R.N. Mohapatra, S. Nussinov, V.L. Teplitz, Y. Zhang, *Supernova bounds on the dark photon using its electromagnetic decay*, Nuc. Phys. B **17**, 890 (2015).

[242] J. von Neumann, *Various techniques used in connection with random digits (Monte Carlo methods)*, Nat. Bureau Standards **12**, 36 (1951).

[243] R.M. Bionta, G. Blewitt, C.B. Bratton, D. Casper, A. Ciocio, R. Claus, B. Cortez, M. Crouch *et al.*, *Observation of a neutrino burst in coincidence with supernova SN 1987A in the Large Magellanic Cloud*, Phys. Rev. Lett. **58**, 1494 (1987).

[244] K. Hirata *et al.* (Kamiokande-II Collaboration), *Observation of a neutrino burst from the supernova SN 1987A*, Phys. Rev. Lett. **58**, 1490 (1987).

[245] E.N. Alekseev, L.N. Alekseeva, V.I. Volchenko, I.V. Krivosheina, *Possible detection of a neutrino signal on 23 February 1987 at the Baksan Underground Scintillation Telescope of the Institute of Nuclear Research*, JETP Lett. **45**, 589 (1987).

[246] N. Panagia, *SN 1987A: The Unusual explosion of a normal type II supernova*, ASP Conf. Ser. **342**, 78 (2005).

[247] M. Meyer, M. Giannotti, A. Mirizzi, J. Conrad, M. Sanchez-Conde, *The Fermi Large Area Telescope as a galactic supernovae axionscope*, arXiv:astro-ph.HE/1609.02350.

[248] M.M. Dolan, G.J. Mathews, D.D. Lam, N.Q. Lan, G.J. Herczeg, D.S.P. Dearborn, *Evolutionary tracks for Betelgeuse*, arXiv:astro-ph.SR/1406.3143v2.

[249] S.J. Smartt, *Progenitors of core-collapse supernovae*, Annual Review of Astronomy and Astrophysics **47**, 63 (2009).

[250] Fermi/LAT Collaboration, *The large area telescope on the Fermi gamma-ray space telescope mission*, Astrophys. J. **697**, 1071 (2009).

[251] V. Tatischeff, *et al.*, *The e-ASTROGAM gamma-ray space mission*, Proc. SPIE **9905**, Space Telescopes and Instrumentation 2016: Ultraviolet to Gamma Ray, 99052N, 2016. Arxiv:astro-ph.IM/1608.03739v2.

[252] A.A. Moiseev, *et al.*, *Compton-pair production space telescope (ComPair) for MeV gamma-ray astronomy*, arxiv:astro-ph.IM/1508.07349v2.

[253] X. Wu, *et al.*, *PANGU: a high resolution gamma-ray space telescope*, Proc. SPIE **9144**, Space Telescopes and Instrumentation 2014: Ultraviolet to Gamma Ray, 91440F, 2014. Arxiv:astro-ph.IM/1407.0710v2.

[254] J. Redondo, *Bounds on very weakly interacting sub-eV particles (WISPs) from cosmology and astrophysics*. Arxiv:hep-ph/0810.3200.

[255] S. Alekhin *et al.*, *A facility to search for hidden particles at the CERN SPS: the SHiP physics case*, Rept. Prog. Phys. **79**, 124201 (2016).

[256] J. Jaeckel, M. Spannowsky, *Probing* MeV *to 90* GeV *axion-like particles with LEP and LHC*, Phys. Lett. B **753**, 482 (2016).

[257] J.L. Hewett *et al.*, *Fundamental physics at the intensity frontier*. ArXiv:hep-ex/1205.2671.

[258] M. Millea, L. Knox, B. Fields, *New bounds for axions and axion-like particles with keV-GeV masses*, Phys. Rev. D **92**, 023010 (2015).

[259] B. Dobrich, J. Jaeckel, F. Kahlhoefer, A. Ringwald, K. Schmidt-Hoberg, *ALP-traum: ALP production in proton beam dump experiments*, JHEP **1602**, 018 (2016).

[260] A. Einstein, *Does the inertia of a body depend on its energy content?*, Ann. der Physik **17**, 981 (1905).

[261] A.A. Michelson, E.W. Morley, *On the relative motion of the Earth and the luminiferous ether*, Am. J. Sci. **34**, 333 (1887).

[262] R.J. Kennedy, E.M. Thorndike, *Experimental establishment of the relativity of time*, Phys. Rev. **42**, 400 (1932).

[263] S. Liberati, *Tests of Lorentz invariance: a 2013 update*, Class. Quant. Grav. **30**, 133001 (2013).

[264] D. Mattingly, *Modern tests of Lorentz invariance*, Living Rev. Relativity **8**, 5 (2005).

[265] OPERA Collaboration, *Measurement of the neutrino velocity with the OPERA detector in the CNGS beam*, arXiv:hep-ex/1109.4897v1.

[266] "Neutrinos sent from CERN to Gran Sasso respect the cosmic speed limit". CERN press release. June 8, 2012. Retrieved June 8, 2012.

[267] I. Mocioiu, M. Pospelov, R. Roiban, *Breaking CPT by mixed non-commutativity*, Phys. Rev. D **65**, 107702 (2002).

[268] R. Gambini, J. Pullin, *Nonstandard optics from quantum space-time*, Phys. Rev. D **59**, 124021 (1999).

[269] N.E. Mavromatos, *Probing Lorentz violating (stringy) quantum space-time foam*, AIP Conf. Proc. 1196, 169 (2009). ArXiv:hep-th/0909.2319v1.

[270] N.E. Mavromatos, *Lorentz invariance violation from string theory*, PoS QG-PH **027** (2007). ArXiv:hep-th/0708.2250.

[271] D. Colladay, *Possible spontaneous breaking of Lorentz and CPT symmetry*, Phys. Atom. Nucl. **63**, 1097 (2000).

[272] R. Bluhm, V.A. Kostelecký, *Spontaneous Lorentz violation, Nambu-Goldstone modes, and gravity*, Phys. Rev. D **71**, 065008 (2005).

[273] R. Bluhm, S.-H. Fung, V.A. Kostelecký, *Spontaneous Lorentz and diffeomorphism violation, massive modes, and gravity*, Phys. Rev. D **77**, 065020 (2008).

[274] V.A. Kostelecký, R. Potting, *Gravity from local Lorentz violation*, Gen. Rel. Grav. **37**, 1675 (2005).

[275] R. Lehnert, *CPT- and Lorentz-symmetry breaking: a review*, arXiv:hep-ph/0611177.

[276] R.M. Barnett *et al.*, *Review of particle properties*, Phys. Rev. D **54**, 1 (1996).

[277] R. Jost, *Eine Bemerkung zum CPT*, Helv. Phys. Acta **30**, 409 (1957).

[278] V.A. Kostelecký, R. Potting, *CPT, strings, and the $K-\bar{K}$ system*, arXiv:hep-th/9211116v1.

[279] O.W. Greenberg, *CPT violation implies violation of Lorentz invariance*, Phys. Rev. Lett. **89**, 231602 (2002).

[280] M. Chaichian, A.D. Dolgov, V.A. Novikov, A. Tureanu, *CPT violation does not lead to violation of Lorentz invariance and vice versa*, arXiv:hep-th:1103.0168v2.

[281] K. Fujikawa, A. Tureanu, *Lorentz invariant CPT breaking in the Dirac equation*. ArXiv:hep-ph/1607.01409.

[282] J.D. Tasson, *What do we know about Lorentz invariance?*, Rep. Prog. Phys. **77**, 062901 (2014).

[283] A. Ashtekar, V. Petkov (eds.), *Springer handbook of spacetime*, Springer Ed. (2014).

[284] T.H. Bertschinger, Natasha A. Flowers, Jay D. Tasson, *Observer and particle transformations and Newton's laws*, arXiv:hep-ph/1308.6572.

[285] R. Bluhm, V.A. Kostelecký, C.D. Lane, N. Russell, *Probing Lorentz and CPT violation with space-based experiments*, Phys. Rev. D **68**, 125008 (2003).

[286] V.A. Kostelecký, M. Mewes, *Signals for Lorentz violation in electrodynamics*, Phys. Rev. D **66**, 056005 (2002).

[287] D. Colladay, V.A. Kostelecký, *Lorentz-violating extension of the standard model*, Phys. Rev. D **58**, 116002 (1998).

[288] D. Colladay, V.A. Kostelecký, *CPT violation and the Standard Model*, Phys. Rev. D **55**, 6760 (1997).

[289] R.B. Mann, U. Sarkar, *Superluminal neutrinos at the OPERA?*, arXiv:hep-ph:1109.5749v2.

[290] D. Colladay, P. McDonald, D. Mullins, *Factoring the dispersion relation in the presence of Lorentz violation*, J. Phys. A **43**, 275202 (2010).

[291] T.D. Gutierrez, *Schrödinger-Pauli equation for the Standard Model extension CPT-violating Dirac equation*. ArXiv:hep-th/1504.01417.

[292] A. Fittante, N. Russel, *Fermion observables for Lorentz violation*, J. Phys. G: Nucl. Part. Phys. **39**, 125004 (2012).

[293] C. Adam, F.R. Klinkhamer, *Causality and radiatively induced CPT violation*, Phys. Lett. B **513**, 245 (2001).

[294] S. Coleman, S.L. Glashow, *High-energy tests of Lorentz invariance*, Phys. Rev. D **59**, 116008 (1999).

[295] V.A. Kostelecký, R. Lehnert, *Stability, causality, and Lorentz and CPT violation*, Phys. Rev. D **63**, 065008 (2001).

[296] R. Lehnert, *Non-local on-shell field redefinition for the SME*, Phys. Rev. D **74**, 125001 (2006).

[297] D. Colladay, V.A. Kostelecký, *Cross sections and Lorentz violation*, Phys. Lett. B **511**, 209 (2001).

[298] R. Casana, M.M. Ferreira Jr, A.R. Gomes, P.R.D. Pinheiro, *Gauge propagator and physical consistency of the CPT-even part of the Standard Model Extension*, Phys. Rev. D **80**, 125040 (2009).

[299] R. Casana, M.M. Ferreira Jr, A.R. Gomes, F.E.P. dos Santos, *Feynman propagator for the nonbirefringent CPT-even electrodynamics of the Standard Model Extension*, Phys. Rev. D **82**, 125006 (2010).

[300] M. Schreck, *Analysis of the consistency of parity-odd nonbirefringent modified Maxwell theory*, Phys. Rev. D **86**, 065038 (2012).

[301] V.A. Kostelecký (ed.), *Proceedings of the fifth meeting on CPT and Lorentz symmetry*, 28 June - 2 July (2010), World Scientific Ed..

[302] V.A. Kostelecký, M. Mewes, *Electrodynamics with Lorentz-violating operators of arbitrary dimension*, Phys. Rev. D **80**, 015020 (2009).

[303] J.B. Araujo, R. Casana, M.M. Ferreira Jr, *Constraining CPT-even and Lorentz-violating nonminimal couplings with the electron magnetic and electric dipole moments*, Phys. Rev. D **92**, 025049 (2015).

[304] H. Belich, L.P. Colatto, T. Costa-Soares, J.A. Helayël-Neto, M.T.D. Orlando, *Magnetic moment generation from non-minimal couplings in a scenario with Lorentz-Symmetry Violation*, Eur. Phys. J. C **62**, 425-432 (2009).

[305] K. Bakke, E. O. Silva, H. Belich, *He–McKellar–Wilkens effect and scalar Aharonov–Bohm effect for a neutral particle based on the Lorentz symmetry violation*, Journal of Physics G: Nuclear and Particle Physics **39**, 055004 (2012).

[306] H. Belich, T. Costa-Soares, M.M. Ferreira Jr., J.A. Helayël-Neto, *Non-minimal coupling to a Lorentz-violating background and topological implications*, Eur. Phys. J. C **41**, 421 (2005).

[307] R. Potting, *Gravity from breaking of local Lorentz symmetry* , J. Phys. Conf. Ser. **171**, 012041 (2009). ArXiv:hep-th/0904.0364.

[308] B.M. Roberts, Y.V. Stadnik, V.A. Dzuba, V.V. Flambaum, N. Leefer, D. Budker, *Limiting P-odd interactions of cosmic fields with electrons, protons and neutrons*, Phys. Rev. Lett. **113**, 081601 (2014).

[309] B.R. Heckel, E.G. Adelberger, C.E. Cramer, T.S. Cook, S. Schlamminger, U. Schmidt, *Preferred-frame and CP-violation tests with polarized electrons*, Phys. Rev. D **78**, 092006 (2008).

[310] M. Nagel, S.R. Parker, E.V. Kovalchuk, P.L. Stanwix, J.G. Hartnett, E.N. Ivanov, A. Peters, M.E. Tobar, *Direct terrestrial test of Lorentz symmetry in electrodynamics to* 10^{-18}, Nature Communications **6**, 8174 (2015).

[311] S.M. Carroll, G.B. Field, R. Jackiw, *Limits on Lorentz- and parity-violating modification of electrodynamics*, Phys. Rev. D **41**, 1231 (1990).

[312] S.S. Chern, J. Simons, *Characteristic forms and geometric invariants*, Ann. Math. **99**, 48 (1974).

[313] Y. Itin, *Wave propagation in axion electrodynamics*, Gen. Rel. Grav. **40**, 1219-1238 (2008).

[314] S.M. Carroll, G.B. Field, *Is there evidence for cosmic anisotropy in the polarization of distant radio sources?*, Phys. Rev. Lett. **79**, 2394 (1997).

[315] R. Jackiw, V.A. Kostelecký, *Radiatively induced Lorentz and CPT violation in electrodynamics*, Phys. Rev. Lett. **82**, 3572 (1999).

[316] M. Chaichian, W.F. Chen, R. Gonzalez Felipe, *Radiatively induced Lorentz and CPT violation in Schwinger constant field approximation*, Phys. Lett. B **503**, 215 (2001).

[317] J.-M. Chung, B.K. Chung, *Induced Lorentz- and CPT-violating Chern-Simons term in QED: Fock-Schwinger proper time method*, Phys. Rev. D **63**, 105015 (2001).

[318] L.-H. Chan, *Induced Lorentz-violating Chern-Simons term in QED and anomalous contributions to effective action expansions.* ArXiv:hep-ph/9907349v2.

[319] J.-M. Chung, P. Oh, *Lorentz and CPT violating Chern-Simons term in the derivative expansion of QED*, Phys. Rev. D **60**, 067702 (1999).

[320] M. Pérez-Victoria, *Exact calculation of the radiatively-induced Lorentz and CPT violation in QED*, Phys. Rev. Lett. **83**, 2518-2521 (1999).

[321] R. Ferrari, M. Raciti, *On effective Chern-Simons term induced by a local CPT-violating coupling using γ_5 in dimensional regularization.* ArXiv:hep-th/1510.04666v1.

[322] R. Jackiw, *When radiative corrections are finite but undetermined*, Int. J. Mod. Phys. B **14**, 2011 (2000).

[323] C. Wang, *Electromagnetic power flow, Fermat's principle, and special theory of relativity*, Optik **126**, 2703-2705 (2015).

[324] M.M. Ferreira Jr, R. Casana, C.E.H. Santos, *Classical solutions for the Carroll-Field-Jackiw-Proca electrodynamics*, Phys. Rev. D **78**, 025030 (2008).

[325] C. Adam, F.R. Klinkhamer, *Causality and CPT violation from an Abelian Chern-Simons-like term*, Nucl. Phys. B **607**, 247-267 (2001).

[326] A.P. Baêta Scarpelli, H. Belich, J.L. Boldo, J.A. Helayël-Neto, *Aspects of causality and unitarity and comments on vortexlike configurations in an Abelian model with a Lorentz-breaking term*, Phys. Rev. D **67**, 085021 (2003).

[327] M. Goldhaber, V. Trimble, *Limits on the chirality of interstellar and intergalactic space*, J. Astrophys. Astron. **17**, 17 (1996).

[328] V.A. Kostelecký, M. Mewes, *Astrophysical tests of Lorentz and CPT violation with photons*, The Astrophysical Journal Letters **689** 1, L1 (2008).

[329] V.A. Kostelecký, M. Mewes, *Lorentz-violating electrodynamics and the cosmic microwave background*, Phys. Rev. Lett. **99**, 011601 (2007).

[330] D.H.T. Franco, A.H. Gomes, *Finite one-loop radiative corrections in the Lorentz- and CPT-violating QED extension*, Proceedings of the Sixth Meeting on CPT and Lorentz Symmetry (CPT'13); arXiv:hep-th/1307.5331v1.

[331] V.A. Kostelecký, C. Lane, A. Peckering, *One-loop renormalization of Lorentz-violating electrodynamics*, Phys. Rev. D **65**, 056006 (2002).

[332] L.H.C. Borges, F.A. Barone, J.A. Helayël-Neto, *Field sources in a Lorentz-symmetry breaking scenario with a single background vector*, Eur. Phys. J. C **74**, 2937 (2014).

[333] G. Arfken, H. Weber, F. Harris, *Mathematical methods for physicists*, 7^{th} Ed, Elsevier (2013).

[334] M. Pospelov, A. Ritz, *Electric dipole moments as probes of new physics*, Ann. Phys. **318**, 119 (2005).

[335] E. Commins, *Electric dipole moments of leptons*, Adv. in Atomic, Molecular and Optical Physics, vol. 40 (1999).

[336] W. Bernreuther, M. Suzuki, *The electric dipole moment of the electron*, Rev. Mod. Phys. **63**, 313 (1991).

[337] C.T. Hill, *Axion induced oscillating electric dipole moments*, Phys. Rev. D **91**, 111702 (2015).

[338] T. Ibrahim, A. Itani, P. Nath, *Electron EDM as a sensitive probe of PeV scale physics*, Phys. Rev. D **90** 5, 055006 (2014).

[339] J.P. Archambault, A. Czarnecki, M. Pospelov, *Electric dipole moments of leptons in the presence of Majorana neutrinos*, Phys. Rev. D **70**, 073006 (2004).

[340] M. Nowakowski, E.A. Paschos, J.M. Rodriguez, *All electromagnetic form factors*, Eur. J. Phys. **26**, 545-560 (2005).

[341] A. Czarnecki, B. Krause, *On the dipole moments of fermions at two loops*, Acta Phys. Polon. B **28**, 829 (1997).

[342] H.H. Patel, *Package-X: a Mathematica package for the analytic calculation of one-loop integrals*, Comput. Phys. Commun. **197**, 276 (2015). ArXiv:hep-ph/1503.01469v2.

[343] M. Haghighat, I. Motie, Z. Rezaei, *Charged lepton electric dipole moment enhancement in the Lorentz violated extension of the standard model*, Int. J. Mod. Phys. A **28** 24, 1350115 (2013).

[344] F.J.M. Farley, K. Jungmann, J.P. Miller, W.M. Morse, Y.F. Orlov, B.L. Roberts, Y.K. Semertzidis, A. Silenko, E.J. Stephenson, *New method of measuring electric dipole moments in storage rings*, Phys. Rev. Lett. **93**, 052001 (2004).

[345] R.M. Talman, J.D. Talman, *EDM planning using ETEAPOT with a resurrected AGS Electron Analogue ring*, Phys. Rev. ST Accel. Beams **18**, 074004 (2015). ArXiv:physics.acc-ph/1503.08494v1.

[346] H. Euler, B. Kochel, *Über die Streuung von Licht an Licht nach der Diracschen Theorie*, Naturwiss. **23**, 246 (1935).

[347] W. Heisenberg, H. Euler, *Folgerungen aus der Diracschen Theorie des Positrons*, Z. Phys. **98**, 718 (1936).

[348] E. Zavattini *et al.* (PVLAS collaboration), *Experimental observation of optical rotation generated in vacuum by a magnetic field*, Phys. Rev. Lett. **96**, 110406 (2006).

[349] A. Cadène, P. Berceau, M. Fouché, R. Battesti, C. Rizzo, *Vacuum magnetic linear birefringence using pulsed fields: status of the BMV experiment*, Eur. Phys. J. D **68**, 16 (2014).

[350] L.H.C. Borges, F.A.B. Rangel, *Traces of Lorentz symmetry breaking in a hydrogen atom at ground state.* ArXiv:hep-ph/1601.04784.

[351] V.V. Flambaum, *Enhanced violation of the Lorentz invariance and Einstein's equivalence principle in nuclei and atoms.* ArXiv:physics.atom-ph/1603.05753v1.

[352] F. Caspers, J. Jaeckel, A. Ringwald, *Feasibility, engineering aspects and physics reach of microwave cavity experiments searching for hidden photons and axions*, JINST **4**, 11013 (2009).

[353] J.A. Lipa, J.A. Nissen, S. Wang, D.A. Stricker, D. Avaloff, *A new limit on signals of Lorentz violation in electrodynamics*, Phys. Rev. Lett. **90**, 060403 (2003).

[354] H. Belich, *et al.*, *Lorentz-violating corrections on the hydrogen spectrum induced by a non-minimal coupling*, Phys. Rev. D **74**, 065009 (2006).

[355] P.A. Bolokhov, M. Pospelov, M. Romalis, *Electric dipole moments as probes of CPT invariance*, Phys. Rev. D **78**, 057702 (2008).

[356] B. Charneski, M. Gomes, R.V. Maluf, A.J. da Silva, *Lorentz violation bounds on Bhabha scattering*, Phys. Rev. D **86**, 045003 (2012).

[357] O. Klein, Y. Nishina, *Über die Streuung von Strahlung durch freie Elektronen nach der neuen relativistischen Quantendynamik von Dirac*, Z. Phys. **52**, 853 (1929).

[358] B. Altschul, *Compton scattering in the presence of Lorentz and CPT violation*, Phys. Rev. D **70**, 056005 (2004).

[359] G. Montagna, O. Nicrosini, F. Piccinini, *Precision physics at LEP*, Riv. Nuovo Cim. 21N9, 1-162 (1998).

[360] SLD collaboration, *Polarized Bhabha scattering and a precision measurement of the electron neutral current couplings*, Phys. Rev. Lett. **74**, 2880 (1995).

[361] I. Bozovic-Jelisavcic, S. Lukic, M. Pandurovic, I. Smiljanic, *Precision luminosity measurement at ILC*, arXiv:physics.acc-ph/1403.7348v1.

[362] S. Dutta, P. Konar, B. Mukhopadhyaya, S. Raychaudhuri, *Bhabha scattering with radiated gravitons at linear colliders*, Phys. Rev. D **68**, 095005 (2003).

[363] R. Bufalo, *On the Bhabha scattering for $z = 2$ Lifshitz QED*, Int. J. Mod. Phys. A **30**, 1550086 (2015).

[364] M. Derrick *et al.*, *Experimental study of the reactions $e^- e^+ \to e^- e^+$ and $e^- e^+ \to \gamma\gamma$ at 29 GeV*, Phys. Rev. D **34**, 3286 (1986).

[365] R. Marshall, *Electron-positron annihilation at high energies*, Rep. Prog. Phys. **52**, 1329 (1989).

[366] R. Casana, M.M. Ferreira, Jr., R.V. Maluf, F.E.P. dos Santos, *Effects of a CPT-even and Lorentz-violating nonminimal coupling on electron-positron scattering*, Phys. Rev. D **86**, 125033 (2012).

[367] S. Mohorovicic, *Möglichkeit neuer Elemente und ihre Bedeutung für die Astrophysik*, Astronomische Nachrichten **253**, 93 (1934).

[368] M. Deutsch, *Evidence for the formation of positronium in gases*, Phys. Rev. **82**, 455 (1951).

[369] S.G. Karshenboim, *Precision study of positronium: testing bound state QED theory*, Int. J. Mod. Phys. A **19**, 3879-3896 (2004).

[370] K. Melnikov, A. Yelkhovsky, *$\mathcal{O}(\alpha^3 \ln \alpha)$ corrections to positronium decay rates*, Phys. Rev. D **62**, 116003 (2000).

[371] B.A. Kniehl, A.A. Penin, *Order $\mathcal{O}(\alpha^3) \ln(1/\alpha)$ corrections to positronium decays*, Phys. Rev. Lett. **85**, 1210, 3065(E) (2000).

[372] A.H. Al-Ramadhan, D.W. Gidley, *New precision measurement of the decay rate of singlet positronium*, Phys. Rev. Lett. **72**, 1632 (1994).

[373] S. Asai, Y. Kataoka, T. Kobayashi, T. Namba, T. Suehara, G. Akimoto, A. Ishida, M.M. Hashimoto, H. Saito, T. Idehara, M. Yoshida, *Precision measurements of positronium decay rate and energy level*, AIP Conf. Proc. **1037**, 43 (2008).

[374] V.A. Kostelecký, A.J. vargas, *Lorentz and CPT tests with hydrogen, antihydrogen, and related systems*, Phys. Rev. D **92**, 056002 (2015).

[375] G.S. Adkins, *Search for CP and CPT violation in positronium decay*; CPT and Lorentz Symmetry, chap. 50, pg 254-257, World Scientific (2012).

[376] S. Aldaihan, D.E. Krause, J.C. Long, W.M. Snow, *Calculations of the dominant long-range, spin-independent contributions to the interaction energy between two nonrelativistic Dirac fermions from double-boson exchange of spin-0 and spin-1 bosons with spin-dependent couplings*. ArXiv:hep-th/1611.01580v1.

[377] R. Pohl *et al.*, *The size of the proton*, Nature **466**, 213 (2010).

[378] C.E. Carlson, *The proton radius puzzle*, Prog. Part. Nucl. Phys. **82**, 59 (2015).

[379] P.J. Mohr, B.N. Taylor, D.B. Newell, *CODATA recommended values of the fundamental physical constants: 2010*, Rev. Mod. Phys. **84**, 1527 (2012).

[380] K. Hagiwara, A.D. Martin, D. Nomura, T. Teubner, *Improved predictions for g-2 of the muon and* $\alpha_{\rm QED}(M_Z^2)$, Phys. Lett. B **649**, 173 (2007).

[381] T. Blum, A. Denig, I. Logashenko, E. de Rafael, B.L. Roberts, T. Teubner, G. Venanzoni, *The muon (g-2) theory value: present and future*, Whitepaper prepared for the US Particle Physics "Snowmass" Self Study; arxiv:hep-ph/1311.2198v1.

[382] F. Jegerlehner, *Leading-order hadronic contribution to the electron and muon g-2*, Eur. Phys. J. C **118**, 01016 (2016).

[383] G.S. Adkins, *Three-dimensional Fourier transforms, integrals of spherical Bessel functions, and novel delta function identities*. ArXiv:math-ph/1302.1830.

Appendix A

Currents in relativistic form

A.1 Introduction

In Chapter 3 we discussed the interparticle potentials between spin-1/2 and spin-1 sources. There, as opposed to the analysis of Chapter 2, we kept terms in the amplitudes up to $\mathcal{O}\left(|\mathbf{p}|^2/m^2\right)$. This meant that our NR approximation should produce effects of this order in the associated potentials and, for this to be correctly implemented, we needed to pay special attention to normalization factors.

Here we present the corrected results in a more succinct way. To do this we divide this appendix in two main sections, where we display the various currents – already with proper normalization – in the fully relativistic and non-relativistic forms, for both spins (and representations, in the case of spin-1). This is useful also for future reference.

The general approach here is the following: for both spin-1/2 and spin-1, we have the (momentum-space) wave function expressed as $\Psi(P) = N_P\psi(P)$, where the global factor N_P represents the (possibly) momentum- and energy-dependent normalization, while $\psi(P)$ is the "true" physically meaningful part of the field. We must also keep in mind that the wave functions rarely appear alone in calculations; they are almost always connected in pairs (bilinears). For the currents this is no exception and they are formally expressed as

$$\begin{aligned} j &= \overline{\Psi}(P')\Gamma\Psi(P) \\ &= N_{P'}N_P\overline{\psi}(P')\Gamma\psi(P) \end{aligned} \tag{A.1}$$

where Γ is any kind of field-independent operator acting on the wave functions with momentum factors, for example. The overbar means complex conjugation or adjoint, as the case may be.

From eq.(2.20) we know that the transition from relativistic to non-relativistic amplitudes involves a few energy-dependent pre-factors and we need to apply our NR approximation, but the question is: at which level should we do it? At the wave function, current or amplitude level? Physically, what we are looking for are the NR amplitudes and, as mentioned above, the wave functions are rarely needed alone. For this reason we do not apply the NR approximations direct to the wave functions. The currents, on the other hand, are pivotal to the construction of any physical process – be it our simple scattering or more complex ones – so it seems appropriate to apply our approximations to the currents and then work out the ensuing amplitudes accordingly.

As mentioned above, besides the normalizations, we also have to include energy factors from eq.(2.20). This means that the actual NR currents are obtained if we make the substitution $j \to j_{\rm NR} = \frac{N_{P'}N_P}{\sqrt{2E_P}\sqrt{2E'_P}}\overline{\psi}(P')\Gamma\psi(P)$, but, using that $E_P = E'_P$ and the fact that $\mathbf{P}^2 = \mathbf{P}'^2 = \mathbf{p}^2 + \mathbf{q}^2/4$, we find

$$j \to j_{\rm NR} = \frac{N_P^2}{2E_P}\overline{\psi}(P')\Gamma\psi(P). \tag{A.2}$$

This is the general prescription for the corrections to be implement in the next sections.

For the sake of convenience, below we present the (correctly) normalized wave functions for the three cases covered[1] spin-1/2 (eq.(2.1)), spin-1 in the vector representation (eq.(3.11)) and spin-1 in the tensor representation (eqs.(3.55) and (3.55)):

$$u(P) = \sqrt{E+m}\begin{pmatrix} \xi \\ \frac{\boldsymbol{\sigma}\cdot\mathbf{P}}{E+m}\,\xi \end{pmatrix} \tag{A.3}$$

$$W^\mu_{\rm lab}(P) = \left[\frac{1}{m}(\mathbf{P}\cdot\boldsymbol{\epsilon})\ ,\ \boldsymbol{\epsilon} + \frac{1}{m(E+m)}(\mathbf{P}\cdot\boldsymbol{\epsilon})\mathbf{P}\right] \tag{A.4}$$

$$B^{0i}(P) = \frac{1}{\sqrt{2}m}\epsilon_{ijk}\boldsymbol{\epsilon}_j\mathbf{P}_k \tag{A.5}$$

$$B^{ij}(P) = \frac{1}{\sqrt{2}}\left\{\epsilon_{ijk}\boldsymbol{\epsilon}_k + \frac{1}{m(E+m)}\left[\mathbf{P}_i(\boldsymbol{\epsilon}\times\mathbf{P})_j - \mathbf{P}_j(\boldsymbol{\epsilon}\times\mathbf{P})_i\right]\right\}, \tag{A.6}$$

and, as usual, we refer to the momenta assignments from Fig. 7.1. For simplicity, in what follows we do not include the coupling constants.

[1] An interesting check that the aforementioned normalizations for the spin-1 wave functions are sensible (at least when it comes to numerical factors) is by looking at their contractions in rest frame. We know that, in the vector representation, $\epsilon_\mu\epsilon^\mu = -1$, which leads to $\boldsymbol{\epsilon}\cdot\boldsymbol{\epsilon} = 1$, as it should. Similarly, if we notice that $B^{0i} = 0$ at rest, we see that the extra $1/\sqrt{2}$ from the normalization is needed to cancel the factor of 2 coming from $\epsilon_{ijk}\epsilon_{ijl} = 2\delta_{kl}$ – this ensures that $\boldsymbol{\epsilon}\cdot\boldsymbol{\epsilon} = 1$ as well.

A.2 Relativistic currents

Since we are dealing with a considerable number of currents (S, PS, V and PV) for basically three different scenarios, it is convenient to organize everything in a systematic way. To facilitate book keeping below I list the currents in their relativistic forms, i.e., no approximations are made yet. This organization is very close to the one presented in Section 2.2.1, which is actually a sub-case of the NR currents presented in the next section.

We shall start by the most common case, that of the usual spin-1/2 fermions. Since we are in the relativistic (general) case, we will keep the overall $(E+m)$ factor stemming from the normalization out of the currents[2] presented below. This will not be necessary for the spin-1 cases, where the normalization factors are simply numbers. In the following m and E refer to the mass and energy of particle 1 (or 2), respectively.

A.2.1 Spin-1/2

The expressions below are exact in the sense that no terms above $\mathcal{O}\left(|\mathbf{p}|^2/m^2\right)$ appear. An overall factor of $E+m$ is implied in all currents.

1) Scalar current (S):

$$\begin{aligned}\bar{u}(p+q/2)\,u(p-q/2) &= \delta\left[1-\frac{1}{(E+m)^2}\left(\mathbf{p}^2-\frac{1}{4}\mathbf{q}^2\right)\right]+ \\ &- \frac{i}{(E+m)^2}\mathbf{q}\cdot(\mathbf{p}\times\langle\boldsymbol{\sigma}\rangle)\end{aligned} \tag{A.7}$$

2) Pseudo-scalar current (PS):

$$\bar{u}(p+q/2)\,i\gamma_5\,u(p-q/2) = -\frac{i}{E+m}\,\mathbf{q}\cdot\langle\boldsymbol{\sigma}\rangle \tag{A.8}$$

3) Vector current (V):

$$\bar{u}(p+q/2)\,\gamma^\mu\,u(p-q/2), \tag{A.9}$$

[2]This was also done in Section 2.2.1.

3i) For $\mu = 0$,

$$\begin{aligned} \bar{u}(p+q/2)\,\gamma^0\,u(p-q/2) &= \delta\left[1+\frac{1}{(E+m)^2}\left(\mathbf{p}^2-\frac{1}{4}\mathbf{q}^2\right)\right]+ \\ &+ \frac{i}{(E+m)^2}\,(\mathbf{q}\times\mathbf{p})\cdot\langle\boldsymbol{\sigma}\rangle \end{aligned} \tag{A.10}$$

3ii) For $\mu = i$,

$$\bar{u}(p+q/2)\,\gamma^i\,u(p-q/2) = \frac{2}{E+m}\left[\delta\mathbf{p}_i - \frac{i}{2}\epsilon_{ijk}\mathbf{q}_j\langle\boldsymbol{\sigma}_k\rangle\right] \tag{A.11}$$

4) Pseudo-vector current (PV):

$$\bar{u}(p+q/2)\gamma^\mu\gamma_5 u(p-q/2) \tag{A.12}$$

4i) For $\mu = 0$,

$$\bar{u}(p+q/2)\,\gamma^0\,\gamma_5\,u(p-q/2) = \frac{2}{E+m}\,\langle\boldsymbol{\sigma}\rangle\cdot\mathbf{p} \tag{A.13}$$

4ii) For $\mu = i$,

$$\begin{aligned} \bar{u}(p+q/2)\,\gamma^i\,\gamma_5\,u(p-q/2) &= \left[1-\frac{1}{(E+m)^2}\left(\mathbf{p}^2-\frac{1}{4}\mathbf{q}^2\right)\right]\langle\boldsymbol{\sigma}_i\rangle + \\ &- \frac{i\delta}{(E+m)^2}\,(\mathbf{q}\times\mathbf{p})_i + \\ &+ \frac{2}{(E+m)^2}\left[(\mathbf{p}\cdot\langle\boldsymbol{\sigma}\rangle)\,\mathbf{p}_i - \frac{1}{4}\,(\mathbf{q}\cdot\langle\boldsymbol{\sigma}\rangle)\,\mathbf{q}_i\right] \end{aligned} \tag{A.14}$$

We notice that the results above, which are the equivalent of $\overline{\psi}(P')\Gamma\psi(P)$ from eq.(A.2), match the ones quoted in Ref. [67] if one makes $E+m \approx 2m$. This substitution is nevertheless justified in the NR limit – even without considering the correction factors from eq.(A.2) – since all of these factors appear in the denominator of terms already containing factors of momenta in the numerator.

A.2.2 Spin-1 (vec. rep.)

Contrary to the spin-1/2 case, where our expressions were exact, here we keep terms only up to and including $\mathcal{O}\left(|\mathbf{p}|^2/m^2\right)$. This means that the following expressions disregard terms of order $\mathcal{O}\left(|\mathbf{p}|^4/m^4\right)$, which are due to the spatial part of the wave functions (that is why we use $\simeq$ instead of $=$).

1) Scalar current (S):

$$\begin{aligned} W^*_\mu(p+q/2)\,W^\mu(p-q/2) &\simeq -\delta + \frac{1}{m^2}\left[1-\frac{2m}{E+m}\right](\mathbf{p}\cdot\boldsymbol{\epsilon}^*)\,(\mathbf{p}\cdot\boldsymbol{\epsilon}) + \\ &- \frac{i}{2m^2}\,(\mathbf{q}\times\mathbf{p})\cdot\langle\mathbf{S}\rangle + \\ &- \frac{1}{4m^2}\left[1+\frac{2m}{E+m}\right](\mathbf{q}\cdot\boldsymbol{\epsilon}^*)\,(\mathbf{q}\cdot\boldsymbol{\epsilon}) \end{aligned} \tag{A.15}$$

2) Pseudo-scalar current (PS):

$$W^*_{\mu\nu}(p+q/2)\,\tilde{W}^{\mu\nu}(p-q/2)) \simeq 2iE\,(\mathbf{q}\cdot\langle\mathbf{S}\rangle) \tag{A.16}$$

3) Vector current (V):

$$J^\mu_{\rm V}(p,q) = 2p^\mu W^*_\nu W^\nu + igq_\nu W^{*\,\alpha}\,(\Sigma^{\mu\nu}_{\rm V})_{\alpha\beta}\,W^\beta \tag{A.17}$$

3i) For $\mu = 0$,

$$\begin{aligned} J^0_{\rm V}(p,q) &= -2E\left\{\delta - \frac{1}{m^2}\left[1-\frac{2m}{E+m}\right](\mathbf{p}\cdot\boldsymbol{\epsilon}^*)\,(\mathbf{p}\cdot\boldsymbol{\epsilon})\right\} + \\ &+ \frac{i}{m}\left[g-\frac{E}{m}\right](\mathbf{q}\times\mathbf{p})\cdot\langle\mathbf{S}\rangle + \\ &+ \frac{1}{m}\left[g-\frac{E}{2m}\left(1+\frac{2m}{E+m}\right)\right](\mathbf{q}\cdot\boldsymbol{\epsilon}^*)\,(\mathbf{q}\cdot\boldsymbol{\epsilon}) \end{aligned} \tag{A.18}$$

3ii) For $\mu = i$,

$$J^i_{\rm V}(p,q) = -\left[2\delta\mathbf{p}_i + ig\epsilon_{ijk}\mathbf{q}_j\langle\mathbf{S}_k\rangle\right] \tag{A.19}$$

4) Pseudo-vector current (PV):

$$J^\mu_{\rm PV}(p,q) = \frac{i}{2}g\epsilon^{\mu\nu\kappa\lambda}q_\kappa W^{*\,\alpha}\left(\Sigma^{\rm V}_{\nu\lambda}\right)_{\alpha\beta}W^\beta \tag{A.20}$$

4i) For $\mu = 0$,

$$J^0_{\rm PV}(p,q) = i\mathbf{q}\cdot\langle\mathbf{S}\rangle \tag{A.21}$$

4ii) For $\mu = i$,

$$\begin{aligned} J^i_{\rm PV}(p,q) &= -\frac{1}{m}\Bigg\{\left[\left(\mathbf{p}-\frac{1}{2}\mathbf{q}\right)\cdot\boldsymbol{\epsilon}\right](\mathbf{q}\times\boldsymbol{\epsilon}^*)_i + \\ &- \left[\left(\mathbf{p}+\frac{1}{2}\mathbf{q}\right)\cdot\boldsymbol{\epsilon}^*\right](\mathbf{q}\times\boldsymbol{\epsilon})_i\Bigg\} \end{aligned} \tag{A.22}$$

A.2.3 Spin-1 (tens. rep.)

Similarly to the vector representation of the spin-1, here we keep terms only up to and including $\mathcal{O}\left(|\mathbf{p}|^2/m^2\right)$. This means that the following expressions disregard terms of order $\mathcal{O}\left(|\mathbf{p}|^4/m^4\right)$, which are due to the spatial part of the wave functions[3] (that is why we use $\simeq$ instead of $=$).

1) Scalar current (S):

$$\begin{aligned} B^*_{\mu\nu}(p+q/2)\,B^{\mu\nu}(p-q/2) &\simeq \delta\left[1-\frac{1}{m^2}\left(1-\frac{2m}{E+m}\right)\mathbf{p}^2+\frac{1}{4m^2}\left(1+\frac{2m}{E+m}\right)\mathbf{q}^2\right]+ \\ &+ \frac{i}{2m^2}\,(\mathbf{q}\times\mathbf{p})\cdot\langle\mathbf{S}\rangle + \\ &+ \frac{1}{m^2}\left[1-\frac{2m}{E+m}\right](\mathbf{p}\cdot\boldsymbol{\epsilon}^*)\,(\mathbf{p}\cdot\boldsymbol{\epsilon})+ \\ &- \frac{1}{4m^2}\left[1+\frac{2m}{E+m}\right](\mathbf{q}\cdot\boldsymbol{\epsilon}^*)\,(\mathbf{q}\cdot\boldsymbol{\epsilon}) \end{aligned} \tag{A.23}$$

2) Pseudo-scalar current (PS):

$$B^*_{\mu\nu}(p+q/2)\,\tilde{B}^{\mu\nu}(p-q/2))\simeq -\frac{i}{m}\,(\mathbf{q}\cdot\langle\mathbf{S}\rangle) \tag{A.24}$$

3) Vector current (V):

$$J^\mu_{\rm V}(p,q) = 2p^\mu B^*_{\lambda\nu}B^{\lambda\nu} + igq_\nu B^{*\,\alpha\beta}\left(\Sigma^{\mu\nu}_{\rm T}\right)_{\alpha\beta\,,\,\sigma\rho}B^{\sigma\rho} \tag{A.25}$$

[3]For the PV current I have set $E+m\approx 2m$ since otherwise the current would be too cumbersome.

3i) For $\mu = 0$,

$$\begin{aligned} J^0_{\rm V}(p,q) &= 2E\left\{\delta - \frac{1}{m^2}\left(1-\frac{2m}{E+m}\right)\left[\delta\mathbf{p}^2 - (\mathbf{p}\cdot\boldsymbol{\epsilon}^*)(\mathbf{p}\cdot\boldsymbol{\epsilon})\right]\right\} + \\ &- \frac{i}{m}\left[g - \frac{E}{m}\right](\mathbf{q}\times\mathbf{p})\cdot\langle\mathbf{S}\rangle + \\ &- \frac{1}{m}\left[g - \frac{E}{2m}\left(1+\frac{2m}{E+m}\right)\right](\mathbf{q}\cdot\boldsymbol{\epsilon}^*)(\mathbf{q}\cdot\boldsymbol{\epsilon}) \end{aligned} \tag{A.26}$$

3ii) For $\mu = i$,

$$J^i_{\rm V}(p,q) = 2\delta\mathbf{p}_i + ig\epsilon_{ijk}\mathbf{q}_j\langle\mathbf{S}_k\rangle \tag{A.27}$$

4) Pseudo-vector current (PV):

$$\begin{aligned} J^\mu_{\rm PV}(p,q) &= 2p^\mu\tilde{B}^*_{\alpha\beta}B^{\alpha\beta} - i\left(\Sigma^{\mu\nu}_T\right)_{\alpha\beta\,,\,\lambda\kappa}\left[p_\nu\left(\tilde{B}^{*\,\alpha\beta}B^{\lambda\kappa} + \tilde{B}^{\alpha\beta}B^{*\,\lambda\kappa}\right) + \right. \\ &- \left.\frac{1}{2}q_\nu\left(\tilde{B}^{*\,\alpha\beta}B^{\lambda\kappa} - \tilde{B}^{\alpha\beta}B^{*\,\lambda\kappa}\right)\right] \end{aligned} \tag{A.28}$$

4i) For $\mu = 0$,

$$J^0_{\rm PV}(p,q) = -i\mathbf{q}\cdot\langle\mathbf{S}\rangle \tag{A.29}$$

4ii) For $\mu = i$,

$$\begin{aligned} J^i_{\rm PV}(p,q) &= -\frac{i}{m}\left[\mathbf{p}_i\,(\mathbf{q}\cdot\langle\mathbf{S}\rangle) + \mathbf{q}_i\,(\mathbf{p}\cdot\langle\mathbf{S}\rangle)\right] + \\ &+ \frac{1}{m}\left\{\left[\left(\mathbf{p}-\frac{1}{2}\mathbf{q}\right)\cdot\boldsymbol{\epsilon}\right](\mathbf{q}\times\boldsymbol{\epsilon}^*)_i + \right. \\ &+ \left.\left[\left(\mathbf{p}+\frac{1}{2}\mathbf{q}\right)\cdot\boldsymbol{\epsilon}^*\right](\mathbf{q}\times\boldsymbol{\epsilon})_i\right\}. \end{aligned} \tag{A.30}$$

A.3 Useful integrals

In Chapters 2 and 3 we calculated interparticle potentials defined via the Fourier transform of the NR amplitude in terms of the momentum transfer, cf. eq.(2.19). In this sense, the following integrals appear

$$\int \frac{d^3\mathbf{q}}{(2\pi)^3}\,\frac{\mathbf{q}_i}{\mathbf{q}^2+m^2}\,e^{i\mathbf{q}\cdot\mathbf{r}} \tag{A.31}$$

$$\int \frac{d^3\mathbf{q}}{(2\pi)^3}\,\frac{\mathbf{q}_i\mathbf{q}_j}{\mathbf{q}^2+m^2}\,e^{i\mathbf{q}\cdot\mathbf{r}} \tag{A.32}$$

$$\int \frac{d^3\mathbf{q}}{(2\pi)^3}\,\frac{\mathbf{q}^{\,2}}{\mathbf{q}^2+m^2}\,e^{i\mathbf{q}\cdot\mathbf{r}} \tag{A.33}$$

It is not difficult to see that these integrals may be obtained starting from the simplest $I_0(r)=\int \frac{d^3\mathbf{q}}{(2\pi)^3}\,\frac{1}{\mathbf{q}^2+m^2}\,e^{i\mathbf{q}\cdot\mathbf{r}}$. Fortunately, this integral is quite standard and its value is given by

$$I_0(r)=\frac{1}{4\pi r}e^{-mr}. \tag{A.34}$$

By applying partial derivatives to eq.(A.34) we are able to extract the other important integrals we need. Below we quote the results used in the main text (the limit $m\to 0$ may be taken):

$$\int \frac{d^3\mathbf{q}}{(2\pi)^3}\,\frac{\mathbf{q}_i}{\mathbf{q}^2+m^2}\,e^{i\mathbf{q}\cdot\mathbf{r}} = \frac{i}{4\pi r^2}\,(1+mr)\,e^{-mr}\hat{\mathbf{r}}_i \tag{A.35}$$

$$\begin{aligned}\int \frac{d^3\mathbf{q}}{(2\pi)^3}\,\frac{\mathbf{q}_i\mathbf{q}_j}{\mathbf{q}^2+m^2}\,e^{i\mathbf{q}\cdot\mathbf{r}} &= \frac{1}{3}\delta_{ij}\delta^3(\mathbf{r}) \\ &+ \frac{1}{4\pi r^3}\left[(1+mr)\delta_{ij}-(3+3mr+m^2r^2)\frac{x_ix_j}{r^2}\right]e^{-mr}\end{aligned} \tag{A.36}$$

$$\int \frac{d^3\mathbf{q}}{(2\pi)^3}\,\frac{\mathbf{q}^{\,2}}{\mathbf{q}^2+m^2}\,e^{i\mathbf{q}\cdot\mathbf{r}} = \delta^3(\mathbf{r})-\frac{m^2}{4\pi r}e^{-mr} \tag{A.37}$$

The presence of the Dirac delta in eq.(A.36) may be better understood by looking at eq.(A.37), which is obtained as its "trace". The fact is that, for $m=0$, there is a cancellation of the $\mathbf{q}^2$ factors in the numerator and denominator of eq.(A.37), which is then reduced to the Fourier transform of unity, the Dirac delta. For $m\neq 0$, the presence of the Dirac delta is also justified, since it retains the spherical symmetry of the left-hand side and recovers the simpler $\delta^3(\mathbf{r})$ once $m\to 0$ [383].